PROTEIN CORONA AND OPTOACOUSTIC PROPERTIES OF GOLD NANOPARTICLES OF DIFFERENT SIZE AND SHAPE

A thesis submitted to The University of Manchester for the degree of Doctor of Philosophy in the Faculty of Biology, Medicine and Health

2019

Rafaela Paz García Álvarez

Supervisors: Prof. Kostas Kostarelos and Prof. Luis M. Liz-Marzán

School of Health Sciences

Blank Page

Table of Contents

LIST OF FIGURES

CHAPTER 1: INTRODUCTION

CHAPTER 3: EXPERIMENTAL METHODOLOGY

CHAPTER 7: *IN VIVO* PROTEIN CORONA ON GOLD NANOPARTICLES

CHAPTER 8: OPTOACOUSTIC PROPERTIES OF GOLD NANOPARTICLES

CHAPTER 9: PROTEIN CORONA AND OPTOACOUSTIC PERFORMANCE

APPENDIX

LIST OF TABLES

CHAPTER 5: *IN VITRO* PROTEIN CORONA ON GOLD NANOPARTICLES

CHAPTER 6: *IN VITRO* PROTEIN CORONA ON GOLD NANOSTARS

CHAPTER 7: *IN VIVO* PROTEIN CORONA ON GOLD NANOPARTICLES

CHAPTER 8: OPTOACOUSTIC PROPERTIES OF GOLD NANOPARTICLES

WORD COUNT: 53186.

Blank page.

ABSTRACT

Nanomaterials designed for biomedical applications are expected to establish contact with physiological fluids, which contain a wide variety of biomolecules and cellular entities. It is now well-accepted that when a nanomaterial comes into contact with a biological fluid, its nature and physico-chemical properties can be affected by the formation of the so-called "protein corona", which leads to a modification of its expected behaviour, fate and pharmacological profile. As a consequence, the protein corona has been studied extensively during the last decade, aiming to describe and define the effect of nanomaterial parameters on the composition of the corona. Similarly, numerous investigations have been performed to understand the effect of the corona itself on a wide range of biological processes. The protein corona has become a critical parameter to be described and understood before the translation of any nanomaterial to biomedical applications.

Among the myriad of available nanomaterials designed and engineered today, gold nanoparticles have attracted a lot of attention due to their plasmonic properties, which confer them interesting optical and thermal characteristics. Due to these properties, gold-based nanostructures have been proposed for several biomedical uses such as drug delivery, biosensing, imaging and disease treatment. Therefore, it is vital to get a deeper understanding on the protein corona formed around this type of nanomaterial.

In this PhD thesis, we focused on the study of the protein corona formed on the surface of gold nanoparticles of different sizes and shapes functionalized with carboxylic polyethylene glycol. Protein corona composition was quantitatively and qualitatively evaluated for gold nanospheres, gold nanorods and gold nanostars of different dimensions. In addition, the *in vivo* protein corona on gold nanoparticles was isolated and analysed for the first time. Lastly, the potential of gold nanoparticles as optoacoustic imaging contrast agents was studied. For this purpose, optoacoustic signals generated by different gold nanoparticles was measured in the absence and presence of protein corona. General results revealed the nanoparticle features strongly affect protein corona composition, which additionally has an impact on the optoacoustic performance of this nanomaterial type.

Blank page.

DECLARATION

I, Rafaela Paz García Álvarez, declare that no portion of the work referred to in the thesis has been submitted in support of an application for another degree or qualification of this or any other university or other institute of learning;

COPYRIGHT

Blank page.

DEDICATIONS AND ACKNOWLEDGEMENTS

This thesis is dedicated to every single person (plus my lovely dog, Ayla) whose actions have helped me, scientifically or emotionally, to go through this challenging period of my life. Thank you from the bottom of my heart.

First of all, I would like to express my gratitude to my two supervisors, Prof. Luis M. Liz-Marzán and Prof. Kostas Kostarelos, for their guidance and advice during this PhD. Thank you very much for this amazing opportunity to make my small contribution to science.

To everybody in the Nanomedicine Lab (The University of Manchester) and the Bionanoplamonics Lab (CIC biomaGUNE), thank you all for your support and help whenever I needed it. In Manchester, special thanks to Adrián Esteban Arranz, he knows he is one of the main reasons I was able to overcome many difficulties. His support really saved me more than once! I feel really grateful to have met someone like him. I would also like to dedicate a special thanks to Neus Lozano Valdés, as she helped me get started in the Nanomedicine Lab and was there to support me since the very beginning. Thanks also to Marilena Hadjidemetriou, as she introduced me and helped me at the beginning of my interactions with the Protein Corona world. In CIC biomaGUNE, I feel especially grateful to Ana Sánchez Iglesias and María Sanromán. Apart from your amazing knowledge of nanoparticle synthesis and science in general, your support, our conversations and moments in the lab really helped me get through some of the most difficult times.

I would also like to express my gratitude towards Prof. Alexander Kuehne, Prof. Twan Lammers and Dr. Dmitry Chigrin, from RHWT Aachen University, for their collaboration, guidance and advice during my two-months stay in Aachen, Germany, for optoacoustic research. I would like also to thank to their teams for their support and help whenever I needed.

Special thanks to Félix Elortza, Mikel Aragortza and Iraide Escobes for their advice and knowledge on Mass Spectrometry and data analysis. It was great working together with them and I could learn a lot thanks to the time and patience they dedicated to me.

Finally, I would like to specially thank my partner, Adrián Barroso, my parents Rosa and Orlando, my brother Héctor, my family and my friends for your infinite support and love. I know I couldn't have done it without you.

Blank page.

PUBLICATIONS

- **R. García-Álvarez**, M. Hadjidemetriou, A. Sánchez-Iglesias, L. M. Liz-Marzán and K. Kostarelos, In vivo formation of protein corona on gold nanoparticles. The effect of size and shape, Nanoscale, 2018, 10, 1256-1264.
- M. Quintanilla, I. García, I. De Lázaro, **R. García-Álvarez**, M. Henriksen-Lacey, S. Vranic, K. Kostarelos and L. M. Liz-Marzán, Thermal monitoring during photothermia: hybrid probes for simultaneous plasmonic heating and near-infrared optical nanothermometry, Theranostics, 2019, 9, 7298-7312.
- **R. García-Álvarez**, L. Chen, A. Nedilko, A. Rix, W. Lederle, V. Pathak, A. Sánchez-Iglesias, T. Lammers, G. Von Plessen, K. Kostarelos, L. M. Liz-Marzán, A. J. C. Kuehne and D. N. Chigrin, Optimizing the geometry of photoacoustically active gold nanoparticles for biomedical imaging, ACS Photonics, 2020, 7, 646-652.

Blank page.

CHAPTER 1: INTRODUCTION

1. Brief History of Nanotechnology.

Theoretical physicist Richard Feynman is widely recognized as one of the most important figures in the history of nanotechnology. Basic principles and concepts for the birth and development of nanoscience and nanotechnology were first proposed in 1959 at the American Physical Society Meeting in California Institute of Technology, during his famous talk "There is Plenty of Room at the Bottom".[1] In this speech, Feynman discussed about the importance of being able to manipulate and control processes at a very small scale. This would imply the ability to control individual atoms and molecules, which theoretically would allow a more detailed investigation. Consequently, this would lead to a deeper insight and explanations of many complex phenomena.

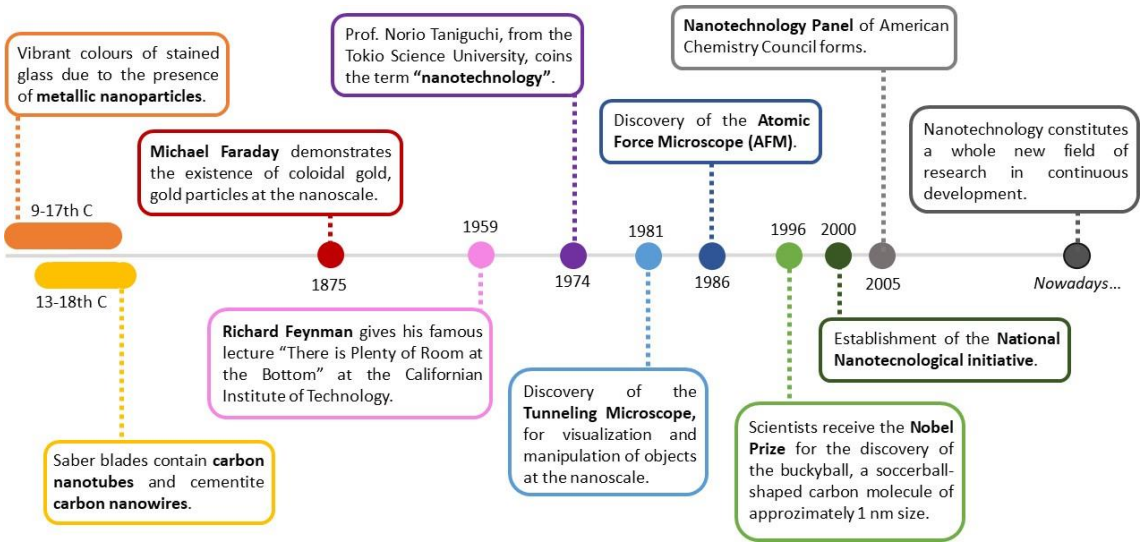

Figure 1: Chronological scheme of the history of Nanotechnology.

The term "nanotechnology" appeared for the first time in a scientific publication in 1974, when Japanese scientist Norio Taniguchi used it to describe the technology to create objects at the nanoscale.[2] Nevertheless, it was not until the invention and development of the Scanning Tunneling Microscope in 1980 by IBM scientists[3] and the later creation and advance on Atomic Force Microscopy[4, 5] that it became possible to visualize and manipulate individual atoms and molecules. These techniques together with important advances on the development of more powerful computers provided the opportunity of thoroughly characterizing different types of nanomaterials (NMs) and hence, to get a

deeper insight of their properties. This knowledge was then applied to the design, development and investigation of novel NMs.

Nanotechnology is nowadays defined as a field of research and innovation focused on the design and creation of objects and devices at the nanoscale. At the nanometre size – a million times smaller than a millimetre – materials exhibit different characteristics in comparison with their macroscopic counterparts. Due to these properties, nanotechnology holds great potential for the development of a great array of NMs for many distinct applications, from environment and energy[6] to medicine and research.[7] Advances on nanotechnology are giving a new perspective and alternative solutions for many different issues present in our society. The following paragraphs will be dedicated to one of the currently most relevant fields of nanotechnology, focused on biomedical application of NMs, Nanomedicine.

2. Nanomedicine.

Nanomedicine is a scientific field of research focused on the application of nanotechnology to medicine.[8] The main purpose of nanomedicine is to achieve a higher quality of life for people all over the world by providing alternative and efficient solutions to a great number of medical problems. With this objective in mind, numerous efforts have been dedicated to the design, development and optimization of many different types of NMs for biomedical purposes. During the last decades, there has been a considerable investment on scientific projects for the production of NMs for medical applications.

One of the main advantages of nano-sized materials when applied to nanomedicine is their small size, which facilitates interactions at the cellular level and allows them to reach places that were thought to be inaccessible.[9, 10] However, it is important to keep in mind that there is a long list of other requirements that nanomedicines must meet depending on the final purpose, such as biocompatibility, high stability, biodegradability or low/none toxicity, among many others. Ideally, nanomedicines must be designed and modified in a certain way that allows control over the interactions and location of the NM with the biological entities within the body.[11] Unfortunately, this objective seems nowadays rather unfeasible due to the limitations of the available techniques for the

characterizations of the material's performance in real-time. At the moment, researchers all over the world are focused not only on NM design, but also in the development of new techniques that allow a detailed investigation of the processes and phenomena that these materials undergo once in touch with biological fluids and entities.[12] Equally important is the improvement on the methodologies used for NM production, as they should ideally be available and economically reachable for everybody. Synthetic protocols are being optimized and modified in order to be easier, cheaper and more convenient and reproducible, as well as simplified for their use by non-specialists.

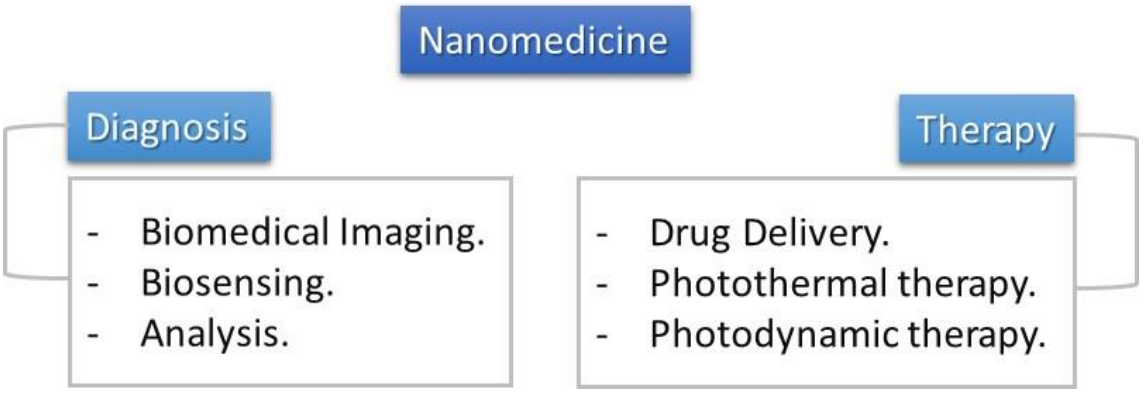

Figure 2: Scheme of biomedical application of Nanomedicine.

Currently, NMs for biomedical applications are generally divided in two main groups with different aims: therapy and diagnosis. Numerous nanoparticles (NPs) have been modified and functionalized in order to use them as drug delivery systems and to target specific organs or parts of the body. Depending on the NM properties, alternative treatments such as photothermal-therapy or photodynamic-therapy have been proposed.[13] Regarding diagnosis applications, myriads of nanostructures of different composition have been manipulated for its use on medical imaging as novel contrast agents as well as for biosensing and analysis.[14] Decades of research and, consequently, of new knowledge about NM synthesis mechanism and functionalization, have given scientists the necessary tools for the creation and production of countless nanostructures with different characteristics and advantages. Relatively recent is the proposal of one of the biggest challenges in nanomedicine, the field of theranostics, which is dedicated to the production of multifunctional NMs with features that allow both diagnosis and therapy in a single nanostructure.[15]

3. Protein Corona.

Any nano-sized material produced for biomedical applications is expected to get in contact with physiological fluids and biological entities present within the body. Exosomes, nucleic acid fragments, lipids, proteins and cells are likely to interact with the injected NM influencing their physico-chemical characteristics and modifying their behaviour.[16] Among these interactions, protein adsorption is one of the most relevant and hence, has been object of study for a long time.

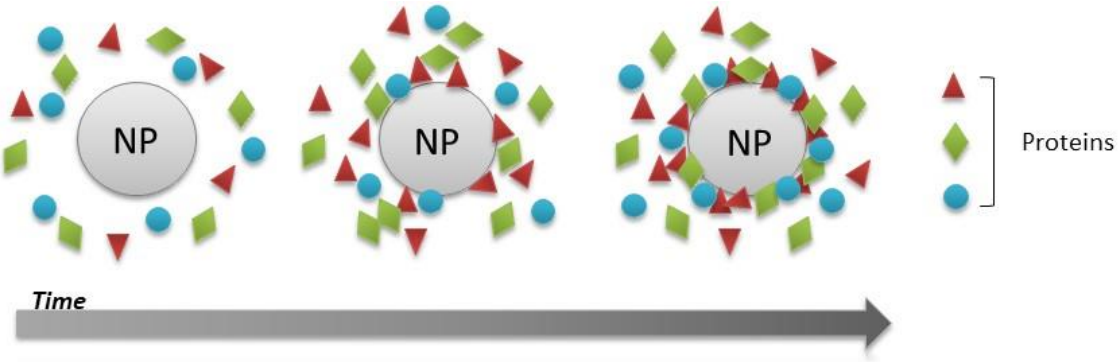

Figure 3: Scheme of the formation of the Protein Corona on a general nanoparticle (NP) over time.

Protein adsorption phenomenon was described for the first time in 1962 by L. Vroman, where he studied the interactions between hydrophobic solid powders and plasma samples.[17] In this paper, he describes how protein interaction changes the surface properties of the material, which becomes hydrophilic. It is important to highlight the preferential absorbance of certain coagulation factors and proteins on the surface as a function of the type of powder observed by Vroman, which indicates that modifications on the wettability of the material are driven not just by the presence of plasma but also by the initial physico-chemical properties of the powders. During several decades, scientists dedicated plenty of efforts to investigate the process of protein adsorption on many different types of materials and NMs, emphasizing the need of new coatings for decreasing and/or avoiding protein interactions and therefore, keeping the initial properties of the NPs untouched.[18, 19] Nevertheless, it was not until 2007 that Cedervall introduced the term “protein corona” (PC) to describe this process and a systematic study of the effect of protein-NP interactions was taken to the molecular level.[20] Nowadays, PC is considered a trending topic in the field of nanotechnology and

countless efforts have been invested in the investigation on the mechanism of the phenomenon and its characterization.[21] This process has become a key parameter that must be adequately defined and understood for any NM proposed for biomedical applications before any translation into clinical trials.[22, 23]

3.1. Description of the Protein Corona.

PC is currently described as a dynamic multi-layered structure formed by proteins adsorbed onto the material surface upon contact with the physiological environment and consequent interaction with proteins.[24] This structure can be divided into two parts known as "soft" and "hard" PC. While the inner layer of tightly bound proteins with a lifetime of several hours has been termed as "hard" corona, the outer layer of weakly bound proteins is called "soft" corona.[25] The "hard" corona is considered as an equilibrium state long enough to confer a new biological identity to the NM. This means that the PC-NP complex and not the initial NM characteristics will determine the behaviour, fate and performance of any material when interacting with the biological media. This statement implies that protein interaction would modify the physico-chemical properties of the synthesized NPs and, therefore, it will lead to changes in biological processes such as cellular uptake, proliferation, cytotoxicity or affect targeting and delivery capabilities of the administered nanostructures.[26]

The existence of the "hard" PC has been a widely discussed topic and hence, it has been extensively investigated. Several publications have supported the formation of an irreversible protein interaction with NM surfaces upon incubation in physiological fluids. Initial studies were focused on the interaction between the NM and one type of protein in particular, where NPs of different compositions were found to form an irreversible layer of protein on their surface.[27] Subsequently, investigations on more complex biological fluids such as serum or full plasma were carried out.[28-30] Results indicate, in general, that NMs effectively interact in an irreversible way with proteins. An *in vitro* study reports an evolution from a loosely towards a tightly attached corona over time.[31] Recently, Hadjidemetriou et al. reported a very interesting study about the PC formed under *in vivo* conditions.[32] Their results indicate that as soon as 10 min post-injection, a stable corona was formed. It is important to highlight that majority of studies have

been focused on the characterization of the "hard" PC, as it is stable enough to be isolated and analysed.

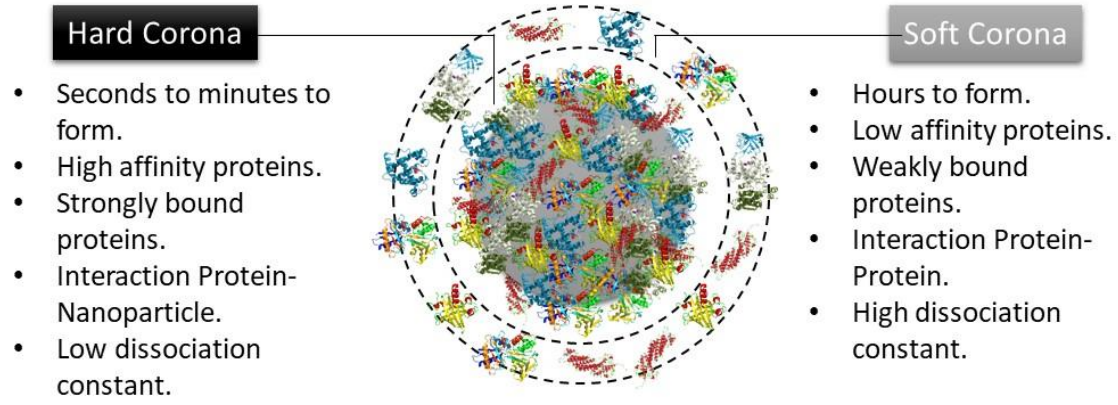

Figure 4: Schematic representation and description of the "soft" and "hard" protein coronas.

In contrast, "soft" corona is constituted by proteins with a lower affinity for the NM surface, which means they are loosely bound to the NP and can be exchanged over time. "Soft" PC is easily detached during the washing process and therefore, its characterization and study have become a rather difficult challenge. Several groups have investigated the "soft" PC by monitoring the interaction of NMs and proteins on real time to get a deeper insight of its mechanism.[33, 34] Nevertheless, it remains as a difficult process to study and, though the main hydrodynamic diameter (D_H) and thickness of the corona can be recorded *in situ* by techniques such as Fluorescence Correlation Spectroscopy (FCS)[35] or Dynamic Light Scattering (DLS)[31], a detailed analysis of its composition has not been performed.

Summarizing, it is important to keep in mind that PC formation is not a static process. Proteins will adsorb and desorb continuously from the NP surface until they reach a steady state. Up to date, it has been reported that highly abundant proteins can be replaced over time by less abundant ones displaying a higher affinity for the NP surface over time.[32]

3.2. Parameters Influencing the Protein Corona.

Process of corona formation is known to be affected by a wide variety of parameters as well as by having an influence on many different biological processes.[36] Physico-chemical characteristics such as functionalization, surface charge, NP size and others are important factors that must be taken into consideration when investigating about PC formation. Similarly, choice of incubation media is also essential, as it will directly impact on PC composition. Equally relevant are the conditions of the experiment such as temperature, time exposure or dynamic/static flow conditions. To be able to adequately study PC formation and composition, it is vital to understand the initial material, the physiological media of interaction and to control the experimental conditions. Next paragraphs will illustrate these ideas with several examples of investigations on PC formation on different NMs.

3.2.1. Nanoparticle Properties.

As mentioned before, NP size plays an important role on the process of PC formation, which influences directly the interaction between the NP surface and the proteins present in the biological media.[37] Surface curvature of the NP, which is mostly dependent on its size, has been proven to be very relevant when investigating protein adsorption on all kind of surfaces. Protein binding affinity is the parameter that will define the adsorption and desorption processes and, in general, protein-NP interactions, and it is as well related to the surface curvature. The higher the surface curvature, as it is in the case of NMs, the lower will be the affinity of the protein for a surface.[38] In addition, when proteins are adsorbed on curved surfaces, they are less likely to undergo conformational changes, though modifications in their structure and function cannot be completely avoided.[39, 40]

Many investigations have focused on the effect of size on PC formation and therefore, numerous studies on a wide variety of NMs have been performed. For example, Dobrovolskaia et al. dedicated efforts to the PC study on the surface of citrate-capped gold nanoparticles incubated in human plasma.[41] In this publication, they examined NPs of 30 and 50 nm diameter size and discovered that more proteins were adsorbed on the smaller NPs. A similar study on silica nanoparticles (SiNPs) was carried out by

Tenzer and co-workers, where they incubated SiNPs of different sizes in blood plasma.[37] Their results showed that NP size has a drastic effect on the binding of almost 40% of the proteins adsorbed on their surface, meaning that has a strong influence on PC composition. Co-polymeric NPs interactions with proteins have also been investigated. In particular, Lundqvist et al. focused on the study of PC on polystyrene NPs of 50 and 100 nm diameter upon exposure to human plasma.[42] In agreement with previous investigations, results indicated that NPs size plays an important role on protein adsorption, modifying the binding constants of the proteins and leading to a different corona composition.

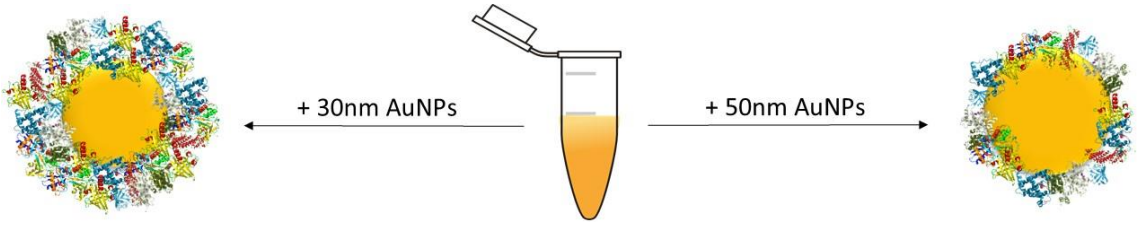

Figure 5: Visual representation of the results obtained by Dobrovolskaia et al.[41] in their study of the size effect on protein corona formation. Smaller nanoparticles display a thicker protein corona.

The way the NPs interact with the proteins present within bio-fluids is also affected by the shape of the NP.[21] For example, anisotropic nanostructures are believed to be more likely to interact with other anisotropic molecules such as deoxyribonucleic acid (DNA).[43] Consequently, it is expected that NP shape exerts an impact on PC formation. As it is widely known, synthetic procedures have been developed and optimized during the last decades and it is currently possible to produce certain NPs on various shapes in a reproducible manner.[44, 45] However, it is important to highlight the low number of publications related to PC dependence on NP morphology with a detailed characterization of its composition. Deng and co-workers investigated corona formation on titanium oxide NPs of different morphologies: nanospheres (NSs), nanorods (NRs) and nanotubes (NTs).[46] Authors found out that certain proteins were present just for the spherical NPs, which would suggest an influence of the shape over protein binding affinity. Similarly, Ma et al. investigated mesoporous SiNPs of spherical and rod-like morphology incubated in single protein solutions.[47] Results showed how these proteins

- human serum albumin (HSA), fibrinogen and globulin - suffered conformational modifications derived from the different NP shape.

Functionalization of the NP surface is a very common strategy for controlling their interactions with proteins. Commonly perceived as a problem because of the way it affects and modifies the bioidentity of the material, PC has been trying to be prevented or minimized by surface modification of the NPs.[18] This strategy aims to confer a "stealth" character to the NM, which also helps to elude immediate opsonisation by immune cells once within the bloodstream. Among the great variety of molecules available for surface modification, zwitterionic polymers[48] and others such as polyethylene glycol[49] have demonstrated to be interesting alternatives. These coatings are able to reduce the amount of proteins adsorbed on the nanoparticle surface, though not to completely avoid protein interactions. In fact, it has been reported by Schöttler et al. that a certain degree of protein adsorption is needed for this "stealth" effect.[50] In this particular publication, authors modified the surface of polystyrene NPs with polyethyleneglycol (PEG) and polyethylethylenephosphate and exposed them to plasma proteins. Results showed that the presence of these polymers could be used to minimize the PC formed around these NPs and to modulate the amount of protein adsorbed. Moreover, this "stealth" property seemed to be related with the abundance of a specific protein, clusterin, within the corona.[51] In addition, it is possible to further manipulate protein adsorption by modifying length and density of the coating. Furthermore, some scientific groups have also pre-coated NPs with protein solutions to observe changes on the behaviour of the material when interacting with biomolecules.[52]

Surface charge is another crucial factor that could have an impact in NP-protein interactions.[21] Positively charged NPs are known to be rapidly recognized by opsonins leading to their elimination from the body and later accumulation in liver and spleen.[53] In order to prevent opsonisation, NPs are usually functionalized with a negatively charged molecule or polymer to display a zeta potential (ZP) value of around -30 - -50 mV.[54] PC studies on positive, neutral and negatively charged AuNPs were performed by Lundqvist et al.,[42] leading to the conclusion that surface charge is a fundamental factor for protein adsorption. Authors discovered that neutral NPs seem to adsorb a smaller amount of proteins and of a lower variety in comparison with their charged

counterparts. Similar comparison was performed by Kah et al.[55] on the surface of rod-like AuNPs.

Summarizing, understanding of relationship between the PC and the NP physico-chemical characteristics is fundamental to be able to partially predict the interactions of a NM upon contact with the physiological environment. Other parameters such as NP composition and nature, hydrophobicity and hydrophilicity must also be considered in order to adequately define corona formation on NMs.

3.2.2. Selection of Biological Media.

In addition to the NP properties, the choice of the physiological milieu is a critical factor that plays a major role on the composition of the PC. The impact of the use of different biological fluids for incubation of NPs and evaluation of protein-NP interaction has been reported by several research groups.[56] One of the first studies focused on this issue was carried out by Maiorano and co-workers.[57] In 2010, they performed a study of the corona formed on the surface citrate-stabilized AuNPs incubated in two different cell culture mediums: Dubelcco Modified Eagle's Medium (DMEM) and Roswell Park Memorial Institute (RPMI). Both media were supplemented with Fetal Bovine Serum (FBS). After examination by several techniques such as Dynamic Light Scattering (DLS) or UV-Visible spectroscopy, it was concluded that, while the corona formed with DMEM seems to evolve and stabilize with time, RPMI corona presented different protein-NP dynamics and leads to a reduced and unstable PC. Interestingly, it was observed that the abundance of the proteins within the corona did not correspond to the amount of proteins on the incubation media, which has been explained by taking into account the different binding constants involved in protein-NP interactions.

Although Maiorano et al.[57] carried out a very complete study, they did not consider the dynamic character of the cell media, which is affected by the biomolecules secreted by the cells in a process known as "cell conditioning". Albanese et al.[58] decided to investigate on the influence of this phenomenon on PC formation and composition. For this purpose, they incubated AuNPs of different size using several cell lines and cell culture media. Authors found out that "cell conditioning" seems to produce NP aggregation together with changes in PC composition, which are dependent on NP

diameter, surface chemistry and cell phenotype. These results indicated that the dynamic nature of the cellular environment must be bear in mind when performing this type of experiments as they can alter the properties of the corona. It is important to highlight that these results must be carefully interpreted as NPs underwent aggregation and lose colloidal stability upon incubation.

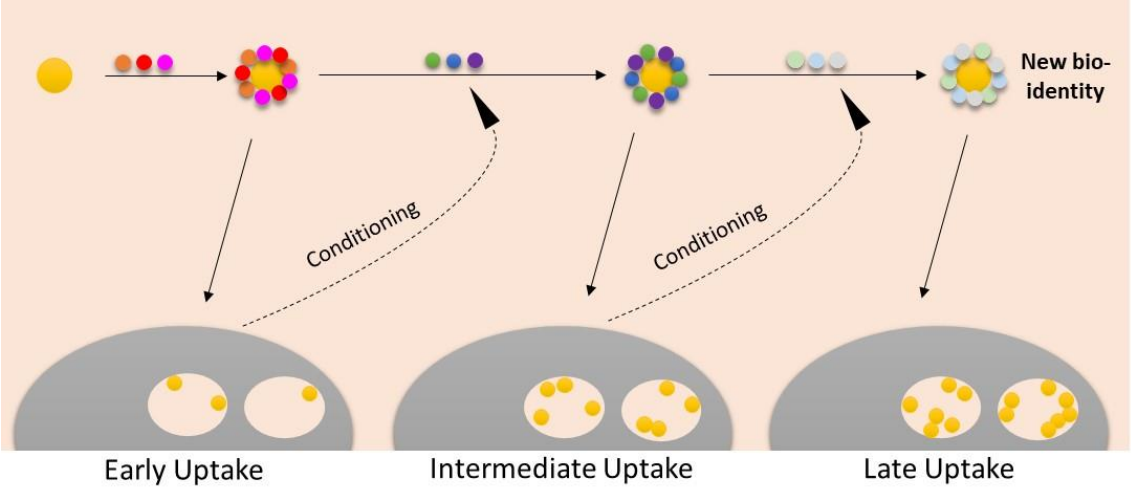

Figure 6: Graphic representation of the effect of cell "conditioning"[58] on protein corona.

Apart from cell culture media, serum and plasma have also been widely used on PC investigations.[57, 59, 60] The main difference between these two physiological medias is that, while plasma is the liquid cell-free part of the blood treated with anticoagulants, serum is the liquid part of blood after coagulation and thus, does not contain clotting factors. In a recent report by Mirshafiee et al.,[61] they presented a comparative study of PC formation on human serum *vs.* human plasma. Significant differences in the amount of protein adsorbed to the surface were observed, revealing that NPs exposed to human plasma exhibited a larger amount than those exposed to human serum. As expected, some differences were reported for PC composition, where a higher fraction of complement proteins and coagulation factors were observed for NPs incubated in human plasma. Another interesting study performed by Solorio-Rodríguez and co-workers[62] focused on the comparison of the corona formed on the surface of SiNPs functionalized with PEG and transferrin after incubation in mouse and human plasma. Once again, significant differences were observed on the composition of the PCs. This study is particularly important as it states that clinical trials performed in animal models

could not be directly translated to clinical use and difference on PC data must be taken into consideration.

As NPs are being proposed for the treatment of many different diseases, they are expected to interact with other physiological fluids apart from blood. Although there are not numerous examples in the literature, some publications have reported studies on PC formation on other biofluids such as lymph, vitreous humour or lining fluids from the respiratory tract.[63-65] Unsurprisingly, PC composition varies depending on the incubation biofluid, which indicates again the importance of the choice of biological milieu for investigation purposes. Finally, it is worth mentioning that researchers have found that changes from one biofluid to another also disturbs the PC, as it is the case of a NP that crosses the blood brain barrier (BBB).[66]

3.2.3. Experimental Conditions.

Although NP properties and incubation media are fundamental for investigation of the phenomenon of PC, the experimental conditions must as well be taken into consideration.[56] A wide variety of parameters such as temperature, exposure time, dynamic/static conditions, plasma/NP concentration or administration route may also have an effect on protein-NP interactions.

In a publication of 2010, Casals and co-workers explored the influence of exposure time on PC formation.[31] Authors incubated citrate-capped gold nanospheres (AuNSs) of different sizes in cell culture media containing 10% of FBS. For this *in vitro* study, several techniques such as DLS, ZP measurements, UV-Visible spectroscopy and Transmission Electron Microscopy (TEM) were utilized to monitor the time evolution of the PC and to characterize the NP-corona complex at every stage of the process. Extraordinarily, results suggested that the corona evolved from a loosely attached transient complex to an irreversible structure. Similarly, Dell' Orco et al.[67] developed a dynamic model to simulate PC formation on NPs surface upon contact with body fluids. Authors proposed this model for the prediction of time evolution and equilibrium composition of the corona based on stoichiometry, rate and affinity constants. The parameters of this model could be easily modified depending on the simulation that needed to be performed.

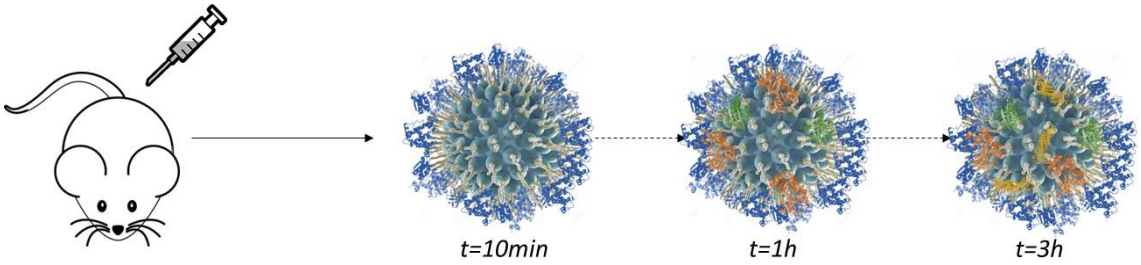

Figure 7: Graphic representation of the time evolution of the protein corona composition after injection in mice, study carried out by Hadjidemetriou et al.[32]

Time evolution of the corona formed onto SiNPs has been investigated by Pisani and co-workers.[68] In this work, authors combined Mass Spectrometry (MS) and computational biology in order to understand the growth of PC around the NP and to define what they called the "interactome", which would refer to the interactions among the proteins of the corona. Finally, a recent study by Hadjidemetriou et al.[32] allowed the study of the *in vivo* PC evolution for the first time. Lipid nano-vesicles were injected on mice and later recovered at different time points by cardiac puncture. A combination of size exclusion chromatography (SEC) and membrane ultrafiltration was utilized to separate the NP-corona complexes from unbound proteins. Analysis by MS revealed that a complex PC was formed as soon as 10 min post-injection. Even though the total amount of protein adsorbed was not significantly different, authors found out that the composition of the corona and the abundance of several proteins fluctuated over time, which indicated a high dynamic character of the PC.

Another important factor that must be taken into consideration is the temperature of the experiment. As it is well-known, body temperature varies depending on the part of the body and its activity. In addition, intracellular temperature is not always constant either. Consequently, it is necessary to get a deeper understanding of the relationship between PC formation and temperature.[21] Surprisingly, there are few publications regarding this matter. As an example, the investigation carried out by Mahmoudi et al.,[69] where they incubated inorganic NPs on a FBS solution. NPs where incubated on a wide range of temperatures, from 5 to 45 °C. Results indicated that, though changes in the temperature may significantly modify PC formation and composition, this is not always the case. In many occasions, NMs are heated in order to perform their task within the body. This is the case, for example, of plasmonic NPs. In order to determine if

plasmonic heating by laser activation influences PC formation and composition, Mahmoudi and co-workers incubated gold nanorods (AuNRs) in FBS solutions and heat them up through plasmonic and traditional thermal heating.[70] Results revealed significant changes on the PC composition formed around low aspect ratio AuNRs. This study highlights the importance of the temperatures at which NPs are exposed and how they can strongly affect their interaction with other molecules.

Time of exposure and temperature are just a couple of examples of environmental parameters that can affect protein-NP interactions.[56] For example, administration route is expected to play a fundamental role on PC formation and composition. Although not yet investigated, different administration routes can be translated into contact with group of molecules and biological entities that will interact and modify the properties of the NM. In addition, plasma concentration as well as NP concentration are expected to affect qualitatively and quantitatively to the PC. Dynamic or static conditions must also be considered as injected NPs and proteins are likely to interact in a different way under flow conditions.

3.2.4. *In Vitro* vs. *In Vivo* Protein Corona.

Nowadays, it is widely accepted that NPs interact with proteins upon contact with physiological fluids leading to PC formation. This multi-layered structure that forms onto the NP surface is known to be able to modify the initial characteristics of NPs giving them a new bioidentity and, consequently, modifying their behaviour, fate and performance.[22] Although PC phenomenon has been intensively studied under *in vitro* conditions, this approximation is likely to differ from the *in vivo* situation due to the strong differences in the experimental conditions between both strategies. In a recent study reported by Palchetti et al.[71], PC formed on liposomes injected into circulating FBS was studied taken as a reference the PC formed under *in vitro* conditions. The main objective of the project was to assess the effect of the shear stress produced by the flow on PC formation. Results indicated that corona composition was significantly influenced by the dynamic flow and, therefore, the PC formed under *in vitro* conditions would considerably differ from its *in vivo* counterpart.

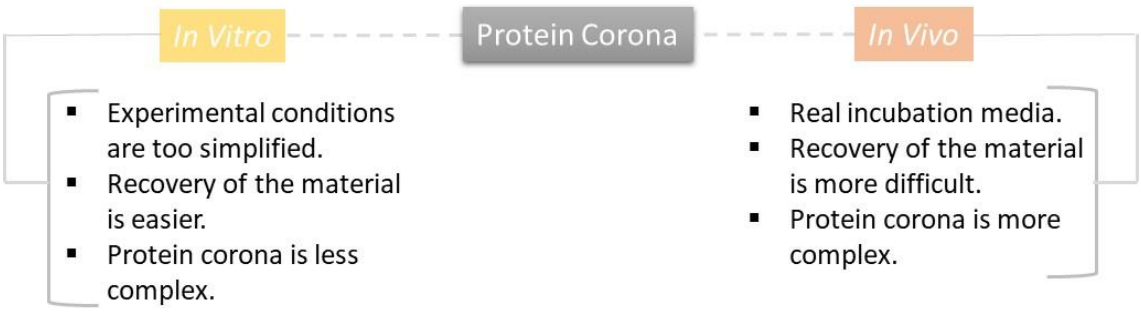

Figure 8: Scheme of the main differences when studying the in vitro and in vivo protein corona.

Up to date, very few studies on the *in vivo* corona of NMs have been performed. Sakulkhu and co-workers[72] were the first ones to present a full characterization of the PC composition formed on the surface of NPs, superparamagnetic iron oxide nanoparticles (SPIONs), under realistic conditions. In this study, NPs were injected in the bloodstream of rats and later recovered by using strong magnets. PC formed after incubation in rat serum were used as reference. Results showed significant differences in corona composition meaning that dynamic conditions strongly influence protein-NP interactions. Similarly, Hadjidemetriou et al.[73] reported an investigation on the *in vivo* PC formed on the surface of liposomes. In this case, NPs were administered to mice through tail vein injection. NPs were recovered by cardiac puncture and a strategy combining SEC and membrane ultrafiltration was used for isolation of the corona-NP complex from unbound proteins. Comparative of *in vitro* and *in vivo* PC composition was carried out by MS, which revealed a wider variety of adsorbed proteins after injection in mice. Authors found out that *in vitro* conditions are far from adequately mimicking the high complexity of the physiological environment and therefore, they cannot be used for prediction of the *in vivo* PC.

In summary, it is important to keep in mind the limitations of the use of data from *in vitro* studies for the prediction of the realistic conditions. Further investigations are needed in order to get a deeper insight of this phenomena and the parameters involved before translation of any NM into clinical trials.

3.3. Protein Corona Influence on other Processes.

PC is known to modify the bioidentity of the initially administered NM, changing its physico-chemical properties and therefore, playing a major role on its interactions with biological entities. As a consequence, several research groups have dedicated plenty of efforts to the investigation of the impact of PC formation on many different processes such as cellular uptake, cytotoxicity, proliferation, targeting capability, drug release or protein fibrillation, among many others.[26, 74, 75] During the next paragraphs, illustrative examples will be given and explained.

3.3.1. Cellular Adhesion and Uptake.

Among the wide variety of cellular processes that can be investigated, scientist have specially emphasized on cellular uptake or cellular internalization of NMs. Remarkably, PC has been reported to decrease but also to increase cellular internalization depending on the NM characteristics, previous corona coating and cell type.[26] In general, many investigations report that NP characteristics play a major role in PC formation, leading to a different cellular interaction. In the majority of the studies, PC has been reported to hinder NP adhesion to the cell membrane, decreasing this way the cellular uptake of the NM.[76] Lesniak and co-workers investigated in the process of cell adhesion in the presence and absence of corona.[77] Cells were exposed to bare and corona coated-SiNPs under very specific conditions. As it is quite difficult to separate the internalization process from the initial adhesion to the material to the cell membrane, cells were incubated at 4 °C in order to shut down other active processes such as cellular uptake. PC is known to be formed around the surface of the NPs to reduce the free energy that the bare NP displays. Results show that, the higher the free energy, the higher the protein adsorption and hence, the lower the adhesion to the cell membrane, as the proteins hinder the interaction between the NPs and the cells.

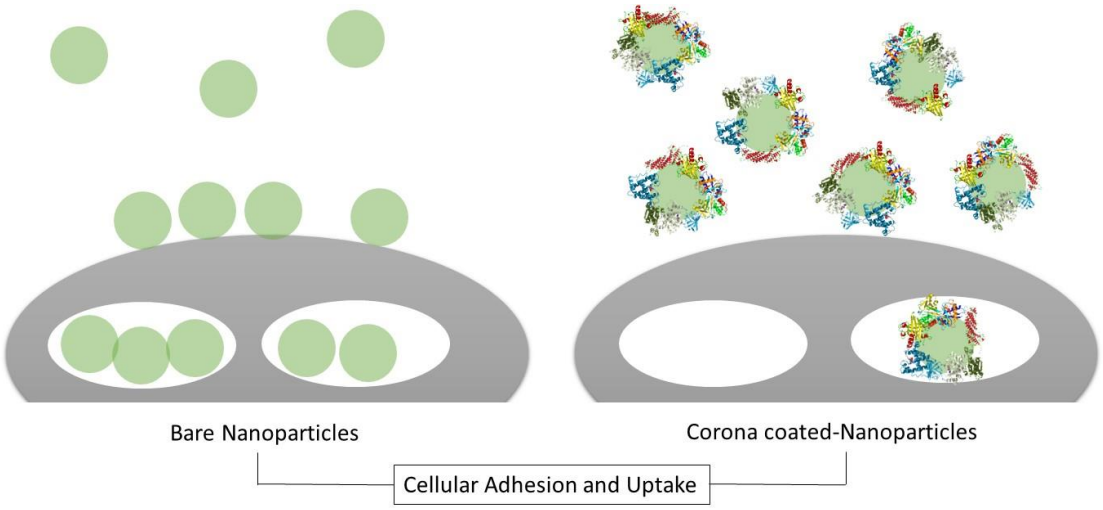

Figure 9: Visual representation of the influence of PC on NP cell adhesion and cell uptake.

Effect of the functionalization on cell internalization has also been investigated. In particular, Pelaz et al.[78] presented a study on PEGylated metallic NPs and their interaction with single protein solutions containing HSA and fibrinogen. As the NPs were fluorescently labelled, the thickness of the corona and evolution over time was monitored by FCS. Coronated and bare-NPs were then exposed to cells and a cell uptake study was performed. Authors found out that PEGylation seemed to reduce cellular internalization in agreement with previous studies in the matter. Together with other similar investigations for NMs of different nature, results concluded that cellular uptake is a process highly dependent on physico-chemical characteristic of the NM, being functionalization the one which influences it the most. In any case, protein adsorption on NP surface generally results in a decrease of NP uptake.

To address the problem of a low cellular uptake of the NPs, scientists decided to use an alternative strategy based on the control and manipulation of the proteins present in the corona. This approach was first used by Mirshafiee et al.[52], where they demonstrated that a pre-coating constituted by gamma proteins produced a corona rich in opsonins. Although this strategy proved to be useful for active targeting, it was still unsuccessful for increasing cellular uptake. Authors concluded that an adequate manipulation of the corona may give possibilities for a different outcome for biological interactions of cells and NPs, though much work must be invested for being able to reach this point of control over the phenomenon of PC.

3.3.2. Toxicity.

Another highly relevant parameter that must be investigated is the toxicity of the material when interacting with biological entities. This issue has been one of the most widely studied regarding NMs for biomedical applications, as the administered nanomedicine must be biocompatible and cause minimal secondary effects to the patient.[79] Consequently, evaluation of the toxicity of many different type of NMs has been intensively carried out during the last decades. Several studies have demonstrated that NP-PC can also influence their toxicity and pathophysiology.

NP toxicity is highly dependent on the surface characteristics, especially on the surface charge. It is widely known that positively charged NPs exhibit a quite high toxicity as they perturb the continuity of the cell membrane,[80] leading to destruction of the barrier followed by cell death. Functionalization of the NP with a wide variety of polymers and molecules has been used as an alternative approach to protect the surface of the cells and increase the biocompatibility of NMs.[81, 82] PEG is one of the most known examples of this strategy and it has been demonstrated that it helps to modify the toxicity profile of several NMs.[19, 49] Protein adsorption is known to further modify the NP physico-chemical characteristics, including the ZP, and therefore, is expected to have an additional effect on the toxicity of NMs.

One way of negatively affecting the physiological environment is by irreversibly modifying the structure of proteins, which consequently influences their ability to change their conformation and perform their biological functions.[39] Several researchers have reported changes on the structure of certain proteins after their interaction with NPs. For example, AuNPs are widely known for playing an important role on fibrillation after stabilizing or destabilizing a specific conformation of certain proteins.[76] Depending on the morphological characteristics of the NP such as size or shape, formation of fibrils can be stopped or induced, which is highly relevant for diseases like Alzheimer's or Parkinson's. In a recent publication by Mirshadegi et al.[83], authors investigated the effect of PC on the fibrillation process by using AuNPs of different shapes. Authors discovered that protein source and concentration are key factors on the PC formed and, consequently, strongly influence the fibrillation process.

Apart from changing the structure of certain proteins, the PC as a whole has been proven to be able to reduce the toxicity of certain NMs and therefore, increase their safety.[26] This was demonstrated for carbon nanotubes (CNTs), a very interesting material that has been extensively proposed for biomedical purposes. This type of NM is known to present a medium-high level of toxicity unless adequately functionalized. Remarkably, De Paoli al.[84] performed a study on toxicity of bare and corona-coated-CNTs on cells. Results showed cytotoxicity was reduced in the case of corona-coated CNTs after exposure to two different cell lines. Ge et al.[85] had also shown comparable results for CNTs by experimental and theoretical means. A similar outcome was observed by Tenzer et al.[86] for SiNPs, where the haemolytic effect of the NPs was reduced by the PC, which protected the cells. As mentioned before, positively charged NPs usually exhibit cytotoxicity due to the disruption of the cell barrier.[80] The role of protection of the PC on this type of NPs was demonstrated by the group of Dawson for polystyrene NPs.[82] Lastly, PC has also been shown to inhibit the generation of radical oxygen species.[87]

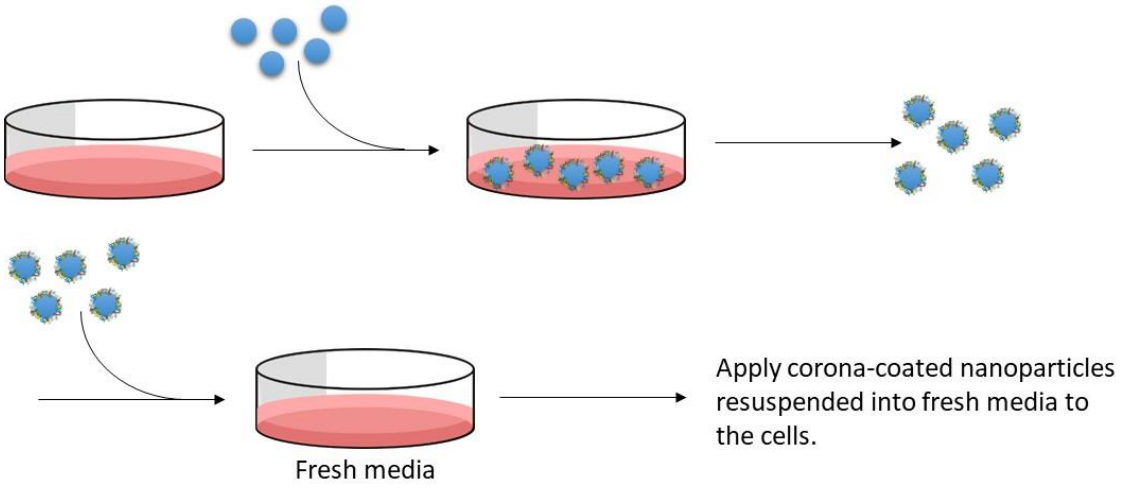

Figure 10: Scheme of an alternative way of performing toxicological assays. Bare-NPs are immersed in media until corona formation, then resuspended in fresh media to be finally added to the cells.

It must be considered that many of these studies have been performed by using toxicological assays originally designed for molecules. This means that these protocol may be not adequate to assess the toxicity of the variety of NMs designed up to now. New strategies and protocols are being developed for the determination of an accurate toxicological profile of NMs.[26]

3.3.3. Targeting Ability.

NMs for biomedical applications are usually designed for active targeting, that is to say, they are specifically functionalized to target a concrete organ of part of the body where the treatment needs to be given.[26] However, the physico-chemical characteristics of the designed NP are modified after interaction with the biological fluids.[22]

Salvati and co-workers were the first group to investigate how PC influences the targeting capability of NMs.[88] In their publication, they showed how transferrin-functionalized SiNPs lose their targeting properties after interaction with proteins. This could be explained by the attachment of proteins on the transferrin preventing the interaction with its binding sites. Another study by Mirsadeghi et al.[83] on AuNPs gave similar results, PC was observed to significantly reduce active targeting of the incubated NM. Although results of other similar studies are in agreement with the previous statements, it must also be considered the investigation of Dai et al.[89] on core-shell NPs, where targeted ability is not significantly affected.

Summarizing, even though in general it is expected that targeting will be reduced by protein adsorption, this does not have to be the case and investigation for different types of NMs must be performed in order to adequately assess their limitations. Targeting disruption will eventually lead to a different biodistribution and fate within the body and hence, it is important to understand it before clinical translation. Nowadays, strategies are being developed towards the use of the PC for targeted drug delivery.[90]

3.3.4. Others.

Cellular uptake, toxicity and targeting are just a few examples of the processes influenced by the new bioidentity conferred to the NPs once exposed to the biological media and interaction with proteins. PC has been shown to have an impact on many other processes such as immune response, drug release, bacterial properties and many others.[26] These studies are a proof of the fundamental character of the corona on biological processes and nanomedicine performance.

3.4. Protein Corona for Biomarker Discovery.

Although PC formation is usually seen as a problem, as it modifies the initial characteristics of the designed NM, some research groups have decided to take advantage of this phenomenon. Apart from using the process itself to increase the drug loading capacity of nanocarriers for biomedical applications, it has been proposed as an alternative tool for biomarker discovery.[91-93]

A biomarker is usually described as a measurable indicator of changes in the biological process and therefore, they are currently use for disease detection. As PC composition is affected by the choice of physiological media, it is expected to observe significant changes in the presence of a biofluid from a patient suffering a disease.[91, 92] The first comparative of PCs formed in plasma from different diseases was performed by Hajipour et al.[94] In this publication, authors incubated polystyrene and silica NPs in plasma from human subjects with different medical conditions: pregnancy, common cold, smoking, diabetes, haemophilia, thalassemia, fauvism, hypercholesterolemia, hypofibrinogenemia, rheumatism and breast cancer. Results showed significant differences on PC composition as a function of the disease. In addition, they introduced the term "personalized protein corona" as a determinant factor in nanomedicine. Several similar investigations have been carried out by other groups to detect the differences among PCs as a function of the disease.[95, 96]

A recent work by Hadjidemetriou and co-workers propose the use of the *in vivo* corona for biomarker discovery.[97] Authors administered lipid-based NPs into mice bearing two different tumour models: subcutaneous melanoma (B16-F10) and human lung carcinoma xenograft (A549). A comprehensive quantitative and qualitative analysis of the coronas was performed by MS. Results demonstrate the advantages of the *in vivo* PC over its *in vitro* counterpart, as the corona formed after injection in mice exhibits a wider range of proteins that could not be detected by incubation in plasma.

Lastly, it is important to mention that the first study on human *in vivo* PC was recently carried out by Kostarelos group.[98] In this scientific publication, authors report the analysis of the human *in vivo* PC onto liposome surfaces after administration of Caelyx

(PEGylated doxorubicin-encapsulated liposomes). Authors showed the potential of using PC for detection of biomarkers in humans.

4. Gold Nanoparticles.

Development and advances of many characterization techniques as well as numerous efforts invested in the understanding of the materials at the nanoscale resulted in the design and production of a wide range of NMs for biomedical applications.[14] Among these endless options, AuNPs have become a very interesting option owing to their optical and thermal properties, given by its plasmonic nature and the so-called "localized surface plasmon resonance" (LSPR) phenomenon.[99] Owing to their amazing optical and thermal properties, gold nanostructures have been proposed for biomedical applications and have demonstrated their great potential as they reached clinical trials. More information and examples will be given in the following paragraphs.

4.1. Localized Surface Plasmon Resonance.

Interactions between light and a metallic surface can result in the formation of hybrid surface waves as a consequence of the light waves coupling with the free electrons of the metallic surface.[100, 101] This phenomenon is widely known as "surface plasmon resonance" (SPR). One of the most important features of these surface plasmons is the ability to trap or confine the light at the metal-dielectric interface, which gives rise to a collective oscillation of electrons at the surface of the material. Confined light can either propagate or localize as a function of the dimensions of the NM.[102, 103]

In particular, in the case of AuNPs being illuminated at an adequate wavelength, electrons of the metallic surface will oscillate and be confined in what is known as LSPR. Differently from propagating plasmons that can be found on the interface between planar surfaces and a dielectric material, electron plasma on metallic NPs is confined into a finite volume. [101] As it is well-known, AuNPs present an absorption band in the electromagnetic spectrum, which occurs when the incident photon frequency is in resonance with oscillating electrons, conferring AuNPs unique properties.[104] AuNPs have been used during centuries for decorative purposes on stained glass. However, the explanation and rationale about the optical properties of these materials was not

provided until Michael Faraday synthesized the first pure colloidal gold sample in 1851 and published a paper regarding its behaviour and interactions with light in 1857.[105] Later in 1908, Gustav Mie and Clark Maxwell joint efforts resulted in a quantitative description of the phenomenon for spherical AuNPs.[106, 107] According to Mie studies, the total extinction cross-section consists of scattering and absorption that is given by the summation of electric and magnetic oscillations. The contribution of both, absorption and scattering, directly depends on the morphology and size of the NP.

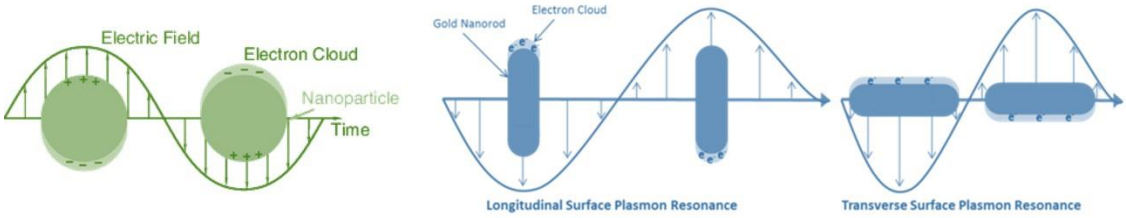

Figure 11: LSPRs for spherical and rod-like gold nanoparticles.[103]

The most important feature of LSPR is the fact that it can be tuned by modifying the structure of the NP.[102, 103] To control this parameter, it is necessary to understand that LSPR directly depends on the frequency of oscillation of the electron on the surface of the metallic NP. At the same time, oscillations frequencies are determined by main four parameters: electron density, effective mass of the electron and size and shape distribution of the charge.[104] This means that, by manipulating size and shape of the NP, the plasmon will also change, which is translated in a modification on the position of the LSPR band, the extinction cross-section and the scattering/absorption ratio. In addition, it is also possible to tune the optical properties by functionalization with photo- or electroactive molecules.[108]

To illustrate the change in the absorption band as a result of the modification of the NP size, the example of AuNSs will be explained. For AuNSs, UV-Visible spectroscopy shows a single absorption band in the spectrum. This is due to the isotropic morphology of the NM, which gives rise to a specific oscillation of electrons and therefore, to a single plasmon band. Usually, for AuNSs of 15 nm diameter, the LSPR band is located at 514 nm.[109] When the size of the NP increases, a bathochromic shift in the wavelength is produced, attributed to electromagnetic retardation for larger NPs.[110] On the contrary, when the NP diameter decreases down to 3 nm, a drop of the intensity of the peak is

observed, explained by quantum size effects. NP of a diameter below 2 nm do not display a plasmon anymore, as there is no space for the surface plasmon to occur.[111]

AuNRs will be utilized as an example to illustrate the influence of the shape on the LSPR band. Among the anisotropic gold nanostructures, AuNRs have specially attracted the attention of the scientific community due to their potential use within the biological window frame and as interconnectors in devices at the nanoscale.[112] UV-Visible spectra of AuNRs show two absorption bands due to the anisotropy of the NP. Shape dependence of the plasmon resonance for ellipsoid nanostructures was already predicted back in 1912 by Gans,[113] who extended the theoretical approach developed by Mie for explaining the plasmonic nature of spherical NPs. In this case, the plasmon resonance is split into two different absorption bands, which correspond to the different orientations of the NM with respect to the polarization of the light. Development and advances on the synthetic mechanism have allowed a control over the synthesis and, consequently, the production a AuNRs of higher purity and in a wide range of aspect ratios (ARs). By changing the ratio between length and width of the rod (AR), the LSPR wavelengths can be tuned.[114-116]

Another consequence derived from the LSPR is the large enhancement of the electromagnetic field, which correlated with the NP shape. Due to this enhanced field, a molecule in the vicinity of the LSPR sees a light intensity stronger than the incident light.[117] This phenomenon is used for the study of interactions at the molecular level, e. g. through the Surface Enhanced Raman Spectroscopy (SERS) technique. Gold nanostars (AuNSts) are especially relevant for sensing applications as they display a high sensitivity to small changes within the dielectric environment.[118] Thanks to their sharp edges and tips, they also provide a particularly high enhancement of the electric field around the NPs. AuNPs assemblies have been designed as well to take advantage of the spaces between them and their application for biosensing.

4.2. Colloidal Gold – Synthesis.

Described as a suspension of AuNPs in a fluid, colloidal gold has been present and used for a very long time. The most widely known example of colloidal gold in history is the

so-called Lycurgus Cup.[119] Produced around the 4th century, this object is a well-known representation of the use of colloidal gold for glass staining. The presence of very small gold particles leads to a beautiful change of colour of the glass depending on the location of the light source. Apart from its uses for decorative purposes, colloidal gold has also been believed to display curative properties and hence, it has been proposed and utilized for medical use for a long time. The first book on colloidal gold preserved to our days and dedicate to the application of colloidal gold for medical purposes was published in 1618 by the philosopher and doctor of medicine Francisco Antonii.[120]

Nevertheless, a proper scientific approach to investigate and describe the properties of colloidal gold did not begin until the 1850s. During this decade, English chemist Michael Faraday was investigating the properties of light and matter and their interactions. It was on 1857 when, accidentally, Faraday synthesized the first examples of metallic colloids, while mounting thin sheets of gold leaf onto microscope slides. Faraday observed a faint red colour in the solution after washing the gold slides, and decided to save these solutions for further examination. One day, he illuminated the mentioned solution and observed a cone of ruby colour appeared. He then realized that this effect should be due to the presence of gold particles of a very small size.[105] These first examples of pure colloidal gold were obtained by using phosphorous to reduce the gold salt present on a solution of gold chloride.

Despite these important realizations, limitations of the techniques available at the time prevented a significant advance on the study of AuNPs until the 2000s. Development and improvement of several techniques such as electron microscopy[3] or atomic force microscopy[4, 5] among many others allowed a detailed characterization and description of the physical and chemical properties of NPs present in the solution. As a result, it became clear that the colour from the solution was indeed due to the presence of gold particles of nanometre size of different sizes and shapes.[105] Further studies revealed that the colour was originated from the oscillations of free electrons at the surface of metallic NPs when illuminated at an adequate wavelength, a phenomenon known as LSPR.[106, 107]

It is widely recognized that NPs present a whole new field of possibilities and properties for many different applications in any field we could think of, from technology and

medicine to environment.[8, 12] Amongst the myriad of NMs that have been discovered, designed and studied, AuNPs have received a great amount of interest from the scientific community due to their amazing optical and thermal properties.[101] As a result, numerous research groups have devoted their efforts to develop a convenient, simple and safe methodology for AuNP synthesis.[44, 121] Thanks to them, protocols are available nowadays for the production of highly monodisperse and stable NPs of different size and shape. However, the mechanism of many of these reactions is yet not fully understood and therefore, studies are still ongoing in this regard. More detailed information about the synthesis of AuNPs utilized for the studies described on this document and their corresponding mechanisms will be described in the following paragraphs.

4.3. Biomedical Applications of Gold Nanoparticles.

As previously mentioned, AuNPs display quite interesting optical and thermal properties and, consequently, have been proposed for a wide variety of biomedical applications.[99, 122] Some examples of AuNPs designed for drug delivery, biosensing, biomedical imaging, disease treatment and well as biofunctional complexes will be given in the next paragraphs.

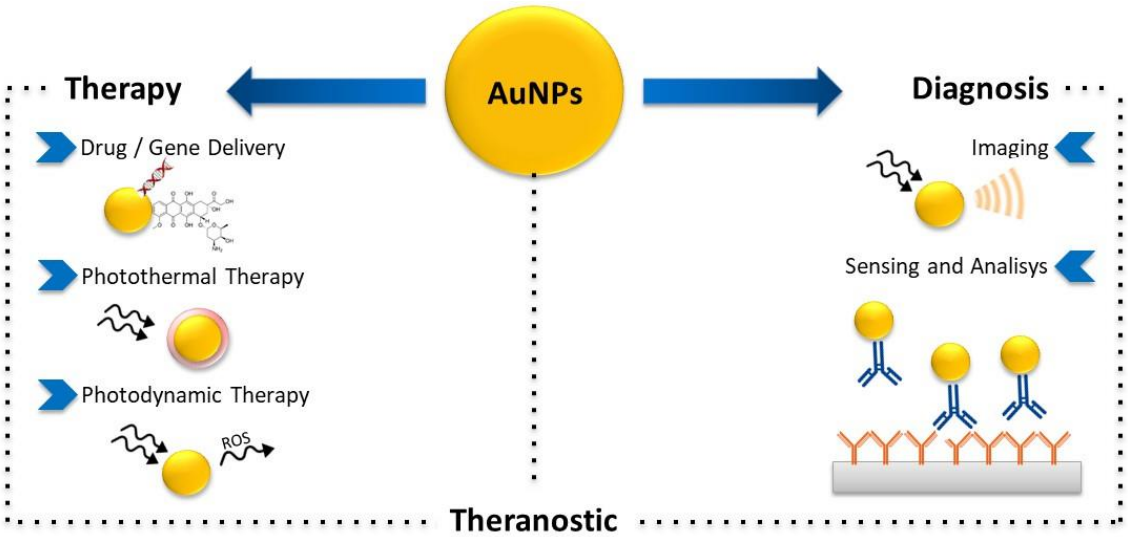

Figure 12: Scheme of the biomedical applications of AuNPs.

4.3.1. Drug Delivery.

When designing nanostructures for drug delivery and therapeutics, it is fundamental to enhance the bioavailability of the drug at the target site, extend the circulation period within the body, control drug release and minimize possible side effects.[10] AuNPs can be engineered in many different ways to fulfill these requirements. Controlling the NP size and shape as well as adequately functionalizing the material are key for creating a useful nanomedicine.[121, 123]

Regarding drug delivery, it is necessary to determine if the nanosystem will work by passive or active targeting. For passive tumour treatments, scientists usually take advantage of their leaky vasculature and their enhanced permeation and retention (EPR) effect, which allows the accumulation of small nanocarriers within the tumour tissue.[124, 125] Of course, the nanocarrier must be adequately functionalized to ensure enough circulation time and avoid immediate opsonisation. In the case of active targeting, NP surface is modified with specific molecules with high affinity towards a specific organ or part of the body, also known as targeting ligands.[126-128] As a result, the specificity of the drug delivery is increased. In general, it is widely accepted that nanocarriers up to 100 nm diameter are the most useful for biomedical applications.[129] Apart of being nano-sized and therefore, able to interact with many bioentities within the physiological fluids, they can also get involved in cellular processes. AuNPs have advantages as, thanks to their optical properties, they can be detected and used for tracking their pathway.

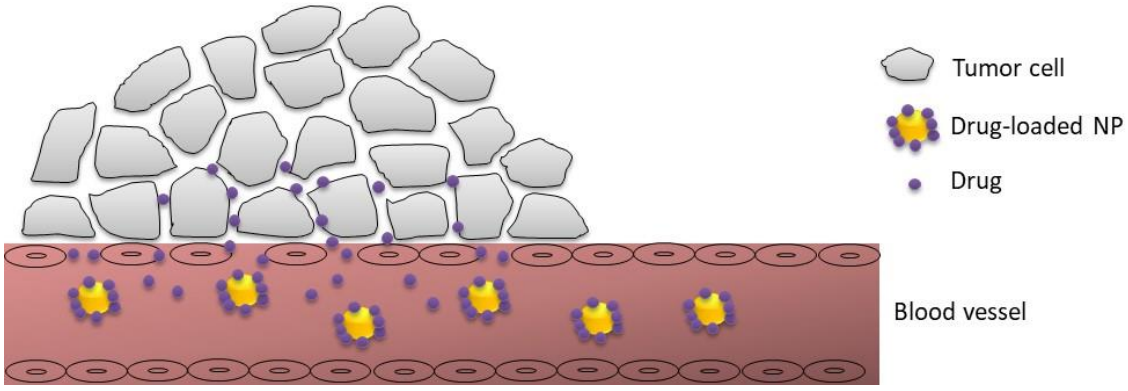

Figure 13: Schematic representation of the use of nanocarriers for drug delivery.

There are several ways to release the content of the carrier, usually by internal or external stimuli such as light, heat or pH change. There are plenty of examples on the

literature of gold-based nanosystems for drug delivery.[10] For instance, Li et al. designed a system composed by PEGylated nanoshells loaded with doxorubicin, a FDA approved drug, for cancer treatment.[130] They used irradiation at the near-infrared (NIR) laser light to induce drug release. Combined action of photo- and chemotherapy allowed an improved performance against the cancer tumour. Similarly, Gibson et al.[131] proposed another gold-based nanocarrier constituted by spherical AuNPs covalently functionalized with plaxitacel, another clinically approved drug.

It must be kept in mind that, during the last decade, AuNPs have been proposed as smart carriers that can be opened and release their content in response to a change of the environment in which they are located.[132] As an example, polymeric drug-loaded capsules containing AuNPs have been reported to take advantage of the photothermal effect for drug release. Carregal-Romero et al.[133] demonstrated that spatial-temporal drug release can be achieved by irradiation of light on the polymeric drug delivery system.

As active targeting displays a higher specificity towards a particular organ or body part, AuNPs surface has been modified with many different target ligands such as oligonucleotides, peptides or antibodies that exhibit the capability of binding a specific receptor overexpressed on the tissue of interest.[126] For instance, AuNPs have been widely functionalized with folic acid for cancer treatment. This is due to the fact that folate receptor is known to be overexpressed on tumour cells in several human cancer types such as lung, ovary, prostate or breast.[134, 135] In addition, AuNP surface has also been modified by linking tumour necrosis factor alfa (TNF-α) for targeting cancer cells.[136]

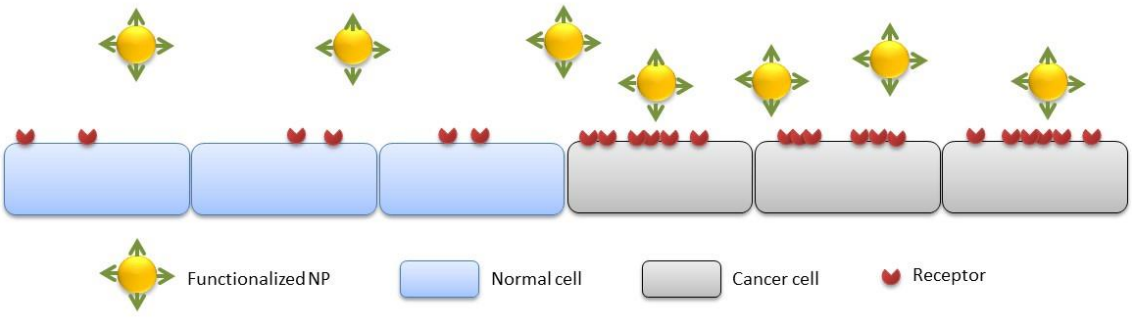

Figure 14: Schematic representation of active targeting.

This factor is highly relevant for cancer treatment as it is overexpressed in solid tumours and as a mediator of haemorrhagic tumours. Concretely, AuNPs of sizes within the 20-100 nm range functionalized with TNF-α have shown preferential accumulation in the tumour vasculature as well as reduced systemic toxicity when compared to non-targeted nanosystems.[137]

4.3.2. Therapy.

When using AuNPs as therapeutic agents, there are several approaches that can be applied depending on the properties of the NM they are based on. One of the most important and promising groups of approaches is the one that takes advantage of the light-related properties of AuNPs, which includes Photothermal Therapy (PTT), Photodynamic Therapy (PDT) and Photoimmunotherapy (PIT).[138] Several examples to illustrate the mechanism and way of action will be given in the following paragraphs.

PTT is based on the electromagnetic irradiation on photosensitive materials for the generation of local heat, which is expected to lead to the elimination or treatment of the diseased tissue. By using this therapeutic mode, it would be possible to have access to tumours with complicated locations and, ideally, it would also allow to avoid surgical interventions.[138] El Sayed et al. studied the optical properties of AuNRs in order to select the most suitable for PTT.[139] Authors found out that AuNRs of 28x8 nm were the most effective heat generators both, theoretically and experimentally. Apart from AuNRs, other gold nanostructures have been proposed and studied such as nanoshells, nanocages (NCs) or nanostars (NSts). As an example of a different shape, Chen et al.[140] reported that PEGylated AuNCs could be passively delivered and accumulated in animal tumours, causing irreversible damage after NIR laser irradiation.

Regarding PDT and PIT, both are based on the use of a photosensitizer that, after irradiation, causes the release of reactive oxygen species (ROS) and the activation of the immune response. ROS will be, in this case, the ones responsible for destroying the tissue of interest. The difference between PDT and PIT is that in PIT photosensitizers are combined with antibodies with the aim or selectively targeting the desired tissue.[138] During the last years, efforts are mainly focused on enhancing the therapeutic treatments by combining PTT and PDT. This particular combination has been reported

to show synergistic effects. For instance, Choi et al.[141] have reported the use of AuNRs-photosensitizers complexes illuminated by two different sources. While the suppression of tumour growth was 79% with PTT alone, it improved and reached a 95% when applying PTT and PDT together.

4.3.3. Diagnosis.

AuNPs display scattering and absorption of light that can be recorded by using UV-Visible spectroscopy. As mentioned before, some AuNPs exhibit these features within the range of the so-called "first biological window" (600-900 nm wavelengths).[142] In addition, they are highly photostable and present a high electronic density. Consequently, they are easily visualized by optical or optoacoustic imaging, flow cytometry and other related techniques. These characteristics make them ideal for biosensing and bioimaging applications that are usually employed for diagnostic purposes.[99, 122]

AuNPs have been extensively applied as contrast agents for optical and optoacoustic imaging as well as for dark field microscopy, two-photon luminescence microscopy, magnetic resonance imaging and X-ray computing tomography, among others.[142, 143] Juts to give an example, Park et al.[144] demonstrated that AuNPs can be used for tracking of their own pathway both, *in vitro* and *in vivo*. Also, the performance of techniques like photoacoustic tomography (PAT) or optical coherence tomography (OCT) has been reported to improve by using AuNPs as exogenous contrast agents.[145, 146] As well, AuNCs have been reported for imaging melanomas, mapping of lymph nodes and imaging of cerebral cortex in animals by applying PAT.[147, 148] Nevertheless, AuNRs are still considered as the preferred plasmonic NPs for bioimaging purposes.[149]

Apart from being very useful for biomedical imaging, countless efforts have been dedicated to AuNP application to biosensing.[122, 150] In particular, scientists have been interested on taking advantage of the change of colour of a solution of AuNPs once aggregation occurs.[151] One example of this is given by Sanromán et al.[152, 153], where they use AuNPs functionalized with DNA strands in order to detect small DNA fragments related with diseases. Upon hybridization, AuNPs aggregate and the colour of the solution changes. This process strongly depends on the concentration of DNA fragments

in the solution, which allows the detection of very small amounts. In addition, AuNPs can be also assembled for detection of biomolecules by SERS.[102]

4.3.4. Theranostics.

This relatively novel field of science is dedicated to the design and development of multifunctional nanosystems that can be used simultaneously as diagnostic and therapeutic tools, all in one. As AuNPs exhibit interesting optical and thermal properties that can be applied to both, diagnosis and therapy, they were soon proposed for this purpose.[154, 155]

Theranostic platforms based on AuNPs have already been proposed and studied in the literature. For example, Khlebtsov et al.[156] investigated silver/gold (Ag/Au) NCs core surrounded by a silica shell containing a NIR photosensitizer for cancer treatment by applying PTT and PDT simultaneously. *In vitro* studies in HeLa cells demonstrated a higher efficacy for the dual system. Another of gold-based theranostic platform was studied by Huang et al.[157], who reported silica-modified AuNRs functionalized with folic acid conjugates as a system with high selective targeting, X-ray computed tomography (X-CT) ability and enhanced PTT effects.

Theranostics has risen as a very interesting alternative or complement to conventional treatments. It benefits from the use of a single nanosystem adequately designed in order to diagnose and treat a disease, and it can also be used as monitoring tool. Although still far from reality, countless efforts are being done for the development of these type of nanomedicines.[15, 132]

4.4. Gold Nanoparticles in Clinical Trials.

Potential and relevance of AuNPs for biomedical applications are illustrated by several gold-based nanosystems that are currently under clinical trials.[158] It is important to mention that one gold-based nanosensor has already been approved by the Food and Drug Administration (FDA).[159] More information about these NMs will be given in the following paragraphs.

The first AuNP-based system approved by the FDA is the Nanosphere Verigene® System.[159] This nanostructure is constituted by AuNPs conjugated to oligonucleotides or antibodies for a higher and more sensitive detection of infectious pathogens and drug resistance markers. Nanosphere Verigene® tests are designed for targeting infections in the bloodstream, respiratory tract and gastrointestinal tract. This system has also shown a good performance for the detection of cardiovascular disease, cancer and autoimmune disease.

Regarding gold-based therapies, Aurimmune has been the first one to reach clinical trials.[160] This system is based on the use of citrate-capped AuNPs that are further functionalized with thiolated PEG and TNF-α, for stabilization and active targeting respectively. These nanosystems have demonstrated their capability to improve the targeting and toxicity within the tumour in comparison with the use of TNF-α alone. Future perspectives aim towards the combination of these gold-based systems with other approved chemotherapies for cancer treatment. Another system currently under clinical trials is AuroShell®.[161] It is based on the use of NPs with a silica core of 120 nm and a gold shell of 15 nm. This nanoplatform is utilized for a therapy called AuroLase®.[161] This therapy has been applied on clinical trials for treatment of head and neck cancer by PTT. The therapy consists on the injection of AuroShell® into the bloodstream of the patient. A waiting period between 12 to 24 hours must occur for the adequate accumulation of the NPs within the tumour. Then, NPs are irradiated with a NIR laser (808 nm) for heating and consequent destruction of the tumour tissue. The system is currently under clinical trials for patients with metastatic lung cancer. For this particular case, a systemic infusion of AuNPs is given to the patients, followed by laser irradiation by an optical fibre via bronchoscopy.

For treatment of artheroesclerotic lesions, there are two delivery techniques for AuNPs and PTT under clinical trials (NANO FIM).[162] In the first case, silica-AuNPs are delivered through a bioengineered on-artery patch. In the second one, silica-gold iron bearing NPs with targeted microbubbles or stem cells are delivered by stent implantation or magnetic navigation. After 12 months, both methods show a similar degree of regression of the lesion volume. It is worth mentioning that for this system, AuroLase® is also used.

Although some gold-based technologies have been quite developed, NP formulation still faces major challenges for clinical translation. Issues such as biodistribution modulation, heterogeneity between human and animal models, biological interplay or NP optimization need to be assessed and understood in order to improve the NP performance and its advancement towards real biomedical application.

4.5. Protein Corona on Gold Nanoparticles.

As previously shown, AuNPs have been proposed for different biomedical applications owning to their remarkable optical and thermal properties.[99, 122] However, *in vivo* evaluation of the behaviour, fate and impact of AuNPs must be investigated and understood taking into account their interaction with biomolecules and the subsequent formation of the PC.[22, 56] Numerous efforts have been dedicated to the study of PC formation on AuNPs and how it influences biological processes.[163]

Time evolution of PC formed on the surface of citrate-capped AuNPs was investigated by Casals and co-workers.[31] Authors found out that spherical AuNPs of diameters ranging between 4-40 nm present a stable corona overtime. In addition, they also reported that AuNPs functionalized with mercaptoundecanoid acid (MUA) lead to a loosely bound corona, which suggests that the stability of the corona highly depends on the coating of the NP as well as the biological media of incubation. Cui et al.[164] focused on the investigation of the influence of surface modification on NP-protein interactions. They synthesized AuNSs and modified their surfaces by using citrate, thioglyclic acid, cysteine and PEG (2 kDa and 5 kDa). NPs were incubated in single protein solutions containing Bovine Serum Albumin (BSA), transferrin and fibrinogen. Results showed the influence of using different functional groups on PC formation.

The first publication regarding size effect on corona formation on AuNPs was reported by Dobrovolskaia et al.[41] Citrate-coated AuNSs of 30 and 50 nm were synthesized and then incubated in human plasma. Results indicated that smaller NPs bind a higher mass of proteins and form a thicker corona. Similar results were reported by other scientific groups. Furthermore, several publications have related the effect of size on PC on other biological processes such as cellular uptake, cytotoxicity or haematocompatibility.[21, 26] Another parameter that is considered to play an important role in protein interactions

is the NPs shape, though few papers have been dedicated to this topic so far. It is worth mentioning the studies of Gagner et al.[39], mainly focused on protein structure after adhesion to AuNSs and AuNRs; and Mirsadeghi et al.[83], who investigated how the process of amyloid beta fibrillation is affected by AuNSs and AuNRs.

Although plenty of research has been done towards understanding PC formation on AuNPs, it is important to keep in mind that majority of the papers are focused on spherical AuNPs.[31, 38, 41] Recently, AuNRs as well as AuNSts have also been investigated, though there are very few papers with a full description of the qualitative and quantitative protein profile of the corona.[83, 165] Also, almost all of these studies are performed under *in vitro* conditions.

5. Optical and Optoacoustic Imaging.

Optical imaging techniques are based on the use of light to obtain information about the molecular and cellular function on animal tissues and on the living body. By illuminating the sample at wavelengths on the range between Ultraviolet (UV) and NIR, images containing information about biomolecular processes and tissue composition can be generated.[166] Some advantages of optical imaging techniques over other imaging methods include: (1) it is a straight-forward process; (2) it exhibits a good ratio cost-effectiveness; (3) it allows real time observation of biomolecular processes; (4) it is a safe technique.

Nonetheless, the main limitation of these techniques is the presence of high scattering and absorption of the applied light by the living tissue. First, scattering causes a decrease in the resolution of the technique due to the loss of directionality of the light as it interacts with the tissue. Secondly, intrinsic absorption due to the presence of molecules such as haemoglobin or melanin results in a reduction of the light intensity which causes a dramatic decrease of the signal to noise ratio. In order to overcome these problems, excitation and emission wavelengths in the NIR window (600-900 nm) have been employed.[142] In this so-called “biological” window, intrinsically strong absorbers such as haemoglobin, melanin, water or lipids absorb the least, which allows obtaining higher signal to noise ratio as well as deeper penetration in the tissue.

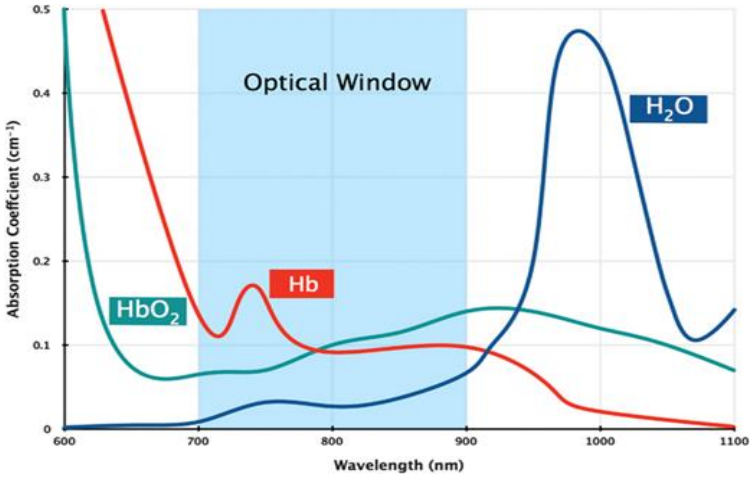

Figure 15: Absorbance spectra of the "biological window" where haemoglobin and water absorb the least.[167]

However, light scattering properties are still limiting the resolution of optical imaging techniques and therefore, optoacoustic imaging approaches have been proposed for improving the resolution and contrast.[168] Based on the optoacoustic phenomenon, the thermo-elastic expansion of NPs after absorbing light, these alternative methods detect the acoustic waves generated, which suffer from much less scattering than light, and use them for generating images of the molecular process or tissue of interest.

Among the different optoacoustic techniques proposed until the moment, hybrid approaches such as Multi Spectral Optoacoustic Tomography (MSOT) are attracting more attention due to the high performance that they show in terms of contrast, resolution and accuracy.[167] A deeper explanation of MSOT as well as its possible applications will be given in the next paragraphs.

5.1. Principle of Optoacoustic Imaging.

Optoacoustic imaging basic operation principle is the following: (1) Firstly, the sample of interest is illuminated with short laser pulses (within the nanosecond range); (2) Then, absorber molecules within the tissue such as haemoglobin, melanin, organic dyes or AuNPs absorb this light; (3) As a consequence of light absorption, a thermo-elastic expansion is produced, which leads to the emission of acoustic waves from the studied tissue; (4) Ultrasonic detectors placed in the vicinity of the illuminated sample recover

the signal from the emitted optoacoustic waves; (5) Finally, a mathematical analysis makes possible to generate high resolution images from the collected data.[167]

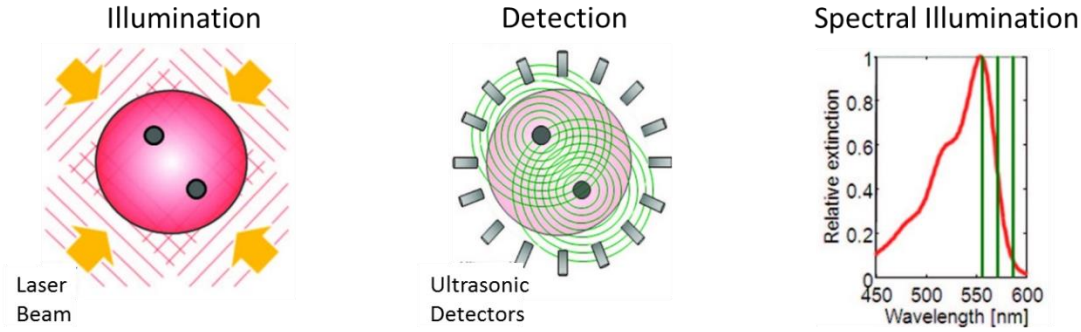

Figure 16: Scheme of the optoacoustic measurement.[145]

5.2. Multiple Spectral Optoacoustic Tomography.

MSOT is a powerful emerging technique in the imaging field that has attracted a lot of attention from the scientific community due to its ability to overcome the major limitations of conventional optical imaging methods while still exhibiting most of the advantages of photonic-based approaches.[167] As other optoacoustic techniques, MSOT exhibits a higher performance in terms of resolution by detecting acoustic waves instead of light from the tissue of interest after illumination. This way, the resolution of the technique is limited by the scattering of the acoustic waves, which is several orders of magnitude lower than in the case of light. As a result, a better signal to noise ratio and a deeper penetration are achieved.

Different anatomic features such as vasculature or melanoma imaging have already been revealed by employing single wavelength methods. However, MSOT allows for multiple wavelength illumination and spectral un-mixing, which allows the detection and resolution of the spectra of multiple absorber molecules at the same time. As it is a tomographic method, a 3D reconstruction can be achieved by recording the ultrasound waves generated in different points of the sample.[167]

It is important to keep in mind the importance of the investigations focused on new processing imaging approaches for improving the sensitivity and quantification power of MSOT. In the case of MSOT, prediction of the sensitivity power of the technique is not straight-forward, as it depends not just on the light diffusion distribution, but also

ultrasound dispersion and characteristic features of each particular sample. Razansky et al.[169] found out that optoacoustic detection limits depend on light penetration distribution and ultrasonic attenuation leading to a nonlinear performance in the detection limit. In their publication, Razansky and co-workers evaluate the dependence of the optoacoustic signal with respect to three parameters: probe concentration, target depth and volume of the target. While for probe concentration the optoacoustic signal was linearly dependent, it was not the case for the other two parameters.

5.3. Gold Nanoparticles as Optoacoustic Tomography Contrast Agents.

Among the numerous AuNPs morphologies that can be synthesized, sphere is the most basic one. It is well-known that AuNSs display an absorption band around 520 nm and that, increasing the size, it is possible to reach 600 nm wavelengths. The main disadvantage using AuNSs for optoacoustic imaging is the decrease on the optoacoustic signal as a result of being out of the "biological window".[142] This is due to the absorption of blood and many other biological molecules within this range, which makes difficult the task of detecting the NPs once injected on the bloodstream. In order to fit their wavelength of absorption within the range of 600-900 nm, AuNSs can be engineered to form an organized assembly that allows to move the LSPR peak towards the NIR region owing to the strong plasmonic coupling effect between adjacent AuNSs.[102] It has been experimentally demonstrated that AuNSs assemblies can be functionalized and designed to display a plasmonic band between 650-1000 nm.

AuNRs have been the most extensively applied for optoacoustic purposes. The anisotropic shape of this NPs gives rise to two different absorption bands in the electromagnetic spectra, one of them within the limits of the biological window. [149] As previously mentioned, AuNRs suitability for optoacoustic applications has been tested and it showed that AuNRs of AR between 3 and 4 seem to be the ones with the best performance.[139] Scattering increases with the size, smaller AuNRs of high AR are preferred as they are expected to absorb more light. These NPs have been investigated for several applications such as lymph node mapping, primary or tumour circulating tumour imaging.[149] For instance, AuNRs functionalized with targeting molecules HER2 and EGFR were successfully used for detection of oral squamous carcinoma cells in a

study by Li et al.[170] In addition, AuNRs were utilized for the *in vivo* study of the cardiovascular system by Taruttis and co-workers, where they were visualized within the bloodstream, with high contrast and good resolution.[171]

Another relevant gold-based structure for optoacoustic imaging is the gold nanoshell, generally constituted by silica spheres coated by a gold shell. After several studies, it was revealed that thinner shells over large cores allow the modulation of the absorption band to be tuned between 800 and 2200 nm.[172, 173] Additionally, Xia and co-workers developed a new replacement methodology for the synthesis of hollow metal nanostructures.[174] This novel protocol allowed the production of more uniform nanoshells. Nevertheless, it is important to keep in mind that nanoshells display higher scattering than NRs that, together with a rather broad absorption spectrum, makes them less effective as optoacoustic imaging agents.[175]

Gold nanoprisms (AuNPrs) have also shown promising results for optoacoustic imaging applications. Malikova and co-workers[176] were the first group to observe and report the spectroscopic signal of AuNPrs. Mirkin group developed a seeded-growth methodology for the production of samples with a higher percentage of AuNPrs, though it was not possible to avoid the secondary formation of pseudospherical NPs.[177] The potential use of this NPs for optoacoustic detection was demonstrated by Bao and co-workers.[178] In this article, authors report the successful application of AuNPrs to the *in vivo* detection of gastrointestinal cancer. They injected PEGylated AuNPrs and used them as signal amplifiers in MSOT to visualize this type of cancer.

In addition to the previously mentioned morphologies, optoacoustic performance of AuNCs has also been investigated.[147] These NPs present characteristics that are similar to those of gold nanoshells, but at much smaller sizes avoiding such an increase in the scattering contribution. Srivatsan and co-workers investigated the performance of AuNCs conjugated to a photosensitizer as a theranostic agent.[179] Authors proved that these complex nanostructures allowed a dual image-guided delivery of the photosensitizer and also improved the efficacy of PDT in murine model. Remarkably, some groups have achieved the synthesis of double-shelled NCs by using different combinations of gold, silver and palladium.[180] The thickness and size of the cage as well as the number of truncated corners can be modulated for tuning the LSPR value. These

NPs are highly reproducible and also quite small, which results in a higher absorption cross-section than the one of traditional dyes.[181]

Last but not least, AuNSts have also been applied for bioimaging applications. Thanks to their spiky morphology, they may present a resonance band within the biological window range.[118] This peak increases with the number branches, their length and the tip sharpness. As they display a very large surface area together with interesting optical and thermal properties, they have been proposed for many different biomedical applications, including optoacoustic imaging.[146] Nie et al. demonstrated the potential of AuNSts for *in vivo* optoacoustic angiography combined with therapeutic monitoring.[182] For this study, AuNSts were conjugated with peptides for active targeting of the tumour. This allowed the performance of the angiography together with PTT. It was proven that optoacoustic imaging gives the possibility of a deeper imaging at a very homogeneous resolution. Other groups have achieved the combination of AuNSts with other NPs such as in the case of Mathiyazhakan and co-workers, who managed to synthesize AuNPs inside liposomes.[183] These complex nanosystems showed a higher optoacoustic signal than AuNSts alone.

5.4. Protein Corona Influence on Optical Properties.

When a NP enters in contact with the biological environment and the physiological fluid is rapidly covered by a "corona" of proteins that will define its new biological identity.[22] During this last decade, numerous publications have been focused in characterizing the PC of numerous different NPs and evaluating its impact in many different processes such as targeting capacity, cellular uptake and pathophysiology.[26, 74] However, little is found in the literature about a possible relationship between the optoacoustic properties of the NM and the possible consequences on them of the formation of a PC. Usually, shifts on the LSPR of AuNPs are mainly used for defining its aggregation state.[151] UV-visible measurements in several papers report a little shift, broadening and decrease on the intensity of the LSPR as a result of the corona formation, though no studies are purely focused on the changes of the imaging properties as a result of the presence of the PC.[31, 184]

Blank page.

CHAPTER 2: OBJECTIVES

1. General Objective.

As previously mentioned, PC has become a trending topic in nanomedicine and biomedical applications since its systematic investigation began in 2007.[20] Nowadays, it is well-known that the bioidentity of any NM is modified upon contact with a physiological fluid, which directly affects their pharmacological and toxicity profile, together with their behaviour and fate within the body.[22] Consequently, PC has become a parameter that must be investigated and understood before any application for biomedical purposes.[163] Among the myriad of NMs designed for biomedical applications, AuNPs have received a lot of attention from the scientific community thanks to their singular optical and thermal properties. As a result, they have been widely proposed and designed as diagnostic and therapeutic platforms.[99]

Taking into consideration this information, we decided to focus this PhD project on the investigation of the PC on AuNPs. After carefully reviewing the published literature on the subject, we realized that the majority of studies on PC formation on AuNPs were carried out utilizing spherical NPs and under *in vitro* conditions.[185] Although investigations on other morphologies can be found, they are very few and do not provide a detailed characterization of the corona profile that interacted with the NP surface.[83, 165, 186] In addition, no studies were found reporting an *in vivo* PC investigation on gold-based nanostructures. Accordingly, this project will be dedicated to provide further information to this scientific knowledge gap, that is to say, we investigate the effect of morphology and *in vivo* conditions on PC formation. Furthermore, we decided to additionally study the optoacoustic properties of AuNPs of different size and shape after interaction with proteins. Surprisingly, there is no information on this matter on the literature and thus, we would like to provide further understanding on this subject.

2. Specific Objectives.

The following sections are dedicated to the description of the individual studies performed during this thesis. These projects were carried out at different research centres and Universities, as a result of the collaborative character of this thesis – co-

supervision at the University of Manchester and CIC biomaGUNE – as well as a brief research stay at RWTH Aachen University.

NPs utilized for all the experiments were functionalized with PEG. The reason for choosing PEGylated NPs is because of its well-known anti-fouling properties. PEGylation is widely used as an anti-opsonisation strategy and it has been shown to partially limit non-specific protein adsorption. Additionally, PEG provides colloidal stability to the NPs when they are in physiological media.[49, 50]

2.1. *In Vitro* Protein Corona Study on Gold Nanoparticles.

This first project is focused on a comparative *in vitro* study of the PC formed on PEGylated AuNSs, AuNRs and AuSts. The aim is to determine the effect of the shape on PC formation.

PC formed onto the surface of PEGylated AuNSs of 70 nm, AuNRs of 75x15 nm and AuNSts of 70 nm was investigated. For that purpose, AuNPs were characterized before and after incubation in human plasma. D_H, ZP and PDI were monitored by DLS. These measurements were carried out before and after incubation to detect the variation on D_H and surface charge upon incubation in the biological media. UV-Visible spectra of AuNPs was also monitored before and after protein interaction to observe a possible shift on the LSPR wavelength of AuNPs.

The protocol followed consisted of: (1) Incubation of the AuNPs on human plasma at 37°C during 10 minutes; (2) Separation of NP-PC complexes from unbound protein by SEC followed by membrane ultrafiltration; (3) Determination of amount of gold by Inductively Coupled Plasma Mass Spectrometry (ICP-MS); (4) Comprehensive analysis of PC qualitative and quantitative composition through Sodium Dodecyl Sulfate Polyacrilamide Gel Electrophoresis (SDS-PAGE) followed by Liquid Chromatography Tandem Mass Spectrometry (LC-MS/MS).

2.2. *In Vitro* Protein Corona Study on Gold Nanostars.

The second project is centred on a comparative PC study formed on PEGylated AuNSts of different spike length. The main aim is the description of the *in vitro* formed PC and the effect of morphological changes of the NP on protein interactions.

For this purpose, PEGylated AuNSts of same quasi-spherical core and different spike length were synthesized. PC formed onto the surface of PEGylated AuNSts under *in vitro* conditions were investigated. Properties of AuNPs were characterized as well by DLS in order to determine the variation of D_H, ZP and PDI before and after formation of the PC. UV-Visible extinction spectra of AuNPs was also monitored. The protocol employed for this investigation was the same as the one described before (Chapter 2; Epigraph 2.1.). Additionally, cell culture studies were carried out to determine the biocompatibility and cellular uptake of these NPs and the influence of the PC on this biological process.

2.3. *In Vivo* Protein Corona Study on Gold Nanoparticles.

The third project is dedicated to the comparative *in vivo* study of the PC of PEGylated AuNSs, AuNRs and AuNSts. The aims are to describe the *in vivo* PC formed on the surface of PEGylated AuNPs and determine the effect of their size and shape on the interaction with proteins.

In this case, PC formed onto the surface of PEGylated AuNSs of 40 and 70 nm, AuNRs of 40x11 and 75x15 nm and AuNSts of 40 and 70 nm under *in vivo* conditions was investigated. Properties of AuNPs were characterized as well by DLS in order to determine the variation of D_H, ZP and PDI before and after formation of the PC. UV-Visible spectra of AuNPs was also monitored.

The followed protocol consisted of: (1) Injection of AuNPs on CD-1 female mice; (2) Recovery of the NPs from the mice 10 min post-injection; (3) Separation of NP-PC complexes from unbound protein by SEC followed by membrane ultrafiltration; (4) Determination of amount of gold by ICP-MS; (5) Comprehensive qualitative and quantitative analysis of the PC composition through SDS-PAGE followed by LC-MS/MS.

The results of this project were published in the journal Nanoscale by the name "*In Vivo* Formation of Protein Corona on Gold Nanoparticles. The effect of Size and Shape".[187]

2.4. Optoacoustic Properties of Gold Nanoparticles.

The fourth project is focused on the determination of the optoacoustic properties of PEGylated AuNPs of different size and shape in aqueous solution. The optoacoustic signal of AuNSs, AuNRs and AuNSts was theoretically simulated as well as experimentally demonstrated by optoacoustic measurements. The main aim was the experimental verification of the simulations.

Theoretical modelling of the optoacoustic performance of the NPs was carried out by Dr. Dmitry Chigrin, at the group Prof. Alexander Kuehne in RHWT Aachen University. Synthesis of the NPs for this study was performed at CIC biomaGUNE and optoacoustic measurements were carried out at RHWT Aachen University in collaboration with Dr. Anne Rix, from Prof. Twan Lammers team.

As the experimental work is in good agreement with the theoretical modelling developed by Dr. Chigrin, the results of this project were published in the journal ACS Photonics by the name "Optimizing the geometry of photoacoustically active gold nanoparticles for biomedical imaging".[188]

2.5. Protein Corona and Optoacoustic Properties of Gold Nanoparticles.

The last project of this thesis is dedicated to the comparative study of the optoacoustic signal of AuNPs in the presence and absence of the corona. The purpose is to determine if there is an influence of the PC on the optoacoustic properties of AuNPs.

For this study, PC-coated AuNSs, AuNRs and AuNSts were prepared by the previously mentioned protocol (Chapter 2; Epigraph 2.1.). Bare- and PC-AuNP complexes were redispersed in milli-Q water and their optoacoustic signals were measured and compared.

3. Relevance of the Project.

AuNPs are one of the most commonly studied NM for biomedical applications due to their remarkable optical and thermal characteristics. Several gold-based nanosystems are currently under clinical trial, which outlines the high potential that these NPs exhibit for the biomedical field.[158] Nevertheless, before being applied for biomedical purposes, gold nanoplatforms behaviour, effect and fate within the biological media must be understood. Nowadays, it is widely recognized that NPs are covered by a layer of proteins upon entrance in the biological milieu and that the PC formed will constitute the new biological identity of the NP.[22] Thus, it is necessary to study PC formation and composition for gold-based nanostructures and how it affects their *in vivo* activity.[185]

Blank page.

CHAPTER 3: EXPERIMENTAL METHODOLOGY

1. Turkevich – Gold Seeds.

The most widely used synthetic route for AuNPs synthesis is based on the scientific work published in 1951 by Turkevich and his colleagues, nowadays well-known as the "Turkevich synthesis".[109] This methodology is based on the reaction between tetrachloroauric acid and trisodium citrate, which leads to AuNP formation. During this reaction, trisodium citrate is used as a reducing agent that allows the transformation of Au^{III} into Au^{0} to form spherical AuNPs. Apart from acting as a reducing agent, excess of trisodium citrate is responsible for the stabilization of the surface of the produced NPs. Although this reaction is considered as the most important landmark in AuNP synthesis, its mechanism is not yet fully disclosed.[189] Many different scientific groups have devoted their work to the study of the mechanism of the Turkevich synthesis by using many different approaches.

Turkevich and his team were the first ones to propose a description for the mechanism for the reaction.[109] They investigated the synthesis with great detail by using several analytical techniques such as electron microscopy, nephelometry and slit-ultramicroscopy. They reached the conclusion that the reaction was governed by a nucleation and diffusional-growth mechanism, which was widely accepted for a long time. Another very important contribution to the field by K. Takiyama et al.[190] remained almost unnoticed despite its great scientific quality. In their publication, Takiyama and co-workers report their investigation of the Turkevich synthesis by using UV-Visible spectroscopy and electron microscopy in combination with a spray. Consequently, an estimation of gold concentration during the course of the reaction was possible. Their results indicate that the number of NPs does not change during the latter part of the reaction.

A great number of these studies were focused on investigating what happens after the reagents are mixed.[191] Changes of colour and several characterization techniques led Chow and Zukoski to believe in a model of reversible aggregation of AuNPs.[192] In other words, it was proposed that large aggregates were formed at the beginning of the reaction giving black and purple colour to the reaction. Then, these big aggregates would

divide leading to the formation of smaller AuNPs, where the colour of the solution would become red. A similar mechanism known as "Ostwald ripening" was proposed by Pong et al.[193], where linear assemblies of clusters resulted in spherical AuNPs after aging and defragmentation via Ostwald ripening.

As a result, several mechanisms have been proposed. Many of the last mechanism proposed for explaining the reaction believe in the formation of intermediate aggregates during the synthesis, which was concluded after UV-Visible spectroscopy and TEM visualization. However, reality is completely different as it has been demonstrated that no large gold aggregates are formed at any time during the Turkevich synthesis.

The most widely accepted mechanism nowadays was proposed in 2010 by Polte et al.[194] In this scientific publication, Polte and co-workers designed a synchrotron set-up for the *in situ* study of the reaction that allowed simultaneous small angle x-ray scattering (SAXS) and x-ray absorption near edge spectroscopy (XANES) measurements for samples in solution. This approach permitted the attainment of accurate data on gold particle concentration and particle size distribution to monitor the particle growth *in situ*. They proposed a seeded-growth mechanism consisting in four steps[194]: 1) gold precursor (Au^{III}) is partially reduced to form small clusters (Au^0); 2) these small clusters combine to form the so-called seeds of about 1.5 nm radius and remaining gold ions are attracted to the surface of these clusters via formation of the electric double layer; 3) and 4) ionic gold is reduced on the surface of the existing seeds – first slowly, then fast – until the precursor is fully consumed. This way, it can be concluded that the number of NPs will be the same as the number as seeds formed during the first part of the reaction, as no new NPs are formed from that point onwards.

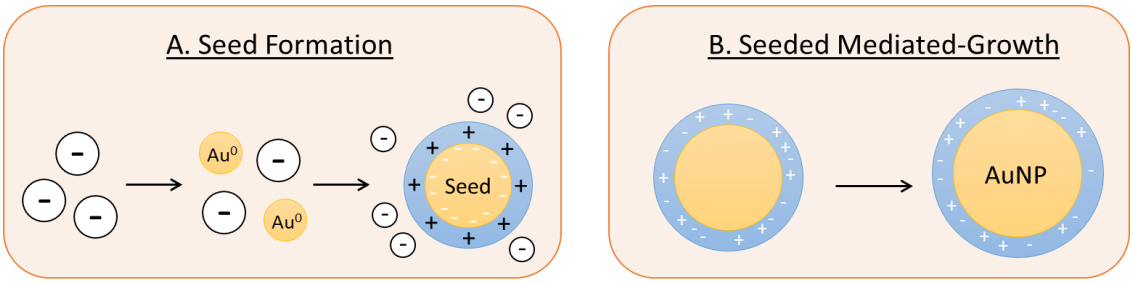

Figure 17: Turkevich mechanism deduced from the study by Polte et al.[194] The mechanism would be divided in 2 parts: A. Seed Formation, which includes the partial

reduction of gold and formation of nanoclusters and their growth up to 1.5 nm radius, and B. Seeded mediated-growth, where the remaining gold ions are reduced on the surface of the existing seeds increasing the diameter of the AuNP.

It is important to keep in mind that, though the work of Turkevich and his co-workers was a fundamental step on the development of AuNP synthesis, their work was based on a previous publication by Ernst. Hauser and J. Edward Lynn in 1940,[195] who had already reported the formation of colloidal gold upon reaction of tetracholoauric acid with trisodium citrate. Up to now, Turkevich reaction has been tuned, improved, studied and further developed in order to have a better control over the size, monodispersity and stability of AuNPs and likewise, to get a deeper understanding of its mechanism.[189, 196] Seeds utilized for synthesis of AuNPs of other geometries involved in our studies were synthesized by this methodology, which is explained in detail below.

2. Gold Nanospheres - Synthesis.

AuNSs of different diameters lead to different optical and thermal properties and hence, it is important to design an appropriate and convenient synthetic strategy for their production. First efforts dedicated to this task where focused on modifying the different parameters that control the Turkevich synthesis[109] and taking into account also further contributions by Frens et al.[197] This strategy leads to the formation of NPs of diameters ranging from 5 to 150 nm. However, the quality of the obtained NPs is quite poor as not only is the size distribution very broad but also shape of NPs are non-uniform, where platonic shapes, rods and others can also be found.

Nowadays, an alternative strategy known as seeded-mediated growth is the most widely used. This approach allows the temporal separation of the nucleation and growth processes within the reaction, leading to a higher control over the size and shape of the NP and consequently, over the monodispersity and quality of the sample.[198, 199] Pioneers in the development of this methodology were Nathan and co-workers, who were able to grow spherical AuNPs by using mild reducing agents such as sodium citrate[200] or hydroxylamine.[201] Although synthesized AuNPs presented improved quality in comparison with previous methodologies, the formation of a second population of anisotropic NPs was also observed. Several efforts were focused on

avoiding the formation of this second population, which was finally achieved by using ascorbic acid[202, 203] as reducing agent or cetyltrimethylammonium bromide[204] as surfactant, among many other molecules.

However, it is particularly interesting for us that the molecule that stabilizes the surface of the NP is labile, as further functionalization by ligand exchange with PEG is required for our studies. Taking this into account, seeded-growth strategy reported by Bastús et al.[110] was selected for growing spherical AuNPs required for our studies. In their publication, Bastús and co-workers focused on the inhibition of the secondary nucleation that occurs during the growth process. By stabilizing the conditions for a homogeneous growth, synthesis of monodisperse and stable AuNSs of a variety of sizes can be obtained, which means a modification of their absorption spectra and hence, different optical properties. After evaluating the effect of several parameters such as temperature, pH and seed concentration, the conditions for an adequate kinetic control were determined, allowing the synthesis of highly monodispersed AuNSs between 10 and 180 nm diameter.

In a typical synthesis, seeds are formed by gold precursor reduction in the presence of trisodium citrate and under strong stirring and high temperature. Once the initial seeds of about 8-10 nm diameter are formed, additional gold precursor and trisodium citrate are added at a lower temperature, which allows the reduction of Au^{III} to Au^{0} on the surface of the already existing seeds without creating new NPs. This process is repeated as many time as needed depending on the final size desired for the NPs. This process is explained more in detail in the paragraphs below.

3. Gold Nanorods - Synthesis.

Although spherical AuNPs display very interesting optical and thermal capabilities, their shape can become a disadvantage for certain biomedical applications. The main limitation of AuNSs is the lack of absorbance in the infrared region of the electromagnetic spectra, which it is an important problem when used for bioimaging purposes.[142] For bioimaging applications, there is a need of NPs that display absorbance within the so-called biological window (600-900 nm) in order to avoid intrinsic biological signals coming from the blood and the tissue. Even if it is possible to synthesize spheres

with an absorbance band within this range, the spheres become far too large (more than 200 nm diameter). AuNRs represent a very attractive alternative as they display an intense band within the desired range, which can be modified by changing the AR of the NP.[112] As mentioned in the introduction, AuNRs, due to their anisotropic shape, exhibit two different plasmon bands named transversal and longitudinal, corresponding to the width and length of the NR respectively.

Nevertheless, the way to achieve a simple and convenient wet chemistry synthetic route for the production of monodisperse and stable AuNRs of well-defined dimensions was not an easy task. During the 1990s, AuNRs were mainly prepared by electrochemical methods based on the use of a molecule as "hard-template" in the presence of a surfactant.[205] Although this synthesis allowed a deeper investigation of the properties of AuNRs, the sample produced was very polydisperse, with a large contribution of other geometries such as spheres and platonic shapes. It was not until 1999, when the first seeded-growth methodology based on wet chemistry was developed for the production of AuNRs,[115] that these NPs started to receive a lot of attention and proposed for many different applications. This synthetic route allows a more convenient and easy production of AuNRs of ARs ranging from 8 to 20 without the need of hard-templates. Up to now, different scientific teams have devoted plenty of efforts to the control and improvement of AuNR synthesis for producing samples of a higher quality, the most important ones being directed by Jana, Murphy and El-Sayed.[114-116, 202]

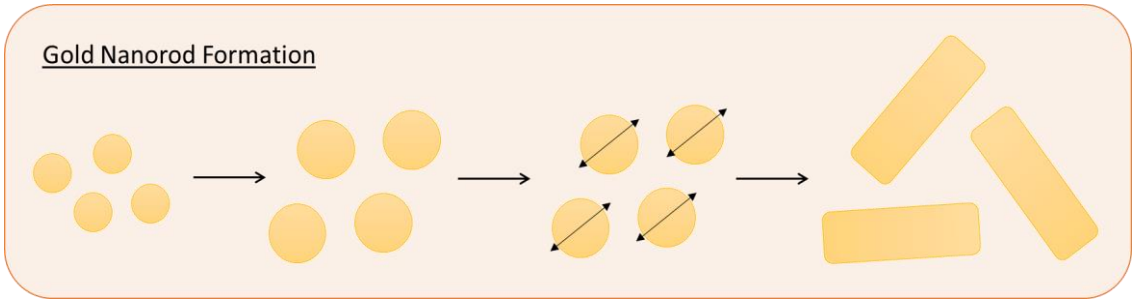

Figure 18: Steps during AuNR synthesis. Small nanoclusters of 1.5 nm are synthesized first and later used as seeds for AuNR formation. After being added to the growth solution the seeds keep growing until the breaking of the symmetry happens, leading to AuNR formation.

Amongst the several approaches for AuNRs synthesis, the protocol initially developed by El-Sayed and Murphy was selected for the production of AuNRs required for our studies.[114-116] This approach is a seeded-growth method based on the use of silver nitrate in the presence of the surfactant cetyltrimethylammonium bromide (CTAB). This synthesis requires kinetic and thermodynamic control which is translated in several parameters that must be taken into account. The first step consists in using a very strong reducing agent for the reduction of Au^{III} to Au^{0} to form very small gold nanoseeds of around 1.5 nm diameter. Afterwards, seeds are added to what is called the growth solution, which contains Au^{III}, silver nitrate and a weak reducing agent. At some point during the reaction the breaking of the symmetry happens, leading to the anisotropic shape of AuNRs. Many investigations have focused on the role of CTAB and silver on AuNR formation and, though the presence of silver and CTAB has been revealed to be fundamental for the correct formation of AuNRs, the mechanism is not fully understood yet.[206] This synthesis allows the production of single crystal gold AuNRs of different ARs. It is important to keep in mind that AuNRs can be divided into single crystal and pentatwinned, depending on the procedure used for obtaining the initial seeds.[116] The procedure followed for synthesis of AuNRs for this study is explained below.

4. Gold Nanostars - Synthesis.

Branched gold nanostructures have also attracted a lot of attention from the scientific community. The main reason is the high sensitivity they display to local changes in the dielectric environment, which is a result of the presence of tips and sharp edges within the NPs.[118] AuNSts exhibit a plasmon band that can be tuned by controlling size of the core and branch length of the NP. As the absorbance band can be modified to be between 600 and 900 nm or even more, these NPs have been proposed for many different applications in biomedicine. Consequently, plenty of efforts have been directed towards the development of a convenient and easy methodology for their synthesis.[117, 207]

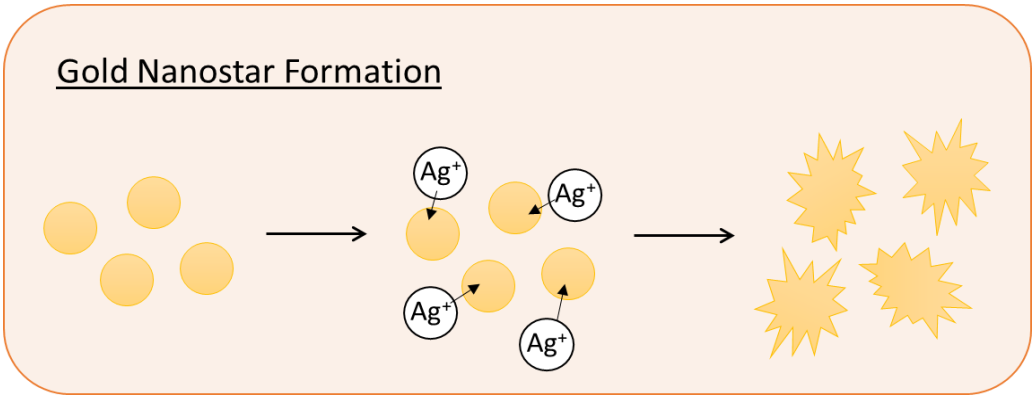

Figure 19. Representation of AuNSt formation. It is believed that silver ions block some facets of gold nanoseeds so gold cannot be deposited there. Therefore, spikes grow on the free facets.

Although both, seedless and seeded-growth methods, can be found in the literature, the second ones present some advantages over the others, such as the higher control over the synthesis, which leads to more homogeneous NPs of a higher monodispersity.[118] In a typical synthesis, gold seeds are prepared and later a growing solution is added for the formation of the tips, where a capping agent is needed.[117] There is plenty of molecules used as capping agents depending on the synthesis, nonetheless we are interested in an easy functionalization after the synthesis and hence, we chose to work following the procedure developed by H. Yuan et al.[208] for the production of surfactant-free AuNSts. In this protocol, Turkevich seeds[109] are prepared and later gold salt is reduced on their surface forming branches after addition of ascorbic acid and in the presence of silver nitrate. While the mechanism has not been fully disclosed, it is believed that the silver ions are able to block some facets of the gold seeds, allowing the gold to be reduced and deposited on the remaining spaces. This synthesis allows the production of AuNSts of different size and tip length by varying seed and silver nitrate amount respectively and was utilized to obtain the NPs used for the studies present in this thesis.

5. Gold Nanoparticle Functionalization.

Gold nanostructures have been functionalized with an incredible number of molecules, polymers and surfactants depending on their final application.[123] In the particular case of biomedical purposes, the nanostructure must be ready to face physiological conditions as it will be eventually injected on the bloodstream. Stability and

biocompatibility are fundamental requirements. However, nowadays there is an additional factor to take into account: the phenomena known as PC.[56]

It is now widely accepted that PC formation leads to a modification of the physicho-chemical properties of the NM, which affects their behaviour, fate and bioidentity.[22] Although there are many other biomolecules present in the blood, proteins are the most abundant and the ones that have a higher impact on the NM characteristics. Sometimes seen as a problem sometimes being taken advantage from, the truth is majority of studies are focused on how to minimize protein adsorption on the surface of NPs while studying the phenomena.[19, 48] Amongst the great number of available molecules, carboxylic PEG with a thiol group was selected for functionalization of all AuNPs required for our studies.[49, 50]

PEG is a widely used polymer for biomedical applications due to its biocompatibility and antifouling capability. Extensively used for *in vivo* experiments, it has been reported to cause no toxicity nor immune response while displaying high solubility and stability in water. This polymer has been shown to be able to reduce protein adsorption upon incubation of NMs when in contact with biological fluids.[50] It has also been reported that the molecular weight of the polymer has an effect on the protein adsorption, the latter being lower when the molecular weight is increased.[19]

The protocol developed by Jana et al.[202] shows a very convenient and easy strategy for functionalization of AuNPs with thiolated PEG based on the ligand exchange reaction. This kind of reaction is typically performed at room temperature and water can be used as a solvent. The reaction can last from a couple of hours to several days. AuNPs are relatively easy to functionalize as the interaction between the stabilizing molecules and the NP surface is usually weaker than the thiol-gold bond and therefore, it can be replaced by the thiol-PEG, which presents a higher affinity for gold. The thiol group would lose the hydrogen atom, which would change for the gold atom of the NP. The nature of the bond that is formed is not completely understood and research is still ongoing.[209] It is believed that the thiol group reacts with the free electrons of the surface of the NP and then, helps stabilizing the surface.

6. Gold Nanoparticle Characterization.

AuNPs synthesis has widely grown during the last decades which means that their characterization has also improved. Several features of AuNPs need to be adequately defined in order to use them for biomedical applications. Typically, a sample of AuNPs must be characterized by different techniques that allow to define their physico-chemical, morphological and optical properties.[210]

6.1. UV-Visible Spectroscopy.

UV-Visible spectroscopy is one of the most popular analytical techniques used in research. In a typical measurement, the sample is illuminated at a range of different wavelengths. This technique is usually employed to study molecules present in the sample, which are able to absorb at some particular wavelengths, producing electronic transitions that can be quantified. This is due to the presence of π-electrons or non-bonding electrons that are able to absorb the light and get to higher level of energy, in other words, the electron goes to an excited state. This technique is very versatile and can be applied for molecule detection, quantification of analytes within a solution, study of molecular interactions with a NP surface or even kinetic studies of many different reactions.[211]

In this work however, UV-Visible spectroscopy was used to characterize AuNPs, which exhibit localized surface plasmon resonances (LSPR), as described above. When illuminated at the resonance wavelength, the collective oscillation of electrons results in a strong absorbance band placed at the visible region or NIR spectral range, depending on the size and shape of the NPs.[101] Analysis of such absorbance bands can provide much information about AuNPs.[212]

6.1.1. Gold Nanospheres.

Spherical AuNPs display an intense single plasmon band usually within 500 to 600 nm depending of the diameter size of the NP. When size increases, the absorbance band is shifted towards higher wavelength values and the signal becomes broader. If the size becomes very large, a second plasmon band will appear as the size would be so big that

more than one plasmon resonance occurs.[110] On the other hand, if the spheres are of a very small size, diameter being under 2 nm, LSPR cannot happen and therefore, no absorbance band will be displayed and just scattering can be recorded.[111] The intensity of the band will depend on the concentration of NPs in the sample.[212]

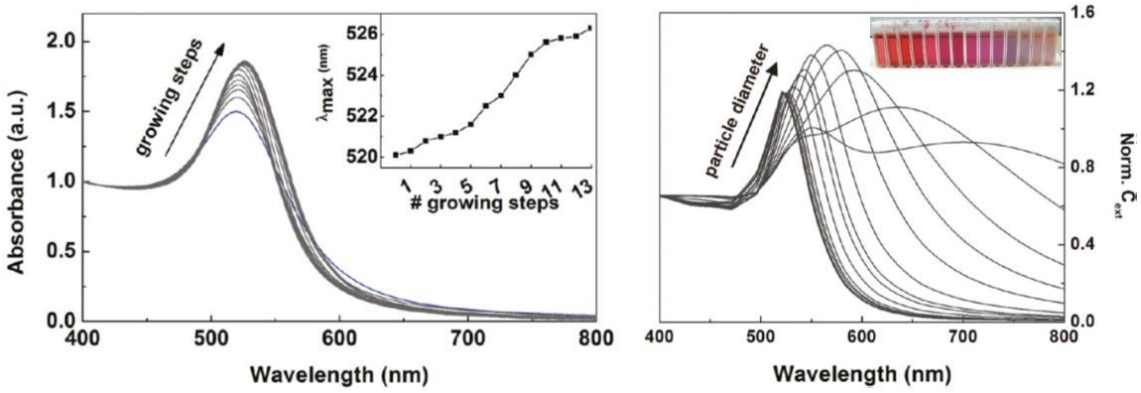

Figure 20: Images from the study on seeded-growth synthesis of AuNPs by Bastús et al.[110] Left: Absorption spectra of AuNSs solutions at different steps within the synthetic procedure; Right) Calculated extinction spectra of AuNSs of different sizes. All spectra are normalized at 400 nm for an easier comparison.

6.1.2. Gold Nanorods.

Although AuNSs already give countless possibilities for biomedical applications, there is a need of NPs that present absorbance within the biological window (600-900 nm) in order to avoid the intrinsic signals coming from the physiological media and tissues.[112] As mentioned before, AuNRs are a very interesting alternative as they display two absorbance bands: transversal and longitudinal. The transversal band exhibits lower intensity and it is located between 500 and 600 nm, depending on the width of the NP. This band usually presents a shoulder which has been reported to be related to the presence of spheres, cubes and other platonic shapes that are formed during AuNR synthesis and therefore, can be used to monitor the purity of the sample. On the other hand, the longitudinal band exhibits a higher intensity and is usually located within the NIR region. Both bands can be tuned by modifying the AR of the AuNR. Intensity ratio between the longitudinal and transversal bands is also an important parameter directly related not just to the dimensions of the NP, but also with the quality of the sample.[116]

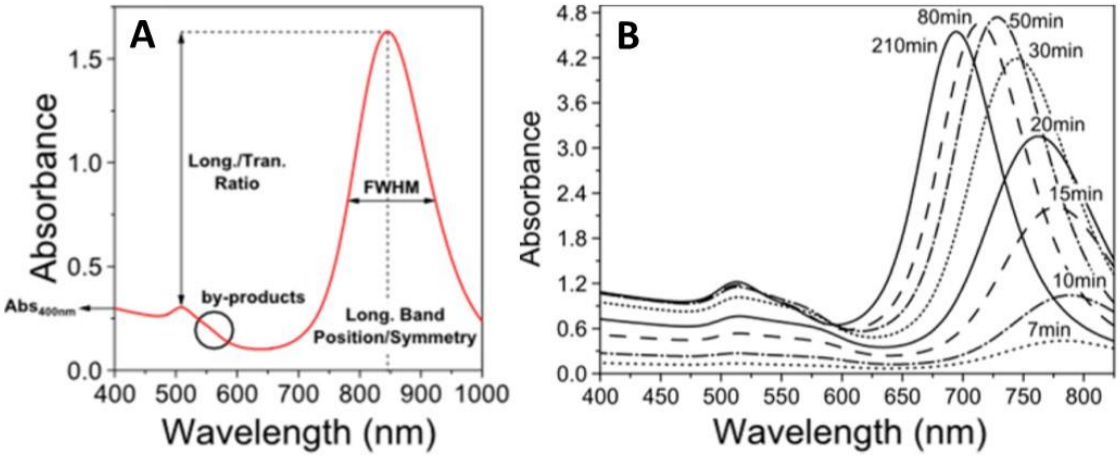

Figure 21: Images from the "Tips and Tricks" guide for AuNRs synthesis published by L. Scarabelli et al.[116] A) Typical UV-Visible spectra of single crystal AuNRs. The longitudinal and transversal peak can be observed as well as the contribution of by-products. B) Growing steps of the seeded-growth synthetic procedure of single crystal AuNRs.

6.1.3. Gold Nanostars.

AuNSts exhibit quite different spectra depending on the synthetic strategy used for their production. While stars synthesized using one-step protocols clearly present two bands of lower wavelengths due to their smaller size, those obtained by other methods display one broader band with a small shoulder within the infrared region of the spectra.[118] In the last case, one corresponds to the plasmon of the spikes while the shoulder corresponds to the core plasmon. Although many efforts have been invested in the development of synthetic routes for AuNSts, there is a limitation related to the polydispersity of the final sample. Independently of the methodology used, AuNSts are not identical and present different number of tips, which is translated in a quite broad branch absorbance band in comparison with the simulation.[208] However, their absorption in the infrared region and plasmon tunability by modification of spike length or size of the NP makes them very useful and relevant for a wide variety of biomedical applications.[207]

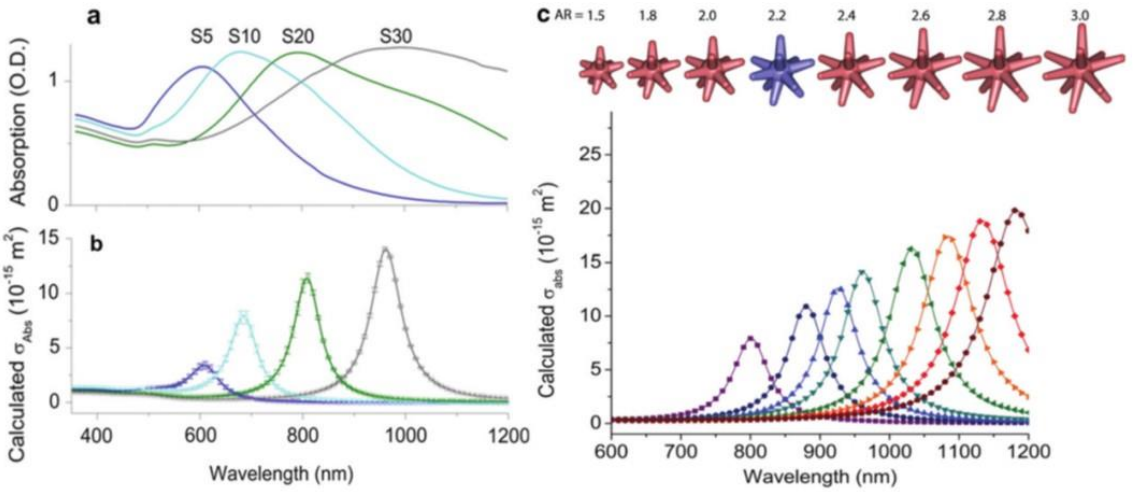

Figure 22: Images from the surfactant-free synthesis of AuNSts published by the group of Vo-Dinh.[208] A) Absorption spectra of AuNSts of different size. B) Corresponding calculated absorption spectra. C) Scatter plotting of polarization-averaged absorptions against AR. The corresponding geometry is on top, where the blue one is the original model of S30 AuNSts.

6.2. Transmission Electron Microscopy.

This microscopy technique can be utilized to determine the morphology and physical dimensions of many NMs.[213] This technique uses an electron beam to visualize the sample. In a typical measurement, a very thin sample or grid of no more than 100 nm height is illuminated with an electron beam. Transmitted rays are then detected and recorded in order to construct an image. Electron illumination poses an advantage in comparison to other optical microscopy techniques, as it is not limited by the wavelength of the visible light. Thanks to this, transmission electron microscopes are able to image with a much higher resolution, allowing the adequate characterization of materials of nanometer size.[214]

AuNPs morphology and dimensions can be analysed by using TEM. In addition, their visualization is particularly easy as gold is a quite heavy atom, which gives a higher contrast to the image. High resolution TEM has been also used for crystallographic studies of different NMs, including AuNPs.[215]

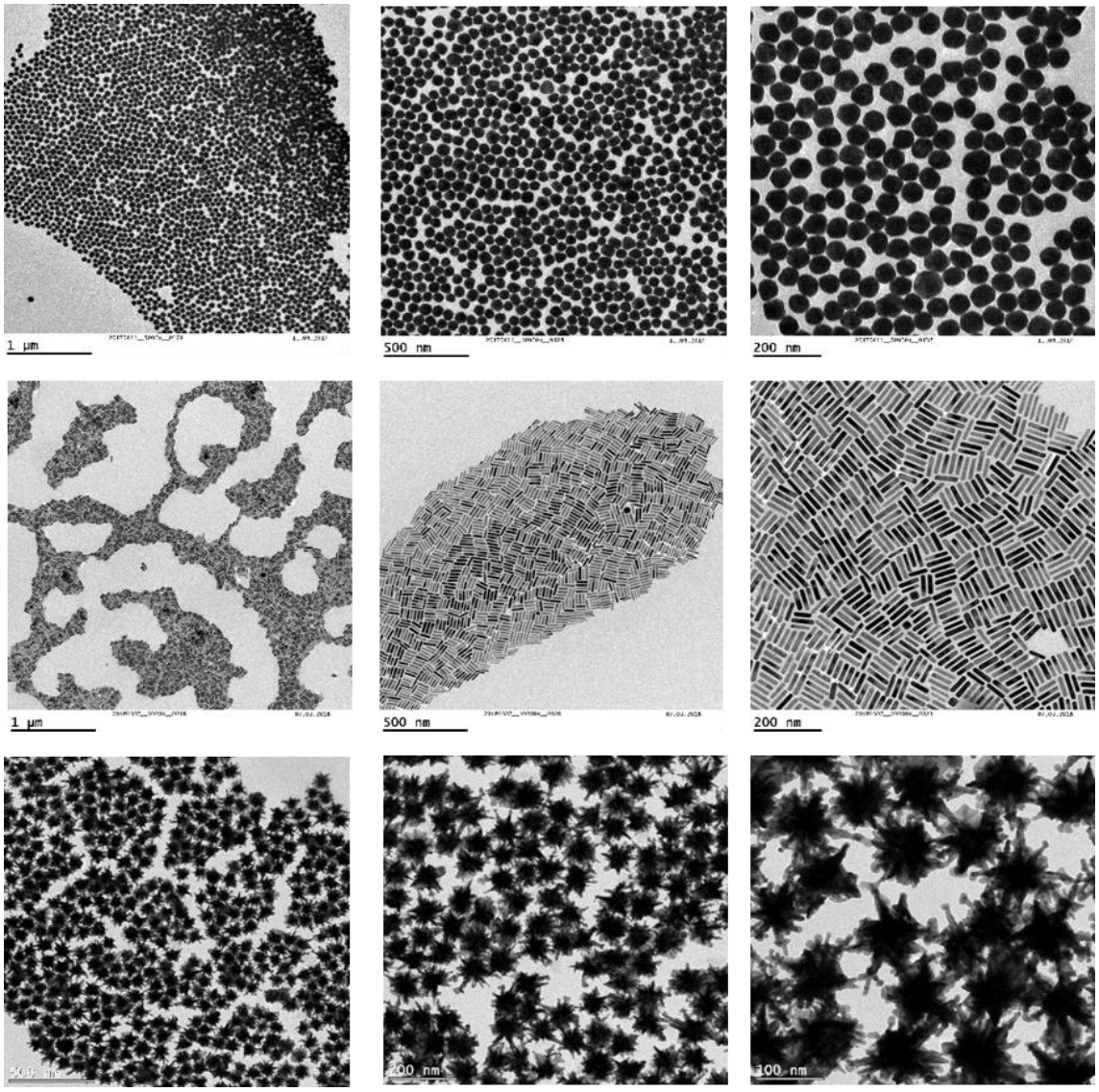

Figure 23. TEM visualization of AuNPs of different morphologies and at different magnifications: row 1 – AuNSs; row 2 – AuNRs; row 3 – AuNSts. This NPs were synthesized and visualized by TEM by myself as initial batches for practice in this synthetic procedure.

6.3. Dynamic Light Scattering.

DLS is an analytical technique usually employed to evaluate the size distribution of NPs and detect the presence of aggregates in the sample. In this instrument, the sample is illuminated by a laser beam. The presence of NPs of different sizes produces distinct fluctuations of the scattering intensity, which are detected and analysed in order to determine their Brownian diffusion coefficient, which can readily correlated to their size. This technique gives hydrodynamic diameter, D_H, of the NPs, which takes into

account the polymer coating or the presence of solvent molecules adsorbed to the NP surface.[216]

DLS has been applied to the characterization of many different colloidal systems such as proteins, polymers and micelles, but also to NPs. Through detailed analysis of the correlation function, diffusion coefficients and polydispersity of the sample be determined.[216] The main limitation of this technique is that the analysis is only straightforward for spherical NPs and hence, the information obtained for anisotropic NMs is not as accurate and needs development of alternative data analysis models. In our case, this technique was utilized before and after functionalization to observe changes in the size distribution and polydispersity for AuNSs and AuNSts, which can be approximated to spheres. Measurements of AuNRs were performed for the sake of comparison but not additional information was extracted as there is a need of a particular model for this anisotropic NP.[217]

6.4. Zeta-potential.

ZP is a parameter that represents the electro-kinetic potential of colloidal systems and it provides information on the surface charge of NPs in solution. Consequently, ZP is strongly related to the stability of NPs in solution, their interaction with other molecules, and the ionic strength of the solution.[218] Back in the 1940s, Derjaguin, Verwey, Landau and Overbeek devoted themselves to develop a theory to explain the colloidal stability of NPs as a function of the total potential energy. Following this theory, the larger the ZP, the greater the repulsive force among NPs and the more stable the suspension.[219]

In a typical measurement, the sample is illuminated by a laser beam in the presence of an electric field. NPs present in the solution respond to the applied electric field at different speeds and thus, produce a distinct scattering of the light which causes a phase shift that can be used to determine the electrophoretic mobility. It is important to keep in mind that ZP is affected not only by the properties of NPs, but also by properties of the solution, such as pH and ionic strength.[218] For this study, ZP was used to observe the changes on the surface charge of the NPs before and after functionalization.

7. Protein Corona.

As mentioned in the introduction, PC is nowadays recognized as a very important parameter that must be taken into account before translating any NP to biomedical applications.[22] Although AuNPs have been described as non-toxic, biocompatible and some gold-based nanosystems have reached clinical trials, deeper investigation of their PC is required for understanding their behaviour and fate.[23]

7.1. Incubation.

Depending on the final application of the designed nanostructure, different experimental approaches can be applied. In this case, it is interesting to study PC formation under different conditions and therefore, *in vitro* and *in vivo* incubations have been performed.[185]

7.1.1. *In Vitro* Incubation.

These type of incubations are the most commonly performed as there is no need of carrying animal experiments. Many different biological fluids such as blood, plasma, protein solutions, FBS and many more, are available for purchase at different companies. Additionally, incubation conditions are more easily controlled, as we can set a particular temperature, time or shaking speed for the experiment. It is also an advantage to know that no sample will be lost during this step, which it cannot be avoided in the case of *in vivo* experiments. However, the limitation lies on the fact that these experiments are not an accurate representation of the real conditions.[73] There are many other parameters that are ignored such as the flow rate, the width of the blood vessels or the presence of cells.

7.1.2. *In Vivo* Incubation.

This approach is utilized for a more realistic representation of the interactions between the NP and other biomolecules present in biological fluids. There are plenty options, though the more utilized models are usually mice and rats.[72, 73] These animals are

available in different strands, which may be more or less adequate depending on the type of experiments that are to be carried out.

It is fundamental to determine the way the NPs are going to be administered to the animal. Majority of NMs are injected in the bloodstream, nonetheless, the injection type (intramuscular, subcutaneous, intravenous, etc) is also important and needs to carefully chosen depending on the study. Same with the approach selected for recovering the sample from the animal for further analysis or if the animal is to be kept alive or terminated (cardiac puncture, orbital, tail, etc). Regarding the sample injected, a certain amount must be selected and several trials must be performed in order to know if more or less amount must be administered or if the sample can or cannot be adequately recovered from the animal. Positively, this approach is the most realistic and gives fundamental information about the behaviour of the system under real conditions.[185]

7.2. Purification of Protein Corona – Gold Nanoparticle complexes.

Once NPs have been allowed to interact with the proteins and the corona has been formed, it is necessary to separate the PC-NP complexes from unbound proteins. The methodology for this step needs to be carefully chosen taking into account the properties of the NPs and the proteins present in the biological media. Several approaches are being currently used, which will be explained shortly in the next paragraphs.

Centrifugation is the most extensively used technique for isolation of PC-NP complexes as it can be applied to a wide range of NMs. It was described for the first time for corona-coated NPs separation by Monopoli et al. in 2013,[220] and is based on the use of several centrifugation steps. In a typical experiment, the sample in presence of unbound proteins would be centrifuged at a determined speed and during a specific time depending on the NM properties. Once the NPs complexes have been spin down, the supernantant containing free proteins would be removed and the sample would be resuspended in another solvent (water or a buffer solution, for example). This process is called washing step and is repeated several time until the analysis of the washing solution gives no signal of protein presence. Although very convenient, easy to perform and applicable to a wide range of NMs, this methodology presents some disadvantages,

such as the strong centrifugal forces (especially for very small or low-density NPs) that may affect to the protein-NP interactions and hence, to the complex stability. It is also possible that some free proteins are being also pulled down by this strong centrifugation and not really removed.

Differential Centrifugation Sedimentation (DCS) has been utilized as an alternative technique to normal centrifugation for PC studies.[221, 222] Also known as two-layer sedimentation method, its use has been extensively applied for determination of the size distribution of NPs with extremely high resolution. This technique is based on the different sedimentation times of the NPs depending on their size. A comparative study was performed by N. Fernández Iglesias et al.[223] In their publication, although no significant differences have been observed regarding the qualitative composition of the PC, it is suggested that DCS presents a higher efficiency in comparison with traditional centrifugation.

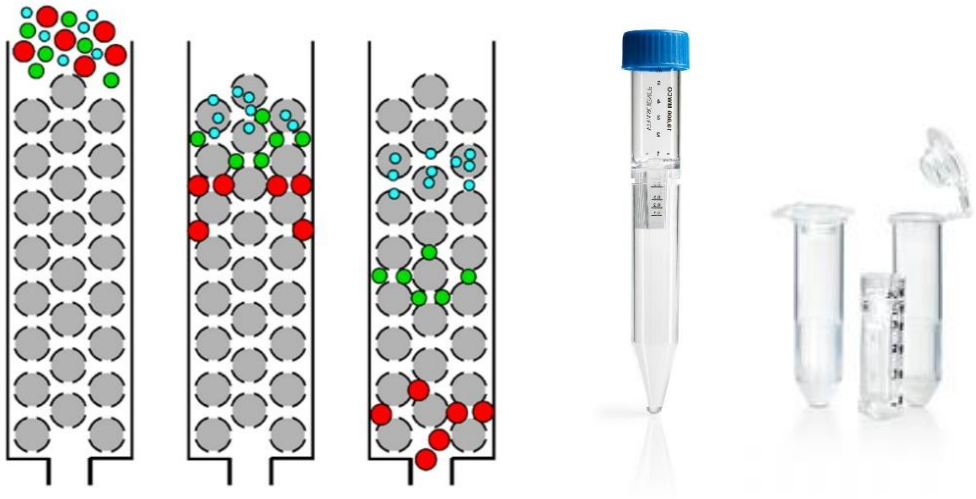

Figure 24. Left – Representation of the principle of SEC;[224] Right – Columns Vivaspin6 and Vivaspin500 for membrane ultrafiltration.[225]

In some cases, it is possible to take advantage of the particular properties of a NM to separate the complex from the physiological media. Sakulkhu and co-workers took advantage of the magnetic NPs for isolating them from unbound proteins.[72] Separation becomes much more simple by using a magnet, though it can just be exclusively used for this kind of NM.

In other occasions, the physico-chemical characteristics of the NP can pose a problem. This is the case of lipidic NPs, whose low density prevents the use of any type of centrifugation for PC-complex purification. Hadjidemetriou et al.[73] developed a methodology to be able to separate protein coronated liposomes from unbound proteins based on the combination of SEC and membrane ultrafiltration. SEC, also known as molecular sieve chromatography, is an analytical technique that allows the separation of molecules in solution by size. Although it has been typically used for separating molecules, in this particular case, it is demonstrated that it can be also successfully applied for NP-protein complexes. However, SEC needs to be complemented with an additional purification step. The reason for this is that this technique alone does not lead to complete separation of unbound proteins from protein-NP complexes and therefore, a second purification step based on the use of membrane ultrafiltration is performed. Centrifugation columns with different membranes are available for purchase and are to be carefully chosen depending on the NM purified. Although centrifugation is still needed, the use of this columns allows to use a much lower centrifugation speed. Even if this technique was firstly designed for the study of PC on the surface of liposomes, it can be optimized for other types of NMs, including AuNPs.

7.3. Physicochemical characterization of Protein Corona – Gold Nanoparticle complexes.

Adequate characterization of the physico-chemical properties of the NPs before and after interaction with proteins is fundamental in order to study the phenomena of PC. For this purpose, NPs are analysed before and after incubation by the following techniques: UV-Visible spectroscopy, TEM, DLS and ZP.[220] Experimental details can be found in epigraph 6. Gold Nanoparticle Characterization.

7.4. Protein Corona Characterization.

Apart from the physico-chemical characterization of the PC-NP complexes, it is also necessary to perform a qualitative and quantitative study of the composition of the PC.

For this purpose, the following techniques are utilized: ICP-MS, Bicinchoninic Acid (BCA) Assay, SDS-PAGE and LC-MS/MS.[220]

7.4.1. Inductively Coupled Plasma Mass Spectroscopy.

This analytical technique is widely used for the detection of the presence of different elements on distinct mixtures. The measurement is based on an ionization source that completely decomposes the sample into its constituent elements and transform the elements into ions. The spectrometer separates these ions as a function of their mass-to-charge ratio and the detector receives an ion signal proportional to the concentration of the ion on the sample. To determine the concentration of a particular element, a calibration of a certified material is used, for instance, reference standards. This powerful technique displays a very high sensitivity, allowing the quantification of elements at concentrations as low as one part in 10^{15} depending on the sample treatment and the available instrument.[226]

Gold can also be quantified by using ICP-MS. However, why not using UV-Visible Spectroscopy? The reason is quite simple. UV-Visible spectroscopy allows the quantification of AuNPs whenever the adsorbed molecules do not affect greatly the signal coming from the AuNPs, in particular, the absorbance at 400 nm.[191] As proteins interact with the NP surface, an increasing of the scattering can be observed under 500 nm wavelength, which directly affects the region usually utilized for gold quantification.

7.4.2. Bicinchoninic Acid Assay.

This popular biochemical colorimetric assay is utilized for the determination of the total concentration of protein present in a solution or sample. The principle of this approach is the reduction of Cu^{II} to Cu^{I} in the presence of protein under alkaline conditions, which results in purple colour due to the formation of bicinchoninic acid which intensity is measured and used for calculation of protein concentration in the solution by comparison with a standard curve. Reduction of copper is mainly caused by some aminoacid residues present on proteins, which includes tryptophan, cysteine and tyrosine.[227, 228] Differently to other methods such as Bradford assay or Lowry Protein

assay as the universal peptide backbone also contributes to colour formation, helping to minimize the variability caused by differences on the composition of proteins.[229, 230]

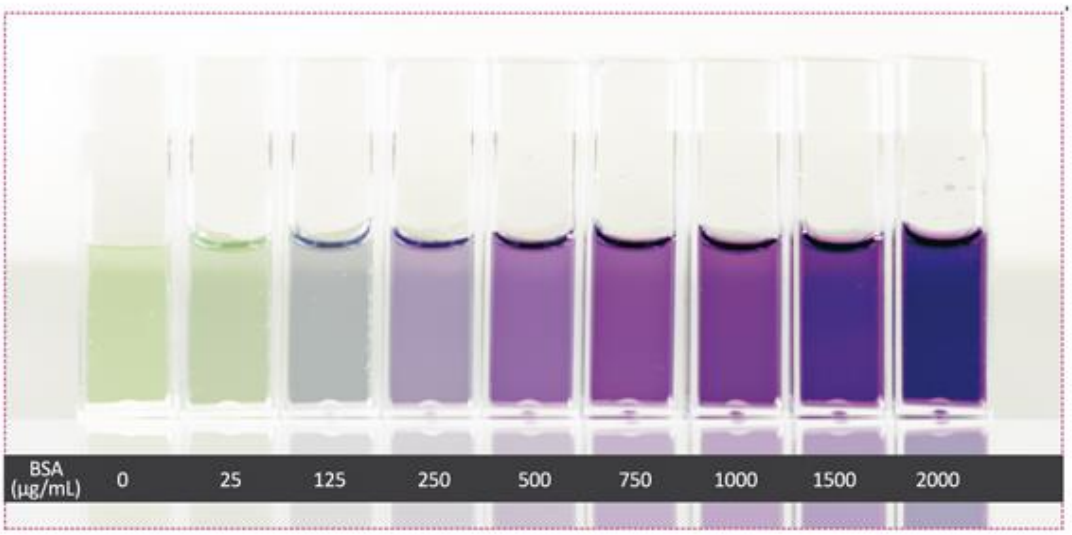

Figure 25: Calibration curve samples prepared with BSA for BCA Assay protein quantification.[231]

7.4.3. Sodium Dodecyl Sulfate Polyacrylamide Gel Electrophoresis.

Gel electrophoresis is a widely used analytical technique used to separate proteins by molecular weight. When proteins are separated by using this technique, they go through a gel matrix, which causes smaller proteins to go faster due to the lower resistance they face.[232, 233] The separation can be affected by the structure or charge of the proteins. However, the use of sodium dodecyl sulfate (SDS) and polyacrylamide gel largely eliminates the influence of these factors, allowing protein separation solely based on polypeptide chain length. SDS is a detergent with a high capacity of denaturing proteins, which binds the protein backbone at a constant molar ratio. By using SDS in the presence of a reducing agent, proteins are unfolded into linear chains with a negative charge that is proportional to the polypeptide chain length.[234]

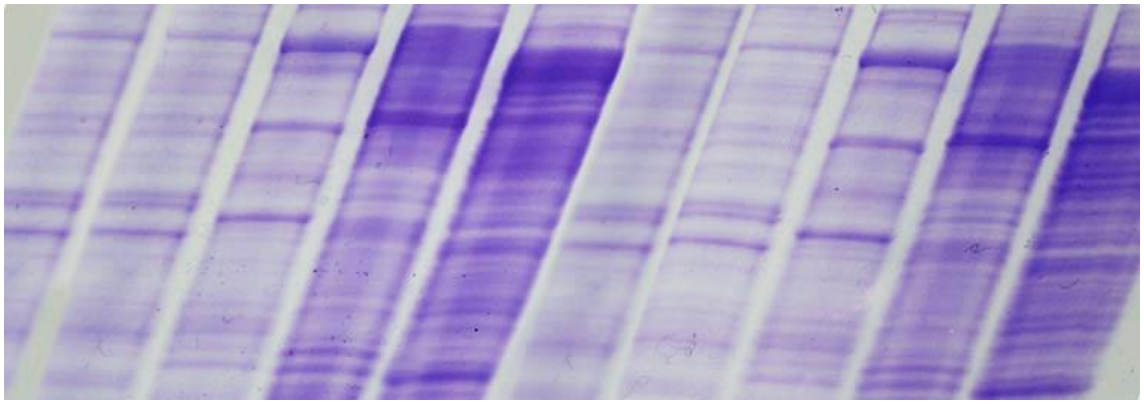

Figure 26. Example of SDS-PAGE gel where many bands can be observed.[235]

7.4.4. Nano Liquid Chromatography Tandem Mass Spectrometry.

This technique has become an essential tool in the field of proteomic analysis as it displays a very high sensitivity and allows the separation and detection of many different proteins within complex mixtures such as blood, plasma and many others. Very small volumes can be used for this analysis, which it is very useful in the case of limited amount of sample.[236] This method uses label-free quantification to determine the relative amount of proteins in a biological sample and so, there is no need of labelling the protein with an isotope or another indicator molecule.

In a typical measurement, gel electrophoresis is used to separate the proteins from the NPs.[220] The bands to be analysed are first excised and later digested prior to introducing them into the instrument. LC is then performed allowing the separation of proteins according to their molecular weight. The sample then reaches the mass spectrometer, where it is ionized and the obtained ions are sorted depending on their mass-to-charge ratio. In the case of PC studies performed on complex fluids, a high amount of proteins can be detected and their relative mass calculated.

Data processing must be handled with care and specific proteomic software is available and recommended for their analysis. Among the different software that can be used at the moment, Scaffold[237] and Progenesis[238] have been some of the most widely used for data processing of PC investigation. They differ on the quantification method, which is based on Spectral Counting in the case of Scaffold, and in Ionic Intensity in the case of Progenesis. Spectral Counting is based on counting the number of spectra identified for

a particular peptide in the sample and then, integrates the result for all measured peptides of the proteins that are quantified. Differently, Ionic Intensity takes advantage of high resolution power from Orbitrap analysers (among others) to extract the intensity of the signal coming from the peptide allowing uncoupling between identification and quantification. Both approaches are very similar and no significant variability is expected.

New approaches are being developed, such as the so-called Intact Protein Expression Spectrometry, which aims for the analysis of intact proteins by LC-MS/MS for determination and quantification of the full protein profile by data reduction software.[239]

8. Optoacoustic Imaging.

Also called Photoacoustic Imaging, it is an emerging imaging modality with great potential for preclinical and clinical research. As mentioned in the introduction, it is a hybrid technique which combines optical illumination and acoustic detection.[167] Optoacoustic imaging allows the delivery of light energy that is absorbed by a the sample, causing a thermo-elastic expansion. This expansion then generates acoustic waves that can be detected by a transducer and used for the construction of an image. Typically, a sample is illuminated at a desired wavelength with a powerful laser, which allows a high degree of penetration in the tissue. However, instead of recovering the signal from scattered light, optoacoustic imaging takes advantage from the fact that acoustic waves are much less scattered than the light and hence, the resolution of the final image is improved. As mentioned before, AuNPs display amazing optical and thermal properties which makes them very interesting for techniques such as optoacoustic imaging.[146] Additionally, by changing their geometry their LSPR wavelength is also modified and hence, it is possible to design a nanostructure to be illuminated at a particular wavelength within the biological window to avoid intrinsic signals from biological tissues.[102]

9. Cell Culture.

Cell culture is a widely used and extremely important tool for scientists all over the world. In the field of nanomedicine, they provide a model system for the study of the interaction of nanomaterials with a basic physiological system, which is fundamental for understanding the behaviour and effect of any nanomaterial on the biochemistry of any body. Cell culture techniques allow us to get more information about processes such as cell internalization, cell toxicity, cell proliferation and many others.

In this particular case, cell studies are focused on the determination of the toxicity and cell internalization of gold nanomaterials in presence and absence of corona. Experiments were performed using two different cell types: A549 (adenocarcinomic human alveolar basal epithelial cells) and 16HBE (human bronchial epithelial cells). These two specific cell lines were chosen with the aim to compare the effect of AuNP exposure to cancer and healthy similar cell types. MTT assay was performed to determine the cytotoxicity of gold nanoparticles with and without protein corona, while ICP-MS, TEM and confocal microscopy techniques were combined for the study of AuNPs internalization by the cells. A more detailed explanation of the techniques and the procedures followed is given in the next section.

Blank page.

CHAPTER 4: EXPERIMENTAL DETAILS

1. Synthesis of Gold Nanoparticles.

1.1. Gold Nanoseeds.

Materials. Hydrogen tetrachloroaurate trihydrate ($HAuCl_4 \cdot 3H_2O$, ≥ 99.9%), trisodium citrate (≥ 98%), hydrochloric acid (HCl, 37%) and nitric acid (HNO_3, 70%) were purchased from Sigma-Aldrich. Milli-Q water was used as a solvent for the synthesis. All glassware was washed with aqua regia (HCl cc:HNO_3 cc; 3:1), rinsed with water, and dried prior to use.

Synthesis. In short, an aqueous solution of $HAuCl_4$ ($5 \cdot 10^{-4}$ M, 250 mL) was placed on a hotplate at a slow stirring rate and high temperature (100 °C). Once boiling started, trisodium citrate (0.152 g, 12.5 mL) was quickly added under vigorous stirring and the mixture was allowed to react for 15 min under vigorous stirring. The final solution had a gold concentration of 0.5 mM.

1.2. Gold Nanospheres.

Materials. Hydrogen tetrachloroaurate trihydrate ($HAuCl_4 \cdot 3H_2O$, ≥ 99.9%), trisodium citrate (≥ 98%), hydrochloric acid (HCl, 37%) and nitric acid (HNO_3, 70%) were purchased from Sigma-Aldrich. Milli-Q water was used as a solvent for the synthesis. All glassware was washed with aqua regia (HCl cc:HNO_3 cc; 3:1), rinsed in water, and dried prior to use.

Synthesis. A volume of 150 mL aqueous solution of trisodium citrate 2.2 mM was prepared and transferred to a three-necked round-bottom flask. The temperature of the mixture was monitored by a thermometer, and was increased until it reached 96 °C, using a condenser to avoid evaporation of the solvent. Once the solution was boiling, 1 mL of $HAuCl_4$ solution 25 mM was injected under vigorous stirring. The colour of the solution changed from yellow to blackish to finally become soft pink after 10 min of reaction. The resulting AuNSs exhibited a diameter of around 10 nm and were used as seeds for the growth of larger spheres. Immediately after the synthesis of these initial seeds, the mixture was cooled down to 90 °C. Subsequently, 1 mL of $HAuCl_4$ 25 mM was

injected under strong stirring. After 30 min, we considered that the reaction has finished and this process was performed again. Next, the sample was diluted by removing 55 mL of the mixture and adding 53 mL of 60 mM sodium citrate solution. This mixture was utilized as a new seed solution, and the process of addition of $HAuCl_4$ was repeated. This cycle was carried out as many times as needed to reach 40 and 70 nm diameters respectively. Once the sample was ready, the reaction was left to cool down at room temperature to be later covered with aluminium foil and stored in the fridge. These samples are stable for months without undergoing any significant change.

1.3. Gold Nanorods.

Materials. Hydrogen tetracholoaurate trihydrate ($HAuCl_4 \cdot 3H_2O$, ≥ 99.9%), sodium borohydride ($NaBH_4$, 99%), hexadecyltrimethylammonium bromide (CTAB, ≥ 99.0%), silver nitrate ($AgNO_3$, 99%), L-ascorbic acid (AA, ≥99.9%), hydrochloric acid (HCl, 37%) and nitric acid (HNO_3, 70%) were purchased from Sigma-Aldrich. Milli-Q water was used as a solvent for the synthesis. All glassware was washed with aqua regia (HCl cc:HNO_3 cc; 3:1), rinsed with water, and dried prior to use.

Synthesis. Gold seeds were synthesized by fast reduction of $HAuCl_4$ (5 mL, 0.25 mM) with freshly prepared $NaBH_4$ (0.3 mL, 10 mM) in an aqueous CTAB solution (100 mM) under vigorous stirring. The colour of the solution changed from yellow to brownish yellow. The seed solution was aged at 27 °C for 30 min before use, to promote the decomposition of sodium borohydride.

Long AuNRs were prepared by adding an aliquot of seed solution (0.6 mL) to a growth solution containing CTAB (250 mL, 100 mM), $HAuCl_4$ (2.5 mL, 50 mM), HCl (4.75 mL, 1 M), ascorbic acid (2 mL, 100 mM) and $AgNO_3$ (3 mL, 10 mM). The mixture was gently shaken and left undisturbed at 30 °C for 2 h. After 2 h of reaction, the solution was centrifuged (6000 rpm, 30 min) to remove excess of reactants and dispersed in an aqueous CTAB solution (100 mL, 1 mM). The resulting AuNRs exhibited dimensions of 70.4±2.5 nm length and 14.5±1.1 nm width.

Short AuNRs were prepared by adding an aliquot of seed solution (3 mL) to a growth solution containing CTAB (250 mL, 100 mM), $HAuCl_4$ (2.5 mL, 50 mM), ascorbic acid (1.88

mL, 100 mM) and $AgNO_3$ (2 mL, 5 mM). The mixture was gently shaken and left undisturbed at 30 °C for 1 h. After 1 h of reaction, the solution was centrifuged twice (8000 rpm, 30 min) to remove the excess of reactants and dispersed in aqueous CTAB solution (100 mL, 1 mM). Obtained AuNRs displayed dimensions of 39.5±1.6 nm length and 11.2±0.9 nm width.

In both cases, once the sample was ready, the reaction was left to cool down at room temperature, then covered with aluminium foil and stored in the fridge. These samples are stable for months without undergoing any significant change.

1.4. Gold Nanostars.

Materials. Hydrogen tetracholoaurate trihydrate ($HAuCl_4 \cdot 3H_2O$, ≥ 99.9%), silver nitrate ($AgNO_3$, ≥ 99.0%) L-ascorbic acid (AA, ≥ 99%), hydrochloric acid (HCl, 37%) and nitric acid (HNO_3, 70%). Milli-Q water was used as a solvent for the synthesis. All glassware was washed with aqua regia (HCl cc:HNO_3 cc; 3:1), rinsed with water, and dried prior to use.

Synthesis A. A certain volume of 14 nm gold nanoseeds (3.75 mL and 5 mL for the preparation of 71.4±1.9 nm and 42.3±1.8 nm diameter AuNSts, respectively) [Au]=0.5 mM, prepared by Turkevich's method, was added to an aqueous solution (250 mL) containing $HAuCl_4$ (1.25 mL, 50 mM) and HCl (0.25 mL, 1 M), followed by fast addition of $AgNO_3$ (0.75 mL, 10 mM) and ascorbic acid (1.25 mL, 100 mM). After 30 s, the reaction was finished and AuNSts are formed. Freshly prepared NSts are not stable and need to be functionalized by addition of stabilizing molecules, as explained on the functionalization section.

Synthesis B. A volume of 10 mL of 14 nm gold nanoseeds [Au]=0.5 mM, prepared by Turkevich's method, was added to an aqueous solution (250 mM) containing $HAuCl_4$ (1.25 mL, 50 mM) and HCl (0.25 mL, 1 M), followed by fast addition of $AgNO_3$ (312 µL, 625 µL, 1.25 mL and 2.5 mL 10 mM respectively, from Stars 4 to Stars 1, different spike length) and ascorbic acid (1.25 mL, 100 mM). After 30 s, the reaction was finished and AuNSts were formed. These NSts are not stable and need to be functionalized by addition of stabilizing molecules, as explained in the functionalization section.

2. Functionalization of Gold Nanoparticles.

Materials. Hexadecyltrimethylammonium bromide (CTAB, ≥ 99.0%) was purchased from Sigma-Aldrich. Mercapto-poly (ethylene glycol) carboxylic acid (α-Mercapto-ω-carboxy PEG, Mw=10KDa) was purchased from Rapp Polymere. Milli-Q water was used as a solvent for the functionalization process.

Functionalization A. AuNSs, AuNRs utilized for the studies presented on Chapters 4 and 6 were synthesized and functionalized by Ana Sánchez Iglesias (CIC biomaGUNE). Synthesis and functionalization of the rest of the NPs was performed by myself. All the mentioned NPs were functionalized with α-Mercapto-ω-carboxy PEG by using the following procedure. An aqueous solution of PEG (20 mL) containing approximately 50 molecules/nm2 was added dropwise to as synthesised AuNPs under vigorous stirring. The mixture was allowed to react for 1 h. PEG-modified AuNPs were centrifuged twice (see previously stated conditions depending on the NP) and finally dispersed in water.

Functionalization B. AuNSts of 40 and 70 nm diameter utilized for the studies presented on Chapters 4 and 6 were synthesized and functionalized by Ana Sánchez Iglesias (CIC biomaGUNE). After the 30 s of AuNSts reaction, an aqueous CTAB solution (3.75 mL, 100 mM) was added the solution containing the freshly prepared AuNSts to enhance their colloidal stability. Afterwards, the solution was centrifuged (3500 rpm, 30 min for 70 nm AuNSts and 5000 rpm, 30 min for 40 nm AuNSts) to remove excess of reactants and dispersed in 100 mL of water. For functionalization with α-Mercapto-ω-carboxy PEG, an aqueous solution of the polymer (20 mL) containing approximately 50 molecules/nm2 was added dropwise to as synthesised AuNPs under vigorous stirring. The mixture was allowed to react for 1 h. PEG-modified AuNPs were centrifuged twice (see previously stated conditions depending on the NP) and finally dispersed in water.

3. Physico-chemical characterization of Gold Nanoparticles.

3.1. UV-Visible Spectroscopy.

UV-Visible optical extinction spectra of AuNPs were recorded before and after interaction with proteins by using an Agilent 8453 UV-visible diode-array

spectrophotometer. Samples were diluted in a total volume of 1 ml using milli-Q water as a solvent and placed on a cuvette of 1 cm optical path length.

3.2. Transmission Electron Microscopy.

Dimensions and morphology of AuNPs involved in this project were monitored by TEM. As the characterization of the NPs was performed at two different locations (CIC biomaGUNE and The University of Manchester), two different instruments were utilized.

CIC biomaGUNE (Chapters 6, 8 and 9). TEM images of the samples before and after PC formation were obtained with a JEOL JEM-1400PLUS transmission electron microscope at an acceleration voltage of 120 Kv using carbon-coated 400 square mesh copper grids. Samples were diluted prior to TEM observation and then, a drop from each colloid (5 µL) was placed onto a carbon-coated copper grid. Excess of suspension was removed with filter paper.

The University of Manchester (Chapters 5 and 7). TEM images of the samples before and after PC formation obtained with a FEI Tecnai 12 BioTwin transmission electron microscope using carbon-coated 400 square mesh copper grids. Samples were diluted prior to TEM observation and then, a drop from each colloid (5 µL) was placed onto a carbon-coated copper grid. Excess of suspension was removed with filter paper.

3.3. Dynamic Light Scattering.

Size distribution of AuNPs was measured by dynamic light scattering before and after protein interaction using a Zetasizer Nano ZS (Malvern, Instruments, UK). This instrument calculates de diffusion speed by recording the illumination patterns of the scattering produced by the NP. The changes of intensity are analysed with a digital autocorrelator that allows the generation of the intensity correlation function, that gives as the value of the diffusion constant. The average particle size and width of the particle size distribution in a colloidal sample can be determined by the assumption of one single NP population (monomodal approximation), which will give as the final plot of the intensity as a function of the size in the form of a Gaussian distribution around the average particle size.

For size distribution measurements, samples were diluted in a total volume of 1 ml using milli-Q water as a solvent, in cuvettes of 1 cm optical path length. A minimum of 3 measurements per sample were made.

3.4. Zeta-Potential.

ZP of AuNPs was measured before and after PC formation using a Zetasizer Nano ZS (Malvern, Instruments, UK). The zeta-potential is a parameter that can be related to the charge acquired by a particle in a given medium. It is determined by the velocity by which the particles move due to electrophoresis. As they are charged, particles will migrate towards an electrode upon application of an electric field. Their speed is proportional to the field strength and also, to the zeta-potential.

For ZP measurements samples were diluted in 1 mL of milli-Q water and placed in Zetasizer disposable folded capillary cells. A minimum of 5 measurements per sample were made.

4. Preparation of Protein Corona-Gold Nanoparticle Complexes.

4.1. *In Vitro* Conditions.

The *in vitro* PC was allowed to form by incubation of AuNPs in a total volume of 1 mL of plasma for 10 min at 37 °C and in an orbital shaker at 250 rpm, setting to mimic *in vivo* conditions. Protein LoBind Eppendorf tubes (Thermofisher Scientific) were used for this experiments. For studies presented in Chapter 4, $5{\cdot}10^{10}$ NPs were incubated in 1 mL of CD-1 mice plasma (Seralab, UK, MSEPLEDTA2-F). For experiments in Chapter 5, $1{\cdot}10^{11}$ NPs were incubated in human plasma (Seralab, UK, Batch HMPLEDTA2-F). Finally, for studies on Chapter 8, $5{\cdot}10^{10}$ NPs were incubated in CD-1 mice plasma (Seralab, UK, Batch MSEPLEDTA2-F).

4.2. *In Vivo* Conditions.

Eight to ten-week old CD-1 female mice were purchased from Charles River (UK). All experiments were performed with prior approval from the UK Home Office under a project license (PPL 70/7763) and in strict compliance with the *UK Home Office Code of*

Practice for the Housing and Care of Animals used in Scientific Procedures. Mice were housed in groups of five with free access to water and kept at temperature of 19-22 °C and relative humidity of 45-65%. Before performing the procedures, animals were acclimatized to the environment for at least 7 days.

CD-1 mice were anesthetized by inhalation of isoflurane and an aqueous solution of 250 µl containing $3.6 \cdot 10^{11}$ NPs, were administered intravenously via lateral tail vein. Blood was recovered 10 min post-injection by cardiac puncture using K2EDTA coated blood collection tubes. Animals were immediately terminated after the recovery of blood. Approximately 0.5-1.0 mL of blood was recovered from each mouse. Plasma was prepared by inverting 10 times the collection tubes to ensure mixing of blood with K2EDTA and subsequent centrifugation for 12 min at 1300 RCF at 4 °C. Supernatant was collected into Protein LoBind Eppendorf tubes (Thermofisher Scientific). For each NP type, plasma sample was obtained by pooling together the blood of 3 mice to achieve a plasma volume of 1 ml. Three experimental replicates were performed and therefore, 9 mice were used in total for each NP type.

5. Isolation and Purification of Protein Corona-Gold Nanoparticle Complexes.

PC-AuNP complexes recovered from *in vitro* and *in vivo* incubations were separated from unbound proteins by SEC. Immediately after recovery from plasma/blood, 1 ml plasma samples were loaded onto a Sepharose CL-4B (Sigma-Aldrich) column (15x1.5 cm) and equilibrated with milli-Q water. A UV-vis spectrophotometer (Agilent Technologies, mentioned in the UV-Visible spectroscopy section) was used to detect the presence of AuNPs in fractions 4, 5 and 6. Fractions containing AuNPs were pulled together and concentrated to 500 µL by using a Vivaspin6 column (10000 MWCO, Sartorious, Fischer Scientific) at 3000 rpm and 4 °C. Subsequently, a Vivaspin500 column (1000000 MWCO, Sartorious, Fischer Scientific) at 3000 rpm and 4 °C was used to further concentrate the sample of 100 µL and ensure adequate separation of PC-AuNP complexes from any remaining unbound large proteins. PC-coated AuNPs were washed 8 times with 100 µL of milli-Q water to remove weakly bound proteins.

6. Physico-chemical Characterization of Protein Corona-Gold Nanoparticle Complexes.

Physico-chemical characteristics of all AuNPs before and after interaction with proteins were monitored by UV-Visible Spectroscopy, TEM and DLS. Experimental details for PC-AuNP complexes are the same as those applied to bare-AuNPs and can be found in Chapter 4, Section 3.

7. Protein Corona Characterization.

7.1. Inductive Coupled Plasma Mass Spectrometry.

The concentration of Au in the samples was determined by ICP-MS (Agilent 7500cx – *Chapters 4 and 6*; ICAP-Q – *Chapter 5*). Samples were digested in presence of aqua regia solution (HNO_3 cc: HCl cc, 1:3) and later diluted in milli-Q water. In a typical experiment, 5 µL of each sample was digested with 1 mL of aqua regia freshly prepared. Then, 100 µL of this solution were diluted in milli-Q water up to a total volume of 5 mL. All samples were measured in triplicate using Iridium 193 as internal standard. Blank samples containing 2% HNO_3 / 0.5% HCl were introduced and run in the instrument before measuring the calibration curve. Calibration samples were prepared at 50, 25, 10, 5, 1 µg/L in 2% HNO_3 / 0.5% HCl from a certified stock solution CMS-2 (Inorganic Ventures, Lakewood, NJ, USA). Wash samples (2% HNO_3 / 0.5% HCl) are prepared and introduced in the instrument to eliminate the memory or carry-over effect previous to measurement of the samples of study.

7.2. Bicinchoninic Acid Assay.

Quantification of protein adsorption on the surface of AuNPs was determined by using a BCA Protein assay kit (Thermofisher Scientific). Pb values, expressed as µg of protein per NP, were then calculated and plotted as the average ± standard error of three independent experiments. For the BCA assay, a calibration curve of 6 points was generated by serial dilutions of bovine serum albumin (BSA) in milli-Q water, with the top standard at a concentration of 2 mg/mL. BCA reagents A and B were mixed at a ratio 50:1 and 200 µL of the BCA mixture were dispensed into 96 well-plates. Then, 25 µL of each standard or 2.5 µL of each sample was added to each well. The plate was incubated

for 30 min at 37 °C and then the absorbance at 574 nm was recorded on a plate reader (Fluostar Omega). Protein concentrations were calculated according to the calibration curve.

7.3. Sodium Dodecyl Sulfate Polyacrilamide Gel Electrophoresis.

Proteins associated with AuNPs ($1 \cdot 10^9$ NPs) were mixed with 20 µL of Novex Tris-Glycine SDS Sample Buffer (2X, Thermofisher Scientific), 4 µL of NuPAGE Sample Reducing Agent (10X, Thermofisher Scientific) and milli-Q water for a final volume of 40 µL and boiled for 2-3 min at 90 °C. Samples were then loaded in Novex WedgeWell 4-20% Tris-Glycine MiniGel of 10 wells (Thermofisher Scientific) and the gel was run for 25-30 min at 225 mV in 10 times diluted Novex Tris-Glycine SDS Running Buffer (10X, Thermofisher Scientific). Staining was performed with Imperial Protein Stain reagent (Thermofisher Scientific) for 1 h and followed by washing in milli-Q water for 2-3 days.

7.4. Nano Liquid Chromatography Tandem Mass Spectrometry.

The University of Manchester – *Chapters 4 and 6.*

Sample digestion – Technician. Bands of interest were excised from the gel and dehydrated using acetonitrile followed by vacuum centrifugation. Dried gel pieces were reduced with 10 mM dithiothreitol and alkylated with 55 mM iodoacetamide. Gel pieces were then washed alternately with 25 mM ammonium bicarbonate followed by acetonitrile. This was repeated, and the gel pieces dried by vacuum centrifugation. Samples were digested with trypsin overnight at 37 °C.

Nano LC – MS measurement - Technician. Digested samples were analysed by LC-MS/MS using an UltiMateR 408 3000 Rapid Separation LC (RSLC, Dionex Corporation, Sunnyvale, CA) coupled to Orbitrap Velos Pro (Thermofisher Scientific) mass spectrometer. Peptide mixtures were separated using a gradient from 92% A (0.1% FA in water, FA = Formic acid) and 8% B (0.1% FA in acetonitrile) to 33% B, in 44 min at 300 nL min, using a 250 mm x 75 µm i.d. 1.7 uM BEH C18, analytical column (Waters). Peptides were selected for fragmentation automatically by data dependant analysis. Data produced were searched using Mascot (Matrix Science UK), against the [Uniprot]

database with taxonomy of [mouse] selected. Data were validated using Scaffold (Proteome Software, Portland, OR).

Protein profile analysis by Scaffold software - Technician. The Scaffold software (version 4.3.2, Proteome Software Inc.) was used to validate MS/MS based peptide and protein identifications and for relative quantification based on spectral counting. Peptide identifications were accepted if they could be established at greater than 95.0% probability by the Peptide Prophet algorithm with Scaffold delta-mass correction. Protein identifications were accepted if they could be established at greater than 99.0% probability and contained at least 2 identified peptides. Protein probabilities were assigned by the Protein Prophet algorithm. Proteins that contained similar peptides and could not be differentiated based on MS/MS analysis alone were grouped to satisfy the principles of parsimony. Semi quantitative assessment of the protein amounts was conducted using normalized spectral counting, NSCs, provided by Scaffold Software. The mean value of NSCs obtained in the three experimental replicates for each protein was normalized to the protein MW and expressed as a relative quantity by applying the following equation:

$$\mathrm{MWNSC_k} = \frac{(\mathrm{NSC/MW})_k}{\sum_{i=1}^{N} (\mathrm{NSC/MW})_i} \times 100$$

where, MWNSCk is the percentage molecular weight normalized NSC for protein k and MW is the molecular weight in kDa for protein k. This equation takes into consideration the protein size and evaluates the contribution of each protein reflecting its relative protein abundance (RPA).

Statistical analysis. Data statistical analysis was carried out using IBM SPSS Statistics software. One-way analysis of variance (ANOVA) followed by the Tukey multiple comparison test were used and p values < 0.05 were considered significant.

CIC biomaGUNE – CIC bioGUNE – *Chapter 5*.

Sample digestion – Technician. Bands of interest were excised from the gel and dehydrated using acetonitrile followed by vacuum centrifugation. Dried gel pieces were reduced with 10 mM dithiothreitol and alkylated with 55 mM iodoacetamide. Gel pieces were then washed alternately with 25 mM ammonium bicarbonate followed by acetonitrile. This was repeated, and the gel pieces dried by vacuum centrifugation. Samples were digested with trypsin overnight at 37 °C.

Sample Digestion - Technician. For tryptic digestion, gel bands were washed in milli-Q water. Reduction and alkylation were performed using ditiothreitol (10 mM DTT in 50 mM ammonium bicarbonate) at 56 °C for 20 min, followed by iodoacetamide (50 mM iodoacetamide in 50 mM ammonium bicarbonate) for another 20 min in the dark. Gel pieces were dried and incubated with trypsin (12.5 µg/mL in 50 mM ammonium bicarbonate) for 20 min on ice. After rehydration, the trypsin supernatant was discarded; Gel pieces were hydrated with 50 mM ammonium bicarbonate, and incubated overnight at 37 °C. After digestion, acidic peptides were cleaned with trifluoroacetic acid (TFA, 0.1%) and dried out in a RVC2 25 speed-vacuum concentrator (Christ). Peptides were resuspended in 10 µL 0.1% FA and sonicated for 5 min prior to analysis.

Nano LC – MS measurement - Technician. The equivalent of approximately 500 ng of each sample was submitted to LC-MS label-free analysis. Peptide separation was performed on a nanoACQUITY UPLC System (Waters) on-line connected to an LTQ Orbitrap XL mass spectrometer (Thermo Electron). An aliquot of each sample was loaded onto a Symmetry 300 C18 UPLC Trap column (180 µm x 20 mm, 5 µm (Waters)). The pre-column was connected to a BEH130 C18 column (75 µm x 200 mm, 1.7 µm (Waters), and equilibrated in 3% acetonitrile and 0.1% FA. Peptides were eluted directly into an LTQ Orbitrap XL mass spectrometer (Thermo Finnigan) through a nanoelectrospray capillary source (Proxeon Biosystems), at 300 nl/min and using a 60 min linear gradient of 3–50% acetonitrile. The mass spectrometer automatically switched between MS and MS/MS acquisition in DDA (Data-Dependent Acquisition) mode. Full MS scan survey spectra (m/z 400–2000; m/z = mass/charge) were acquired in the orbitrap with mass resolution of 30000 at m/z 400. After each survey scan, the six

most intense ions above 1000 counts were sequentially subjected to collision-induced dissociation (CID) in the linear ion trap. Precursors with charge states of 2 and 3 were specifically selected for CID. Peptides were excluded from further analysis during 60 s using the dynamic exclusion feature.

Protein profile analysis by Progenesis software - Technician. Progenesis LC-MS (version 2.0.5556.29015, Nonlinear Dynamics) was used for the label-free differential protein expression analysis. One of the runs was used as the reference to which the precursor masses in all other samples were aligned to. Only features comprising charges of 2+ and 3+ were selected. The raw abundances of each feature were automatically normalized and logarithmized against the reference run. Samples were grouped in accordance to the comparison being performed, and an ANOVA analysis was performed. A peak list containing the information of all the features was generated and exported to the Mascot search engine (Matrix Science Ltd.). This file was searched against a Uniprot/Swissprot database restricted to Homo sapiens entries, and the list of identified peptides was imported back to Progenesis LC-MS. Protein quantitation was performed based on the three most intense non-conflicting peptides (peptides occurring in only one protein), except for proteins with only two non-conflicting peptides. The significance of expression changes was tested at protein level, and proteins with a p-value ≤ 0.05 were selected for further analyses. Protein abundances were loaded onto Perseus software and log2 transformed for the generation of the heatmaps.

8. Optoacoustic Imaging.

Optoacoustic spectra and imaging were acquired on a Visualsonics Vevo LAZR. AuNP and PC-AuNP complexes analysis was performed in tubing phantoms, where air bubble free polyurethane tubing (Polyurethane Intravascular Tubing, 0.025 x 0.040 in, INSTECH) was filled with an aqueous dispersion of the respective NPs (0.1-1 mg/mL) and then placed into a custom built rack and immersed in water. The detector head was immersed in the water reservoir above the tubing phantoms and 4 tubes were analyzed at the same time. One of the tubes was filled with milli-Q water to be used as a blank. The immersed tubes wer then subjected to optoacoustic imaging delivering optoacoustic excitation spectra and at the maximum wavelength cross section images of the plastic tubing are recorded.

9. Cell Culture.

9.1. MTT Assay.

Description. The MTT assay is a widely extended method utilized to measure the metabolic activity as an indicator of cell viability, proliferation and cytotoxicity. This colorimetric assay is based on the reduction of a yellow tetrazolium salt (3-(4,5-dimethylthiazol-2-yl)-2,5-diphenyltetrazolium bromide), most commonly known as MTT, to purple formazan crystals as a consequence of the metabolic activity of cells. Viable cells contain NAD(P)H-dependent oxidoreductase enzymes that are able to reduce the MTT to formazan. Consequently, insoluble formazan crystals are dissolved using a solubilisation solution. Afterwards, the quantification of the resulting coloured solution is carried out by measuring the absorbance at 550 nm using UV-vis spectroscopy. The darker the solution, the greater the number of metabolically active cells.

MTT Assay. MTT assay (Sigma Aldrich, kit) was performed for every NP (triplicates) at 3 different concentrations (1 mM, 0.1 mM and 0.01 mM) and in presence and FBS-free and FBS-containing DMEM. Both A549 and 16HBE cells well plated in 96-well plates, a total of 120 wells for each cell line containing $1 \cdot 10^4$ cells (A549) and $2 \cdot 10^4$ cells (16HBE) per well. The cell media used for both cases was Dulbecco's Modified Eagle Medium (DMEM, Gibco, ThermoFisher Scientific). Note that half of the amount of A549 cells are plated as they naturally grow and reproduce very fast. After 24 h, 100 µL of AuNSts (1 to 4) are added directly to the wells without removing any previous media. This is to minimize disruption of the cells and to avoid that they lift up during removal of the media. Cell viability was measured after 24 h of exposure of cells to AuNPs. Afterwards, for the MTT assay, all supernatants were removed and 100 µL of DMEM/FBS (FBS, Gibco, Thermofisher Scientific) containing MTT reagent (diluted 1:10) were added to every well. The samples were left for 1 h isolated from the light and at 37 °C. To remove the MTT containing reagent, plates were upturned, pressed dry and 100 µL of DMSO (dimethyl sulfoxide) were added to each well. Intensity of the colour of the solution was read at 550 nm.

9.2. Inductive Coupled Plasma Mass Spectrometry.

Description. ICP-MS was used for detecting the amount of gold that was internalized by both cell lines (A549 and 16HBE) after 24-exposure to the presence of AuNPs. The procedure of incubation and sample preparation for ICP-MS treatment is explained in detail below.

ICP-MS. ICP analysis was performed for every NP (triplicates) at 1 mM concentration and in presence and FBS-free and FBS-containing DMEM. Both A549 and 16HBE cells well plated in 24-well plates containing $5 \cdot 10^4$ cells (A549) and $1 \cdot 10^5$ cells (16HBE) per well. The cell media used for both cases was Dulbecco's Modified Eagle Medium (DMEM, Gibco, Thermofisher Scientific). Note that half of the amount of A549 cells are plated as they naturally grow and reproduce very fast. After 24 h, the media was removed and 300 µL of AuNSts (1 to 4), diluted in DMEM with and without FBS, were added to the wells, where they were left for 24 h. Next, supernatants were removed and wells were washed with 150 µL of Phosphate-Buffered Saline (PBS; Gibco, Thermofisher Scientific) and 150 µL of trypsin (Thermofisher Scientific). This mixture was all pooled in the supernatant sample. A further 200 µL of trypsin was added to the cells to bring them into suspension and then, 800 µL of DMEM/FBS were utilized to quench the trypsin. Samples were then centrifuged and the supernatant removed and reserved for treatment before ICP-MS measurements by following the protocol mentioned in Chapter 3, ICP-MS Experimental Detail Section.

9.3. Transmission Electron Microscopy.

Description. TEM was utilized for the visualization of the AuNPs internalized by the cells. The procedure and treatment of the sample for preparing the sample for TEM observation is explained below.

TEM. For TEM sample preparation, 4 small petri dishes containing 4 mL of DMEM media with 2 plates containing $2.5 \cdot 10^5$ A549 cells and 2 plates containing $5 \cdot 10^5$ 16HBE cells respectively. Note that half of the amount of A549 cells were plated taking into account their fast growth rate. After 24 h, media is removed and 3 mL of AuNPs, diluted in DMEM (Gibco, Thermofisher Scientific) with and without FBS (Gibco, Thermofisher Scientific),

were added to the cells and left for 24 h. The concentration tested in this case was 1 mM. Afterwards, the supernatants were removed and wells were washed twice with 1 mL of PBS (Gibco, Thermofisher Scientific) each. Next, 1 mL of tripsyn was added and, once cells were detached, 3 mL of media were added. Cells were washed 3 times in Sorensens phosphate buffer (0.1 M, pH 7.4) at 300 g, 4 °C for 5 min. Cells were fixed for 10 min at room temperature using a mixture of formaldehyde and glutaraldehyde in Sorensens buffer, being the final concentrations 2% and 2.5% respectively. The fixative was replaced with a new fixative and samples were left at 4°C for 2 h. Fixative was removed in 3 washes of 5 min each using Sorensens buffer (300 g, 4 °C). Cell pellets were transferred to solubilised agar (a 2% w/v solution of low melting weight agar in Sorensens buffer) and 100 µL were added directly to the cell pellet. Samples were flicked and immediately centrifuged at 3600 rpm for 5 min at 20 °C. Cell pellets could be visualized in the lower part of the agarose. Samples were placed on ice for approximately 1 h in order to harden. Pieces of cell-containing agarose were cut in cubes of approximately 1 mm^3 size, and then transferred to glass vials for the addition of a 1% solution of OsO4 (Sigma Aldrich, ≥99%) in Sorensens buffer (300 µL added to each sample). Samples were left lightly capped on ice, in the dark, for 1 h. Next, samples were washed 3 times with Sorensens buffer, with no centrifugation needed from this point on as the samples are solid. A dehydration series of water:ethanol (50, 70, 90 and 100%; Sigma Aldrich, ≥ 99.5%) was carried out, 10 min each, followed by a final 2 steps on 100% acetone (Sigma Aldrich, ≥ 99.9%). Samples were embedded beginning with a 1:1 acetone:spurr (Spurr resin – Pelco – TEM lab) mix, followed by a 1:2 acetone:spurr and then 100% spurr, all for 30 min. Finally, samples were transferred to BEEM embedding capsules and pure spurr resin was added. Samples were cured at 60 °C for 48 h, before 100 nm slices were cut using glass knives. Slices were transferred to 100 square grids and visualized by TEM.

9.4. Confocal Microscopy.

Description. Confocal microscopy was utilized for visualization of the AuNPs internalized by cells. For this purpose, different dyes were applied for easier visualization of the

different parts of the cells and, therefore, to detect in which parts of the cell AuNPs can be located. The procedure is explained in the following paragraph.

Confocal Microscopy. A549 and 16HBE cells were incubated and exposed to AuNPs following the same procedure stated previously (MTT assay, Experimental Details). Two different dyes were applied to the cells before visualization by confocal microscopy: Fluorescein diacetate (FDA – Green; Invitrogen, Thermofisher Scientific) for the cell cytoplasm and 4',6'-diamidino-2-phenylindole (DAPI – Blue; Invitrogen, Thermofisher Scientific) for the nucleus. Media was removed and cells were washed 2 times with 200 µL of PBS. Then, a volume of 150 µL of diluted solution of FDA and another of DAPI were added to the cells and left to stain during 15min.Cells were washed 3 times with 200 µL of PBS. Finally, cells were then examined using Zeiss 780 multiphoton CLSM using the 40X objective. Images were then processed using Zeiss microscope software ZEN. Excitation/emission wavelength: 490/526 nm (FDA) and 358/461 (DAPI) nm.

Blank page.

CHAPTER 5: *IN VITRO* PROTEIN CORONA ON GOLD NANOPARTICLES

1. Focus of the Study.

The first part of this work focused on a detailed analysis of the PC formed onto the surface of AuNPs under *in vitro* conditions. Among the myriad of parameters that have been studied and reported in the literature, we discovered that morphology was not deeply investigated and that, the few publications regarding this matter were not focused on AuNPs but on other kinds of NMs.[46, 47] As AuNP synthesis is well developed and optimized, we decided to focus our first study on the investigation of the influence of morphology on PC formation and composition.

For this purpose, we applied a designed and optimized purification process previously described and published by Kostarelos's group for the isolation of the PC-NP complex.[73] In this context, we present an *in vitro* study of the PC formed around AuNPs of 70 nm size and different morphologies: AuNSs, AuNRs and AuNSts. All AuNPs involved in this study were adequately functionalized with carboxylic PEG of molecular weight of 10 kDa. Plasma from CD-1 female mice was chosen as incubation media for this project. For PC formation, AuNPs were incubated in mice plasma for 10 minutes at 250 rpm and at 37°C of temperature in an incubator shaker. Afterwards, AuNP-PC complexes were separated from loosely and unbound proteins by a combination of SEC followed by membrane ultrafiltration. Physico-chemical properties of AuNPs before and after interaction with proteins was monitored by DLS, ZP measurements, UV-Visible Spectroscopy and TEM. PCs formed after plasma incubation were qualitatively and quantitatively analysed by LC-MS/MS revealing a quite complex corona for all AuNPs.

2. Results. Physico-Chemical Characterization.

All AuNPs utilized for this project were synthesized by seeded-growth methods extensively optimized and reported in the literature and at the biomaGUNE group.[109, 110, 114-116, 208] AuNPs were then functionalized with thiolated carboxylic PEG (Molecular weight - Mw =10 KDa) by a ligand exchange methodology and adequately washed to separate from unbound polymer before any PC experiment.[202] Characterization of the

initially produced AuNPs is summarized in Figures 27 and 28 and Table 1. Physico-chemical and morphological characterization of AuNPs before and after PC formation was carried out by DLS, ZP measurements, UV-Visible spectroscopy and TEM.

	AuNSs		AuNRs		AuNSts	
	No PC	PC	No PC	PC	No PC	PC
D_H (nm)	111.1±0.7	118.0±2.6	24.9±0.3	139.8±22.1	122.0±1.3	132.3±1.7
ZP (mV)	-44.1±1.5	-20.9±3.3	-28.8±0.4	-17.6±1.9	-33.6±0.2	-24.5±6.3
PDI	0.050±0.024	0.121±0.032	0.378±0.003	0.403±0.038	0.101±0.007	0.231±0.030

Table 1. Effect of in vitro PC formation on the physico-chemical properties of AuNPs before and after interaction with proteins: D_H (nm), ZP (mV) and polydispersity index (PDI).

PEGylation is known to limit protein interaction with the NM surface once they get in contact with a biological fluid.[49] Nonetheless, it has been demonstrated that it cannot fully supress protein adsorption and hence, PC formation cannot be eliminated.[19] In fact, in a recent study by S. Schöttler et al.[50], it was demonstrated that the well-known ¨stealth¨ effect is not exclusively due to the polymer. Instead, it is actually a secondary effect, consequence of the adsorption of certain proteins in the corona. In agreement with previous findings, PEGylated AuNPs involved in this study were found to interact with proteins after incubation in plasma.

Size distribution of AuNPs before and after protein interaction was monitored by DLS (Figure 26). In general, isotropic NPs are expected to show a single band when examined by DLS. In our case, AuNSs and AuNSts, which are pseudo-isotropic, displayed a single band in agreement with our expectations. The width of the band was higher for AuNSts size distribution profile, which can be explained by the higher PDI that characterizes this NP type. AuNSts morphology is quite complicated and can be defined by the number of spikes, their length and their width. Nonetheless, although we could theoretically establish these parameters, it is extremely difficult at the experimental level to control these features. As a result, even if researchers can synthesize AuNSts with the same total diameter, it is expected that the sample produced will contain AuNSts of different morphological features.[207, 208] On the other hand, we have AuNRs displaying a clearly

anisotropic shape. AuNRs exhibit two bands, which can be explained by their anisotropic morphology.[83, 186] After interaction with proteins, PDI values for AuNSs and AuNSts increased and bands became broader indicating a more polydisperse size distribution.

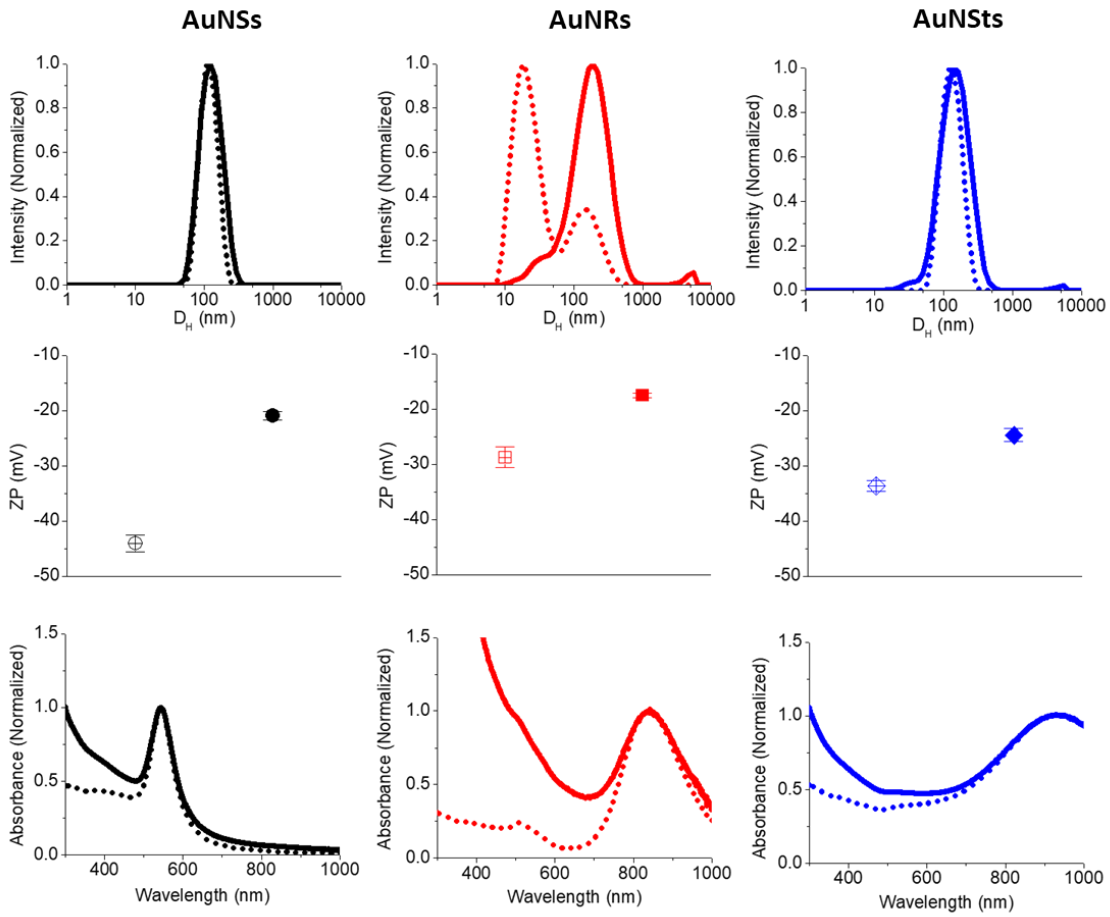

Figure 27. The effect of PC formation on the physicochemical properties of AuNPs. DLS size distribution, ZP and UV-VIS extinction spectra are depicted for AuNPs before (dotted lines) and after (solid lines) interaction with CD-1 female mice plasma.

D_H was not significantly changed, which is different from what is already reported in the literature. As previously mentioned, several groups have investigated effect of *in vitro* PC on physico-chemical properties of AuNPs, specifically spheres, using several sizes ranging from 5 to 80 nm.[38, 41] In all cases, approximately a double of the initial D_H was observed after interaction with proteins. This difference may be related to the different functionalization of the NPs. While the mentioned studies are focused on citrate capped AuNPs, the ones used in this particular project are PEGylated (Mw=10 KDa). In a comparative study between citrate-capped and PEGylated AuNPs, Benetti et al.[240]

found PEGylation reduced the amount of protein adsorbed and therefore, a smaller shift of the D_H band. Regarding AuNRs, the two initial bands merged into one, in agreement with previous studies.[83, 241] Although an increase in AuNRs size after protein incubation has been reported by Kah et al.[186], this difference was more likely due to aggregation as the final size was much higher than the one presented in this study. Again, this phenomenon is explained by the lower anisotropy displayed by PC-AuNR complexes.

ZP measurements before and after protein interaction are presented in Figure 26. Surface charge of AuNPs prior to exposure to mice plasma was negative, displaying a value around -25 mV. Nonetheless, interaction with proteins lead towards a less negative ZP value, indicating interaction with proteins of different charges. These results are in agreement with data reported in the literature and are usually explained by the attachment of neutral and positively charged proteins onto the NP surface.[41] It is believed that proteins interact with the NP surface by electrostatic forces (among others such as Van der Waals) by a sequential binding. This would allow the interaction of a negatively charged surface with proteins of the same type of charge. Nevertheless, the initial charge of the NP, negative in our case, still plays a major role on PC formation and influences the proteins that will interact with the NP surface.

Additionally, UV-Visible spectra of AuNPs before and after incubation were recorded, the result being displayed in Figure 26. Monitoring changes on the plasmon band is very important as they give information about the aggregation state and changes on the dielectric environment of the NP. Interestingly, no significant shift in the LSPR band was observed after interaction with plasma proteins. In previous studies, while for positively charged AuNPs a clear shift towards higher values can be seen,[186, 241] the shift is almost non-existent for negatively charged AuNPs.[57, 184] Remarkably, positively charged NPs seem to be more likely to aggregate and, in several occasions, the shift observed on the plasmon band is due to NP aggregation more than a change of the NP morphology. This may be explained by the higher amount of proteins that is able to interact with the surface of positively charged NP in comparison with their neutral and negatively charged counterparts. Therefore, a negatively charged polymer coating (as carboxylic PEG) is able to minimize PC formation as well as helping the stabilization of the NP even after incubation with proteins.

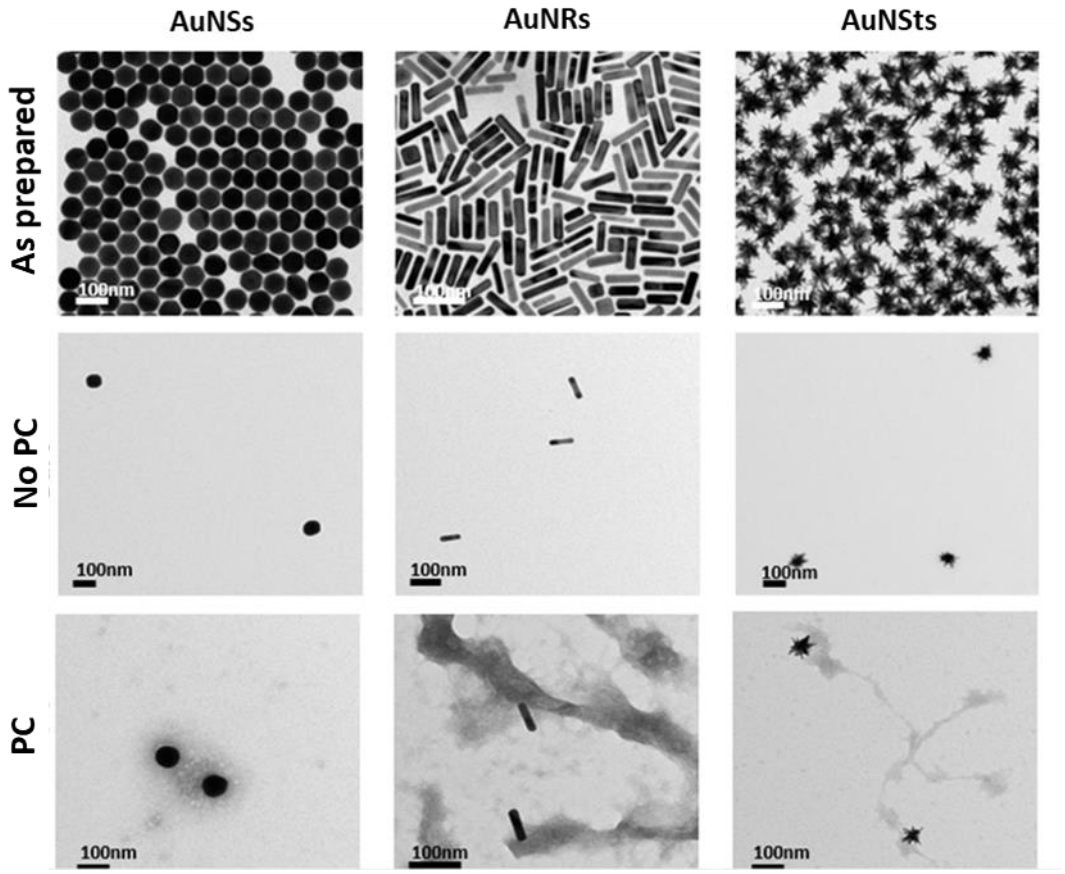

Figure 28. Representative TEM images of AuNPs, as prepared, bare and after interaction with CD-1 mouse plasma. All scale bars are 100 nm.

Morphological properties of all AuNPs involved in this study were monitored by TEM visualization before and after incubation in plasma (Figure 28). In all cases, proteins surrounding the NPs can be observed. No reshaping or changes in the structure of the NPs was detected. It is worth highlighting the presence of more fibre-like structures in the case of AuNRs and AuNSts than for AuNSs.

3. Results. Protein Corona Characterization.

Proteins adsorbed on AuNPs were separated from their surface by SDS-PAGE and PC profiles were visualized by Imperial Protein Staining (Figure 29B). Quantification of protein adsorbed per NP was obtained combining results from BCA Assay, used for protein content determination, and ICP-MS, performed for gold quantification. As it can be observed in Figure 28A, the amount of protein adsorbed on AuNSs and AuNSts does differ from the one adsorbed by AuNRs. Although there is a couple of studies on shape

comparison and PC, no quantification was performed in those cases and therefore, no comparative is possible.[46, 47] Taking a look at the graph, AuNRs seem to be the ones that adsorb a lower amount of proteins per NP, though the difference was found not to be statistically significant. This would be understandable as, among all AuNPs involved in this study, AuNRs are the ones displaying a smaller total surface area, as the number of NPs injected is the same. Regarding AuNSs and AuNSts, results suggest that they adsorb a similar amount of protein despite having very different morphologies. If we focus on the NP surface, this result is difficult to explain, as AuNSts display a much higher surface area than a AuNSs of the same diameter due to the presence of multiple branches on their surface. However, the steric impediment constituted by the spikes of the AuNSts must also be taken into consideration. These two parameters may have opposite effects: while a higher surface area is expected to facilitate protein-NP interactions, the presence of spiky branches may hinder this process.

Additionally, Figure 29C illustrates the corresponding Venn diagram where the common unique protein of the three AuNPs used in the study can be observed. For all NPs, quite complex PCs were revealed. A total number of 229 common proteins were found for the three different morphologies. Some variations are found in the number of unique proteins for the different NPs, which indicates that PC composition was influenced by the NP shape. In particular, AuNSs revealed a total of 36 proteins, more than AuNSts (18 proteins) and AuNRs (9 proteins). Also, several proteins were found to be shared just between two of the three compared morphologies, indicating NP shape as an important factor for PC composition. In a previous study carried out by Deng et al.[46], PC composition of TiO_2 NPs of different morphology (NSs, NRs and NTs) were also compared. Similar results were obtained in this case, where protein identification was carried out by 2D gel electrophoresis and a total of 20 proteins were identified for NSs, 7 for NRs and 8 for NTs. Figure 29D displays a classification of identified proteins in the corona with respect to their MW. It can be observed that the protein profiles are very similar for all AuNPs. Proteins of MW<80 contribute to 75-80% of the PCs formed for all the different AuNPs in agreement with previous investigations.[32, 73, 242] Altogether, these results show that shape affects quantitatively and qualitatively PC formation of AuNPs.

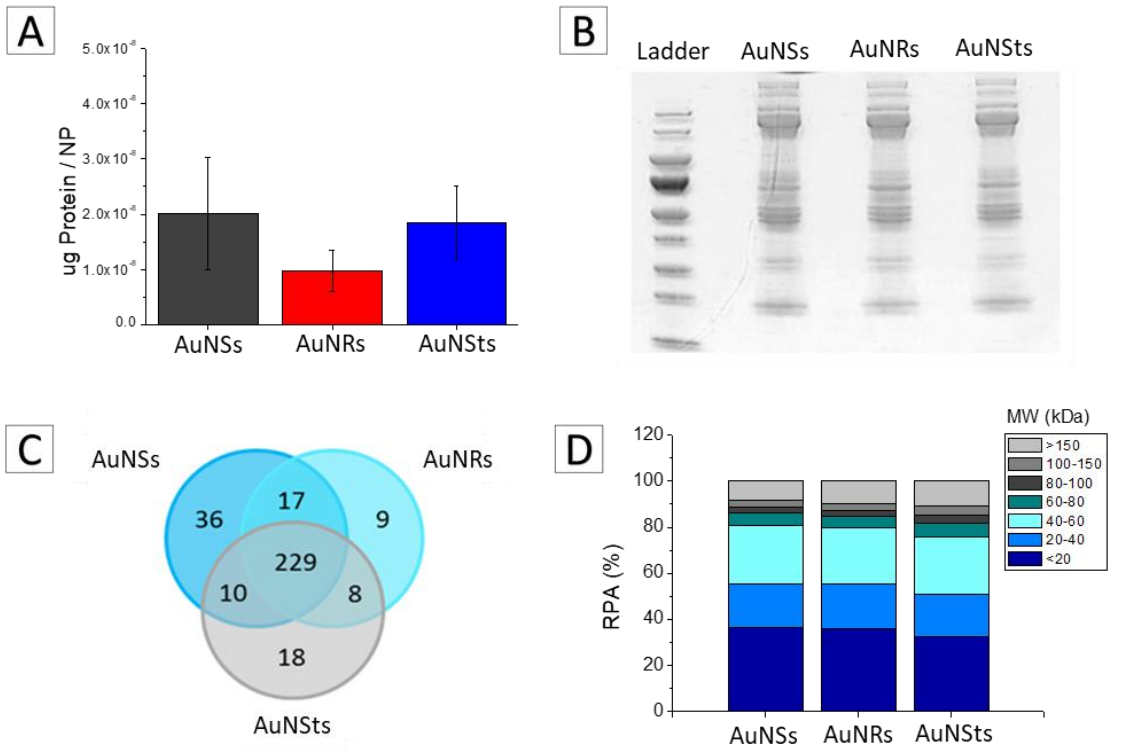

*Figure 29. Comparison of protein adsorption profiles on AuNPs after PC formation. (A) Imperial protein stained SDS-PAGE gel of proteins associated with AuNPs. (B) Comparison of the amount of proteins adsorbed onto AuNPs. The values of µg protein/NP represent the average and standard deviation from three independent experiments (*** indicates p<0.001). (C) Venn diagram displaying the number of unique proteins identified in the in vitro formed coronas, and their respective overlaps. (D) Classification of identified corona proteins, according to their molecular mass.*

Finally, to get a deeper insight on the influence of NP morphology on *in vitro* PC formation, relative protein abundance (RPA) was calculated for each identified protein. Table 2 summarizes the top 20 most abundant proteins adsorbed onto the AuNPs surface. Alpha-2-macroglobulin (A2M) is the most abundant protein for all AuNPs analysed. This protein is a protease inhibitor implicated in fibrillation processes and related with AD.[243] The presence of this protein may be related with the fibre-like structures previously visualized by TEM. Previous publications by Dobrovolskaia et al.[41] and Schäffler et al.[38] reported fibrinogen and serum albumin as the most abundant proteins on the PC of spherical AuNPs. Other related investigations on AuNPs of different functionalization also report serum albumin as the most abundant protein,

which suggests an important role of the NP material in protein interaction. In our case, serum albumin occupies the second place among the top 20 abundant proteins and therefore, it is expected to play an important role on the PC.

AuNSs		AuNRs		AuNSts	
Identified protein	**RPA**	**Identified protein**	**RPA**	**Identified protein**	**RPA**
Alpha-2-macroglobulin	3.01±1.98	Alpha-2-macroglobulin	4.12±0.41	Alpha-2-macroglobulin	4.18±1.59
Serum albumin	2.55±2.10	Serum albumin	2.47±1.00	Serum albumin	2.33±1.72
Ig mu chain C region (Fragment)	2.04±1.13	Fibrinogen gamma chain	2.11±0.14	Ig mu chain C region (Fragment)	1.98±0.17
Apoa1 protein	2.04±1.76	Fibrinogen beta chain	1.90±0.21	Fibrinogen beta chain	1.93±0.24
Fibrinogen beta chain	1.91±0.80	If kappa light chain (Fragment)	1.71±0.40	Fibrinogen gamma chain	1.92±0.14
Fibrinogen gamma chain	1.83±0.84	Anti-colorectal carcinoma light chain	1.60±0.31	Complement C3	1.76±0.25
Apolipoprotein A-I	1.67±0.90	Igk protein	1.56±0.33	Apoe protein	1.73±0.25
Complement C3	1.41±0.08	MCG114299 (Fragment)	1.41±0.24	Apolipoprotein A-I	1.67±0.49
Igk protein	1.41±0.45	Complement C3	1.40±0.13	Apoa1 protein	1.55±1.54
Anti-colorectal carcinoma light chain	1.34±0.35	Serine protease inhibitor A3K	1.35±0.19	Fibrinogen alpha chain	1.48±0.25
IgG1 heavy chain VDJ region (Fragment)	1.31±0.33	Fibrinogen alpha chain	1.32±0.13	Protein Ighv1-42	1.45±0.20
MCG114299 (Fragment)	1.28±0.00	Igk protein	1.29±0.18	If kappa light chain (Fragment)	1.33±0.36
Apoe protein	1.24±0.30	Apoe protein	1.28±0.17	MCG114299 (Fragment)	1.33±0.09
Serine protease inhibitor A3K	1.19±1.06	Ig mu chain C region (Fragment)	1.27±0.34	Anti-colorectal carcinoma light chain	1.23±0.33
ENSMUSG00000076577 protein	1.16±0.39	Apolipoprotein A-I	1.26±0.44	Serine protease inhibitor A3K	1.22±0.58
Igk protein	1.15±0.36	ENSMUSG00000076577 protein	1.25±0.21	IgG1 heavy chain VDJ region (Fragment)	1.21±0.80
If kappa light chain (Fragment)	1.15±1.00	Protein Igkv6-13	1.12±0.21	Igk protein	1.19±0.36
Fibrinogen alpha chain	1.14±0.52	IgG1 heavy chain VDJ region (Fragment)	1.11±0.47	Protein Ighv1-81 (Fragment)	1.14±0.08
Protein Ighv1-81 (Fragment)	1.09±0.17	Protein Ighv1-81 (Fragment)	1.10±0.30	Complement factor H	1.04±0.17
Protein Ighv1-18 (Fragment)	1.01±0.16	Uncharacterized protein	1.04±0.11	Uncharacterized protein	0.98±0.20

Table 2. Most abundant (top 20) proteins identified in the in vitro PC of AuNPs, as identified by LC-MS/MS. RPA values represent the average and standard deviation from three different experiments.

4. Conclusions – Summary of findings.

Current literature gives very limited information about the effect of NP shape on the process of PC formation. Consequently, the present chapter was focused on the investigation of the influence of the NP morphology on the formation of the PC. In this particular case, AuNPs of three different shapes were incubated under *in vitro* conditions in mice plasma in order to study the interactions between proteins and AuNP surfaces.

The methodology developed by Hadjidemetriou et al. was successfully adapted to the recovery and purification of PC-AuNP complexes. Our results indicated that the physico-chemical characteristics of AuNPs were modified due to the interaction of the NP surface

with the proteins and the physiological media. No specific shape-dependent effect could be inferred from these physico-chemical modifications.

A qualitative and quantitative analysis of the protein profile of the corona was performed for every AuNP type. Results showed a very complex PC for every NP shape. Interestingly, the protein profile of the PC was found to be modified as a function of the NP morphology, which leads to our final conclusion: AuNP morphology has an important influence on the protein profile of PCs formed around AuNPs.

Blank page.

CHAPTER 6: *IN VITRO* PROTEIN CORONA ON GOLD NANOSTARS

1. Focus of the Study.

After carefully review of the available literature on PC on AuNPs and the results reported in the previous chapter, we dedicated a further effort toward understanding the influence of NP morphology on PC formation and composition. While there is an extensive body of literature regarding AuNSs and AuNRs, there is barely a single publication that has investigated the PC formed around AuNSts.[165] For these reasons, we continued our studies towards an adequate definition of PC on AuNSts, which are particularly interesting because of their outstanding thermal and optical properties owing to their plasmonic nature. The presence of sharp tips makes them especially sensitive to changes on the environment and therefore, they have been proposed for biosensing applications. Among the numerous synthetic protocols that can be found in the literature, we chose to work with the methodology published by Yuan et al.,[208] where AuNSts are produced without the presence of a surfactant and hence, they are quite easy to functionalize. We decided to produce AuNSts with different spike length and constant quasi-spherical core in order to investigate the effect of small morphological changes on protein-NP interactions. It is important to highlight the importance of using an adequate synthetic approach, which allows the control of spike length by simply changing a reaction parameter.

In this context, we present an *in vitro* study of the PC formed around AuNSts of constant core size and different spike length here named as AuNSts 1, AuNSts 2, AuNSts 3 and AuNSts 4 (from larger to shorter spike length). All AuNPs involved in this study were functionalized with carboxylic PEG (MW = 10 kDa). Human plasma was chosen as incubation media for this project. For PC formation, AuNPs were incubated in human plasma for 10 minutes at 250 rpm and at 37°C of temperature in an incubator shaker. In this case, human plasma was chosen aiming to obtain the human *in vitro* PC. Afterwards, AuNP-PC complexes were separated from loosely and unbound proteins by a combination of size exclusion chromatography followed by membrane ultrafiltration. Physico-chemical properties of AuNPs before and after interaction with proteins were monitored by DLS, ZP measurements, UV-Visible Spectroscopy and TEM. PCs formed

after plasma incubation were qualitatively and quantitatively analysed by LC-MS/MS revealing a quite complex corona for all AuNPs. Additionally, cell uptake and toxicity of AuNSts of different spike length with and without PC were investigated and compared for a healthy and a cancer cell line.

2. Results. Physico-chemical Characterization.

AuNSts were prepared by a silver-assisted seeded-growth methodology previously reported by H. Yuan et al.[208] This surfactant-free synthesis allows to control the length of the branches by simply changing the amount of silver nitrate ($AgNO_3$) used during the reaction. A smaller amount of $AgNO_3$ results on AuNSts of shorter spikes without modifying the diameter of the NP core, while a larger amount of $AgNO_3$ leads to sharper branches. A total number of four AuNSs of different spike length were prepared. Samples were named AuNSs 1 AuNSts, AuNSts 3 and AuNSts 4, being AuNSts 1 the one with longer spikes and AuNSts 4 the one with shorter spikes. AuNSts were functionalized with thiolated PEG (Mw = 10 KDa) containing carboxylic acid-functional groups immediately after synthesis by ligand exchange in order stabilize the NP surface and avoid the usual reshaping process.[202, 244]

	AuNSts 1		AuNSts 2		AuNSts 3		AuNSts 4	
	No PC	PC	No PC	PC	No PC	PC	No PC	PC
D_H (nm)	96.6±0.4	172.5±3.1	81.9±0.8	187.4±2.9	69.3±0.7	134.4±2.5	62.4±0.3	115.4±2.0
ZP (mV)	-45.1±1.4	-15.2±0.3	-44.2±1.7	-13.7±0.2	-46.7±0.8	-14.1±0.2	-40.0±2.2	-13.4±0.1
PDI	0.149±0.009	0.269±0.010	0.204±0.002	0.282±0.004	0.282±0.004	0.371±0.011	0.284±0.0.015	0.482±0.024

Table 3. Effect of in vitro PC formation on the physico-chemical properties of AuNPs before and after interaction with proteins: D_H (nm), ZP (mV) and PDI.

Initial characterization of all NPs involved in this study is summarized in Figures 29 and 30 and Table 3. Physico-chemical and morphological characteristic of the samples before and after interaction with human plasma were assessed by UV-Visible Spectroscopy, TEM, DLS and ZP measurements. TEM visualization revealed well-dispersed and fairly monodispersed samples with quasi-spherical core of similar size. Measurements of total diameter, core diameter and spike length were determined by image analysis of at least 300 AuNSts. D_H and PDI were analysed by DLS measurements. Results showed a single

band for AuNSts 1 and AuNSts 2, while a smaller peak appears in the case of AuNSts 3 and AuNSts 4. This smaller band may be attributed to a higher level of anisotropy of these type of stars in comparison with their spikiest counterparts. Functionalization with carboxylic PEG results in ZP with negative values. Tip-confined LSPRs were determined by UV-Visible spectroscopy: AuNSts 1 – 830 nm, AuNSts 2 – 780 nm, AuNSts 3 – 686 nm and AuNSts 4 – 542 nm.

Plasmonic response of AuNSts before and after incubation with plasma proteins was recorded by UV-Visible Spectroscopy (Figure 30). It is surprising to observe that, contrary to the usually reported red-shift of the absorbance band of the material after protein interaction, a shift towards lower wavelength values is presented instead for all AuNPs involved in our study. This blue-shift appears to increase when the length of the AuNSts branch decreases and is often attributed to the reshaping of the tips.[244] AuNSts are especially prone to suffer this effect due to their morphological properties, which involve the presence of high energetic facets that must be stabilized by using an adequate surfactant or stabilizing agent. However, it seems that even though the surface was protected with a polymeric coating, interaction with proteins affects somehow NP shape, especially for AuNSts 3 and AuNSts 4. This could be explained by an insufficient coverage of the AuNSts, which is likely to occur when smaller NPs are functionalized with a high molecular PEG coating as the density of the polymer will not be high enough.[245] It is also important to notice that PEG grafting has been defined for NPs with a very regular surface such as spheres or rods, whereas for AuNSts due to their more irregular shape, the density is not so easy to predict. It is also true that this blue-shift may be a consequence of an increase in the Rayleight scattering due to protein adsorption.

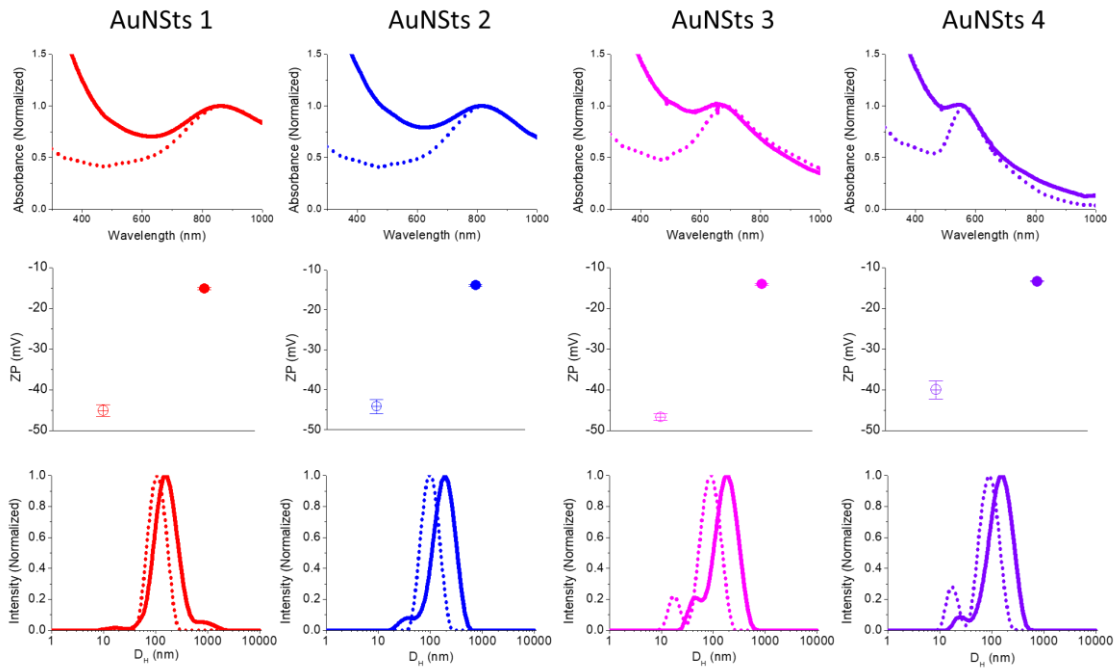

Figure 30. Representation of the physicochemical characteristics of all AuNSts involved in the study. Colours correspond to the different AuNPs: red – AuNSts 1, blue – AuNSts 2, magenta – AuNSts 3 and violet – AuNSts 4. Physico-chemical properties: 1st row – UV-Visible spectra; 2nd row – Surface Charge and 3rd row – H_D. Black line and coloured line correspond to the NP before and after PC formation, respectively.

ZP measurements before and after interaction with plasma proteins demonstrated that the surface charge of all AuNSts remains negative after protein adsorption, which is in agreement with previous studies.[38, 41] However, it is evident from the graphical representation that all ZPs have shifted towards less negative values, which suggests a preferential interaction with positively charged proteins. It has been previously established that negatively charged NPs do not exclusively interact with positively charged proteins as electrostatic interactions are not the only force involved. Neutral, positive and negatively charged proteins can be found in the corona, regardless the surface charge of the studied material. The presence of negatively charged proteins is usually explained by a sequential protein binding model, where positively charged proteins are the first ones to be adsorbed on the NP surface, followed by negative ones.[246]

PDI and D_H modifications due to PC formation were monitored by DLS. As it can be observed in Figure 30, both PDI and D_H were found to increase after interaction with proteins, which is in agreement with previous findings.[187] Difference between final and initial D_H was calculated and plotted for better comparison (Figure 31). Interestingly, a trend can be observed: the shorter the spike, the higher the difference in D_H, which suggests that the volume of the corona is higher for AuNSts with shorter spikes.

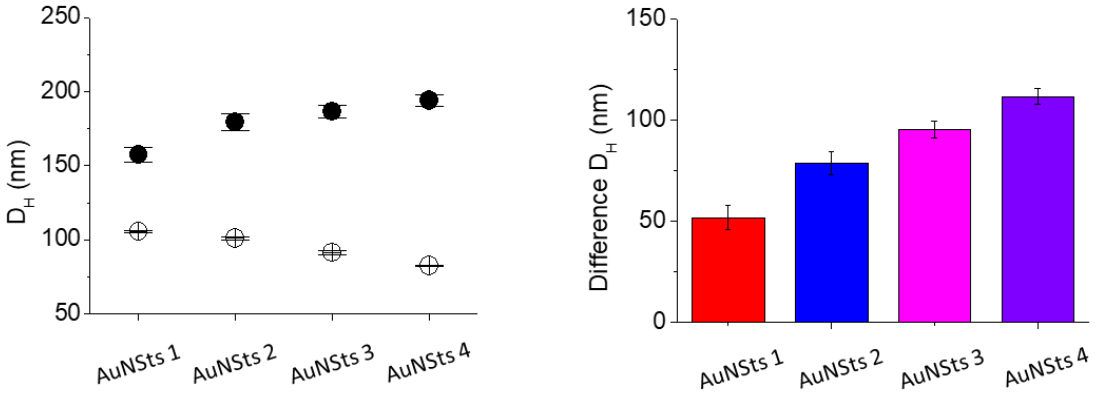

Figure 31. Representation of the difference in D_H before and after PC formation. First graph represents the initial D_H (black) and final D_H (red, after interaction with proteins). Right graph is a representation of this difference for each of the AuNSts, which corresponds to the mean and standard deviation for 4 individual replicates.

Finally, TEM visualization shows no significant changes in AuNSts morphology as well as good dispersion of corona coated-NPs after incubation with human plasma (Figure 32). As previously mentioned, although UV-Visible spectroscopy suggests a reshaping of some of the AuNSts involved in this study, the difference is not visible by TEM. Again, the blue-shift may be explained by increase of Rayleight scattering due to protein interactions and not by morphological changes.

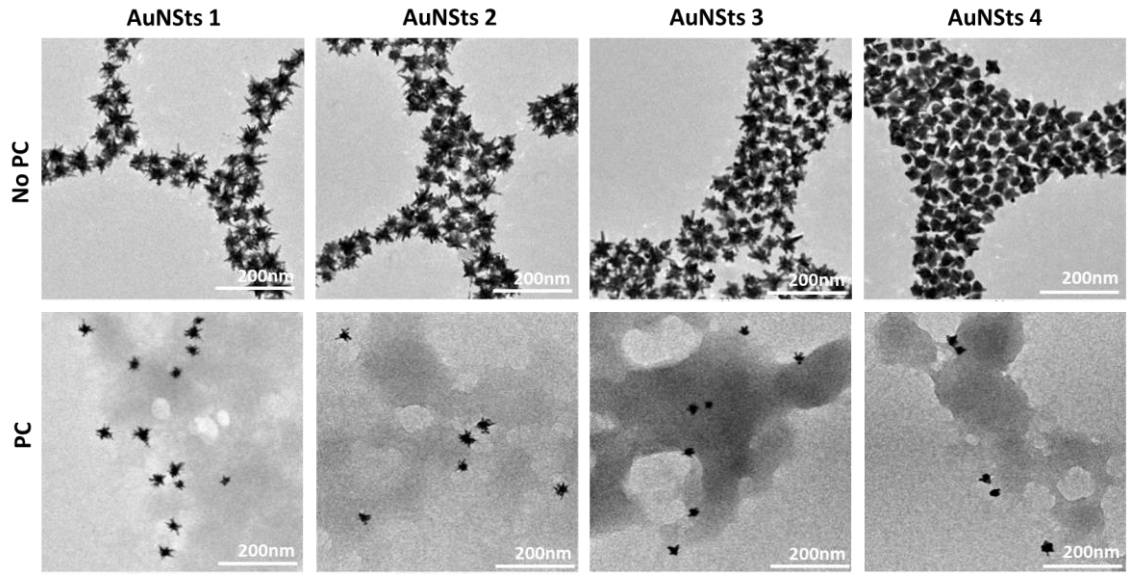

Figure 32. Morphological characterization of the AuNSts by TEM before and after protein interaction. From left to right: AuNSts 1, AuNSts 2, AuNSts 3 and AuNSts 4.

3. Results. Protein Corona Characterization.

Proteins of corona coated-AuNPs were separated by SDS-PAGE and their protein profile was visualized by Imperial Protein Staining. Figure 33 illustrates that PC composition was both qualitatively and quantitatively affected by the spike length of AuNSts. An interesting trend can be observed: the larger the spike, the lower the amount of proteins that interact with the surface of the NP. These results were further confirmed by quantification of gold and proteins present on these complexes by ICP-MS and BCA Assay respectively, which allowed calculation of the μg of protein adsorbed per NP. Although we have previously reported a comparative study showing that size and shape of the NP were important parameters when defining the corona,[187] it was surprising to observe a significant change in PC composition as a consequence of a small change in the morphology of one specific type of NP. These results suggest that PC formation is highly sensitive to the morphological properties of the NM. We hypothesize that proteins may be able to interact much more easily with AuNSts with shorter spikes as the steric impediment is lower than in the case of AuNSts with longer spikes.

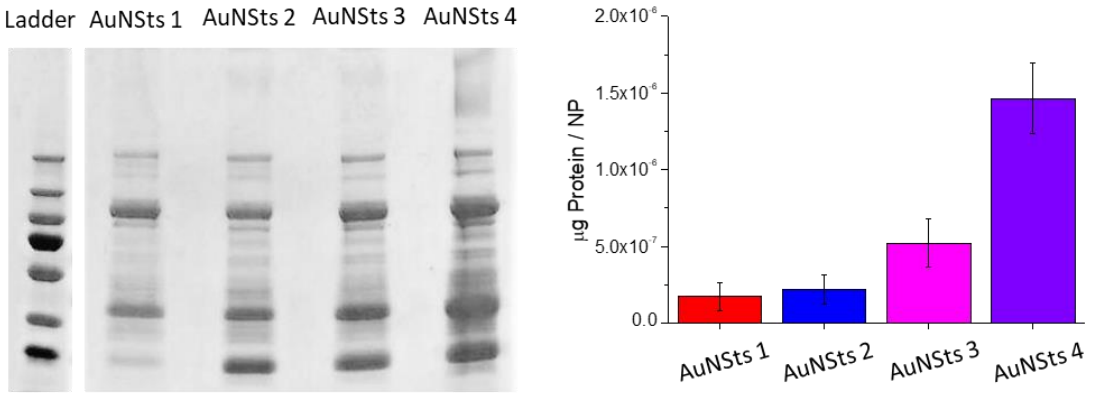

Figure 33. Left: SDS-PAGE gel showing the protein profile of the corona of the different AuNPs utilized in this study; Right: Information from ICP-MS (gold content) and BCA assay (protein content) was used to calculate and represent the mass of protein adsorbed per AuNP. The values correspond to the mean and standard deviation of 4 individual replicates.

A comprehensive comparison of PC profiles for the different types of AuNSts was carried out by Nano LC-MS/MS, while data analysis was performed by using Progenesis Software. This technique is extensively used for the detection of a great number of molecules in complex samples such as biological fluids, and it allowed detection of around 150 different proteins on the corona formed on the surface of our AuNSts. Figure 5 illustrates the protein profile of all NPs involved in the study classifying the proteins by their MW. As it can be seen in the graph, almost 40% of the corona is constituted by proteins of MW oscillating between 40 and 79 kDa. For all NPs, contribution of proteins of MW between 80 and 150 kDa is less than 10%. As reported previously by other scientific groups, 80% of the corona is defined by proteins of MW below 80 kDa.[73, 242] It is important to notice that these studies were done under dynamic conditions and for lipid NP. In our previous *in vivo* PC study on AuNPs, similar results were obtained. This suggests that type of incubation (static or dynamic) does not seem to have a significant influence on the Mw of the adsorbed proteins. Some fluctuations in the RPA of the different proteins is observed depending on the type of star, though these changes do not follow a particular trend. A similar graphical representation illustrates the protein profile of AuNSts classifying proteins by biological function (Figure 34). Immunoglobulins are the most abundant type of protein on the PC of AuNSts, making

up around 30-40% of the corona. This family of proteins plays a critical role in the response of the immune system when an unknown NM or exogenous object enters the body.[243] Also known as antibodies, immunoglobulins are chemically described glycoproteins produced by white blood cells and are able to specifically recognize and bind antigens such as bacteria or viruses, contributing to their elimination. Presence of this kind of protein is usually thought to be desirable as they are responsible for cellular uptake. However, it was recently demonstrated that pre-coating a NP with opsonins does not lead to an increased cellular internalization.[52] Another protein family quite abundant in the corona is acute phase proteins, which constitute 20-25% of the corona of AuNSts. This kind of proteins can be divided in positive and negative acute phase proteins and are usually segregated in response to injury or inflammation. Other protein families present in the corona are coagulation proteins (around 10%), complement proteins (around 10%) and in a smaller percentage, lipoproteins and tissue leakage proteins. It is important to notice that albumin itself already constitutes around 20% of the corona.[243]

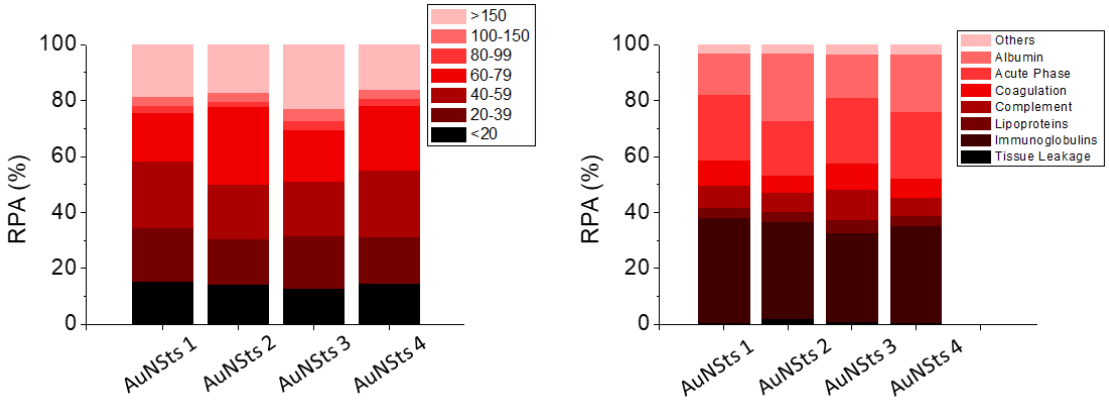

Figure 34. Left graph represents the proteins of the PC of the NPs classified by their MW. Right graph is similar but the classification of proteins is made by biological function.

Top 20 most abundant proteins found on the corona of AuNSts are summarized in Table 4. It can be observed that HSA is the most abundant protein for all AuNSts involved in this study. These results are in agreement with previous investigations on the PC formed on the surface of AuNPs where, independent of size, shape or functionalization of the NP, HSA was as well found to the be at the top of the most abundant protein list.[41, 59] This protein plays a fundamental role on the transport of many different biomolecules

through the body. Several studies have revealed that HSA presence in the corona modulates its physico-chemical properties and influences other biological processes such as cell internalization or cytotoxicity.[247] As it can be observed in the table, HSA represents approximately the 15-25% of the corona of all AuNSts under investigation and therefore, it could probably affect interaction with other biological entities.

AuNSts 1		AuNSts 2		AuNSts 3		AuNSts 4	
Description	**Average %NA**	**Description**	**Average %NA**	**Description**	**Average %NA**	**Description**	**Average %NA**
Serum albumin	14.60	Serum albumin	23.95	Serum albumin	15.32	Serum albumin	20.58
Ig kappa chain C region	10.86	Alpha-2-macroglobulin	10.73	Alpha-2-macroglobulin	12.73	Ig kappa chain C region	10.56
Alpha-2-macroglobulin	10.67	Ig kappa chain C region	9.75	Ig kappa chain C region	9.37	Alpha-2-macroglobulin	10.46
Ig gamma-1 chain C region	8.28	Ig mu chain C region	7.26	Ig gamma-1 chain C region	7.48	Haptoglobin	7.75
Haptoglobin	8.08	Ig gamma-1 chain C region	6.57	Ig alpha-1 chain C region	4.92	Ig gamma-1 chain C region	6.41
Ig mu chain C region	5.74	Haptoglobin	3.71	Haptoglobin	4.85	Ig mu chain C region	6.36
Ig alpha-1 chain C region	4.76	Ig alpha-1 chain C region	3.67	Complement C3	4.44	Ig alpha-1 chain C region	4.32
Fibrinogen gamma chain	3.52	Fibrinogen gamma chain	2.16	Ig mu chain C region	3.82	Fibrinogen gamma chain	2.55
Complement C3	3.33	Immunoglobulin lambda-like polypeptide 5	2.15	Fibrinogen gamma chain	3.21	Complement C3	2.28
Immunoglobulin lambda-like polypeptide 5	2.38	Complement C3	2.09	Apolipoprotein B-100	2.67	Immunoglobulin lambda-like polypeptide 5	2.12
Fibrinogen beta chain	2.25	Ig lambda-2 chain C regions	1.88	Fibrinogen beta chain	2.46	Fibrinogen alpha chain	1.89
Apolipoprotein B-100	1.99	Apolipoprotein B-100	1.83	Fibrinogen alpha chain	2.09	Ig lambda-2 chain C regions	1.63
Ig lambda-2 chain C regions	1.97	Fibrinogen beta chain	1.74	Immunoglobulin lambda-like polypeptide 5	1.74	Fibrinogen beta chain	1.61
Fibrinogen alpha chain	1.88	Alpha-1-antitrypsin	1.10	Ceruloplasmin	1.48	Apolipoprotein B-100	1.37
Ceruloplasmin	1.11	Ceruloplasmin	1.10	Ig lambda-2 chain C regions	1.43	Ceruloplasmin	1.32
Complement C4-B	0.96	Fibrinogen alpha chain	1.07	Inter-alpha-trypsin inhibitor heavy chain H2	1.40	Apolipoprotein A-I	1.19
Alpha-1-antitrypsin	0.94	Apolipoprotein A-I	1.06	Complement C4-B	1.33	Alpha-1-antitrypsin	1.15
Fibronectin	0.91	Complement C4-B	0.93	Plasma protease C1 inhibitor	1.02	Plasma protease C1 inhibitor	1.11
Inter-alpha-trypsin inhibitor heavy chain H2	0.87	Plasma protease C1 inhibitor	0.91	C4b-binding protein alpha chain	0.90	Inter-alpha-trypsin inhibitor heavy chain H2	0.78
Apolipoprotein A-I	0.84	Inter-alpha-trypsin inhibitor heavy chain H2	0.85	Alpha-1-antitrypsin	0.89	Complement C4-B	0.68

Table 4. Most abundant (top 20) proteins identified in the in vitro PC of AuNSts, as identified by LC-MS/MS. Average %NA values represent the average and standard deviation from three different experiments.

Interestingly, even though around 150 different proteins have been detected within the corona, the abundance of the top 20 proteins is enough to define more than 75% of the corona composition. In other words, although the variety of proteins is quite rich, majority of the proteins contribute in a very low proportion in comparison to the top 20 ones. Apart from HSA, several immunoglobulins can be found within the table, which is expected knowing that this protein family represents 30-40 % of corona proteins. Additionally, complement proteins, fibrinogen and A2M are also observed.

Data analysis was carried out by using Progenesis proteomic Software. Protein profile of AuNSts 1 was compared individually with protein profiles of the other AuNSts. Progenesis was utilized to detect the significant changes on RPA of individual proteins. Figure 33 shows the heatmaps obtained by using Perseus Software representing the difference in the amount of certain proteins of AuNSts 2, AuNSts 3 and AuNSts 4 in comparison with those of AuNSts 1. Proteins present in higher amount are displayed in red, while proteins present in lower amount are displayed in green. Looking attentively the heatmaps, one can observe a trend where the differences in the number of these particular proteins increase when the spike length changes, changing from 33 in the case of AuNSts 2 to 41 in the case of the comparison with AuNSts 4. These results suggest confirm that the slightest change in the morphology of AuNSts may have an impact on the PC composition.

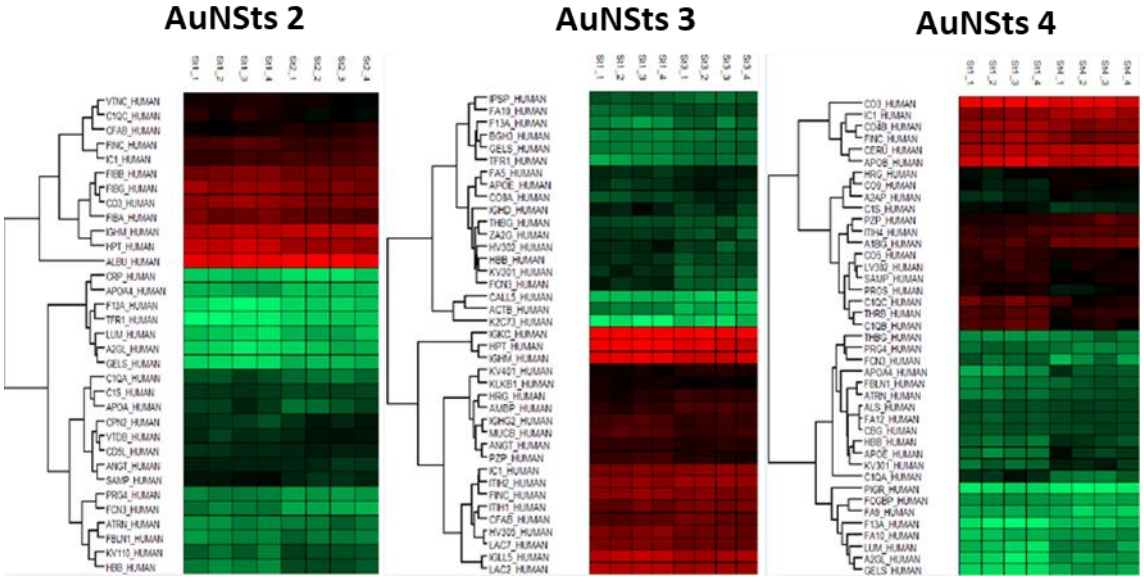

Figure 35. Heatmaps showing common proteins on the surface of AuNSts and their relative amount with respect to AuNSts 1.

Finally, cell internalization of AuNSts of different spike length in absence and presence of PC was investigated. Firstly, toxicity of the material at 3 different concentrations (0.01 mM, 0.1 mM and 1 mM) was evaluated by MTT assay (Figure 36). No significant toxicity was reported, which is in agreement with numerous studies on biocompatibility of AuNPs.[248]

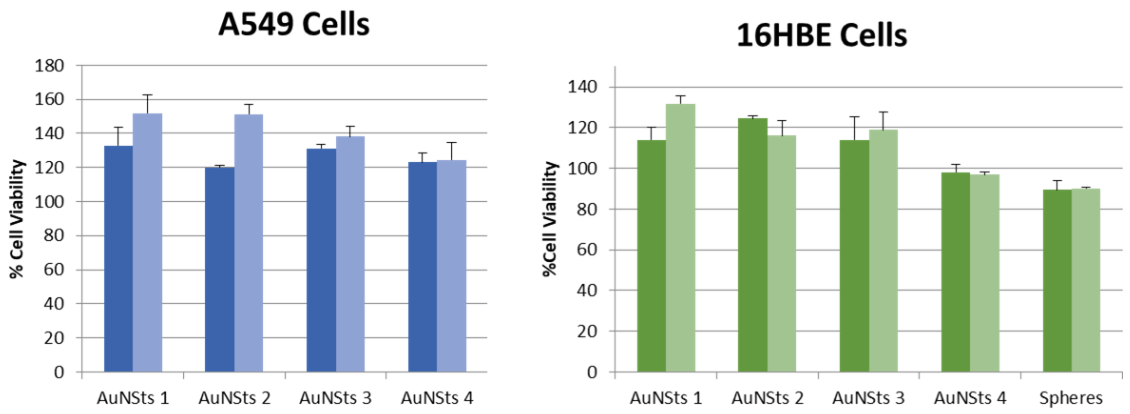

Figure 36: MTT Assay results for A549 and 16HBE cell lines in presence and absence of PC. The values correspond to the mean and standard deviation of 4 individual replicates.

Figure 37 shows a graphical representation of the amount of gold (in µg) detected per cell. Although the general amount of internalized gold is quite low in absence of PC, A549 cell line displays a higher uptake than 16HBE cell line, which could be explained by the higher activity usually exhibited by cancer cell lines. In the case of 16HBE cell line, PC produces a rise of the internalization.

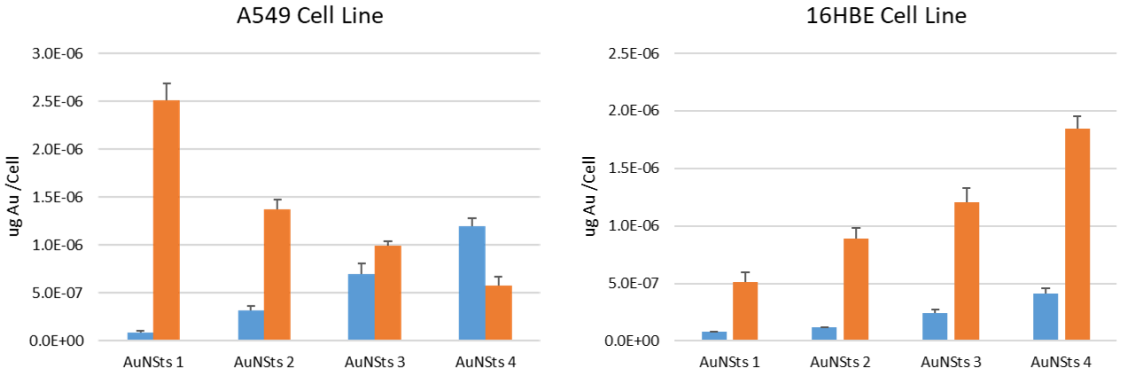

Figure 37. Cell internalization results for A549 and 16HBE cell lines in presence (orange) and absence (blue) of PC. The values correspond to the mean and standard deviation of 4 individual replicates.

Numerous publications have been focused on PC influence on cellular uptake, though both increase and decrease of the internalization have been reported and thus, NP characteristics and experimental protocols must be carefully chosen and defined.[26] Remarkably, A549 cells present opposite trend with and without PC coating. In order to confirm these results, TEM and confocal microscopy were used to try to visualize AuNSts

1 and AuNSts 4 in A549 cells (Figures 38 and 39). Unfortunately, no AuNPs are clearly observed, which may be due to the very small amount of gold internalized.

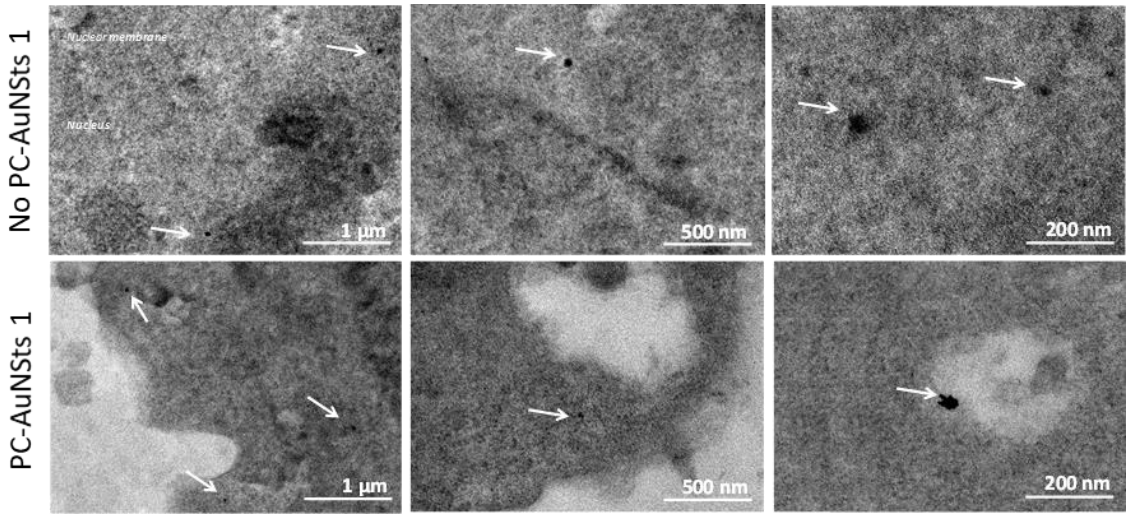

Figure 38. TEM visualization of AuNSs 1 with and without corona internalized in A549 cells. It was not possible in many occasions to distinguish between cell vesicles and AuNSs as the quality of the image was not good enough.

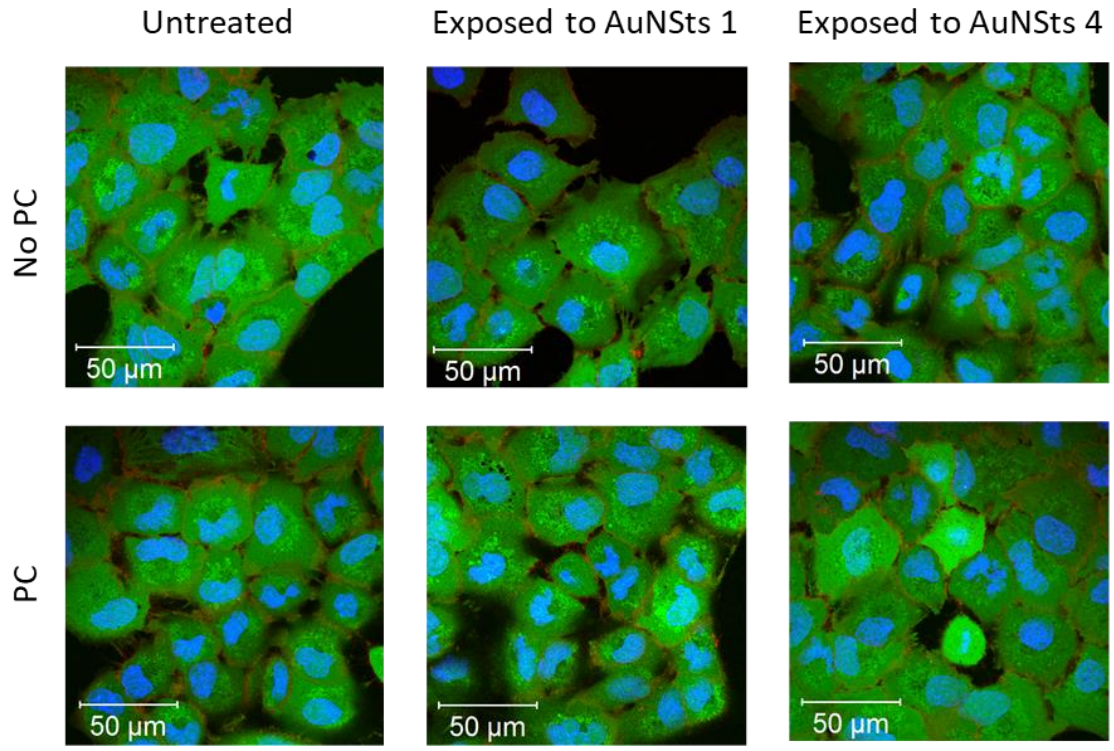

Figures 39: Confocal microscopy images of A549 cells before and after AuNSs exposure.

4. Conclusions – Summary of findings.

In this particular case, the investigation focused on the effect of the length of the spikes of AuNSts on PC formation. AuNSts with four different spike lengths and similar core size were incubated in plasma under *in vitro* conditions for the study of protein-NP interactions.

Regarding the physico-chemical characteristics of NPs before and after incubation, our results suggest that the spike length is an important parameter that must be taken into account in order to predict PC formation on a NP. In particular, a tendency to interact with a higher number of proteins is showed to be dependent on the spike length of the AuNSt: the shorter the spike, the larger the amount of proteins that interact with the NP surface.

Qualitative and quantitative analysis of the proteins attached on each AuNSt surface revealed complex PC formed for all AuNSt, being the protein profiles different depending on the spike length of the NP. In addition, the amount of certain proteins was found to fluctuate as a function of the type of AuNSt, highlighting once again the importance of the differences in the morphology of a NP.

Finally, a cell culture study was carried out to investigate the toxicity and cell internalization of these AuNSts. Two different cell types were used: A549 and 16HBE. AuNSts were found to be non-cytotoxic for both cell types. Interestingly, cell internalization studies suggested an important influence of the spike length for the internalization of both, bare- and corona-coated AuNSts, which also depends on the cell type. More experiments would be required to confirm these results.

Blank page.

CHAPTER 7: *IN VIVO* PROTEIN CORONA ON GOLD NANOPARTICLES

1. Focus of the Study.

Previous chapters have been dedicated to the study and characterization of the PC formed onto the surface of PEGylated AuNPs. In particular, previous projects have been focused on how physico-chemical parameters such as the dimensions and the morphology of the NP may influence PC formation and composition. The results obtained confirmed our hypothesis, clearly showing that the shape of the NP plays a fundamental role on PC formation. Although this information is important and must be taken into consideration for further studies, it is important to keep in mind that these experiments were performed under *in vitro* conditions and therefore, they are not fully representative of a realistic situation. Previous investigations carried out by Kostarelos group on the PC formed on lipidic NPs have shown that the *in vivo* formed PC is significantly different from its *in vitro* counterpart and thus, though the information obtained from the latter is very useful, it does not completely correspond with the real picture.[73] Many fundamental parameters characteristic of *in vivo* incubations such as dynamic flow, contact with other biological entities within the blood and their interactions are being somehow overlooked and ignored. Therefore, in order to get more realistic results, we decided to focus our next project on the preparation, isolation and characterization of the *in vivo* PC formed on the surface of AuNPs after injection in CD-1 female mice.

For this purpose, a previously developed methodology for the separation of the *in vivo* PC on liposomes was applied. We present here a detailed study of *in vivo* PC formation and composition after blood circulation of AuNPs of different dimensions and morphology aiming to investigate the effect of size and shape on the PC constituted under *in vivo* blood flow conditions. AuNRs and AuNSts with overall sizes of 40 and 70nm were intravenously administered and recovered from the blood circulation of mice, to be later isolated and purified. AuNSs were not included in this study as we were not able to separate them from blood. Physico-chemical properties of *in vivo* formed PC-AuNP complexes were characterized by DLS, ZP measurements, UV-Visible Spectroscopy and

TEM. Likewise, PC-NP profiles were qualitatively and quantitatively characterized by high-resolution LC-MS/MS based proteomics.

2. Results. Physico-Chemical Characterization.

The synthesis of AuNRs and AuNSts was based on extensively reported seeded-growth methods,[114-116, 208] followed by functionalization with thiolated PEG (MW = 10kDa) containing a carboxylic acid end-functional group.[202] Initial characterization of the AuNPs used in this study is summarized in Figures 37 and 38, and Table 5. DLS, ZP, UV-Visible spectroscopy and TEM measurements were performed prior to intravenous administration of AuNPs, to assess their properties and morphology. TEM images revealed well dispersed NPs of the following dimensions: AuNRs of 40x11 and 70x15 nm and AuNSts of 40 and 70 nm total diameter. Whereas DLS measurements of AuNSts show a single peak for the D_H, AuNRs exhibited two different peaks, mostly due to their anisotropic shape. All AuNPs were functionalized with PEG containing carboxylic acid groups, which conferred a negative surface charge indicated by a ZP value around -28 mV. LSPRs were determined by UV-Visible spectroscopy to be 701 nm and 853 nm for short and long AuNRs, respectively, while the tip-confined LSPR for small and big AuNSts are 763 nm and 940 nm, respectively.

	AuNRs 40		AuNSts 40		AuNRs 70		AuNSts 70	
	No PC	PC	No PC	PC	No PC	PC	No PC	PC
D_H (nm)	21.2±0.1	83.3±7.5	82.1±2.7	80.0±0.7	24.9±0.3	75.7±6.2	122.0±1.3	93.4±4.1
ZP (mV)	-28.6±1.5	-36.8±2.1	-29.3±0.2	-31.8±2.9	-28.8±0.4	-20.3±0.9	-33.6±0.2	-18.9±0.4
PDI	0.786±0.002	0.315±0.088	0.245±0.008	0.232±0.080	0.378±0.003	0.388±0.110	0.101±0.007	0.388±0.017

Table 5. Effect of in vivo PC formation on the physico-chemical properties of AuNPs before and after interaction with proteins: D_H (nm), ZP (mV) and PDI.

Even though the overall protein adsorption is known to be hindered by functionalization of NPs with PEG, it cannot be fully supressed and a certain amount of plasma proteins do adsorb on the NP surfaces, irrespective of the density and MW of the PEG coating.[19, 41, 50] In agreement with these previous findings, we found in the present study that PEGylated AuNPs are not completely inert and interact with plasma proteins upon intravenous administration in rodents. To investigate the *in vivo* formation of PC, AuNPs

were intravenously administered via tail injection in CD-1 mice and recovered by cardiac puncture, 10 min post-injection. Apart from being inexpensive, robust and readily available, CD-1 mice are an outbread strain, widely employed for biomedical research and are ideal as a general multipurpose model for safety and pharmacological testing.[249] Cardiac puncture is employed in order to collect a single, good quality and large amount of blood from the experimental animals.[250] Plasma was then prepared from recovered blood by centrifugation. A protocol combining SEC and membrane ultrafiltration was used for the isolation of AuNP-corona complexes from unbound and loosely bound plasma proteins, as previously described.

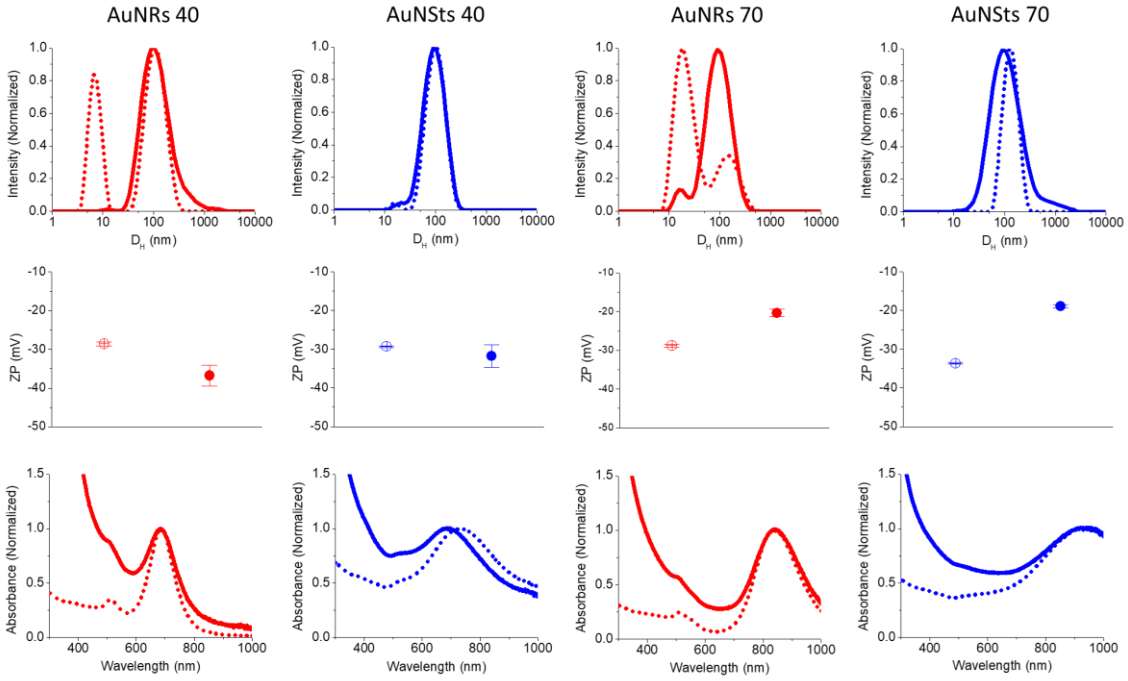

Figure 40. The effect of PC formation on the physico-chemical properties of AuNPs. DLS size distribution, ZP and UV-VIS extinction spectra are depicted for AuNRs and AuNSts before (dotted lines) and after (solid lines) interaction with CD-1 mouse plasma in vivo. Z-potential values are given before (empty dot) and after (full dot) PC formation, error bars refer to the standard deviation of 4 individual measurements.

DLS and ZP comparative measurements before and after *in vivo* incubation demonstrated that, in all cases, the D_H did not change significantly and the surface charge remained negative. These results are in agreement with previous studies suggesting that negatively charged NPs do not exclusively interact with positively

charged proteins, as electrostatic interactions are not the only driving force behind NP-corona interactions.[38, 41] Interestingly, only for 70nm AuNRs and AuNSts the ZP was shifted toward less negative values, suggesting preferential interaction with positively charged proteins. The presence of negatively charged proteins can be explained by a sequential model of protein binding, in which positively charged proteins initially bind the NP, followed by negatively charged ones.[41] In the case of AuNRs, DLS measurements show that the initial distribution with two peaks merges into a single one after interaction with proteins, which has been previously reported by E. Yeo et al.[241] for AuNRs of 46x20 nm incubated in human serum under *in vitro* conditions, and is likely related to a less anisotropic morphology of the formed complex upon protein adsorption.

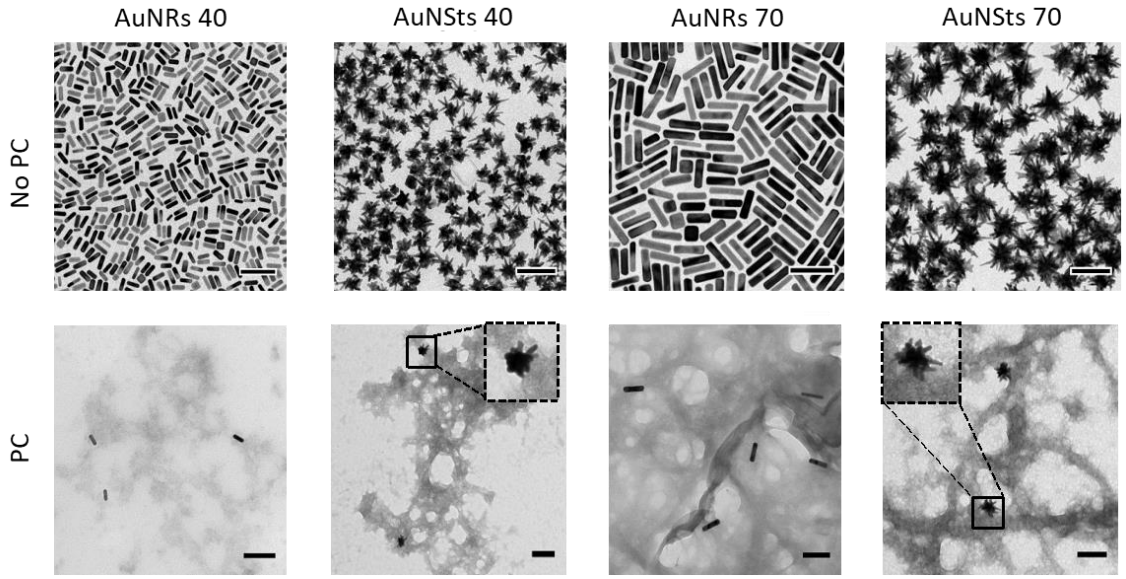

Figure 41. Representative TEM images of AuNRs and AuNSts, before (upper panel) and after (lower panel) interaction with CD-1 mouse plasma in vivo. All scale bars are 100 nm.

Regarding the plasmonic response of AuNPs, it has been reported that *in vitro* interaction of AuNPs with plasma proteins leads to a 5-10 nm red-shift in the LSPR band of spherical AuNPs when recorded in a biological medium, due to an increase in the local refractive index around the particles.[57, 184] We recorded the UV-Visible spectra before and after *in vivo* administration and recovery of AuNRs and AuNSts. As shown in Figure 37, no significant changes were observed in the LSPR position, except for a blue-shift in

the case of 40 nm AuNSts, which may be related to partial reshaping of AuNSts. The morphology of AuNSts involves highly energetic facets, which are likely to undergo reshaping unless properly stabilized by a suitable capping agent, typically containing thiol groups.[251] An example of a similar observation has been reported for AuNSts capped with polyvinylpyrrolidone (PVP), which readily reshaped by simply adding small amounts of CTAB.[244] We investigated by TEM the reshaping of AuNSts as a result of its *in vivo* interaction with plasma proteins. As shown in Figure 39 TEM images of AuNSts (and AuNRs) after recovery and purification revealed well-dispersed NPs in the presence of protein molecules adsorbed onto their surface, as expected for PC formation. Several washing steps were performed to confirm the PC-NP complex was correctly isolated from the free proteins.

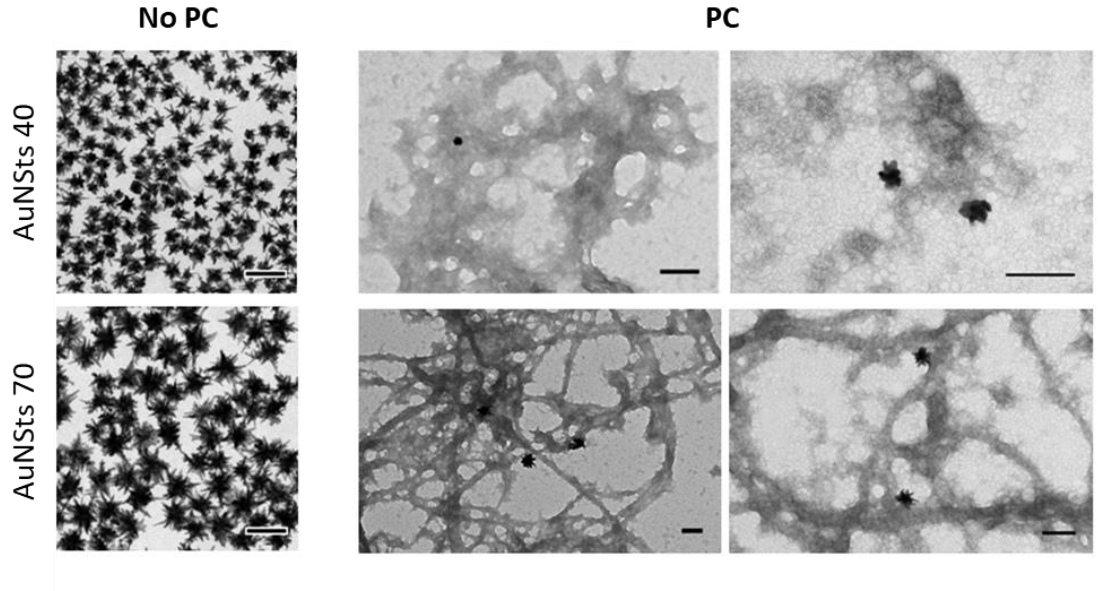

Figure 42. TEM visualization of AuNSts 40 and 70 nm before and after interaction with proteins. AuNSts 40 nm undergo reshaping after PC formation while AuNSts 70 nm morphology is kept intact.

TEM images confirm that 40 nm AuNSts had undergone reshaping, while AuNSts of 70 nm remained intact (Figure 42). As the conditions of the experiments have been the same for all NPs during the whole experiment, the reshaping process could be explained by the different size of the NPs. Even though AuNSts employed in this study are capped

with thiolated PEG, the high MW (10kDa) is likely to lead to insufficient surface coverage for smaller AuNSts. PC-coated NPs showed fibre-like structures.

3. Results. Protein Corona Characterization.

Proteins adsorbed on AuNPs *in vivo* were separated by SDS-PAGE and visualized by Imperial Protein staining (Figure 43). The composition of PCs was found to quantitatively and qualitatively differ between the different types of AuNPs, as a first indication that size and shape do influence PC formation under *in vivo* blood-flow conditions. As illustrated in Figure 43A, 70 nm AuNSts were found to adsorb a significantly larger amount of protein, which could be explained by the higher surface area that AuNSts exhibit as compared to their rod-like counterparts. Indeed, SDS-PAGE results show that AuNSts adsorbed a larger amount of protein than AuNRs, which was further reinforced by quantification of the total amount of protein adsorbed onto the different types of AuNPs, as illustrated in Figure 43B.

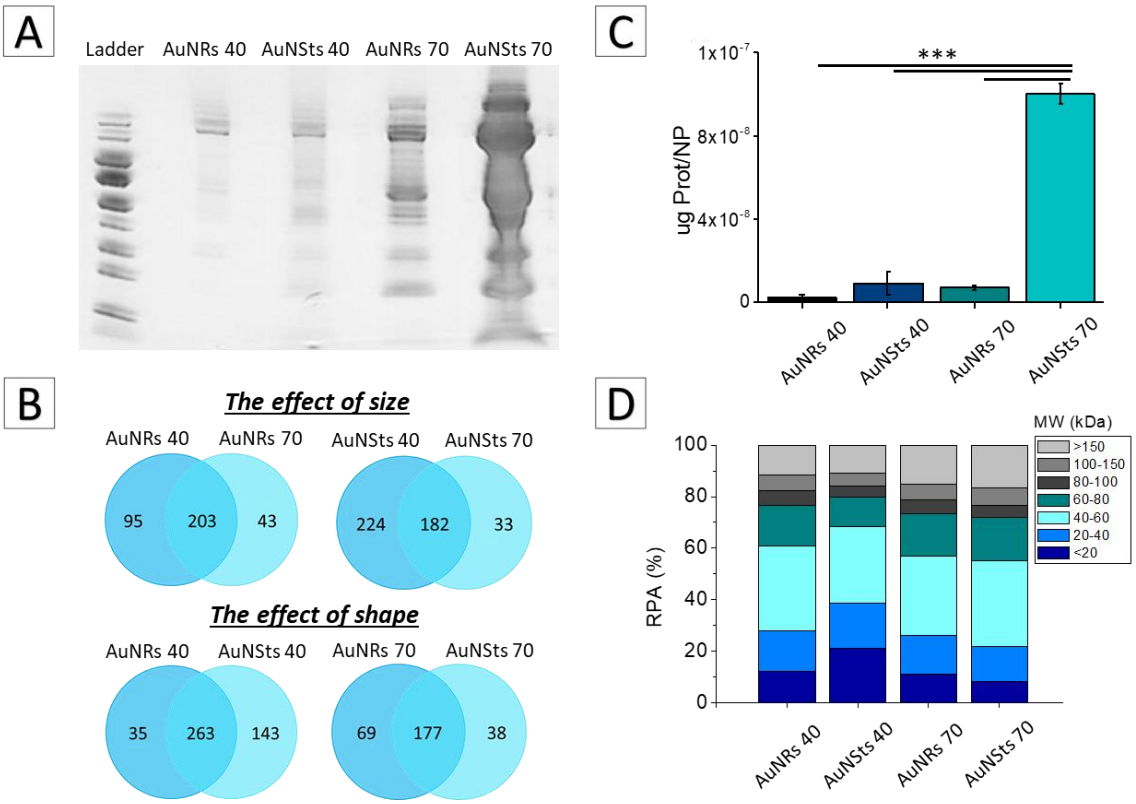

*Figure 43. Comparison of protein adsorption profiles on AuNPs after in vivo protein corona formation. (A) Imperial protein stained SDS-PAGE gel of proteins associated with AuNPs in vivo. (B) Comparison of the amount of proteins adsorbed onto AuNPs. The values of µg protein/NP represent the average and standard deviation from three independent experiments (n=3 CD-1 mice/group; 4 independent experiments replicated). *** indicates p<0.001. (C) Venn diagram displaying the number of unique proteins identified in the in vivo formed coronas, and their respective overlaps. (D) Classification of identified corona proteins, according to their molecular mass.*

A comprehensive comparison of the PC profiles for the different types of AuNPs was carried out by LC-MS/MS. The Venn diagrams displayed in Figure 43C indicate the number of common and unique proteins identified after digestion of corona-covered AuNPs of different size and shape. Our results suggest that, the total amount of adsorbed protein (Figure 43B) does not necessarily reflect the complexity of PC composition (Figure 43C). For instance, even though a significantly larger amount of protein was found to adsorb onto 70 nm AuNSts as compared to 40 nm AuNSts, the total number of identified proteins was significantly higher in the case of 40 nm AuNSts (n=406 for 40 nm AuNSts; n=215 for 70 nm AuNSts). We hypothesize that protein exchange and protein interaction are affected by the presence of the spikes, so that the shorter the spike, the easier protein exchange will be, and as a consequence the higher the number of different proteins that are able to interact with the NP surface. On the other hand, reshaping of 40 nm AuNSts could more easily allow protein replacement, resulting in a higher complexity of their PC. In addition, 40 nm AuNSts also display a significantly higher number of different proteins than the corresponding 40 nm AuNRs, while having a similar total amount of adsorbed protein. We thus find that small AuNPs show a more complex PC than that on their larger counterparts. We however find an opposite behaviour for 70 nm NPs, where AuNRs seem to present a PC with a higher number of protein types than AuNSts of a similar size.

To better understand the effect of AuNP size and shape on the *in vivo* PC formation, the RPA of each identified protein was calculated and surface-bound proteins were classified according to their molecular mass (Figure 43D). Interestingly, 40 nm AuNSts present a significantly larger amount of proteins with MW<20 kDa, and a slightly larger

abundance of proteins with MW=20-40 kDa than the other AuNPs. Previous studies by Pozzi et al.[242] and Hadjidemetriou et al.[73] on liposomal NPs show, under *in vitro* dynamics and *in vivo* conditions, respectively, a tendency toward interaction with low MW proteins. Our study is in agreement with this observation, as proteins with MW<80 kDa contribute to 75-80% of the PCs for all AuNPs.

Table 6 summarizes the most abundant (top 20) proteins adsorbed onto the AuNPs surface. Serum albumin was found to be the most abundant protein in all cases. The presence of serum albumin on the corona of AuNPs has been previously reported for spherical AuNPs of different sizes under *in vitro* conditions.[59] While preferential adsorption of opsonins such as immunoglobulins and complement proteins enhance phagocytosis, leading to NP removal from blood, serum albumin and apolipoproteins are known to extend blood circulation. The second most abundant protein for all AuNPs employed was found to be A2M, a protease inhibitor and cytokine transporter and it is usually related to formation of fibres.[243] It is noteworthy that, even though the two most abundant proteins are the same for all AuNPs, regardless of size and shape, only 10 out of the top 20 proteins are common for all of them (those on the top 20 may be found in the total list of proteins), which have different RPA values depending on the NP type. For example, whereas 40 nm AuNPs present arginine succinate synthase and plasma kallikrein proteins within their top 20, 70 nm AuNPs do not. On the contrary, 70 nm AuNPs display alpha-1B-glycoproteins, ceruloplasmin, alpha-1-antitrypsin and serpina1a proteins, which are not present in 40 nm AuNPs. This may mean that NP size plays an important role in protein-NP interactions, such that some proteins show a higher tendency to attach to NPs, depending on their size.

It should however be kept in mind that the procedure applied for this study may pose certain limitations. First of all, it is not possible to recover all of the AuNPs injected into the mice and hence, the PC analysis is necessarily limited to the recovered NPs. Moreover, recovery of proteins from metallic NPs is a rather difficult task, as some proteins are difficult to detach from the NP surface without disruption. As a consequence, the analysis of PC composition is obviously limited to the proteins that could be effectively recovered.

AuNRs 40		AuNSts 40		AuNRs 70		AuNSts 70	
Identified Protein	**RPA**	**Identified Protein**	**RPA**	**Identified Protein**	**RPA**	**Identified Protein**	**RPA**
Serum albumin	5.16±2.39	Serum albumin	3.71±2.85	Serum albumin	7.52±0.87	Serum albumin	8.19±0.84
Alpha-2-macroglobulin	4.30±0.64	Alpha-2-macroglobulin	3.70±1.24	Alpha-2-macroglobulin	6.13±0.37	Alpha-2-macroglobulin	7.80±0.32
		Serine protease inhibitor		Serine protease inhibitor		Serine protease inhibitor	
Fibrinogen beta chain	2.29±0.90	A3K	2.44±1.81	A3K	4.83±0.86	A3K	6.01±1.01
Apolipoprotein A-I	2.27±0.22	Fibrinogen beta chain	2.37±0.53	Apolipoprotein A-I	3.24±0.47	Fibrinogen beta chain	3.99±1.71
Complement factor H	2.12±0.26	Apolipoprotein E	2.31±0.37	Fibrinogen beta chain	2.51±0.92	Alpha-1B-glycoprotein	3.11±0.36
Serine protease inhibitor							
A3K	2.07±1.06	Fibrinogen gamma chain	2.07±0.25	Fibrinogen gamma chain	2.28±0.92	Fibrinogen gamma chain	2.99±1.48
Ig mu chain C region							
(Fragment)	1.71±0.29	Apolipoprotein A-I	1.98±1.21	Complement C3	2.10±0.34	Apolipoprotein A-I	2.57±0.80
		Ig mu chain C region					
Fibrinogen gamma chain	1.64±0.56	(Fragment)	1.87±0.69	Apolipoprotein E	1.71±0.23	Apolipoprotein E	1.98±0.67
Argininosuccinate synthase	1.62±0.54	Complement factor H	1.73±0.17	Murinoglobulin-1	1.71±0.10	Fibrinogen alpha chain	1.94±0.74
		If kappa light chain					
Plasminogen	1.61±0.20	(Fragment)	1.61±0.05	Complement factor H	1.68±0.38	Murinoglobulin-1	1.93±0.17
				Ig mu chain C region			
Protein Ighv7-1 (Fragment)	1.55±0.28	Complement C3	1.33±0.84	(Fragment)	1.67±0.28	Complement factor H	1.63±0.34
		IgM heavy chain VDJ					
Apolipoprotein E	1.50±0.45	region (Fragment)	1.29±0.54	Alpha-1B-glycoprotein	1.35±0.31	Apoa1 protein	1.55±2.69
Complement C3	1.49±0.93	Beta-globin	1.13±0.25	Fibronectin	1.28±0.31	Complement C3	1.31±0.18
						Ig mu chain C region	
Beta-globin	1.25±0.08	Fibrinogen alpha chain	1.08±0.22	Plasminogen	1.15±0.10	(Fragment)	1.31±0.58
Betaine--homocysteine S-		Protein Ighv7-1					
methyltransferase 1	1.18±0.45	(Fragment)	1.04±0.52	Alpha-1-antitrypsin 1-3	1.13±0.18	Ceruloplasmin	1.25±0.21
		Argininosuccinate					
Apolipoprotein C-III	1.18±0.32	synthase	1.01±0.45	Serpina1a protein	1.12±0.07	Fibronectin	1.25±0.35
		Complement factor				Serine protease inhibitor	
Plasma kallikrein	1.17±0.35	properdin	0.94±0.54	Fibrinogen alpha chain	1.09±0.38	A3N	1.20±0.24
Murinoglobulin-1	1.08±0.12	Plasminogen	0.92±0.26	Beta-globin	1.09±0.27	Murinoglobulin-2	1.18±0.28
				Protein Ighv7-1			
Apolipoprotein C-I	1.04±0.45	Plasma kallikrein	0.86±0.24	(Fragment)	1.01±0.22	Alpha-1-antitrypsin 1-3	1.16±0.04
Fructose-bisphosphate							
aldolase B	1.04±0.47	Fibronectin	0.85±0.20	Ceruloplasmin	0.97±0.19	Serpina1a protein	1.12±0.03

Table 6. Most abundant (top 20) proteins identified in the in vivo PC of AuNPs, as identified by LC-MS/MS. RPA values represent the average and standard deviation from three different experiments, each using n=3 mice/group.

In a broader context, we propose that the investigation and understanding of *in vivo* PC formation and composition are necessary towards the development of adequate gold-based NP systems for biomedical applications. Although usually seen as an obstacle, the PC also provides new opportunities such as NPs manipulation to control their interaction with proteins, optimization of drug loading or discovery of biomarkers. Nevertheless, it is crucial to perform a comprehensive characterization of the PC under realistic *in vivo* conditions, in order to understand the interaction of NPs with the physiological media and its consequences.

4. *In Vitro* vs. *In Vivo.*

Although our experiments were not designed for a detailed comparative study of *in vitro* vs. *in vivo* PC, results obtained from our previous investigations can be utilized to get a preliminary and approximate idea of the influence of the incubation method on PC formation. Remarkably, there is an evident lack of *in vivo* PC studies, which is reflected by the very few publications regarding the matter. In fact, as far as we know, there is

just one scientific paper dedicated to the comparison of PCs formed under *in vitro* and *in vivo* conditions.[73]

This particular research project was carried out by Hadjidemetriou et al.[73] for the investigation of the influence of the incubation characteristics on PC formation and composition. For this study, liposomes were incubated in mice plasma (*in vitro* PC) and injected and later recovered from mice (*in vivo* PC). Likewise, they developed an alternative methodology for the isolation and purification of the PC-NP complexes based on the combination of SEC and membrane ultrafiltration. Physico-chemical properties of liposomes before and after interaction with proteins were monitored by DLS, ZP, UV-VIS and TEM. PCs were qualitatively and quantitatively analysed by LC-MS/MS for a detailed and statistical comparison of the corona profiles. Results show clear differences between the *in vitro* and *in vivo* formed PCs, demonstrating that artificial conditions cannot adequately represent a realistic case.

After comparing some of our results from PC investigations on AuNPs, we observe that the amount of protein attached to the NP seems to be higher when the NPs are injected in mice. This results are in agreement with Hadjidemetriou studies, where researchers found out a higher amount of proteins on the surface of *in vivo* incubated lipidic NPs. Qualitative and quantitative differences were also observed for the PC profiles of AuNPs injected on rodents and incubated in plasma. These results were also observed in Hadjidemetriou et al. study on liposomes. A wider number of unique proteins was observed for *in vivo* formed PCs in comparison with its *in vitro* counterpart. As mentioned before, *in vitro* and *in vivo* approaches of study are quite different and, in particular, *in vitro* methodologies irremediably ignore factors such as the dynamic flow or the presence of other biological entities. When injected in the blood stream, NPs are expected to interact with a higher amount and variety of proteins as they travel through different parts of the body and are immersed in different environments within this time.

Summarizing, though this particular project is not dedicated to the comparative study of *in vitro* and *in vivo* PCs, information from previous investigations together with this one can offer an initial and approximate idea of the differences that might be expected. Interestingly, results are in agreement with a previous project on PC on liposomes, which

suggests that these effects may be coming mainly from the incubation conditions, as they were observed for NPs of different nature (AuNPs and liposomes).

5. Conclusions – Summary of findings.

This study allowed the analysis and characterization of the *in vivo* PC on the surface of AuNPs for the first time. A methodology previously developed for PC-liposome isolation was successfully applied for purification of PC-AuNP complexes. As it was possible to recover enough sample from mice, the analysis of the formed PC of AuNRs and AuNSts was positively carried out. Unfortunately, this was not the case for AuNSs and therefore, this NP type could not be included in this study.

Physico-chemical characteristics were analysed before and after interaction with proteins. Results showed that interactions between proteins and the NP surface lead to a modification of the initial physico-chemical properties of AuNPs. Interestingly, 40 nm AuNSts morphology was modified after protein adsorption.

Quantitative and qualitative analysis revealed a striking difference on the amount of protein adsorbed by 70 nm AuNSts, being these NP the ones displaying the higher amount of protein adsorbed per NP. Interestingly, though 70 nm AuNSts present the higher amount of proteins, these is not translated in a larger number of different proteins. Additionally, study of the protein profile of the coronas of AuNPs indicated the influence of both parameters, size and shape, on the different PC profiles of each NP.

Remarkably, despite the different nature of the NPs used in the present study, our results are in agreement with those previously published by Hadjidemetriou et al.[73] for PC-liposome complexes. In general terms, *in vivo* PCs of AuNPs present a higher complexity than its *in vitro* counterparts.

Blank page.

CHAPTER 8: OPTOACOUSTIC PROPERTIES OF GOLD NANOPARTICLES

1. Focus of the Study.

As mentioned along the previous chapters, AuNPs constitute a type of NM with a great potential due to their interesting optical and thermal properties. It is currently well-established that AuNPs' properties mainly arise from their plasmonic nature. When a metallic NP is irradiated at their localized surface plasmon resonance (LSPR) wavelength, free electrons on the NP surface oscillate at the corresponding frequency and, as a consequence, produce strong absorption and scattering with an intense extinction band in the UV-Visible-NIR spectrum also known as plasmon band. This LSPR is responsible for the optical and thermal properties of AuNPs and therefore, countless efforts have been invested on the understanding and study of this particular process. The LSPR strongly depends on the NP morphology and hence, numerous investigations have been dedicated toward the development and optimization of synthetic procedures that allow the production of AuNPs of a wide variety of shapes such as spheres, rods, stars, bipyramids, triangles and many others.

Owing to their interesting properties, gold-based NMs have been proposed for a myriad biomedical applications including drug delivery systems, biosensing and biomedical imaging. In this chapter, we focus on their potential as optoacoustic imaging contrast agents. As a result of the LSPR absorption, AuNPs exhibit what is known as plasmonic heating, which has been described in detail for AuNRs and AuNSts. When these AuNPs are excited with pulsed light at the adequate wavelength repetitively, this leads to periodic heating and thermal expansion and contraction of the particles as well as the surrounding medium. Interestingly, this phenomenon can be detected in the form of emitted ultrasonic waves by utilizing a conventional ultrasound transducer.

Optoacoustic Imaging has been introduced as an interesting alternative or a complementary tool for biomedical imaging research as it presents some advantages over traditional imaging. For example, it is not affected by fluorescence damping as only the excitation light beam needs to penetrate through the tissue. In addition, while light suffers from attenuation due to absorption and scattering of biological structures, ultrasound waves can travel through the tissue almost unhindered. It is also important

to note that, the LSPR of AuNPs can be tuned by tailoring their morphology to specifically fit within the NIR region (600-900 nm), commonly known as the therapeutic window. Up to now, mainly AuNRs, AuNSts and gold nanoshells have been intensively applied. Nevertheless, the complete parameter space of NP size, length, diameter and other degrees of freedom with respect to their optimal photoacoustic performance has not been optimized and the contributions of the individual factors are not well understood. This lack of understanding leads to application of unsuitable or underperforming AuNP architectures and limited optoacoustic contrast in imaging applications.

In collaboration with Prof. Alexander Kuehne group, Dr. Dmitry Chigrin and Prof. Twan Lammers team, we developed a theoretical description of the optoacoustic experiment to identify the optimal AuNP geometry with absorption in the therapeutic window and high absorption efficiency. While the optimal structure is probably impossible to obtain, we developed AuNSts as a structural equivalent and compared the theoretical results with experimental data from four AuNSts samples with different tip-lengths.

2. Results. Physico-Chemical Characterization of AuNPs.

Gold nanostructures involved in the present study were synthesized by several seeded-growth methodologies available in the literature[109, 110, 114-116, 208] and, subsequently functionalized with thiolated PEG of a MW of 10 KDa in order to stabilize their surfaces and make the structure more biocompatible.[202] Physico-chemical properties of AuNPs were characterized by the following techniques: DLS, ZP, UV-Visible Spectroscopy and TEM. Characterization of these NPs is summarized in Figures 44-47. The morphology and dimensions of the NPs was studied and analysed by TEM. Diameter of AuNSs, length and width of AuNRs, as well as total diameter, core diameter and spike length of AuNSts were determined. These data are summarized in Table 7.

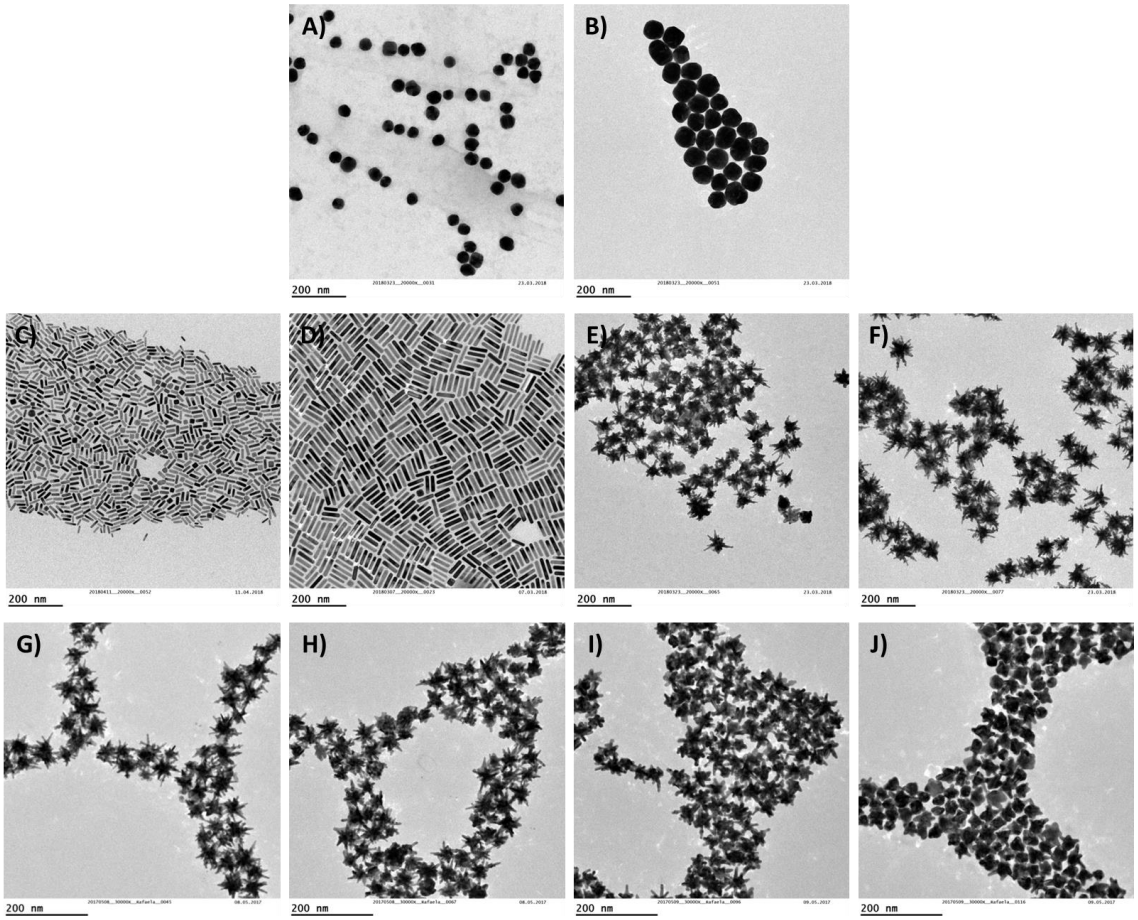

Figure 44 shows the TEM images of: A) AuNSs 40nm; B) AuNSs 70 nm; C) AuNRs Length 40nm; D) AuNRs Length 70nm; E) AuNSts 40nm; F) AuNSts 70nm; G)-J) AuNSts of different spike length and same core size, from longer to shorter spike.

		Total Diameter / nm	Length / nm	Width / nm	Spike Length / nm	Core Diameter / nm
AuNSs	A	41.1±1.0	-	-	-	-
	B	70.2±1.9	-	-	-	-
AuNRs	C	-	41.9±2.0	11.5±1.2	-	-
	D	-	72.0±2.1	15.2±2.1	-	-
AuNSts	E	42.0±1.0	-	-	9.2±1.3	23.8±2.0
	F	71.9±2.3	-	-	18.9±1.4	32.2±2.1
	G	60.1±3.1	-	-	16.7±1.0	25.9±2.5
	H	54.6±3.2	-	-	14.4±1.2	25.3±2.6
	I	49.0±3.3	-	-	11.5±1.1	25.7±2.5
	J	40.1±2.3	-	-	7.2±1.3	25.3±2.1

Table 7 summarizes the dimensions obtained for all AuNPs involved in this study.

First of all, D_H and PDI of our samples were evaluated by DLS measurements. It is well-known that this technique provides information about the aggregation state and average size in solution of spherical NPs. AuNSs and AuNSts can be approximated to a spherical shape and therefore, we can observe a single band in the DLS graph for 40 and

70 nm AuNSs and AuNSts. The width of the band gives representation of the sample PDI, the wider the band the higher the PDI. In our case, AuNSts exhibit a higher PDI index, which was expected as the control over the morphological characteristics of AuNSts is limited.[207, 208] DLS measurements of AuNRs were carried out for the sake of comparison of the signal. As AuNRs are anisotropic, two different bands are obtained in the DLS graphs corresponding to this NP type.[252] It is possible to obtain more information about the dispersion of the sample and the behaviour of the NPs in solution of this kind of NPs, however, specific algorithms and simulations are needed.

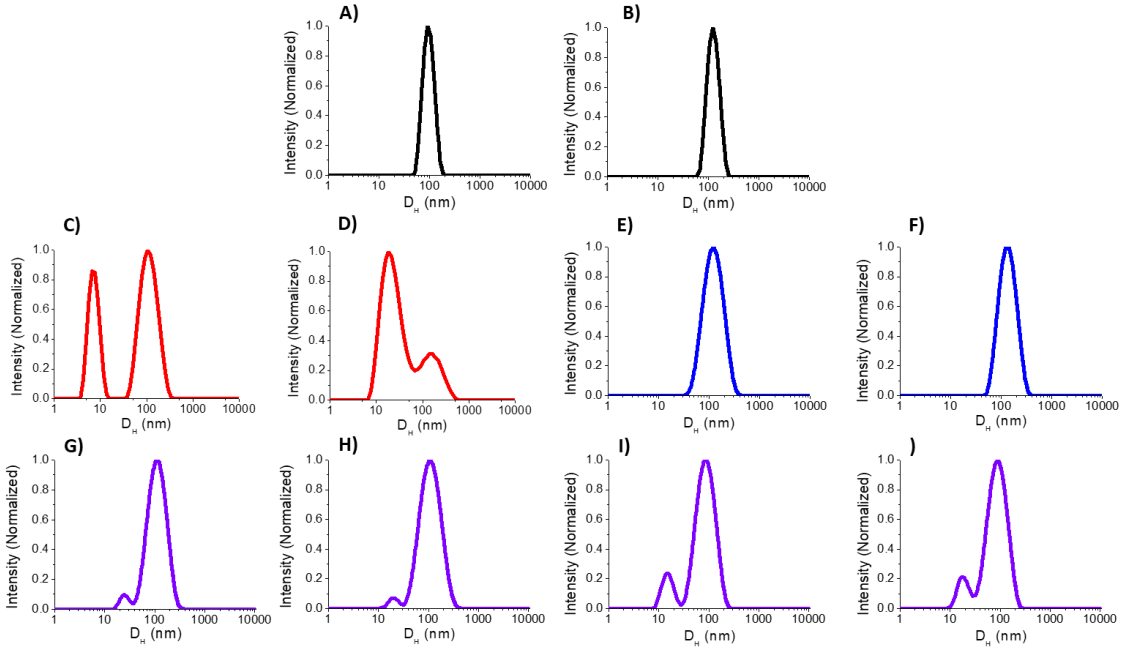

Figure 45. DLS measurements of: A) AuNSs 40nm; B) AuNSs 70 nm; C) AuNRs Length 40nm; D) AuNRs Length 70nm; E) AuNSts 40nm; F) AuNSts 70nm; G)-J) AuNSts of different spike length and same core size, from longer to shorter spike.

Secondly, ZP measurements were carried out to determine the surface charge of the NPs. As mentioned above, all AuNPs were functionalized with thiolated carboxylic PEG (Mw = 10 KDa) and, hence, they show a main signal at negative ZP values. The presence of a single peak on the spectra plots indicates a homogeneous surface charge of our samples.

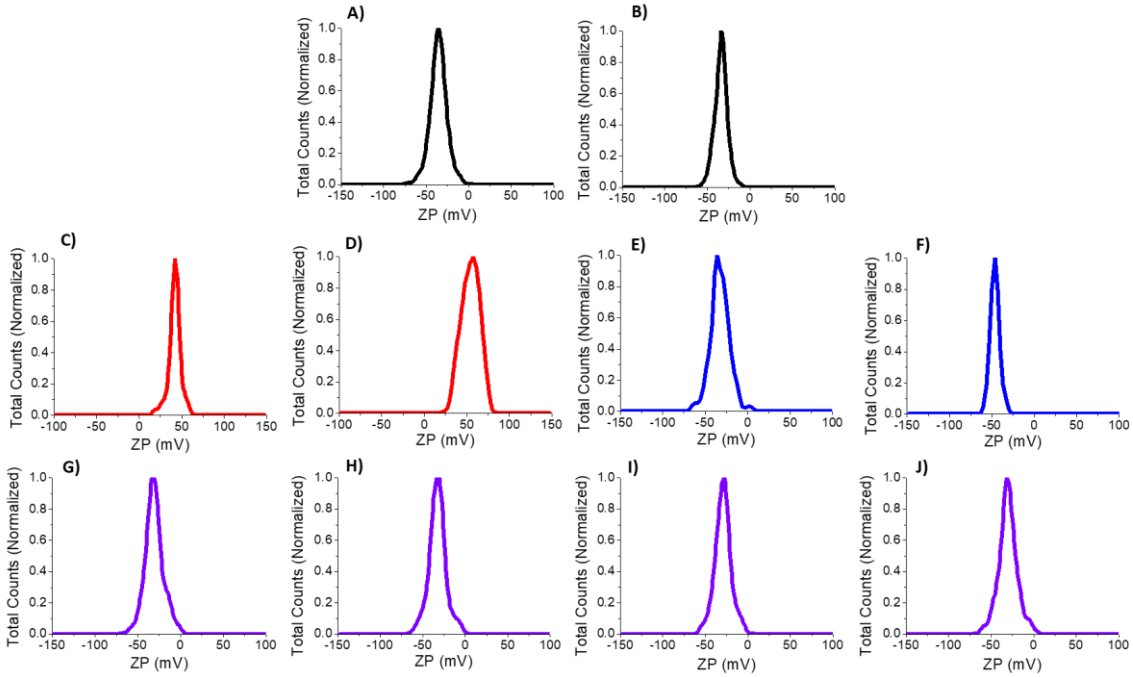

Figure 46. ZP measurements of: A) AuNSs 40 nm; B) AuNSs 70 nm; C) AuNRs Length 40 nm; D) AuNRs Length 70 nm; E) AuNSts 40 nm; F) AuNSts 70 nm; G)-J) AuNSts of different spike length and same core size, from longer to shorter spike.

UV-Visible-NIR spectroscopy was utilized to characterize the absorption properties of AuNPs. In the case of AuNSs, the spectrum shows a single and narrow LSPR band that reflects the high quality and monodispersity of the sample. The absorbance maxima are: 532 nm for 40 nm and 542 nm for 70 nm AuNSs. Regarding AuNRs, their spectra present two different bands corresponding to transverse and longitudinal LSPR modes that arise due to the anisotropic morphology of the NRs. The ratio between the intensities of this two bands is considered a suitable measure for the quality of AuNRs (the ratio should be at least 3, but depends on the aspect ratio of the NRs). Longitudinal plasmon bands were located at the wavelengths of 747 nm for 40 nm AuNRs and 893 nm for 70 nm ones. Finally, UV-visible-NIR spectra of AuNSts shows a main and broad plasmon band at higher wavelengths together with a small shoulder at lower wavelengths. This is explained by the particular morphology of this nanostructure, which presents LSPR modes corresponding to their semi-spherical core, and the total diameter of the NP.[208] The broad bands arise from a higher polydispersity, both in the total dimensions and in the length and sharpness of the spikes in each AuNSt.

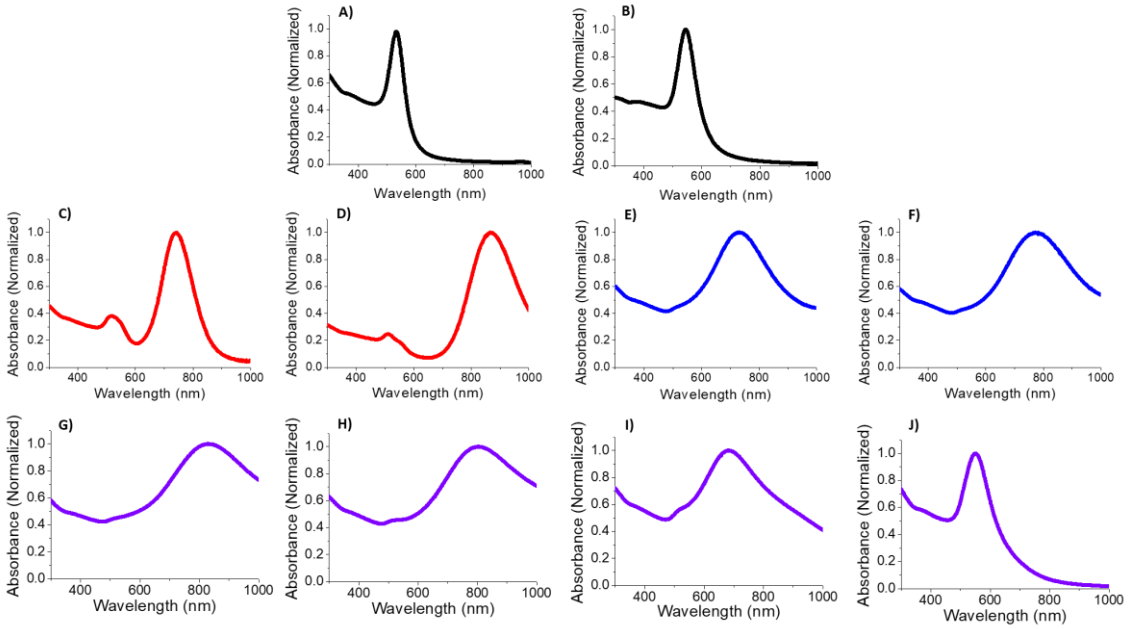

Figure 47: UV-Visible-NIR spectra of: A) AuNSs 40 nm; B) AuNSs 70 nm; C) AuNRs Length 40 nm; D) AuNRs Length 70 nm; E) AuNSts 40 nm; F) AuNSts 70 nm; G)-J) AuNSts of different spike length and same core size, from longer to shorter spike.

Prof. Alexander Kuehne and Dr. Dmitry Chigrin, together with their teams, have performed simulations that were compared with the experimental optoacoustic performance of AuNPs presented in this chapter. As a consequence, a scientific paper presenting this study has been recently submitted (Appendix). The content of the paper is described in the remainder of this chapter.

3. Results and Discussion. Theoretical and Experimental Optoacoustic Performance of AuNPs.

The main objective of the theoretical simulations designed and performed by Prof. Kuehne and Dr. Chigrin was the identification of the optimal morphology and dimensions of AuNPs for optoacoustic imaging. We assume that the ideal nanostructure may, at least at the present time, be impossible to obtain and therefore, we propose the use of AuNPs of different morphologies and compare their experimental optoacoustic performance with their simulated behaviour.

For a more straight-forward comparison of the optoacoustic performance, the optoacoustic signal of AuNPs was analysed by the point source model.[253, 254] In this

model, it is considered that the optoacoustic signal generated by a single NP is proportional to its absorption cross-section (σ_a) and the fluence of the laser illumination (Φ) at the source location (x). After taking into account the attenuation undergone by the laser when travelling through the sample by applying the Lambert-Beer law, we obtain the following expression:

$$S_{\text{PA}} \propto W_0 \frac{\sigma_a}{\sigma_e}\left(1 - \exp\left(-\frac{\sigma_e L}{m} c\right)\right) \qquad \text{Eq.1}$$

Where W_0 is the power of the laser at the sample entrance, σ_e is the extinction cross-section of the NP, L is the sample length, m is the mass of a single NP and c represents the weight concentration of NPs. When the concentration is very low ($\sigma_e Lc/m \ll 1$), Eq.1 is reduced to the following expression:

$$S_{\text{PA}} \propto W_0 L \frac{\sigma_a}{m} c = \alpha c \qquad \text{Eq.2}$$

Where the linear dependence of the optoacoustic signal on sample concentration and absorption cross-section can be observed. Constant α is interpreted as the optoacoustic efficiency of the NP at low concentrations. As a consequence, to maximize the optoacoustic efficiency of a NP, we must also maximize its absorption cross-section. However, for larger concentrations ($\sigma_e Lc/m \ll 1$) the optoacoustic signal saturates towards a constant value:

$$S_{\text{PA}} \propto \frac{\sigma_a}{\sigma_e} \qquad \text{Eq.3}$$

In this case, the optoacoustic efficiency now depends in the ratio between the absorption cross-section and the extinction cross-section. This leads to the first design principle for optimal optoacoustic probes: an ideal probe should exhibit maximal absorption and minimal scattering efficiencies.

It is well-known that small NPs display a high absorption and low scattering values, which is desirable for an optoacoustic probe. Nonetheless, spherical NPs usually display absorption at wavelengths out of the biological window, which greatly affects their potential as imaging probes.[255] One way to solve this problem would be to modify the morphology of the NP by elongating it in one dimension of the space, which would allow to tune the absorption band towards the NIR region.[255] Consequently, we arrive to the

second design principle for optoacoustic probes: NP size must be kept small but elongated towards one dimension of the space.

The previously mentioned requirements are satisfied by long, high aspect ratio AuNRs or nanowires.[256] Consequently, we performed several calculations of the absolute absorption cross-section and relative absorption at the absorption maxima of AuNRs of different aspect ratios. For the simulations, water was utilized as theoretical solvent and assumed to have a refractive index of 1.33.[257] Results indicate an expected shift towards longer wavelengths when the length of the AuNR increases. This leads to a larger NP volume, which is translated in an increase of the absolute absorption and a reduction of the relative absorption. An optimal compromise between these two trends is achieved for AuNRs of 12nm diameter and a length among 40 and 100nm. Although these AuNRs exhibit large absolute and relative absorption at the NIR region, they have been reported to suffer from degradation due to Rayleigh instability, which leads to the breakage of the AuNRs into smaller pieces consequently losing their NIR absorption over time.[258, 259]

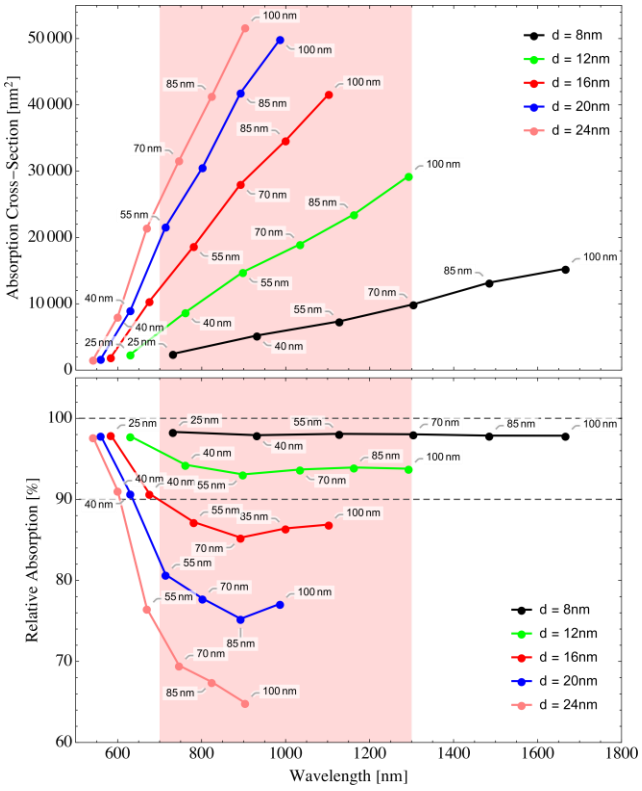

Figure 48. Absolute absorption cross-section (top) and relative absorption (bottom) of AuNRs at their respective absorption maxima, as a function of a corresponding

wavelength. Results for different NR diameters and lengths are shown. The light red area marks the NIR transparency window of biological tissue. This image and corresponding calculations have been developed by Dr. Dmitry Chigrin and his team.

Alternative gold NMs that also satisfy the two mentioned requirements are AuNSts. This NP type is typically constituted by a quasi-spherical core and numerous sharp tips. Their particular plasmonic response is interpreted as the hybridization of the plasmon polaritons of the core and the branches (approximated to small and long rods).[260] AuNSts present a NIR absorption similar to the one of AuNRs, translated in a large absolute and relative absorption.[261] For AuNSts, we calculated the absorption cross-section and relative absorption at the absorption maximum wavelength for different geometries. In particular, AuNSts with tips larger than 10nm are considered to satisfy both conditions of an ideal optoacoustic probe.

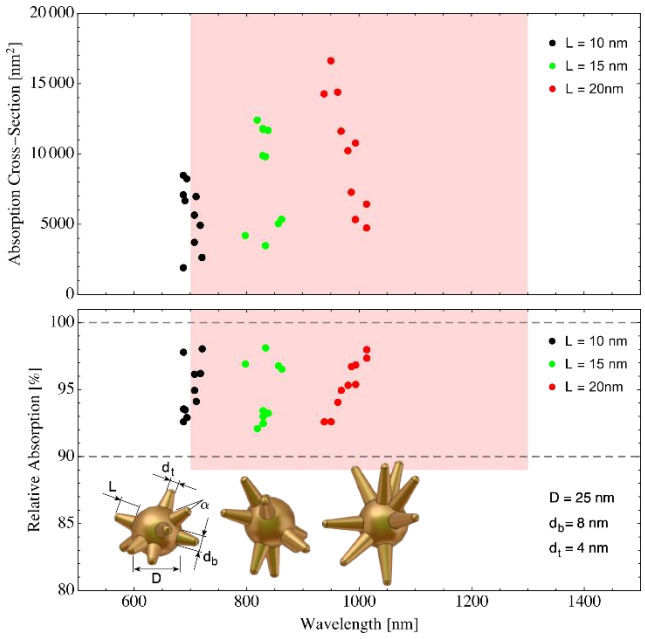

Figure 49. Absolute absorption cross-section (top) and relative absorption (bottom) of AuNSts at their respective absorption maxima, as a function of a corresponding wavelength. Results for different NSts geometries are shown. Representation examples of the geometries with relevant dimensions are provided as insets. The light red area marks the NIR transparency window of biological tissue. Calculation and further visualizations with TEM was performed by Dr. Dmitry Chigrin and Prof. Alexander Kuehne teams.

To confirm our theoretical predictions, we determined the extinction, absorption and scattering coefficients of dispersions of AuNRs and AuNSts with geometries fulfilling the conditions for optimal photoacoustic performance. AuNRs of length of 38.0±3.8nm and diameter of 10.0±1.0nm were employed. AuNRs were stabilized with CTAB molecules and dispersed in water. AuNSts were functionalized with PEG for better stabilization. Geometrical parameters of the AuNSts were determined through inspection of at least 100 particles in TEM images. The average equivalent diameter of the AuNSts was 45.0 ± 5.0 nm, with an average core diameter of 25.0 ± 2.0 nm. Experimental results of these measurements are presented in Figure 47a and 47b. Experimental measurement indicate a relative absorption of 87.3% and 85.7% for AuNRs and AuNSts respectively. These results are in good agreement with theoretical calculations, which show relative absorption values of 94.5% for AuNRs and 97.1% for AuNSts.

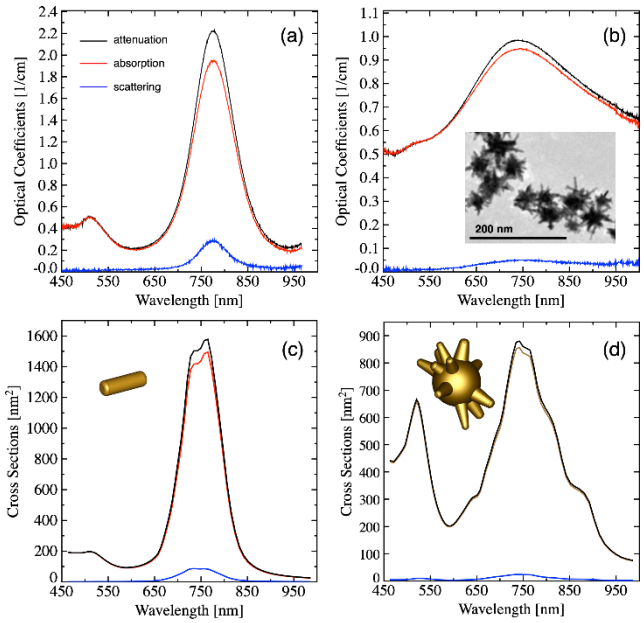

Figure 50. Top panel: Experimental attenuation (extinction), absorption and scattering coefficients for NRs (a) and NSts (b). Inset shows a TEM image of NSts. Simulated shapes have been obtained by Dr. Dmitry Chigrin.

We thus proceed to the study and comparison of the optoacoustic performances of the optimal AuNRs and AuNSts. AuNSs of around 40nm of diameter were included as an example of a non-optimized structure. Theoretical optoacoustic signal of these NPs was calculated by using Eq.1 and the values of the extinction and absorption cross-section reported in Figure 47c and 47d. For AuNSs, the attenuation cross-section was averaged

from over 100 realizations. Optoacoustic performance of both AuNRs and AuNSts was found to be very superior to the one of AuNSs. To give an example, for a concentration of gold of 0.4g/L, the signal enhancement with respect to AuNSs was of 55 times for AuNRs and 35 times for AuNSts. Total optoacoustic signal, understood as the sum over the wavelength interval 690-900nm, was found to be dependent on the concentration, showing a characteristic saturation behavior (Figure 48c).

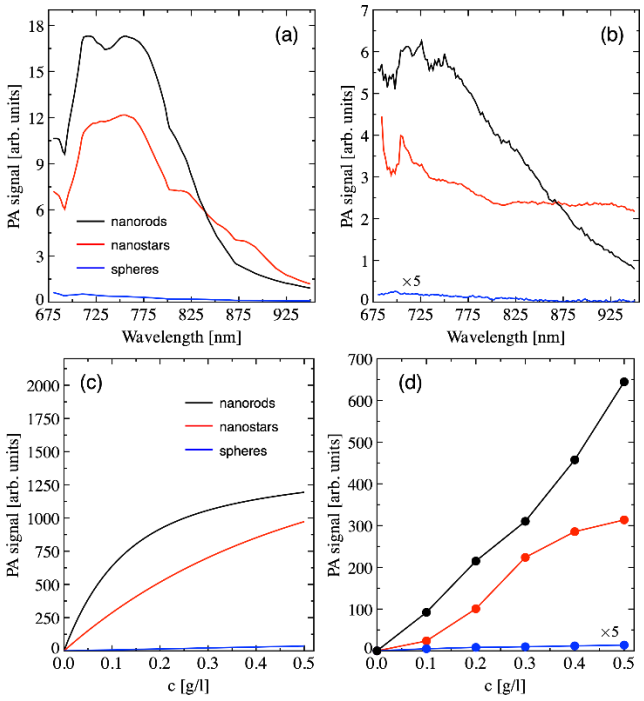

Figure 51. Top panel: Photoacoustic signal as a function of excitation laser wavelength. Theoretical (a) and experimental (b) data are shown for a concentration c=0.4 g/L. Bottom panel: Theoretical (c) and experimental (d) total photoacoustic signal over a wavelength range from 690 nm to 900 nm, as a function of concentration. Data for AuNRs (black), AuNSts (red) and AuNSs (blue) are shown. Experimental photoacoustic signal for AuNSs is multiplied by a factor 5. Theoretical data has been simulated by Dr. Dmitry Chigrin.

Experimental results are in agreement with theoretical predictions. For a concentration of 0.4 g Au/L, AuNSts signal was enhanced 25-fold with respect with AuNSs, while AuNRs optoacoustic signal was enhanced 35-fold. The dependence of the optoacoustic signal on the Au concentration follows the expected saturation trend. Nevertheless, it is important to note that higher concentration of AuNRs deviate from this behavior, which

could be explained by the additional non-linear characteristic of the optoacoustic process that were not taken into consideration in our model.

4. Conclusions – Summary of findings.

The present project was the result of a collaboration with Prof. Alexander Kuehne, Dr. Dimitry Chigrin, Prof. Twan Lammers and their respective teams. The main focus of this investigation was the determination of the optimal morphology and dimensions of AuNPs for optoacoustic performance. Our approach was a combination of theoretical simulation and experimental detection of the optoacoustic signal of selected NPs.

Our results indicated a good agreement of experimental data with theoretical simulations, which confirmed that the selected model was adequate for simulation of the optoacoustic signal of AuNPs at low concentrations. Among the three NP types, AuNRs and AuNSts exhibited a very good performance, with AuNRs displaying a higher optoacoustic signal than AuNSts.

As expected, the optoacoustic signal was found to be dependent on the concentration of the sample. Nevertheless, whereas AuNSts reach a saturation stage, ANRs at higher concentrations deviate from this behaviour, which was explained by an additional non-linear characteristic of the optoacoustic process that was not taken into consideration in this model.

Summarizing, this project led to two important design principles of optoacoustic probes:
a) An ideal probe should exhibit maximal absorption and minimal scattering efficiencies;
b) NP size must be kept small but elongated towards one dimension of the space.

Blank page.

CHAPTER 9: PROTEIN CORONA AND OPTOACOUSTIC PERFORMANCE

1. Focus of the Study.

In the previous chapter, the focus was on the characterization and optimization of the optoacoustic properties of AuNPs of different sizes and morphologies for their application in Optoacoustic Imaging. This emerging bioimaging modality is capable of providing structural and functional information about tissue by using either endogenous or exogenous contrast agents.[166, 262] It allows a deeper penetration than currently available optical imaging-based techniques, which is combined with high quality image resolution. Nevertheless, as these materials are expected to be injected or administered to a potential patient and therefore, they will eventually be exposed to physiological fluids. As we showed in previous chapters, this translates into a fast interaction of the contrast agent (the NM in our case) with the biomolecules present within the biofluid, giving rise to the PC, leading to a modification of the performance, behaviour and fate of the NM.[26, 56]

In this last thesis chapter, we focus on the investigation of the possible influence of PC formation on the optoacoustic performance of AuNPs, a topic that has not been discussed in the literature, as far as we have seen. For this purpose, AuNPs of different morphology (spheres, rods and stars) and size (40 and 70 nm) were synthesized and exposed to mice plasma for PC formation. The optoacoustic performance of bare- and corona-coated AuNPs was evaluated and compared. Interestingly, our results suggest that PC enhances the optoacoustic signal of the NP, which may be related to a thermo-elastic expansion effect of the protein coating.

2. Results. Physico-chemical Characterization of bare and corona-coated AuNPs.

AuNSs, AuNRs and AuNSts of two different sizes (40 and 70 nm) were synthesized by following seeded-growth protocols available in the literature[109, 110, 114-116, 208] and then functionalized with thiolated carboxylic PEG of MW 10KDa.[202] Physico-chemical characterization of the NPs before and after interaction with plasma proteins was monitored by several techniques such DLS, ZP and UV-Visible-NIR Spectroscopy.

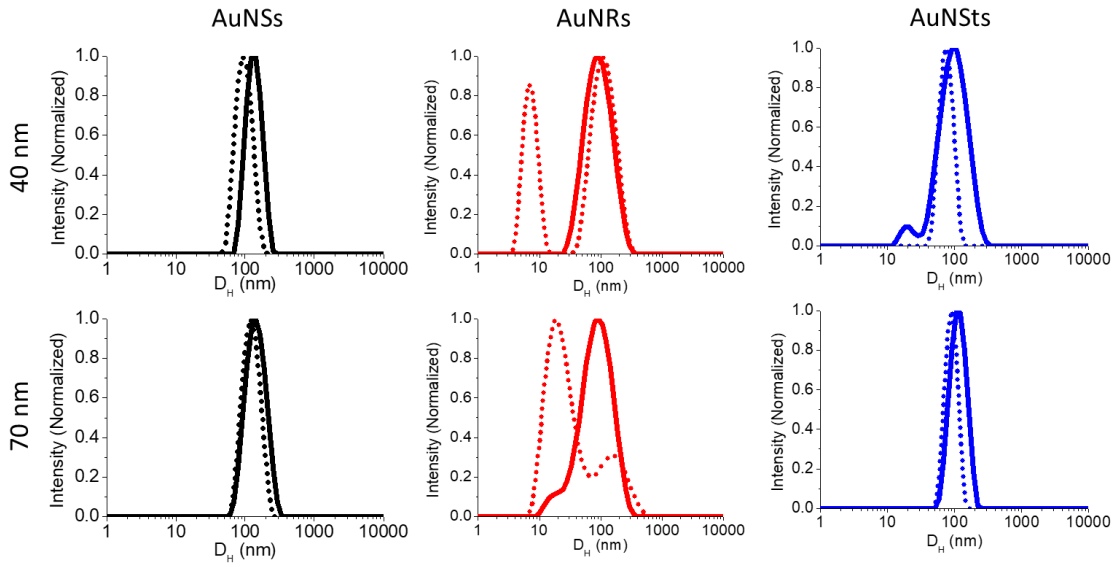

Figure 52. Size distribution measured by DLS, of all AuNPs involved in this study before (dotted line) and after (continuous line) incubation with plasma proteins.

Firstly, the D_H of all NPs involved in this project were measured by DLS. In the case of the more isotropic NPs (spheres and stars), a rather small variation in the size distribution was observed, which was expected taking into consideration previous results (See Chapter 4). This increase on the D_H value is explained by the attachment of proteins to the NP surface, which also results in a higher PDI value. Due to their anisotropy, AuNRs present two initial well-defined bands within the size distribution. These two initial bands merge into a main and broad single band after exposure to plasma proteins, suggesting that protein adsorption reduces the anisotropy of the final PC-AuNR complex.

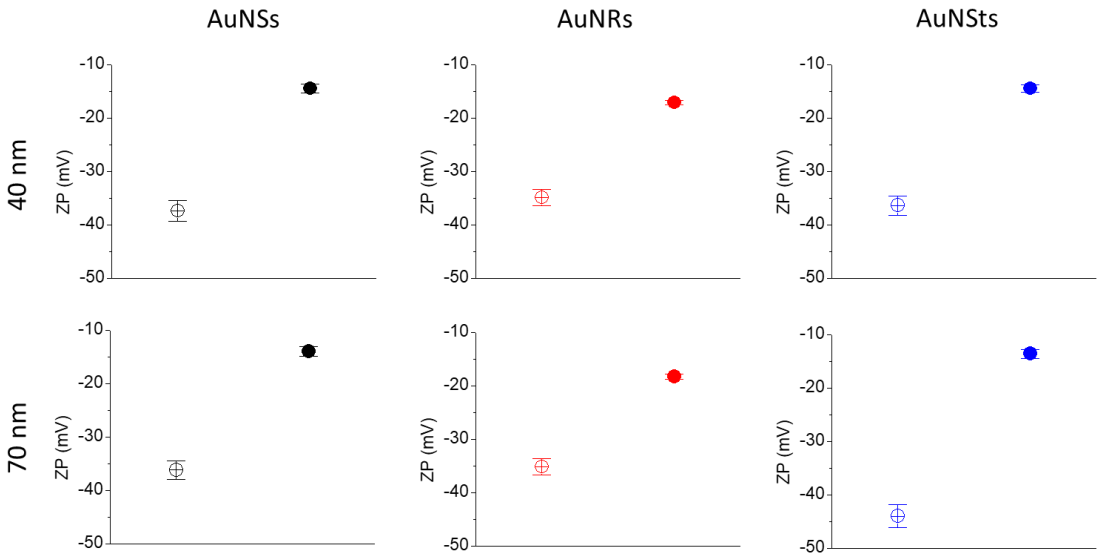

Figure 53. Graphical representation of the change of ZP due to protein adsorption: before (dotted line) and after (continuous line) plasma exposure.

Secondly, ZP measurements were performed to monitor the changes undergone by the surface charge of NPs after being in contact with plasma proteins. Due to the surface functionalization with carboxylic PEG (Mw=10 kDa), all AuNPs show an initial negative surface charge. However, PC-AuNP complexes exhibit less negative values as a result of interaction with proteins. This trend is clearly observed for all NP types.

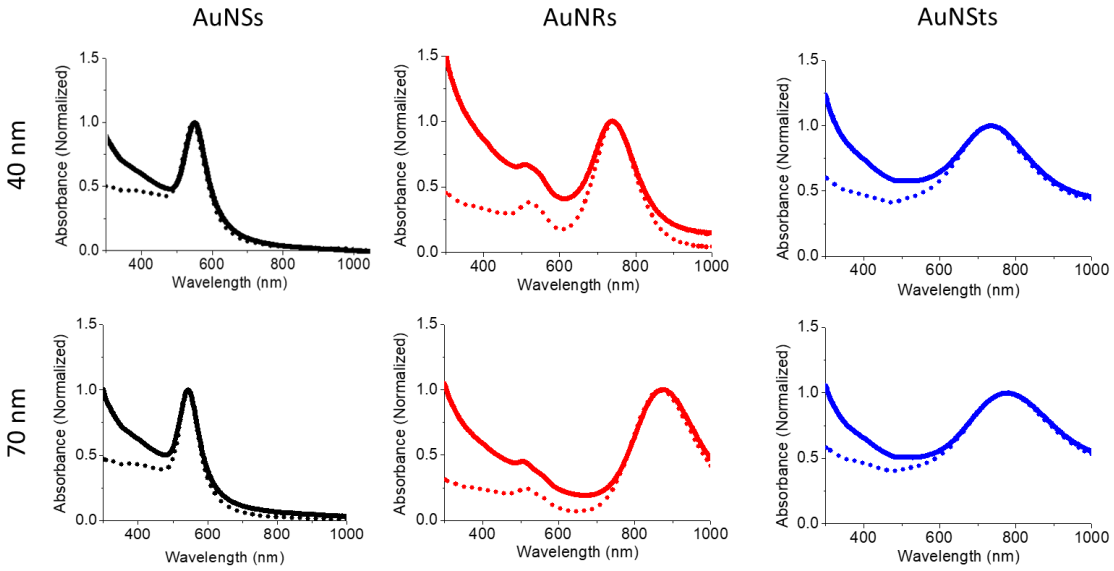

Figure 54. UV-Visible-NIR spectra of AuNPs before (dotted line) and after (continuous line) interaction with plasma proteins.

UV-Visible-NIR spectroscopy was also carried out to detect modifications on the plasmon bands of AuNPs after protein adsorption. As observed in the plots, the position of the plasmon bands was barely affected by the presence of the PC. Notwithstanding, protein adsorption translated into higher Rayleigh scattering at lower wavelengths. These results are in agreement with similar measurements previously carried out and described in Chapter 4. As the NP characterization confirms the PC formation on the surface of all AuNPs involved in this study, both bare- and protein-AuNP complexes were used to test their optoacoustic activity.

3. Optoacoustic Measurements and Discussion.

For an adequate measurement of the optoacoustic signal of AuNPs (bare- and corona-coated) an imaging system VEVO LAZR was utilized. Samples were prepared by injecting 25 µL of NP solution in plastic tubes, always filling one of the tubes with milli-Q water for background signal detection. It is essential to avoid the formation of bubbles as they can interfere and modify the optoacoustic signal. Vessel containing the tubes was filled with milli-Q water and placed on the VEVO imaging station. This imaging station combines high frequency ultrasound and optoacoustics into one single platform, leading to a high resolution anatomical, functional and molecular imaging system. It allows for optimal positioning, quick set-up and alignment as well as real-time monitoring of several parameters. An LZ transducer was used for the detection and measurement of the optoacoustic signal once the samples were adequately placed. This transducer combines high ultrasound technology with an integrated fibre optic cable for high-energy laser light delivery. Different concentrations of AuNPs were utilized.

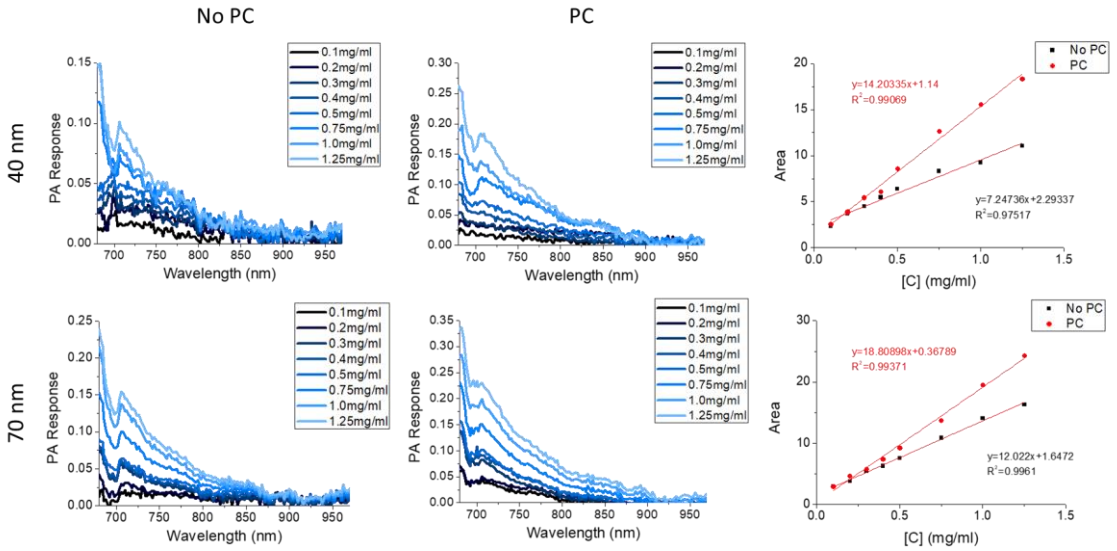

Figure 55. Graphical representation of the optoacoustic signal emitted by AuNSs in presence and absence of PC. In addition, the area under the curves was plotted against the concentration of gold to detect differences between the bare and corona-coated samples.

We first measured AuNSs. As expected, the optoacoustic signal from this NP type is quite low due to the low wavelength of their plasmon band (<600 nm). Therefore, measurements at high NP concentration were performed to get a measurable signal. In order to easily see these differences, the areas under the curves were measured and plotted against NP concentration. In this new graphical representation, a linear increase of the optoacoustic signal and the concentration was clearly observed. The higher optoacoustic signal of larger AuNSs is mainly due to the position of its maximum absorption band located at higher wavelengths. Interestingly, although at very low concentrations the optoacoustic signal is very similar, PC-coated NPs exhibited a slightly more intense optoacoustic activity at higher concentrations.

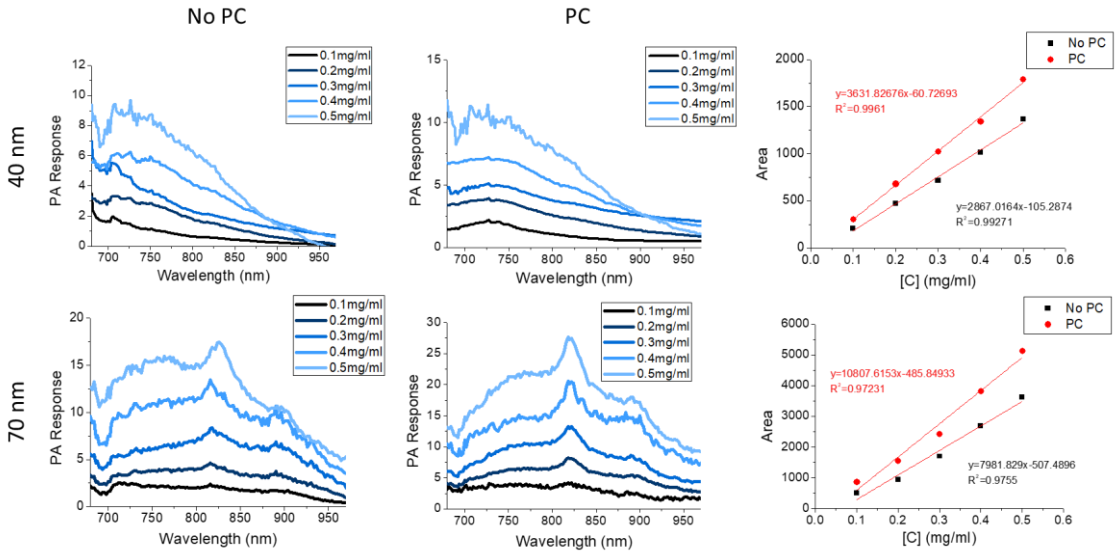

Figure 56. Graphical representation of the optoacoustic signal emitted by AuNRs in presence and absence of PC. In addition, the areas under the curves were plotted against the concentration of gold to detect differences between bare and corona-coated samples.

The optoacoustic potential of AuNRs was then evaluated. As previously mentioned, AuNRs are one of the most promising NP types for imaging applications and therefore, it is not surprising to observe that they display a quite strong optoacoustic signal at low concentrations. The profile of the spectra is different from the one of AuNSs due to the different plasmonic properties. The absorbance of AuNRs is intense, even for a small amount of gold and is located within the first biological window, which results in a higher optoacoustic signal. Larger AuNRs exhibit a higher optoacoustic performance than smaller ones. Similar to what was observed for AuNSs, PC-coated NPs display a slightly superior optoacoustic activity than their bare counterparts, suggesting an enhancement caused by the presence of the PC. It is important to highlight that this enhancement is observed even at the lowest gold concentration.

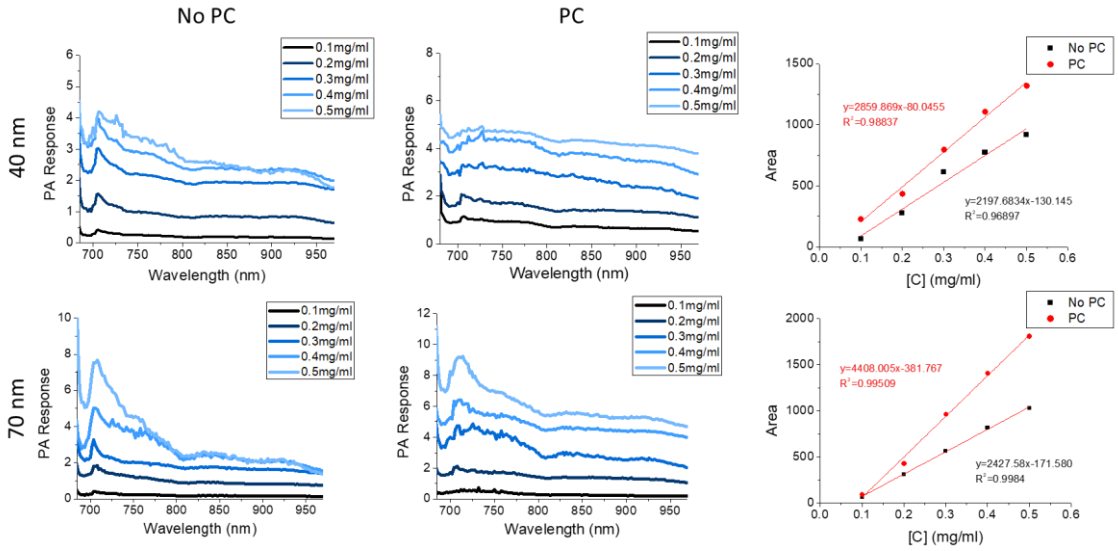

Figure 57. Graphical representation of the optoacoustic signal emitted by AuNSts in presence and absence of PC. In addition, the areas under the curves were plotted against the concentration of gold to detect differences between bare and corona-coated samples.

Lastly, the optoacoustic performance of AuNSts of different sizes, in presence and absence of PC was monitored. AuNSts also display a very intense optoacoustic signal, though not as high as those exhibited by AuNRs. The optoacoustic performance is very similar for both NP sizes and it highly depends on the concentration of gold utilized. Again, our results suggest an enhancement of the optoacoustic performance in presence of the corona coating for both AuNSt samples.

The optoacoustic performances of all AuNPs involved in this study, in presence and absence of PC, were compared. For this purpose, the areas under the curves of the optoacoustic signal spectra were measured and plotted vs. the concentration of gold utilized. The results indicate that corona-coated AuNRs 70 nm exhibit the best optoacoustic performance, while AuNSs displayed the poorest optoacoustic signals. In order to easily compare their performance, we analysed the optoacoustic signal generated in the phantom using a point source model. The signal emitted from a single NP, modelled as a point source, is proportional to the absorption cross-section of the NP, represented as σ_a, and the fluence of the laser radiation at the source location. If we take into consideration the attenuation undergone by the laser when it travels through the sample applying the Lambert-Beer law, we obtain the following expression:

$$S_{PA} \propto W_0 \frac{\sigma_a}{\sigma_e}\left(1 - \exp\left(-\frac{\sigma_e L}{m} c\right)\right) \qquad \text{Eq.1}$$

Where σ_e is the extinction cross-section, W_0 the excitation of the laser power, c the NP concentration, m the mass of a single NP and L the length of the sample. Assuming a very low concentration, $\sigma_e Lc/m \ll 1$ the previous equation is reduced to the following expression:

$$S_{PA} \propto W_0 L \frac{\sigma_a}{m} c = \alpha c \qquad \text{Eq.2}$$

Which demonstrates the linear dependence of the optoacoustic signal on the sample concentration and the absorption cross-section. The optoacoustic constant α (Equations on Figure 58B), which is interpreted as the optoacoustic efficiency under these conditions was calculated for every sample and displayed in the Table in Figure 58C. The values displayed in Figure 58C confirm the superior optoacoustic performance of PC-coated NPs in comparison with their bare counterparts.

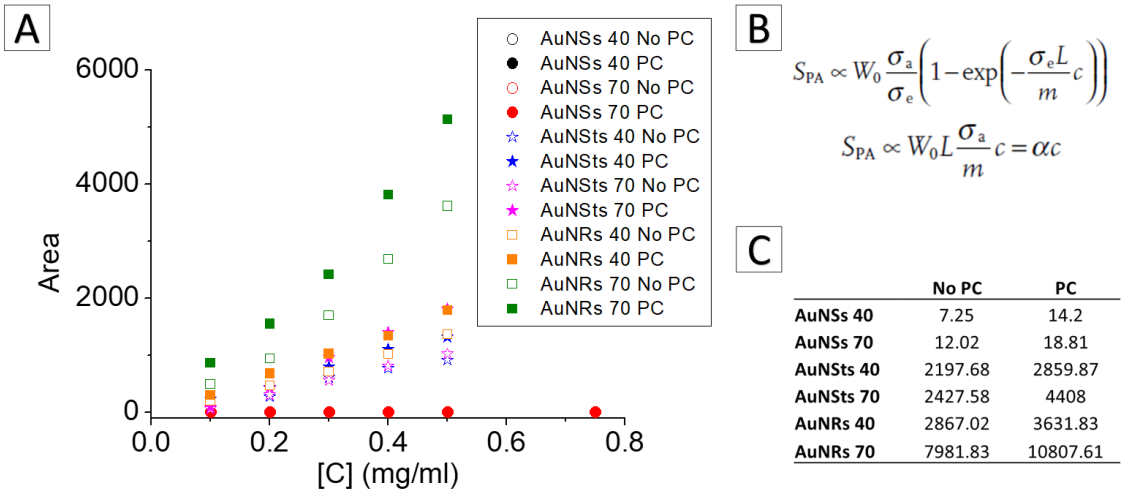

	No PC	PC
AuNSs 40	7.25	14.2
AuNSs 70	12.02	18.81
AuNSts 40	2197.68	2859.87
AuNSts 70	2427.58	4408
AuNRs 40	2867.02	3631.83
AuNRs 70	7981.83	10807.61

Figure 58. (A) Graphical representation of the optoacoustic performance of AuNPs; (B) Equations utilized to calculated the optoacoustic constant α; (C) Table containing the optoacoustic constants for all AuNPs, in presence and absence of protein corona.

This enhancement is an interesting feature that seems strongly related to the presence of a protein coating around the NPs surface. To understand this phenomenon, we searched in the literature for similar cases. In previous publications, an enhancement of the optoacoustic performance of AuNPs was reported to be caused by melanin[263] and silica[253] coatings, respectively. In both works, the authors explained the higher

optoacoustic signal obtained for coated NP by the so called “thermal confinement” phenomenon.

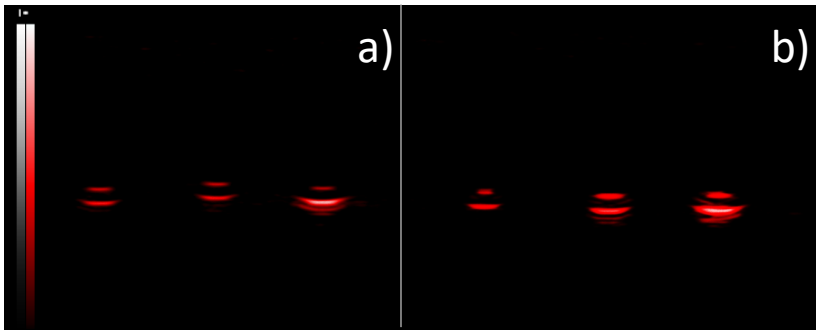

Figure 59. Optoacoustic signal of AuNRs 70 nm. A) 0.1, 0.2 and 0.3 mg/mL AuNRs in absence of corona. B) 0.1, 0.2 and 0.3 mg/mL AuNRs in presence of the corona. As can be observed on the comparative image, the increase on the area is not translated in a sharp enhancement of the optoacoustic signal.

In a typical optoacoustic experiment on pristine AuNPs in aqueous media, the NPs would be illuminated by excitation laser pulses and their optoacoustic signal would be measured. As previously mentioned, the optoacoustic performance of AuNPs is strongly related with their ability to generate heat when irradiated at specific wavelengths. Due to the large heat capacity of water, the heat generated by the AuNPs is efficiently cooled and dispersed very rapidly, which makes the signal drop. In other words, the optoacoustic ability of AuNPs is more dependent on the thermal expansion of the liquid layer in the vicinity of the NP than on the NP itself. Consequently, the possibility of controlling the optoacoustic efficiency by modifying the NP surface with a thermal insulator coating has been proposed. The main result is a synergistic effect between the optical absorbing core and an insulating shell that allows for the design and development of nanoprobes with a better optoacoustic performance.

The effects of the silica[253] and melanin[263] coatings were evaluated by two different groups, which demonstrated that the enhancement of the optoacoustic signal on the coated-NPs was caused by the thermal insulating character of the coating. Nevertheless, the protocol followed by these authors cannot be directly applied to our case. This is mainly due to the complexity of a PC coating, which is in fact composed by a wide variety of different proteins and other biomolecules and thus, approximations cannot be so

easily applied. Even if we are not able to prove it, we hypothesize that the PC is acting as a thermal insulator, leading to the enhancement of the optoacoustic signal of AuNPs.

4. Conclusions – Summary of findings.

On this last thesis chapter, the project focused on the investigation of the influence of the PC on the optoacoustic performance of AuNPs. For this purpose, the optoacoustic signal given by AuNSs, AuNRs and AuNSts of different sizes were measured in absence and presence of corona.

Interestingly, the optoacoustic performance of corona-coated AuNPs was found be superior to that exhibited by bare AuNPs, regardless of the morphology or size of the NP. Optoacoustic signal displays a linear dependence with the concentration of the sample, independent of the size and shape of the morphology and of the presence or absence of the corona. Results of further calculations indicated 70 nm AuNRs displayed the highest optoacoustic performance among all the NPs involved on this study, being the PC-AuNRs superior to their bare counterparts.

The enhancement of the optoacoustic signal observed in our results could be explained by the so-called “thermal confinement effect”. The protein layer around the NP would act as a thermal insulator that concentrates the heat, and would finally lead to a stronger acoustic wave. This phenomenon has been reported in the literature for other NMs such as silica-coated AuNPs and melanin-coated AuNPs. Unfortunately, in those cases a theoretical simulation was utilized in order to confirm the data, which is a rather unfeasible task at the moment due to the complexity of the corona coating.

Blank page.

GENERAL CONCLUSIONS

In general terms, the presented thesis aimed at revealing novel and relevant information related to AuNPs, a very interesting NM extensively proposed as an alternative platform for nanomedicine applications. In this regard, we decided to focus our investigation towards two particular topics, PC formation and optoacoustic performance of AuNPs.

The first part of our research was dedicated exclusively to the study of the PC per se, where the influence of experimental conditions, such as NP morphology and NP size were evaluated. Our results revealed that physico-chemical characteristics of AuNPs, such as size distribution, PDI, surface charge and UV-Visible spectra were modified as a consequence of their interaction with proteins. Quantitative and qualitative analysis of the corona of all AuNPs displayed a high complexity, and showed that the amount of protein adsorbed, as well as the PC profile, were affected by NP size and NP shape. Additionally, AuNSts of different spike length were selected for cell culture studies centred on cell toxicity and cell internalization. AuNSts displayed very low to no toxicity towards A549 and 16HBE cell types. Results of our cell internalization studies suggested that both PC and NP shape have a strong influence on the internalization process. Nevertheless, additional investigations would be needed to confirm these data.

Although the study of PC under *in vitro* conditions is very helpful and gives important data about the interactions of NMs with physiological fluids, we decided to go a step further and performing an *in vivo* PC experiment using CD-1 mice. As a result, we obtained for the first time information about the *in vivo* PC of AuNPs. AuNRs and AuNSts were successfully recovered from the mice and separated from the blood and therefore, study of the physico-chemical characteristics of the PC-AuNP complexes and the characterization of the corona were performed. Results indicated a higher complexity of the *in vivo* PC over its *in vitro* counterpart, their corona profiles and amount of protein adsorbed being influenced by NP size and NP shape.

We then developed a study on optoacoustic imaging of AuNPs. Optoacoustic imaging holds great potential as an alternative tool for medicine, bioimaging and research applications. In particular, gold nanostructures display a powerful optoacoustic signal due to their plasmonic properties and therefore, have been object of study during recent

years. In this collaboration project with Prof. Alexander Kuehne, Dr. Dimitry Chigrin and Prof. Lammers' teams, we focused on the identification of the most relevant parameters of AuNPs design in order to maximize their optoacoustic performance. This project has led to the development of a theoretical model that allowed the determination of two basic guidelines that can be applied to the design of new NPs and NMs with different shapes for optoacoustic imaging purposes: a) An ideal probe should exhibit maximal absorption and minimal scattering efficiencies; b) NP size must be kept small but elongated towards one dimension of the space. Our results indicate that both AuNRs and AuNSts fulfill these requirements.

Finally, our last experiment was dedicated to the effect of PC on the optoacoustic performance of AuNPs of different sizes and shapes, which joined together the two main topics of this thesis: PC and optoacoustic imaging. Remarkably, an enhancement of the optoacoustic signal was observed in the presence of protein coating. This phenomenon could be explained by the corona acting as a thermal insulator coating, leading to an amplified optoacoustic signal. Unfortunately, due to the high complexity of the corona coating, it was not possible to theoretically prove the so-called "thermal confinement" phenomenon.

Blank page.

FUTURE DIRECTIONS

Research and results summarized in this thesis have revealed new and relevant information about different topics of scientific interest such as optoacoustic properties of AuNPs, PC formation on diverse AuNPs and PC effect on optoacoustic performance. This novel information is essential for the adequate design and development of NMs for nanomedicine applications. Nevertheless, there are plenty of options to continue with the investigations presented in this thesis. Below, some proposal for further experiments will be described:

- A complete study of the *in vitro* PC of AuNPs, including AuNSs, AuNRs and AuNSts of 40 and 70 nm. This study would allow to describe the effect of size and shape on the PC formed around AuNPs, improving and completing the results from Chapter 4. Additionally, this project would allow to compare the PC and the stability of NPs after interaction with proteins under *in vitro* and *in vivo* conditions and to further understand the results of Chapter 6.
- Results of Chapter 5 could be improved by designing a similar set of experiments, but adding AuNSs of diameter similar to the core of the AuNSts to be able to compare them with AuNSts of different spike lengths. These would be applicable to cell culture studies, where cell treatment and visualization for TEM should be performed with adequate assessment of experts to improve the quality of the obtained images.
- Plasma is quite a complex mixture of proteins and other biomolecules and therefore, its study is quite complex. It would be useful to carry out protein corona studies in single protein solutions or solutions containing 2-5 different proteins in order to simplify the experimental approach and get additional information of the interaction of certain proteins with the NP surface.
- AuNSts are very interesting NPs with an important distinctive feature with respect to AuNSs, on their surface there are two principal elements present, gold and silver. The interaction with any molecule would be expected to be affected by the characteristics of the surface, therefore the presence of silver would potentially have an effect on interaction and functionalization.

Regarding PC investigations, several alternative techniques are available for the study of interactions between molecules and NMs, such as circular dichroism or isothermal titration calorimetry and many others. Optoacoustic set-up could be modified to get more realistic information about the optoacoustic performance on NPs in physiological media. Summarizing, these are just some of numerous paths that can be chosen for continuing with this research.

Blank page.

APPENDIX – Optimizing the geometry of photoacoustically active gold nanoparticles for biomedical imaging

Gold nanoparticles represent a versatile class of materials, with potential application in various fields, including photoacoustic imaging.[264-266] Pulsed excitation of plasmonic gold nanoparticles leads to periodic heating and thermal expansion and contraction of the particle, as well as the surrounding medium, which can be recorded as ultrasound waves using a conventional ultrasound transducer.[267] For biomedical imaging, photoacoustics is advantageous over fluorescence imaging, as only the excitation light beam needs to penetrate through the tissue.[254] Light becomes attenuated due to absorption and scattering by biological structures, while ultrasound waves can travel through tissue almost unhindered. Tissue exhibits the least absorption and background scattering in the near infrared region, from about 700 to 1300 nm, which is why this spectral region is commonly described as the tissue transparency window.[268] Depending on the shape and size of the plasmonic gold particles, the plasmon extinction can be spectrally shifted into the desired examination window, to gain information also from deep underneath the skin.[266]

A wide variety of synthetic strategies have been developed to obtain gold nanoparticle shapes in a controlled fashion, ranging from spheres, shells, bipyramids and rods to cages and stars.[44, 269] Edges and tips present in some geometries lead to enhancement of the electromagnetic field in these tapers and the emergence of hotspots, where the plasmon-polaritons relax thermally (via electron-phonon coupling).[270] However, different shapes also exhibit different ratios between absorption and scattering, which may be limiting the applicability of such gold nanostructures in photoacoustic imaging.[252, 271] To date, mainly gold nanorods, nanocages, and nanoshells have been applied for biomedical photoacoustic imaging.[262, 263, 272-275] However, the complete parameter space of nanoparticle size, length, diameter and other degrees of freedom with respect to their optimal photoacoustic performance have not been optimized and the contributions of the individual factors are not well understood. This lack of understanding leads to the use of unsuitable or underperforming gold nanoparticle architectures and limited photoacoustic contrast in imaging applications.

Here, we identify the most important parameters for plasmonic nanoparticle design enabling identification of the optimal gold nanoparticle shape and size for maximized photoacoustic efficiency within the tissue transparency window. While the optimal structure is probably impossible to obtain, we approach this ideal by developing suitable size and shape ranges for gold nanorods and gold nanostars. We compare their actual photoacoustic performance with model simulations.

The photoacoustic signal generated by a small plasmonic nanoparticle as part of an ensemble can be described using a point source model.[263, 267] In this case, the signal from a single nanoparticle is proportional to its absorption cross-section σ_a and the fluence of the laser radiation Φ at the source location x:

$$s_{\mathrm{PA}}(x) \propto \sigma_a \Phi(x) = \sigma_a \frac{W(x)}{S} \quad \text{Eq. 1}$$

Here W(x) is the power of the laser radiation and S is the laser beam cross section area. In analysing the total photoacoustic signal, one has to consider that the laser radiation is attenuated as it passes through the sample (see Figure 52a). Using the Beer-Lambert law:

$$W(x) = W_0 \exp\left(-\sigma_e \frac{N}{V} x\right) \quad \text{Eq. 2}$$

the photoacoustic signal from the thin layer dx at position x can be estimated as:

$$s_{\mathrm{PA}}(x) \frac{N}{V} S dx \propto \sigma_a W_0 \exp\left(-\sigma_e \frac{N}{V} x\right) \frac{N}{V} dx \quad \text{Eq.3}$$

Here W_0 is the power of the laser at the sample entrance, σ_e is the extinction cross-section of the nanoparticle, N is the total number of nanoparticles, V is the total illuminated volume and N⁄V is the nanoparticle density. After integration over the sample length L, the total photoacoustic signal is given by:

$$S_{\mathrm{PA}} \propto W_0 \frac{\sigma_a}{\sigma_e}\left(1 - \exp\left(-\frac{\sigma_e L}{m} c\right)\right) \quad \text{Eq.4}$$

Here the weight concentration of nanoparticles c has been introduced:

$$c = m \frac{N}{V} \quad \text{Eq. 5}$$

m being the mass of a single particle.

The total photoacoustic signal is plotted in Figure 1b-c as a function of nanoparticle concentration, for different absorption and extinction cross-sections. It can be seen that two distinct regimes exist. For small concentrations ($\frac{\sigma_e L}{m} c \ll 1$), the total photoacoustic signal is linearly dependent on the concentration and the absorption cross-section:

$$S_{\mathrm{PA}} \propto W_0 L \frac{\sigma_a}{m} c = \alpha c \quad \text{Eq. 6}$$

where α is the photoacoustic efficiency at low concentrations. In order to maximize the photoacoustic efficiency for low concentrations, the absorption cross-section has to be maximized. For large concentrations ($\frac{\sigma_e L}{m} c \gg 1$), the total photoacoustic signal saturates towards a constant value:

$$S_{\mathrm{PA}} \propto \frac{\sigma_a}{\sigma_e} \quad \text{Eq.7}$$

To maximize the photoacoustic efficiency in this case, the absorption cross-section has to be maximized with respect to the extinction cross-section. These observations allow to formulate a first design principle for achieving high performance of the photoacoustic point source: (i) the absorption cross-section of the nanoparticle has to be maximised, not only with respect to its absolute value, but also with respect to the extinction cross-section. Therefore, an ideal photoacoustic probe should display maximal absorption and minimal scattering efficiencies.

For small nanoparticles, the absorption cross-section is proportional to the imaginary part of the particle polarizability α, $\sigma_a \sim \mathrm{Im}\alpha$. The scattering cross-section, σ_s, is proportional to the absolute value squared of the polarizability, $\sigma_s \sim |\alpha|^2$. The polarizability itself is proportional to the particle volume v. Therefore, the absorption cross-section of a plasmonic nanoparticles scales with the particle volume, while its scattering cross-section does with the volume squared, v^2. This results in the dominance of absorption over scattering for the particles with a small volume.[255] Unfortunately, this effect is accompanied by a shift of the plasmon resonance towards the plasma frequency, and so away from the near-infrared (NIR) transparency window of biological tissue. It is well-known that, the plasmon resonance frequency can be shifted towards longer wavelengths by elongating the particle geometry.[255] Combining this with the requirement that the particle volume must be kept small, one arrives at the second design rule for achieving optimal performance of the nanoparticle photoacoustic source:

(ii) the nanoparticle volume has to be kept small with simultaneous increase of one nanoparticle dimension. This requirement can be satisfied by using small nanoparticles with a large aspect ratio.

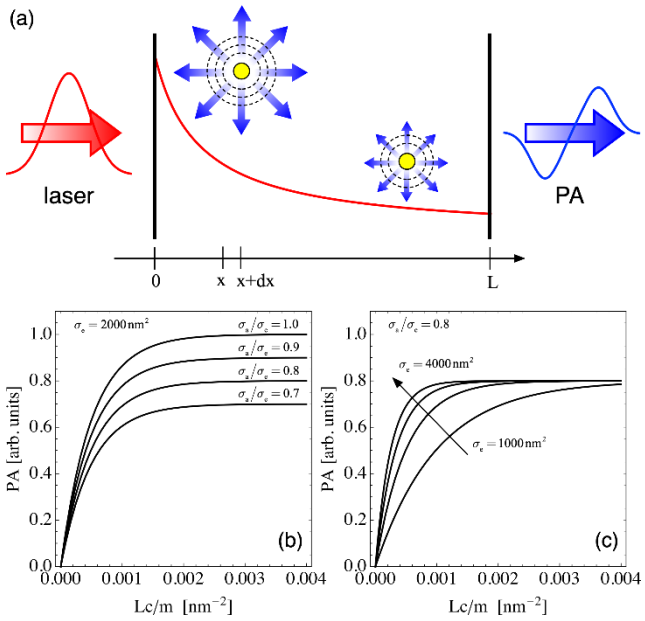

Figure 60. (a) A sketch of photoacoustic signal recording. Gold nanoparticles are heated by an incident laser radiation and generate ultrasound signal. The intensity of the laser beam drops as it propagates through the sample. b) Photoacoustic signal normalized to incident power, as given by Eq. (1) for different fractions of absorption in the extinction cross-sections (70-100%). The extinction cross-section is assumed to be equal to σ_e=2000 nm^2. c) Photoacoustic signal for different extinction cross-sections, from σ_e=1000 nm^2 to σ_e=4000 nm^2. The fractions of absorption in the extinction cross-sections is 80%. With increasing concentration, the photoacoustic signal increases linearly for at low concentrations, while at high particle concentrations of particles, the signal saturates.

Obvious candidates for an optimal photoacoustic source are long, high-aspect ratio nanorods or nanowires.[256] We thus calculated the absolute absorption cross-section and relative absorption of gold nanorods at their absorption maxima, for different diameters and lengths (different aspect rations), as a function of a corresponding wavelength (Figure 60). Relative absorption is defined as the ratio of the absorption to extinction cross-sections, σ_a/σ_e. All calculations were performed using a commercial solver, CST Studio Suite. We employed a finite element solver with the plane-wave excitation linearly polarized along the long axis of the nanorod, in combination with far-

field monitors. Open boundary conditions were used to simulate an infinite water background. Water was assumed to have a refractive index of 1.33. The Johnson-Christy values were used for the wavelength-dependent dielectric constant of gold.[257] It can be clearly seen that, an increase of the nanorod length leads to a shift of the resonance towards longer wavelengths (Figure 61). An increase of the nanoparticle volume results in the simultaneous increase of the absolute absorption and reduction of the relative absorption.

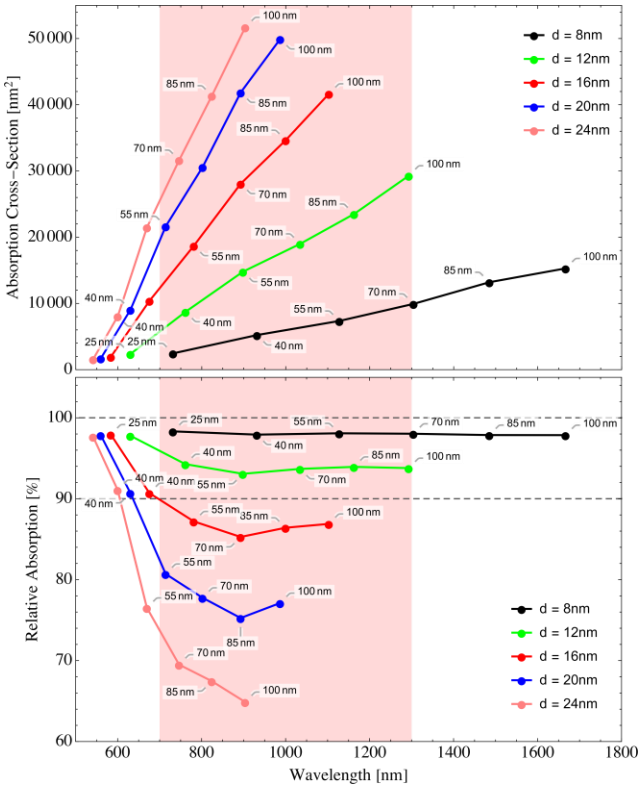

Figure 61. Absolute absorption cross-section (top) and relative absorption (bottom) of gold nanorods at their respective absorption maxima, as a function of a corresponding wavelength. Results for different nanorod diameters and lengths are shown. The light red area marks the NIR transparency window of biological tissue.

A reasonable compromise between these two trends is achieved for nanorods with diameter $d = 12$ nm and length between $l = 40$ nm and $l = 100$ nm. These nanorods demonstrate both large absolute and relative absorption in the NIR transparency window of biological tissue (Figure 61). However, such high aspect ratio gold nanorods have been reported to suffer from degradation due to Rayleigh instability,[258, 276] i.e. breakage of high aspect ratio gold nanostructures into smaller pieces over time. This

degradation is accompanied by a shift of the resonant absorption band towards the visible spectral range, considerably reducing the NIR absorption efficiency over time.

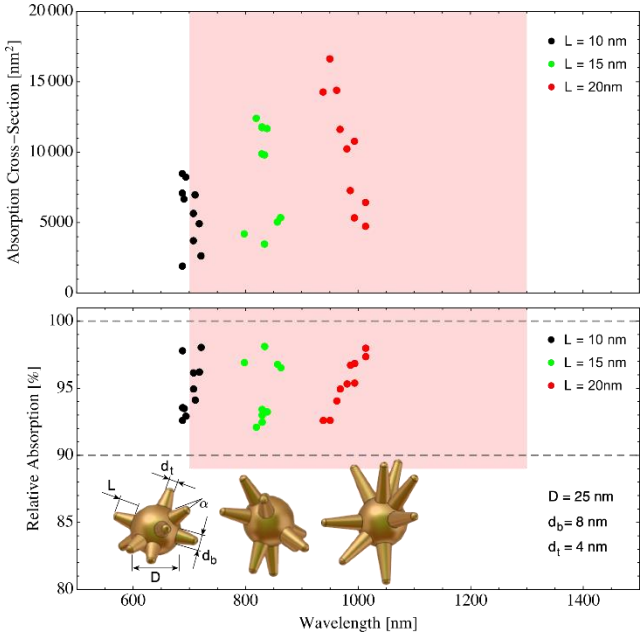

Figure 62. Absolute absorption cross-section (top) and relative absorption (bottom) of gold nanostars at their respective absorption maxima, as a function of a corresponding wavelength. Results for different nanostars geometries are shown. Representation examples of the geometries with relevant dimensions are provided as insets. The light red area marks the NIR transparency window of biological tissue.

A compromise between long term stability of the nanoparticle and high absorption efficiency in the NIR spectral range is offered by gold nanostars.[259] Nanostars consist of a small quasi-spherical core (typical diameter 10-25 nm) and many sharp tips (typical length: 5-25 nm). Their plasmonic response can be roughly understood by considering hybridization of particle plasmon polaritons of the core and the high aspect ratio nanorods representing nanostar tips.[260] Due to the large spectral separation between the corresponding plasmon polariton resonances, the NIR absorption efficiency of gold nanostars resembles that of high aspect ratio gold nanorods, demonstrating both large absolute and relative absorption.[261] We calculated the absolute absorption cross-section and relative absorption at the absorption maximum wavelength for different nanostar geometries, as shown in Figure 55. Three geometries were considered. They all had a core diameter of D=25 nm, and radii of the tips bottom and tips top of d_b=8 nm and d_b=4 nm, respectively. Results for 10 random realizations for tip lengths L=10 nm,

15 nm and 25 nm, are shown. Every realization differs by number and placement of the tips, with an average number of tips ⟨N⟩=10 and a standard deviation σ_N=4. For all nanostar geometries, both absolute and relative absorption are high and comparable with those of long aspect ratio nanorods. Nanostars with tips length larger than L=10 nm satisfy both conditions for an optimal photoacoustic probe, as defined above.

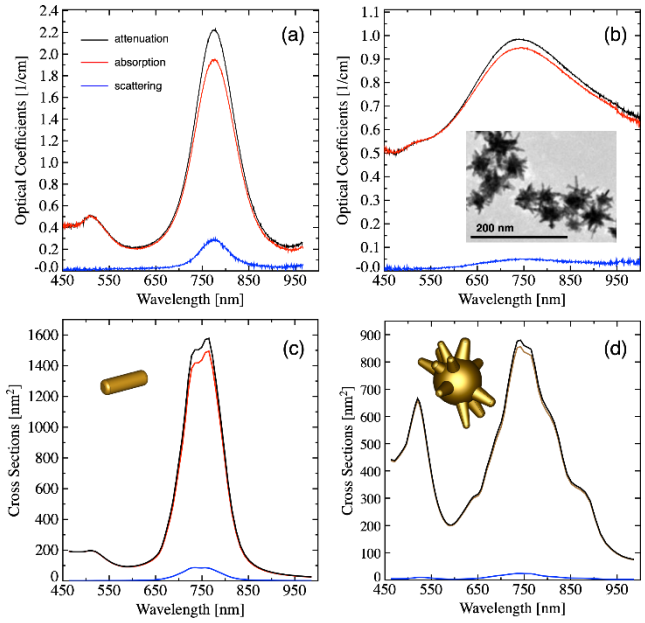

Figure 63. Top panel: Experimental attenuation (extinction), absorption and scattering coefficients for nanorods (a) and nanostars (b). Inset shows a TEM image of nanostars. Relative absorption at the absorption maximum is 87.3% and 95.7% for nanorods and nanostars, respectively. Measurements were performed for different concentrations of nanorods and nanos-tars. Bottom panel: Theoretical extinction, absorption and scattering cross-section for gold nanorods (c) and gold nanostars (d). All spectra were averaged over 100 random realizations of the corresponding geometries. Insets show representative examples of simulated structures. Relative absorption values at the absorption maxima is are 94.5% and 97.1% for nanorods and nanostars, respectively.

In order to confirm our theoretical predictions, we determined the attenuation (extinction), absorption and scattering coefficients of dispersions of gold nanorods and nanostars, with geometries fulfilling the conditions for optimal photoacoustic performance. Gold nanorods with average length of 38.0 ± 3.8 nm and diameter of 10.0 ± 1.0 nm were used. The rods were stabilized by cetyltrimethylammonium bromide (CTAB) and dispersed in water. Gold nanostars were synthetized following previously

reported protocols.[117, 207, 277] Geometrical parameters of the nanostars were determined through inspection of at least 100 particles in TEM images. The average equivalent diameter of the nanostars was 45.0 ± 5.0 nm, with an average core diameter of 25.0 ± 2.0 nm. Experimental attenuation, absorption and scattering coefficients are shown for nanorods and nanostars in Figure 55a and 55b, respectively.

The measurements were performed by using an integrating sphere setup. The setup consists of an Andor spectrometer (iDus 420 CCD camera and Shamrock 303i spectrograph) and an integrating sphere with barium sulfate coating (UPB-150-ARTA from Gigahertz-Optik). Both nanoparticle types demonstrated pronounced resonances in the NIR transparency window near 750 nm, with absorption dominating over scattering. The resonance band of nanostars was found to be largely broadened, compared to nanorod resonances, due to higher dispersity in nanostar geometries. Both nanoparticle types show high relative absorption at the maximum wavelength, with 87.3% and 95.7% for nanorods and nanostars, respectively.

Calculated attenuation, absorption and scattering cross-sections for gold nanorods and gold nanostars are shown in Figure 56c and 56d, respectively. All spectra were calculated for linearly polarized plane wave excitation and averaged over 100 realizations of randomly oriented nanorods (c) and nanostars (d) geometries. The best fit to the experimental data was obtain for nanorods with average length $\langle L\rangle$=38.0 nm, standard deviation of σ_L=2 nm and average diameter $\langle d\rangle$=12.0 nm with σ_d=1.0 nm. For the nanostars, the best fit was obtained for a core diameter of 25 nm, an average number of tips of $\langle N\rangle$=6 with σ_N=4, length of tips $\langle L\rangle$=10.0 nm with σ_L=2.0 nm, diameter of the tip at the top of $\langle d_t \rangle$=4.0 nm with $\sigma_{(dt)}$=1.0 nm and taper opening angle of $\langle\alpha\rangle$=8.0° with σ_α=2°. The calculated spectral position of the plasmon resonance modes, as well as the relative and absolute absorption values, are in good agreement with the experimental data. Both types of nanoparticles demonstrated large relative and absolute absorption efficiencies, with relative absorption at maximum wavelength being 94.5% and 97.1% for nanorods and nanostars, respectively.

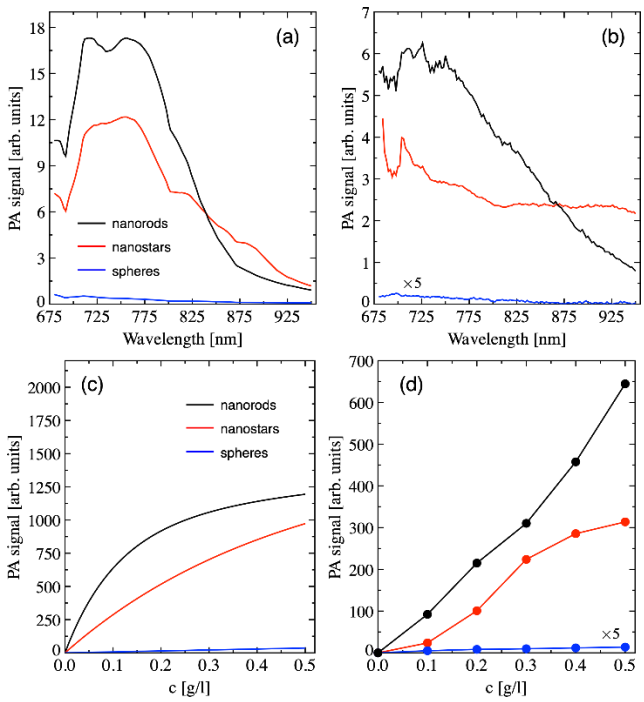

Figure 64. Top panel: Photoacoustic signal as a function of excitation laser wavelength. Theoretical (a) and experimental (b) data are shown for a concentration c=0.4 g/L. Bottom panel: Theoretical (c) and experimental (d) total photoacoustic signal over a wavelength range from 690 nm to 900 nm, as a function of concentration. Data for nanorods (black), nanostars (red) and nanospheres (blue) are shown. Experimental photoacoustic signal for nanospheres is multiplied by a factor 5.

We thus proceeded to investigate the photoacoustic signal for optimized nanorods and nanostar geometries. For comparison, we also include the results for a non-optimized plasmonic nanostructure, namely nanospheres of comparable diameter (d = 44 nm), as shown in Figure 64. We calculated the theoretical photoacoustic signal using Eq. (1) and the absorption and extinction cross sections reported in Figure 4c-d for gold nanorods and nanostars (Figure 64a, 64c). For gold nanospheres we determined the attenuation cross section by averaging over 100 realizations, with an average diameter of 44 nm and a standard deviation of 6 nm (not shown here). The length of the sample was assumed to be 600 µm, which corresponds the length of the experimentally used phantom. The numerical value of the laser power at different wavelengths was obtained from the literature.[278] The average mass of the gold nanoparticles was calculated using their averaged volume and density (ρ=19300 kg/m^3).[279] The photoacoustic signal from both nanorods and nanostars was found to follow the spectral shape of the attenuation cross

section, being considerably stronger than the signal from gold nanospheres across all excitation wavelengths and concentrations (Figure 64a and 64c). For a concentration of c=0.4 g/l, the signal enhancement was as large as 55 and 35 times for nanorods and nanostars, respectively (see Figure 64a). The dependence of the total photoacoustic signal as a function of concentration, calculated as a sum over the wavelength interval from 690 nm to 900 nm, shows the expected and characteristic saturation behavior (compare with Figure 53b-c). While the absorption cross section for gold nanorods is larger than that for nanostars, the photoacoustic signal from nanorods grows faster for low concentrations but also saturates at lower values due to the smaller relative absorption.

Photoacoustic measurements of synthesized[117, 207, 277] nanorods, nanostars and nanospheres were performed on a Visualsonics Vevo LAZR. The gold nanoparticles were analyzed in tubing phantoms (air bubble free polyurethane intravascular tubing, 0.025 x 0.040 in, INSTECH), as an aqueous dispersion of the corresponding nanoparticle concentration. The previously described gold nanorods, nanostars and nanospheres were used. The spectral dependence of the photoacoustic signal shows good qualitative agreement with the theoretical prediction. For a concentration of c=0.4 g/L, the signal enhancement with respect to the signal from nanospheres is as large as 35- and 25-fold for nanorods and nanostars, respectively. The concentration dependence of the photoacoustic signal showed the expected saturation character for all concentrations in the case of nanostars. However, for gold nanorods the photoacoustic signal deviated substantially from the expected trend for large concentrations (c>0.4 g/L). We attribute this behavior to additional nonlinearities of the photoacoustic process, which are not considered by our model.

In conclusion, we have developed a theoretical model for the photoacoustic response of gold nanoparticles, considering their size, tip length and taper angle, as well as batch heterogeneity. This model allows to formulate two simple constraints for nanoparticles properties, to obtain an optimal photoacoustic performance in the tissue transparency window. We demonstrate that gold nanorods and nanostars can be designed to fulfil both constraints. While gold nanorods exhibit slightly better performance, their bio-compatibility and cytotoxicity might limit their application.[270] Gold nanostars might

represent the superior geometry with comparable performance and better biocompatibility. However, previous studies have shown that biocompatibility can be improved by coating the gold nanoparticles with inert materials.[263] In the future, the here developed model will allow modelling the performance of gold nanoparticles for a variety of further applications. Furthermore, the model represents a means to derive guidelines for the development of other nanoparticle shapes and materials for photoacoustic imaging applications.

Blank page.

REFERENCES

1. Feynman, R.P., *There is Plenty of Room at the Bottom.* Engineering and Science, 1976. **23**(5): p. 15.
2. Taniguchi, N., *On the Basic Concept of Nanotechnology.* Proceedings of the International Conference on Production Engineering Tokyo, 1974: p. 6.
3. D. M. Eigler and E.K. Schweizer, *Positioning single atoms with a scanning tunnelling microscope.* Nature, 1990. **344**: p. 3.
4. G. Binning and C.F. Quate, *Atomic Force Microscope.* Physical Review Letters 1986. **56**(9): p. 5.
5. D. Rugar and P. Hansma, *Atomic Force Microscopy.* Physics Today, 1990. **43**(10): p. 3.
6. M. R. Wiesner and J.-Y. Bottero, *Environmental Nanotechnology*. 2007.
7. V. S. Saji, H. C. Choe, and K.W.K. Yeung, *Nanotechnology in biomedical applications: a review.* International Journal of Nano and Biomaterials 2010. **3**(2): p. 21.
8. B. Y. S. Kim, J. T. Rutka, and W.C.W. Chan, *Nanomedicine.* The New England Journal of Medicine, 2010. **363**: p. 10.
9. M. De, P. S. Ghosh, and V.M. Rotello, *Applications of Nanoparticles in Biology.* Advanced Materials, 2008. **20**: p. 17.
10. A. Z. Mirza and F.A. Siddiqui, *Nanomedicine and drug delivery: a mini review.* International Nano Letters, 2014. **4**: p. 7.
11. R. Mout, et al., *Surface functionalization of nanoparticles for nanomedicine.* Chemical Society Reviews, 2012. **41**(7): p. 5.
12. S. Hua and S.Y. Wu, *Advances and Challenges in Nanomedicine*. 2019.
13. S. Nazir, et al., *Nanomaterials in combating cancer: Therapeutic applications and developments.* Nanomedicine: Nanotechnology, Biology, and Medicine, 2014. **10**: p. 5.
14. M. Bellah, S. M. Christensen, and S.M. Iqbal, *Nanostructures for Medical Diagnosis.* Journal of Nanomaterials, 2012. **1**: p. 21.
15. N. Ahmed, H. Fessi, and A. Elaissari, *Theranostic applications of nanoparticles in cancer.* Drug Discovery Today, 2012. **17**(17-18): p. 7.
16. D. Docter, et al., *The nanoparticle biomolecule corona: lessons learned - challenge accepted?* Chemical Society Reviews, 2015. **44**: p. 28.
17. Vroman, L., *Effect of Adsorbed Proteins on the Wettability of Hydrophilic and Hydrophobic Solids.* Nature, 1962. **196**: p. 2.
18. D. F. Moyano, et al., *Fabrication of Corona-Free Nanoparticles with Tunable Hydrophobicity.* ACS Nano, 2014. **8**(7): p. 8.
19. R. Gref, et al., *"Stealth" corona-core nanoparticles surface modified by polyethylene glycol (PEG): influences of the corona (PEG chain length and surface density) and of the core compositionon phagocytic uptake and plasma protein adsorption.* Colloids and Surfaces B: Biointerfaces, 2000. **18**(3-4): p. 14.
20. T. Cedervall, et al., *Understanding the nanoparticle-protein corona using methods to quantifyexchange rates and affinities of proteins for nanoparticles.* Proceedings of the National Academy of Sciences, 2007. **104**: p. 6.
21. M. Mahmoudi, et al., *Protein-Nanoparticle Interactions: Opportunities and Challenges.* Chemical Reviews, 2011. **111**: p. 28.
22. M. Monopoli, et al., *Biomolecular coronas provide the biological identity of nanosized materials.* Nature Nanotechnology, 2012. **7**: p. 8.
23. Caracciolo, G., *Clinically approved liposomal nanomedicines: lessons learned from the biomolecular corona.* Nanoscale, 2018. **10**: p. 6.
24. C. D. Walkey and W.C.W. Chan, *Understanding and controlling the interaction of nanomaterials with proteins in a physiological environment.* Chemical Society Reviews, 2012. **41**: p. 22.

25. P. C. Ke, et al., *A Decade of the Protein Corona.* ACS Nano, 2017. **11**(12): p. 4.
26. S. Zanganeh, et al., *Protein Corona. Opportunities and Challlenges.* International Journal of Biochemistry and Cell Biology, 2016. **75**: p. 5.
27. E. D. Kaufman, et al., *Probing protein adsorption onto mercaptoundecanoid acid stabilized gold nanoparticles and surfaces by quartz crystal microbalance and zeta-potential measurements.* Langmuir, 2007. **23**: p. 10.
28. H. Wang, et al., *The Nature of a Hard Protein Corona Forming on Quantum Dots Exposed to Human Blood Serum.* Small, 2016. **12**(45): p. 9.
29. G. Caracciolo, et al., *Lipid composition: a "key" factor for the rational manipulation of the liposome-protein corona by liposome design.* The Royal Society fo Chemistry Advances, 2015. **5**: p. 9.
30. M. M. Yallapu, et al., *Implications of protein corona on physico-chemical and biological properties of magnetic nanoparticles.* Biomaterials, 2015. **46**: p. 12.
31. E. Casals, et al., *Time Evolution of the Nanoparticle Protein Corona.* ACS Nano, 2010. **4**(7): p. 10.
32. M. Hadjidemetriou, Z. Al-Ahmady, and K. Kostarelos, *Time-evolution of in vivo protein corona onto blood-circulating PEGylated liposomal doxorubicin (DOXIL) nanoparticles.* Nanoscale, 2016. **8**: p. 12.
33. L. Shang and G.U. Nienhaus, *In Situ Characterization of Protein Adsorption onto Nanoparticles by Fluorescence Correlation Spectroscopy* Accounts of Chemical Research, 2017. **50**: p. 9.
34. H. Wang, et al., *The protein corona on nanoparticles as viewed from a nanoparticle-sizing perspective.* WIREs Nanomedicine and Nanotechnology, 2018: p. 9.
35. S. Milani, et al., *Reversible versus Irreversible Binding of Transferrin to Polystyrene Nanoparticles: Soft and Hard Corona.* ACS Nano, 2012. **6**(3): p. 10.
36. S. A. Ahsan, C. M. Rao, and M.F. Ahmad, *Nanoparticle-Protein Interaction: The Significance and Role of Protein Corona.* Cellular and Molecular Toxicology of Nanoparticles - Advances, 2018. **1**: p. 24.
37. S. Tenzer, et al., *Nanoparticle Size is a Critical Physicochemical Determinant of the Human Blood Plasma Corona: A Comprehensive Quantitative Proteomic Analysis.* ACS Nano, 2011. **5**(9): p. 13.
38. M. Schaffler, et al., *Serum protein identification and quantification of the corona of 5, 15 and 80 nm gold nanoparticles.* Nanotechnology, 2013. **24**(26): p. 10.
39. J. E. Gagner, et al., *Effect of gold nanoparticle morphology on adsorbed protein structure and function.* Biomaterials, 2011. **32**(12): p. 7241.
40. J. S. Gebauer, et al., *Impact of the Nanoparticle - Protein Corona on Colloidal Stability and Protein Structure.* Langmuir, 2012. **28**: p. 7.
41. M. A. Dobrovolskaia, et al., *Interaction of colloidal gold nanoparticles with human blood: effects on particle size and analysis of plasma protein binding profiles.* Nanomedicine: Nanotechnology, Biology, and Medicine, 2009. **5**: p. 12.
42. M. Lundqvist, et al., *Nanoparticle size and surface properties determine the protein corona with possible implications for biological impacts.* Proceedings of the National Academy of Sciences, 2008. **105**(38): p. 6.
43. S. E. Baker, et al., *Covalently bonded adducts of DNA oligonucleotides with single wall carbon nanotubes: synthesis and hybridization.* Nano Letters, 2002. **2**: p. 5.
44. M. Grzelczak, et al., *Shape control on gold nanoparticle synthesis.* Chemical Society Reviews, 2008. **37**: p. 10.
45. A. Shavel and L.M. Liz-Marzán, *Shape control on iron oxide nanoparticles.* Physical Chemistry Chemical Reviews, 2009. **11**: p. 5.
46. Z. J. Deng, et al., *Differential plasma protein binding to metal oxide nanoparticles.* Nanotechnology, 2009. **20**: p. 10.

47. Z. Ma, et al., *Impact of Shape and Pore Size of Mesoporous Silica Nanoparticles on Serum Protein Adsorption and RCBs Hemolysis.* ACS Applied Materials and Interfaces, 2014. **6**: p. 8.
48. K. P. García, et al., *Zwitterionic-Coated "Stealth" Nanoparticles for Biomedical Applications: Recent Advances in Countering Biomolecular Corona Formation and Uptake by the Mononuclear Phagocyte System.* Small, 2014. **10**(13): p. 14.
49. Q. Dai, C. Walkey, and W.C.W. Chan, *Polyethylene Glycol Backfilling Mitigates the Negative Impact of the Protein Corona on Nanoparticle Cell Targeting.* Angewandte, 2014. **53**: p. 4.
50. S. Schottler, et al., *Protein adsorption is required for stealth effect of poly(ethylene glycol)- and poly(phosphoester)-coated nanocarriers.* Nature Nanotechnology, 2016. **11**: p. 6.
51. M. Aoyama, et al., *Clusterin in the protein corona plays a key role in the stealth effect of nanoparticles against phagocytes.* Biochemical and Biophysical Research Communications, 2016. **480**(4): p. 6.
52. V. Mirshafiee, et al., *Impact of pre-coating on the protein corona composition and nanoparticle cellular uptake* Biomaterials, 2016. **75**: p. 10.
53. M. Mahmoudi, A. S. Milani, and P. Stroeve, *Synthesis, surface architecture and biological response of superparamagnetic iron oxide nanoparticles for application in drug delivery: a review.* International Journal of Biomedical Nanoscience and Nanotechnology, 2010. **1**(2-4): p. 5.
54. M. S. Ehrenberg, et al., *The influence of protein adsorption on nanoparticle association with cultured endothelial cells.* Biomaterials, 2009. **30**(4): p. 8.
55. J. C. Y. Kah, et al., *Protein Coronas on Gold Nanorods Passivated with Amphiphilic Ligands Affect Cytotoxicity and Cellular Responseto Penicillin/Streptomycin.* ACS Nano, 2014. **8**(5): p. 13.
56. V. H. Nguyen and B.-J. Lee, *Protein corona: a new approach for nanomedicine design.* International Journal of Nanomedicine, 2017. **12**: p. 15.
57. G. Maiorano, et al., *Effects of Cell Culture Media on the Dynamic Formation of Protein-Nanoparticle Complexes and Influence on the Cellular Response.* ACS Nano, 2010. **4**(12): p. 11.
58. A. Albanese, et al., *Secreted Biomolecules Alter the Biological Identity and Cellular Interactions of Nanoparticles.* ACS Nano, 2014. **8**(6): p. 12.
59. S. Schottler, et al., *Protein source and choice of anticoagulant decisively affects nanoparticle protein corona and cellular uptake.* Nanoscale, 2016. **8**: p. 11.
60. D. Pozzi, et al., *Sruface chemistry and serum type both determine the nanoparticle-protein corona.* Journal of Proteomics, 2015. **119**: p. 9.
61. V. Mirshafiee, et al., *The importance of selecting a proper biological milieu for protein corona analysis in vitro: Human plasma versus human serum.* The International Journal of Biochemistry and Cell Biology, 2015. **75**: p. 8.
62. A. Solorio-Rodríguez, et al., *A comparison of the human and mouse protein corona profiles of functionalized SiO_2 nanocarriers.* Nanoscale, 2017. **9**: p. 10.
63. A. Kumar, et al., *Enrichment of the immunoregulatory proteins in the biomolecular corona of nanoparticles within human respiratory tract lining fluid.* Nanomedicine: Nanotechnology, Biology, and Medicine, 2016. **12**(4): p. 11.
64. D. Bonvin, et al., *Protein Corona: Impact of Lymph Versus Blood in a Complex In Vitro Environment.* Small, 2017. **1**: p. 13.
65. D. H. Jo, et al., *Nanoparticle-protein complexes mimicking corona formation on ocular environment.* Biomaterials, 2016. **109**: p. 9.
66. A. Cox, et al., *Evolution of Nanoparticle Protein Corona Across the Blood-Brain Barrier.* ACS Nano, 2018. **12**(7): p. 9.

67. D. Dell'Orco, et al., *Modeling the Time Evolution of the Nanoparticle-Protein Corona in a Body Fluid.* PLOS One, 2010. **5**(6): p. 8.
68. C. Pisani, et al., *The timeline of corona formation around silica nanocarriers highlights the role of the protein interactome.* Nanoscale, 2017. **9**(5): p. 12.
69. M. Mahmoudi, et al., *Temperature: The "Ignored" Factor at the NanoBio Interface.* ACS Nano, 2013. **7**(8): p. 9.
70. M. Mahmoudi, et al., *Variation of Protein Corona Composition of Gold Nanoparticles Following Plasmonic Heating.* Nano Letters, 2014. **14**: p. 7.
71. S. Palchetti, et al., *The protein corona of circulating PEGylated liposomes.* Biochimica et Biophysica Acta, 2016. **1858**: p. 8.
72. U. Sakulkhu, et al., *Ex situ evaluation of hte composition of the protein corona of intravenously injected superparamagnetic nanoparticles in rats.* Nanoscale, 2014. **6**: p. 12.
73. M. Hadjidemetriou, et al., *In Vivo Biomolecule Corona Around Blood-Circulating, Clinically Used and Antibody-Targeted Lipid Bilayer Nanoscale Vesicles.* ACS Nano, 2015. **9**(8): p. 15.
74. C. Corbo, et al., *The impact of nanoparticle protein corona on cytotoxicity, immunotoxicity and target drug delivery.* 11, 2016. **1**(20): p. 81.
75. P. Foroozandeh and A.A. Aziz, *Merging Worlds of Nanomaterials and Biological Environment: Factor Governing Protein Corona Formation on Nanoparticles and Its Biological Consequences.* Nanoscale Research Letters, 2015. **10**: p. 12.
76. P. Wang, et al., *Interaction of gold nanoparticles with proteins and cells.* Science and Technology of Advanced Materials, 2015. **16**: p. 15.
77. A. Lesniak, et al., *Effects of the Presence and Absence of Protein Corona on Silica Nanooparticle Uptake and Impact on Cells.* ACS Nano, 2012. **6**(7): p. 13.
78. B. Pelaz, et al., *Surface Functionalization of Nanoparticles with Polyethylene Glycol: Effects on Protein Adsorption and Cellular Uptake.* ACS Nano, 2015. **9**(7): p. 13.
79. M. Mahmoudi, et al., *Cell "vision": complementary factor of protein corona in nanotoxicology.* Nanoscale, 2012. **4**(8): p. 5461.
80. Frohich, E., *The role of surface charge in cellular uptake and cytotoxicity of medical nanoparticles.* International Journal of Nanomedicine, 2012. **7**: p. 15.
81. Q. Peng, et al., *Preformed albumin corona, a protective coating for nanoparticles based drug delivery systems.* Biomaterials, 2013. **34**: p. 10.
82. F. Wang, et al., *The biomolecular corona is retained during nanoparticle uptake and protects the cells from damage induced cationic nanoparticles until degraded in the lysosomes.* Nanomedicine 2013. **9**: p. 10.
83. S. Mirshadegi, et al., *Protein corona composition of gold nanoparticles/nanorods affects amyloid beta fibrillation process.* Nanoscale, 2015. **7**: p. 10.
84. S. H. De Paoli, et al., *The effect of the protein corona composition on the interaction of carbon nanotubes with human blood platelets.* Biomaterials, 2014. **35**: p. 13.
85. C. C. Ge, et al., *Binding of blood proteins to carbon nanotubes reduces toxicity.* Proceedings of the National Academy of Sciences, 2011. **108**: p. 6.
86. S. Tenzer, et al., *Rapid formation of plasma protein corona critically affects nanoparticle pathophysiology.* Nature Nanotechnology, 2013. **8**: p. 10.
87. A. Manke, L. Wang, and Y. Rojanasakul, *Mechanisms of nanoparticle-induced oxidative stress and toxicity.* BioMed Research International, 2013: p. 15.
88. A. Salvati, et al., *Transferrin-functionalized nanoparticles lose their targeting capabilities when a biomolecule corona adsorbs on the surface.* Nature Nanotechnology, 2013. **8**: p. 7.
89. Q. Dai, et al., *Monoclonal Antibody-Functionalized Multilayered Particles: Targeting Cancer Cells in the Presence of Protein Coronas.* ACS Nano, 2015. **9**(3): p. 10.

90. J. Y. Oh, et al., *Cloacking nanoparticles with protein corona shield for targeted drug delivery.* Nature Communications, 2018. **9**: p. 9.
91. S. Palchetti, et al., *Exploitation of nanoparticle-protein corona for emerging therapeutic and diagnostic applications.* Journal of Material Chemistry B, 2016. **4**: p. 6.
92. M. Hadjidemetriou and K. Kostarelos, *Evolution of the nanoparticle corona.* Nature Nanotechnology, 2017. **12**: p. 3.
93. C. Corbo, et al., *Presonalized protein corona on nanoparticles and its clinical implications.* Biomaterials Science, 2017. **5**(3): p. 10.
94. M. J. Hajipour, et al., *Personalized protein coronas: a "key" factor at the nanobiointerface.* Biomaterials Science, 2014. **2**: p. 12.
95. M. J. Hajipour, et al., *Personalized disease-specific protein corona influences the therapeutic impact of graphene oxide.* Nanoscale, 2015. **7**: p. 17.
96. V. Colapicchioni, et al., *Presonalized liposome-protein corona in the blood of breast, gastric and pancreatic cancer patients.* The International Journal of Biochemistry and Cell Biology, 2015. **75**: p. 10.
97. M. Hadjdemetriou, et al., *A novel scavenging tool for cancer biomarker discovery based on the blood-circulating nanoparticle protein corona.* Biomaterials, 2019. **188**: p. 12.
98. M. Hadjdemetriou, et al., *The Human In Vivo Biomolecule Corona onto PEGylated Liposomes: A Proof-of-Concept Clinical Study.* Advanced Materials, 2019. **31**(4).
99. S. Ashraf, et al., *Gold-Based Nanomaterials for Applications in Nanomedicine.* Topics in Current Chemistryº, 2016. **370**: p. 34.
100. W. L. Barnes, A. Dereux, and T.W. Ebbesen, *Surface plasmon subwavelength optics.* Nature, 2003. **424**: p. 7.
101. M-C. Daniel and D. Astruc, *Gold Nanoparticles: Assembly, Supramolecular Chemistry, Quantum-Size-Related Properties, and Applications towards Biology, Catalysis, and Nanotechnology.* Chemical Reviews, 2004. **104**: p. 54.
102. Liz-Marzán, L.M., *Tailoring Surface Plasmons through the Morphology and Assembly of Metal Nanoparticles.* Langmuir, 2006. **22**(1): p. 10.
103. C. Burda, et al., *Chemistry and Properties of Nanocrystals of Different Shapes.* Chemical Reviews, 2005. **105**(4): p. 78.
104. K. L . Kelly, et al., *The Optical Properties of Metal Nanoparticles: The Influence of Size, Shape, and Dielectric Environment.* The Journal of Physical Chemistry B, 2003. **107**(3): p. 10.
105. Faraday, M., *The Bakerian Lecture - Experimental relations of gold (and other metals) to light.* Philosophical Transactions 1857. **147**: p. 37.
106. Horvath, H., *Gustav Mie and the scattering and absorption of light by particles: Historic developments and basics.* Journal of Quantitative Spectroscopy and Radiative Transfer, 2009. **110**: p. 13.
107. Mie, G., Annalen der Physics, 1908. **25**.
108. R. Shenhar and V.M. Rotello, *Nanoparticles: Scaffolds and Building Blocks* Accounts of Chemical Research, 2003. **36**(7): p. 13.
109. J. Turkevich, C.S. P, and J. Hillier, *A study of the nucleation and growth processes in the sysnthesis of colloidal gold.* Discussions of the Faraday Society, 1951. **11**: p. 21.
110. N. G. Bastús, J. Comenge, and V. Puntes, *Kinetically Controlled Seeded Growth Synthesis of Citrate-Stabilized Gold Nanoparticles of up to 200 nm: Size Focus versus Ostwald Ripening.* Langmuir, 2011. **27**: p. 8.
111. U. Kreibig and M. Vollmer, *Optical Properties of Metal Clusters*. 1995: Springer
112. X. Huang, S. Neretina, and M.A. El-Sayed, *Gold Nanorods: From Synthesis and Properties to Biological and Biomedical Applications.* Advanced Materials, 2009. **21**(48): p. 31.
113. Gans, R., Annalen der Physiks, 1912. **342**(5).

114. M. Liu and P. Guyot-Sionnest, *Mechanism of Silver(I)-Assisted Growth of Gold Nanorods and Bipyramids.* The Journal of Physical Chemistry B, 2005. **109**(47): p. 9.
115. B. Nikoobakht and M.A. El-Sayed, *Preparation and Growth Mechanism of Gold Nanorods (NRs) Using Seed-Mediated Growth Method* Chemistry of Materials 2003. **15**(10).
116. L. Scarabelli, et al., *A "Tips and Tricks" Practical Guide to the Synthesis of Gold Nanorods* The Journal of Physical Chemistry Letters, 2015. **6**(21): p. 10.
117. P. S. Kumar, et al., *High-yield synthesis and optical response of gold nanostars* Nanotechnology, 2008. **19**: p. 6.
118. G. Chirico, M. Borzenkov, and P. Pallavicini, *Gold Nanostars: Synthesis, Properties and Biomedical Application*. 2015: Springer.
119. I. Freestone, et al., *The Lycurgus Cup - A Roman Nanotechnology.* Gold Bulletin, 2007. **40**(4): p. 8.
120. Antonii, F., *Panacea Aurea-Auro Potabile*. 1618: Hamburg: Ex Bibliopolio Frobeniano.
121. P. Zhao, N. Li, and D. Astruc, *State of the art in gold nanoparticle synthesis.* Coordination Chemistry Reviews, 2013. **257**: p. 28.
122. T. K. Sau and D.V. Goia, *Biomedical Applications of Gold Nanoparticles*. 2012: Springer.
123. R. Cao-Milán and L.M. Liz-Marzán, *Gold nanoparticle conjugates: recent advances toward clinical applications.* Expert Opinion on Drug Delivery, 2014. **11**(5): p. 12.
124. H. Maeda, et al., *Vascular permeability enhancement in a solid tumor: various factors, mechanisms involved and its implications.* International Immunopharmacology, 2003. **3**(3): p. 10.
125. Greish, K., *Enhanced permeability and retention of macromolecular drugs in solid tumor: a royal gate for targeted anticancer nanomedicines.* Journal of Drug Targeting, 2007. **15**(7-8): p. 7.
126. M. Srinivasarao and P.S. Low, *Ligan-Targeted Drug Delivery.* Chemical Reviews, 2017. **117**: p. 32.
127. J. M. De la Fuente and C.C. Berry, *Tat Peptide as an Efficient Molecule To Translocate Gold Nanoparticles into the Cell Nucleus.* Bioconjugate Chemistry, 2005. **16**(5): p. 5.
128. D. P. O'Neal, et al., *Photo-thermal tumor ablation in mice using near infrared-absorbing nanoparticles.* Cancer Letters, 2004. **209**(2): p. 6.
129. R. A. Sperling, et al., *Biological Applications of gold nanoparticles.* Chemical Society Reviews, 2008. **37**: p. 13.
130. X. Li, et al., *PEGylated PAMAM dendrimer-doxorubicin conjugate-hybridized gold nanorod for combined photothermal-chemotherapy.* Biomaterials, 2014. **35**(24): p. 9.
131. J. D. Gibson, B. P. Khanal, and E.R. Zubarev, *Paclitaxel-functionalized gold nanoparticles.* Journal of the American Chemical Society, 2007. **129**(37): p. 9.
132. D. Liu, et al., *The Smart Drug Delivery System and Its Clinical Potential.* Theranostics, 2016. **6**(9): p. 18.
133. S. Carregal-Romero, M. Ochs, and W.J. Parak, *Nanoparticle-functionalized microcapsules for in vitro delivery and sensing.* Nanophotonics, 2012. **1**: p. 10.
134. G. L. Zwicke, G. A. Mansoori, and C.J. Jeffrey, *Utilizing the folate receptor for active targeting of cancer nanotherapeutics.* Nano Reviews, 2012. **3**: p. 11.
135. Y. Lu and P. S. Low, *Folate-mediated delivery of macromolecular anticancer therapeutic agents.* Advanced Drug Delivery Reviews, 2002. **54**(5): p. 19.
136. N. A. Koonce, et al., *Combination of Gold Nanoparticle-Conjugated Tumor Necrosis Factor-α and Radiation Therapy Results in a Synergistic Antitumor Response in Murine Carcinoma Models.* International Journal of Radiation Oncology Biology Physics, 2015. **93**(3).
137. F. C. Victor and A.B. Gottlieb, *TNF-α adn apoptosis: implications for the pathogenesis and treatment of psoriasis.* Journal of Drugs in Dermatology, 2002. **1**.

138. S. Hwang, et al., *Gold nanoparticle-mediated photothermal therapy: current status and future perspective.* Nanomedicine (Lond), 2003. **9**(13): p. 20.
139. M. A. Mackey, et al., *The Most Effective Gold Nanorod Size for Plasmonic Photothermal Therapy: Theory and In Vitro Experiments.* The Journal of Physical Chemistry B, 2014. **118**(5): p. 8.
140. J. Chen, et al., *Gold Nanocages: Engineering Theri Structure for Biomedical Applications.* Advanced Materials, 2005. **17**(18): p. 7.
141. B. Jang, et al., *Gold nanorod-photosensitizer complex for near-infrared fluorescence imaging and photodynamic/photothermal therapy in vivo.* ACS Nano, 2011. **5**(2): p. 9.
142. J. Ripoll, B. Koberstein-Schwarz, and V. Ntziachristos, *Unleashing Optics and Optoacoustics for Developmental Biology.* Trends in Biotechnology, 2015. **33**(11): p. 13.
143. Y. Peng, et al., *Recent Advances in Optical Imaging with Anisotropic Plasmonic Nanoparticles* Analytical Chemistry, 2015. **87**: p. 16.
144. J. Park, et al., *Two-photon-induced photoluminescence imaging of tumors using near-infrared excited gold nanoshells.* Optics Express, 2008. **16**(3): p. 10.
145. Ntziachristos, V., *Going deeper than microscopy: the optical imaging frontier in biology.* Nature Methods, 2010. **7**(8): p. 12.
146. W. Li and X. Chen, *Gold nanoparticles for photoacoustic imaging.* Nanomedicine (Lond), 2015. **10**(2): p. 22.
147. W. Li, et al., *Gold nanocages as contrast agents for optoacoustic imaging.* Contrast Media and Molecular Imaging, 2011. **6**: p. 8.
148. S. E. Skrabalak, et al., *Gold Nanocages: Synthesis, Properties and Applications.* Accounts of Chemical Research, 2008. **41**(12): p. 9.
149. S. Manohar, C. Ungureanu, and T.G.V. Leeuwen, *Gold nanorods as molecular contrast agents in photoacoustic imaging: the promises and the caveats.* Contrast Media and Molecular Imaging, 2011. **6**: p. 12.
150. X. Yu, Y. Jiao, and Q. Chai, *Applications of Gold Nanoparticles in Biosensors.* Nano LIFE, 2016. **6**(2): p. 1064.
151. H. Aldewachi, et al., *Gold nanoparticle-based colorimetric biosensors.* Nanoscale, 2018. **10**: p. 16.
152. M. Sanromán-Iglesias, et al., *Sensitivity Limit of Nanoparticle Biosensors in the Discrimination of Single Nucleotide Polymorphism.* ACS Sensors, 2016. **1**(9): p. 7.
153. M. Sanromán-Iglesias, et al., *Nanoparticle-Based Discrimination on Single-Nucleotide Ploymorphism in Long DNA Sequences.* Bioconjugate Chemistry, 2017. **28**(4): p. 4.
154. J. Guo, et al., *Gold nanoparticles enlighten the future of cancer theranostics.* International Journal of Nanomedicine, 2017. **12**: p. 22.
155. Y. Liu, W. Ma, and J. Wang, *Theranostics of Gold Nanoparticles with an Emphasis on Photoacoustic Imaging and Photothermal Therapy.* Current Pharmaceutical Design, 2018. **24**(23): p. 10.
156. B. Khlebtsov, et al., *Nanocomposites Containing Silica-Coated Gold-Silver Nanocages and Yb-2,4-Dimethoxyhematoporphyrin: Multifunctional Capability of IR-Luminescence Detection, Photosensitization, and Photothermolysis.* ACS Nano, 2011. **5**(9): p. 13.
157. P. Huang, et al., *Folic acid-conjugated Silica-modified gold nanorods for X-ray/CT imaging-guided dual-mode radiation and photo-thermal therapy.* Biomaterials, 2011. **32**(36): p. 14.
158. A. C. Anselmo and S. Mitragotri, *A Review of Clinical Translation of Inorganic Nanoparticles.* The APPS Journal, 2015. **17**(5): p. 14.
159. C. Ward, et al., *Performance evaluation of the Verigene (Nanosphere) and FilmArray (BioFire) molecular assays for identification of causative organisms in bacterial bloodstream infections.* European Journal of Clinical Microbiology and Infectious Diseases, 2015. **34**(3): p. 10.

160. Center, N.I.o.H.C., *TNF-Bound Colloidal Gold in Treating Patients With Advanced Solid Tumors*. 2006-2012.
161. Inc., N.B., *Pilot Study of Aurolase (tm) Therapy in Refractory and/or Recurrent Tumors of the Head and Neck.* 2009-2017.
162. University, U.M., *Plasmonic Nanophotothermal Therapy of Atherosclerosis (NANOM-FIM).* 2011-2019.
163. F. Charbgoo, et al., *Gold nanoparticle should understand protein corona for being a clinical nanomaterial.* Journal of Controlled Release, 2018. **272**: p. 15.
164. M. Cui, et al., *Quantitative study of protein coronas on gold nanoparticles with different surface modifications.* Nano Research, 2014. **7**(3): p. 8.
165. A. D'Hollander, et al., *Limiting the protein corona: A successful strategy for in vivo active targeting of anti-HER2 nanobody-functionalized nanostars.* Biomaterials, 2017. **123**: p. 9.
166. V. Ntziachristos and D. Razansky, *Optical and Opto-acoustic Imaging*. 2013: Springer.
167. V. Ntziachristos and D. Razansky, *Molecular Imaging by Means of Multispectral Optoacoustic Tomography (MSOT).* Chemical Reviews, 2010. **110**: p. 12.
168. A. Taruttis, G. M. Van Dam, and V. Ntziachristos, *Mesoscopic and Macroscopic Optoacoustic Imaging of Cancer.* Cancer Research, 2015. **75**(8): p. 12.
169. D. Razansky, J. Baeten, and V. Ntziachristos, *Sensitivity of molecular target detection by multispectral optoacoustic tomography (MSOT).* The International Journal of Medical Physics Research and Practice, 2009. **36**(3): p. 7.
170. P-C. Li, et al., *In vivo Photoacoustic Molecular Imaging with Simultaneous Multiple Selective Targeting Using Antibody-Conjuugated Gold Nanorods.* Optics Express, 2008. **16**(23): p. 11.
171. A. Taruttis, et al., *Real-time imaging of cardiovascular dyamics and circulating gold nanorods with multispectral optoacoustic tomography.* Optics Express, 2010. **18**(19): p. 11.
172. S. J. Oldenburg, et al., *Infrared extinction properties of gold nanoshells.* Applied Physics Letters, 1999. **75**: p. 10.
173. C. Loo, et al., *Nanoshell-enabled photonics-based imaging and therapy of cancer.* Technology in Cancer Research and Treatment, 2004. **3**(1): p. 8.
174. Y. Sun, B. T. Mayers, and Y. Xia, *Template-Engaged Replacement Reaction: A One-Step Approach to the Large-Scale Synthesis of Metal Nanostructures with Hollow Interiors.* Nano Letters, 2002. **2**(5): p. 6.
175. J. R. Cole, et al., *Photothermal Efficiencies of Nanoshells and Nanorods for Clinical Therapeutic Applications.* The Journal of Physical Chemistry C, 2009. **113**(28): p. 5.
176. N. Malikova, et al., *Layer-by-Layer Assembled Mixed Spherical and Planar Gold Nanoparticles: Control of Interparticle Interactions.* Langmuir, 2002. **18**(9): p. 4.
177. J. E. Millstone, et al., *Observation of a Quadrupole Plasmon Moder for a Colloidal Solution of Gold Nanoprisms.* Journal of the American Chemical Society, 2005. **127**(15): p. 2.
178. C. Bao, et al., *Gold nanoprisms as optoacoustic signal nanoamplifiers for in vivo bioimaging of gastrointestinal cancers.* Small, 2013. **9**: p. 10.
179. A. Srivatsan, et al., *Gold Nanocage-Photosensitizer Conjugates for Dual-Modal Image-Guided Enhanced Photodynamic Therapy.* Theranostics, 2014. **4**(2): p. 12.
180. M. A. Mahmoudi and M.A. El-Sayed, *Metallic double shell hollow nanocages: the challenges of their synthetic techniques.* Langmuir, 2012. **28**(9): p. 9.
181. J. Chen, et al., *Gold Nanocages: Bioconjugation and Their Potential Use as Optical Imaging Contrast Agents* Nano Letters, 2005. **5**(3): p. 5.
182. L. Nie, et al., *In Vivo Volumetric Photoacoustic Molecular Angiography and Therapeutic Monitoring with Targeted Plasmonic Nanostars* Small, 2014. **10**(8): p. 9.

183. M. Mathiyazhakan, et al., *Non-invasive controlled release from gold nanoparticle integrated photo-responsive liposomes through pulse laser induced microbubble cavitation.* Colloids and Surfaces B: Biointerfaces, 2015. **126**: p. 6.
184. A. L. Chen, et al., *Changes in Optical Properties of Plasmonic Nanoparticles in Cellular Environments are Modulated by Nanoparticle PEGylation and Serum Conditions* Nanoscale Research Letters, 2016. **11**: p. 12.
185. M. Wang, et al., *Nanoparticle-proteome in vitro and in vivo.* Journal of Material Chemistry B, 2018. **6**: p. 16.
186. J. C. Y. Kah, et al., *Exploiting the Protein Corona around Gold Nanorods for Loading and Triggered Release.* ACS Nano, 2012. **6**(8): p. 11.
187. R. García-Álvarez, et al., *In vivo formation of protein corona on gold nanoparticles. The effect of their size and shape.* Nanoscale, 2018. **10**: p. 9.
188. R. García-Álvarez, et al., *Optimizing the Geometry of Photoacoustically Active Gold Nanoparticles for Biomedical Imaging.* ACS Photonics, 2020. **7**: p. 7.
189. M. Wuithschick, et al., *Turkevich in New Robes: Key Questions Answered for the Most Common Gold Nanoparticle Synthesis.* ACS Nano, 2015. **9**(7): p. 20.
190. Takiyama, K., *Formation and Aging of Precpitates. VIII. Formation of Monodisperse Nanoparticles (1) Gold Sol Particles by Sodium Citrate Method.* Bulletin of the Chemical Society of Japan, 1958. **31**(8): p. 9.
191. T. Hendel, et al., *In Situ Determination of Colloidal Gold Concentrations with UV-Vis Spectroscopy: Limitations and Perspectives* Analytical Chemistry, 2014. **86**: p. 10.
192. M. K. Chow and C.F. Zukoski, *Gold Sol Formation Mechanism: Role of Colloidal Stability.* Journal of Colloid and Interface Science, 1994. **165**(1): p. 13.
193. B-K. Pong, et al., *New Insights on the Nanoparticle Growth Mechanism in the Citrate Reduction of Gold(III) Salt: Formation of the Au Nanowire Intermediate and Its Nonlinear Optical Properties* The Journal of Physical Chemistry C, 2007. **111**(17): p. 7.
194. J. Polte, et al., *Mechanism of Gold Nanoparticle Formation in the Classical Citrate Synthesis Method Derived from Coupled In Situ XANES and SAXS Evaluation.* Journal of the American Chemical Society, 2010. **132**(4): p. 6.
195. E. A. Hauser and J.E. Lynn, *Experiments in Colloid Chemistry*. 1940: McGraw-Hill.
196. Polte, J., *Fundamental growth principles of colloidal metal nanoparticles - a new perspective.* Cryst Eng Comm, 2015. **17**: p. 22.
197. Frens, G., *Controlled Nucleation for the Regulation of the Particle Size in Monodisperse Gold Suspensions.* Nature Physical Science, 1973. **241**: p. 3.
198. S. D. Perrault and W.C.W. Chan, *Synthesis and Surface Modification of Highly Monodispersed, Spherical Gold Nanoparticles of 5-200 nm.* Journal of the American Chemical Society, 2009. **131**(47): p. 2.
199. N. C. Bigall, et al., *Monodisperse Platinum Nanospheres with Adjustable Diameters from 10 to 100 nm: Synthesis and Distinct Optical Properties.* Nano Letters, 2008. **8**(12): p. 5.
200. K. R. Brown, D. G. Walter, and M.J. Natan, *Seeding of Colloidal Au Nanoparticle Solutions. Improved Control of Particle Size and Shape.* Chemistry of Materials, 2000. **12**(2): p. 8.
201. K. R. Brown and M.J. Natan, *Hydroxylamine Seeding of Colloidal Au Nanoparticles in Solution and on Surfaces.* Langmuir, 1998. **14**(4): p. 3.
202. N. R. Jana, L. Gearheart, and C.J. Murphy, *Seeding Growth for Size Control of 5-40 nm Diameter Gold Nanoparticles.* Langmuir, 2001. **17**(22): p. 5.
203. J. Rodríguez-Fernández, et al., *Seeded Growth of Submicron Au Colloids with Quadrupole Plasmon Resonance Modes.* Langmuir, 2006. **22**(16): p. 4.
204. A. P. Leonov, et al., *Detoxification of Gold Nanorods by Treatment with Polystyrenesulfonate.* ACS Nano, 2008. **2**(12): p. 8.

205. C. A. Foss, M. J. Tierney, and C.R. Martin, *Template synthesis of infrared-transparent metal microcylinders: comparison of optical properties with the predictions of effective medium theory.* The Journal of Physical Chemistry, 1992. **96**(22): p. 7.
206. S. E. Lohse and C.J. Murphy, *The Quest for Shape Control: A History of Gold Nanorod Synthesis.* Chemistry of Materials, 2013. **25**(8): p. 12.
207. S. Barbosa, et al., *Tuning Size and Sensing Properties in Colloidal Gold Nanostars.* Langmuir, 2010. **26**(18): p. 8.
208. H. Yuan, et al., *Gold nanostars: surfactant-free synthesis, 3D modelling, and two-photon photoluminescence* Nanotechnology, 2012. **23**(7): p. 15.
209. E. Pensa, et al., *The Chemistry of the Sulfur-Gold Interface: In Search of a Unified Model.* Accounts of Chemical Research, 2012. **45**(8): p. 10.
210. J. B. Hall, et al., *Characterization of nanoparticles for therapeutics.* Nanomedicine, 2007. **2**(6): p. 15.
211. A. B. Djurisic, et al., *Optical Properties of Oxide Materials.* UV-VIS and Photoluminescence Spectroscopy for Nanomaterials Characterization, 2013: p. 15.
212. L. Yu and A. Andriola, *Quantitative gold nanoparticle analysis methods: A review.* Talanta, 2010. **82**(3): p. 7.
213. Kumar, C.S.R., *Transmission Electron Microscopy Characterization of Nanomaterials.* 2014.
214. D. B. Willliams and C.B. Carter, *The Transmission Electron Microscope*. 1996: Springer. 15.
215. Malatesta, M., *Trasnmission electron microscopy for nanomedicine: novel applications for long-established techniques.* European Journal of Histochemistry, 2016. **60**: p. 5.
216. Ramos, A.P., *Dynamic Light Scattering Applied to Nanoparticle Characterization.* Micro and Nano Technologies, 2017. **4**: p. 12.
217. G. Videen and D. Secker, *Focus Issue: Light Scattering by Non-Spherical Nanoparticles.* Optics Express, 2001. **8**(6): p. 2.
218. J. D. Clogston and A.K. Patri, *Zeta Potential Measurement.* Methods in Molecular Biology, 2011. **697**: p. 8.
219. Oshima, H., *The Derjaguin-Landau-Verwey-Oberbeek (DLVO) theory of colloid stability* Electrical Phenomena at Interfaces and Biointerfaces, 2012. **1**: p. 8.
220. M. P. Monopoli, et al., *Formation and Characterization of the Nanoparticle-Protein Corona* Nanomaterial Interfaced in Biology 2013: p. 19.
221. O. Vilanova, et al., *Understanding the Kinetics of Protein-Nanoparticle Formation* ACS Nano, 2016. **10**(12): p. 9.
222. A. M. Davidson, et al., *Sensitive Analysis of Protein Adsorption to Colloidal Gold by Differential Centrifugal Sedimentation.* Analytical Chemistry, 2017. **89**(12): p. 8.
223. N. Fernández-Iglesias and J. Bettmer, *Complementary mass spectrometric techniques for the quantification of the protein corona: a case of study on gold nanoparticles and human serum proteins* Nanoscale, 2015. **7**: p. 8.
224. Creative-Biostructure. Available from: www.creative-biostructure.com.
225. Inc, V.P.; Available from: www.vivaproducts.com/.
226. Taylor, H.E., *Inductively Coupled Plasma-Mass Spectrometry*. 2001: Academic Press.
227. P. K. Smith, et al., *Measurement of protein using bicinchoninic acid.* Analytical Biochemistry, 1985. **150**(1): p. 10.
228. K. J. Wiechelman, R. D. Braun, and J.D. Fitzpatrick, *Investigation of the bicichoninic acid protein assay: identification of the groups responsible for color formation.* Analytical Biochemistry, 1988. **175**(1): p. 7.
229. R. J. Kessler and D.D. Fanestil, *Interference by lipids in the determination of protein using bicinchoninic acid.* Analytical Biochemistry, 1986. **159**(1): p. 5.
230. R. E. Brown, K. L. Jarvis, and K.J. Hyland, *Protein measurement using bicinchoninic acid: elimination of interfering substances.* Analytical Biochemistry, 1989. **180**(1): p. 4.

231. SRL, C.; Available from: www.cyanagen.com/.
232. Colligan, J.E., *Current Protocols in Science: Electrophoresis*. 2002: John Wiley and Sons.
233. Laemmli, U.K., *Cleavage of Structural Proteins during the Assembly of the Head of Bacteriophage T4.* Nature, 1970. **227**: p. 6.
234. J. Svasti and B. Panijpan, *SDS-Polyacrilamide Gel Electrophoresis.* Journal of Chemical Education, 1977. **54**(9): p. 3.
235. Scientific, T.
236. M. Gaspari and G. Cuda, *Nano LC-MS/MS: A Robust Setup for Proteomic Analysis*. Methods in Molecular Biology. 2011: Humana Press.
237. Searle, B.C., *Scaffold: a bioinformatic tool for validating MS/MS-based proteomic studies.* Proteomics, 2010. **10**(6): p. 5.
238. R. Zhang, et al., *Evaluation for computational platforms of LC-MS based label-free quantitative proteomics: A global view.* Journal of Proteomics and Bioinformatics, 2010. **3**(9): p. 6.
239. H. Wang and S. Hanash, *Intact-Protein Based Sample Preparation Strategies for Proteome Analysis in Combination with Mass Spectrometry.* Mass Spectrometry Reviews, 2005. **24**: p. 14.
240. F. Benetti, et al., *Gold nanoparticles. role of size and surface chemistry on blood protein adsorption.* Journal of Nanoparticle Research, 2013. **15**: p. 9.
241. E. L. L. Yeo, et al., *Protein Corona around Gold Nanorods as a Drug Carrier for Multimodal Cancer Therapy.* ACS Biomaterials Science and Engineering, 2017. **3**(6): p. 12.
242. S. Palchetti, et al., *Influence of the dynamic flow environment on nanoparticle-protein corona: From protein patterns to uptake in cancer cells.* Colloids and Surfaces B: Biointerfaces, 2017. **153**: p. 9.
243. J. Schaller, et al., *Human Blood Plasma Proteins: Structure and Function*. 2008: Wiley.
244. L. Rodríguez-Lorenzo, et al., *Reshaping and LSPR tuning of Au nanostars in the presence of CTAB.* Journal of Material Chemistry, 2011. **21**: p. 6.
245. C. D. Walkey, et al., *Nanoparticle size and surface chemistry determine serum protein adsorption and macrophage uptake.* Journal of the American Chemical Society, 2012. **134**: p. 9.
246. U. Sakulkhu, et al., *Protein Corona Composition of Superparamagnetic Iron Oxide Nanoparticles with Various Physico-Chemical Properties and Coatings.* Scientific Reports, 2014. **4**: p. 9.
247. A. M. Merlot, D. S. Kalinowski, and D.R. Richardson, *Unraveling the mysteries of serum albumin - more than just a serum protein.* Frontiers in Physiology, 2014. **5**: p. 7.
248. N. Khlebstov and L. Dykman, *Biodistribution and toxicity of engineered gold nanoparticles: a review of in vitro and in vivo studies* Chemical Society Reviews, 2011. **40**: p. 25.
249. R. Chia, et al., *The origins and uses of mouse outbred stocks.* Nature Genetics, 2005. **37**(11): p. 6.
250. S. Parasuraman, R. Raveendran, and R. Kesavan, *Blood sample collection in small laboratory animals.* Journal of Pharmacology and Pharmacotherapeutics, 2010. **1**(2): p. 7.
251. Y. Wang, et al., *Stabilization and Encapsulation of Gold Nanostars Mediated by Dithiols.* Small, 2015. **11**(34): p. 7.
252. P. K. Jain, et al., *Calculated Absorption and Scattering Properties of Gold Nanoparticles of Different Size, Shape, and Composition: Applications in Biological Imaging and Biomedicine.* The Journal of Physical Chemistry B, 2006. **110**(14): p. 11.
253. Y. Shi, et al., *Thermally confined shell coating amplifies the photoacoustic conversion efficiency of nanoprobes.* Nano Research, 2016. **9**(12): p. 14.

254. S. Mallidi, G. P. Luke, and S. Emelianov, *Photoacoustic Imaging in Cancer Detection: Diagnosis and Treatment Guidance.* Trends in Biotechnology, 2011(29): p. 9.
255. L. Novotny and B. Hecht, *Principles of Nano-Optics.* Cambridge University Press, 2012.
256. D. Baranov, et al., *Synthesis of Flexible, Ultrathin Gold Nanowires in Organic Media.* Langmuir, 2008(24): p. 5.
257. P. B. Johnson and R.W. Christy, *Optical Constants of the Noble Metals.* Physical Review B, 1972(6): p. 9.
258. S. Xu, P. Li, and Y. Lu, *In SItu Atomic-Scale Analysis of Rayleigh Instability in Ultrathin Gold Nanowires.* Nano Research, 2018(11): p. 7.
259. A. Guerrero-Martínez, et al., *Nanostars Shine Bright for You. Colloidal Synthesis, Properties and Applications of Branched Metallic Nanoparticles.* Current Opinion on Colloids and Interface Science, 2011(16): p. 9.
260. F. Hao, et al., *Plasmon Resonances of a Gold Nanostar.* Nano Letters, 2007(7): p. 3.
261. H. Yuan, et al., *In Vivo Particle Tracking and Photothermal Ablation Using Plasmon-Resonant Gold Nanostars.* Nanomedicine: Nanotechnology, Biology, and Medicine, 2012(8): p. 8.
262. D. Wu, et al., *Contrast Agent for Photoacoustic and Thermoacoustic Imaging: A Review.* International Journal of Molecular Sciences, 2014. **15**: p. 24.
263. T. Repenko, et al., *Strong Photoacoustic Signal Enhancement by Coating Gold Nanoparticles with Melanin for Biomedical Imaging.* Advanced Functional Materials, 2018. **28**: p. 8.
264. W. Li and X. Chen, *Gold nanoparticles for optoacoustic imaging.* Nanomedicine (Lond), 2015. **10**(2): p. 22.
265. B. Cox, et al., *Quantitative Spectrocopic Photoacoustic Imaging: A Review.* Journal of Biomedical Optics, 2012(17): p. 23.
266. E. C. Dreaden, et al., *The Golden Age: Gold Nanoparticles for Biomedicine.* Chemical Society Reviews, 2012(41): p. 39.
267. M. Xu and L.V. Wang, *Photoacoustic Imaging in Biomedicine.* Review of Scientific Instruments, 2006(77): p. 25.
268. V. J. Pansare, et al., *Review of Long-Wavelength Optical and NIR Imaging Materials: Contrast Agents, Fluorophores, and Multifunctional Nano Carriers.* Chemistry of Materials, 2012(24): p. 15.
269. M. Hu, et al., *Gold Nanostructures: Engineering Their Plasmonic Properties for Biomedical Applications* Chemical Society Reviews, 2006(35): p. 10.
270. Y. Wang, et al., *Comparison Study of Gold Nanohexapods, Nanorods and Nanocages for Photothermal Cancer Treatment.* ACS Nano, 2013(7): p. 9.
271. L. Jauffred, et al., *Plasmonic Heating of Nanostructures.* Chemical Reviews, 2019. **119**(13): p. 43.
272. K. Wilson, K. Homan, and S. Emelianov, *Biomedical Photoacoustics beyond Thermal Expansion Using Triggered Nanodroplet Vaporization for Contrast-Enhanced Imaging.* Nature Communications, 2012(3): p. 8.
273. J. V. Jokerst, et al., *Gold Nanorods for Ovarian Cancer Detection with Photoacoustic Imaging and Resection Guidance via Raman Imaging in Living Mice.* ACS Nano, 2012(6): p. 11.
274. Y. Wang, et al., *Photoacoustic Tomography of a Nanoshell Contrast Agent in the in Vivo Rat Brain.* Nano Letters, 2004(4): p. 3.
275. X. Yang, et al., *Photoacoustic Tomography of a Rat Cerebral Cortex in Vivo with Au Nnaocages as an Optical Contrast Agent.* Nano Letters, 2007(7): p. 4.
276. S. Karim, et al., *Morphological Evolution of Au Nanowires Controlled by Rayleigh Instability.* Nanotechnology, 2006(17): p. 5.
277. J. Pérez-Juste, et al., *Gold Nanorods: Synthesis, Characterization and Applications.* Coordination Chemistry Reviews, 2005(249): p. 31.

278. S. E. Bohndiek, et al., *Development and Application of Stable Phantoms for the Evaluation of Photoacoustic Imaging Instruments.* PLOS One, 2013(8): p. 14.
279. Y. A. Cengel and M.A. Biles, *Thermodynamics: An Engineering Approach.* 8th Edition, McGraw-Hill Education, 2014.